AD-A189 323 CORPUS CHRISTI INNER HARBOR SHOALING INVESTIGATION(U) 1/3
CAVER (TROY V) DOVER NJ T M SMITH ET AL. SEP 87
WES/TR/HL-87-13

UNCLASSIFIED F/G 13/2 NL

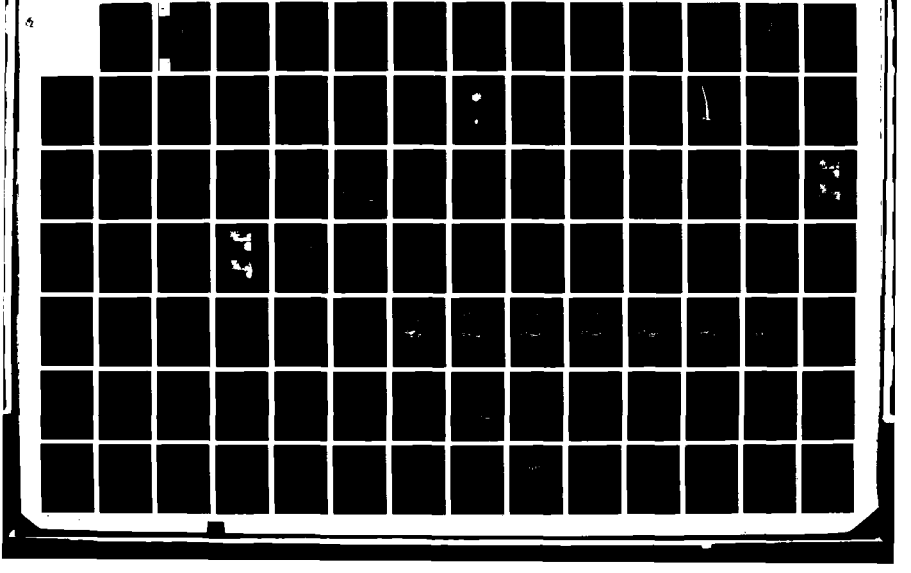

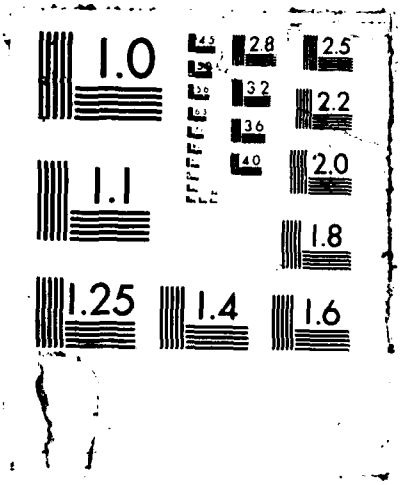
1.0
1.1
1.25
1.4
1.6
1.8
2.0
2.2
2.5
2.8
3.2
3.6
4.0

US Army Corps of Engineers

TECHNICAL REPORT HL-87-13

CORPUS CHRISTI INNER HARBOR SHOALING INVESTIGATION

by

Tamsen M. Smith, William H. McAnally, Jr., Allen M. Teeter

Hydraulics Laboratory

DEPARTMENT OF THE ARMY
Waterways Experiment Station, Corps of Engineers
PO Box 631, Vicksburg, Mississippi 39180-0631

September 1987
Final Report

Prepared for US Army Engineer District, Galveston
Galveston, Texas 77553-1229

HYDRAULICS LABORATORY

Destroy this report when no longer needed. Do not return it to the originator.

The findings in this report are not to be construed as an official Department of the Army position unless so designated by other authorized documents.

The contents of this report are not to be used for advertising, publication, or promotional purposes. Citation of trade names does not constitute an official endorsement or approval of the use of such commercial products.

Unclassified

SECURITY CLASSIFICATION OF THIS PAGE

REPORT DOCUMENTATION PAGE

Form Approved OMB No. 0704-0188

AD-A189 323

1a. REPORT SECURITY CLASSIFICATION Unclassified	1b. RESTRICTIVE MARKINGS
2a. SECURITY CLASSIFICATION AUTHORITY	3. DISTRIBUTION/AVAILABILITY OF REPORT Approved for public release; distribution unlimited.
2b. DECLASSIFICATION/DOWNGRADING SCHEDULE	
4. PERFORMING ORGANIZATION REPORT NUMBER(S) Technical Report HL-87-13	5. MONITORING ORGANIZATION REPORT NUMBER(S)
6a. NAME OF PERFORMING ORGANIZATION USAEWES Hydraulics Laboratory 6b. OFFICE SYMBOL (If applicable) WESHE-?	7a. NAME OF MONITORING ORGANIZATION
6c. ADDRESS (City, State, and ZIP Code) PO Box 631 Vicksburg, MS 39180-0631	7b. ADDRESS (City, State, and ZIP Code)
8a. NAME OF FUNDING/SPONSORING ORGANIZATION USAED, Galveston 8b. OFFICE SYMBOL (If applicable)	9. PROCUREMENT INSTRUMENT IDENTIFICATION NUMBER
8c. ADDRESS (City, State, and ZIP Code) PO Box 1229 Galveston, TX 77553-1229	10. SOURCE OF FUNDING NUMBERS PROGRAM ELEMENT NO / PROJECT NO / TASK NO / WORK UNIT ACCESSION NO

11. TITLE (Include Security Classification)

Corpus Christi Inner Harbor Shoaling Investigation

12. PERSONAL AUTHOR(S)

Smith, Tamsen M.; McAnally, William H., Jr.; Teeter, Allen M.

13a. TYPE OF REPORT	13b. TIME COVERED	14. DATE OF REPORT (Year, Month, Day)	15. PAGE COUNT
Final report	FROM _____ TO _____	September 1987	216

16. SUPPLEMENTARY NOTATION

Available from National Technical Information Service, 5285 Port Royal Road, Springfield, VA 22161.

17. COSATI CODES			18. SUBJECT TERMS (Continue on reverse if necessary and identify by block number)
FIELD	GROUP	SUB-GROUP	Corpus Christi Bay; Corpus Christi Harbor; Estuaries; Numerical modeling; Sedimentation

19. ABSTRACT (Continue on reverse if necessary and identify by block number)

A combination of numerical models was used to test alternatives for shoaling prevention in Corpus Christi Harbor, Texas. The vertically averaged model system, TABS-2, was used to simulate contributions of sediments by bay waters to the sediment load. The laterally averaged estuarine model, LAEMSED, was used to simulate density currents in the channel and sedimentation that occurs at the harbor entrance.

Applications of the models testing advance maintenance, removal of industrial discharges and withdrawals, advance maintenance in conjunction with a sill, and movement of the disposal areas showed a 20 percent decrease in shoaling as a result of industrial activity removal, a 75 percent decrease in sediments entering the bay channel due to disposal area relocation, and practically no effect on shoaling rates resulting from advance maintenance.

(Continued)

20. DISTRIBUTION/AVAILABILITY OF ABSTRACT	21. ABSTRACT SECURITY CLASSIFICATION
☒ UNCLASSIFIED/UNLIMITED ☐ SAME AS RPT ☐ DTIC USERS	Unclassified
22a. NAME OF RESPONSIBLE INDIVIDUAL	22b. TELEPHONE (Include Area Code) / 22c. OFFICE SYMBOL

DD Form 1473, JUN 86 *Previous editions are obsolete*

19. ABSTRACT (Continued).

Appendix A presents the results of a reconnaissance survey on shoaling conditions in Corpus Christi Harbor. Appendix B describes the TABS-2 numerical modeling system, and Appendix C describes the theoretical aspects of LAEMSED.

PREFACE

This report describes and presents the results from the Corpus Christi Harbor Shoaling Investigation performed by the US Army Engineer Waterways Experiment Station (WES) for the US Army Engineer District, Galveston (SWG). The study was conducted by personnel of the Hydraulics Laboratory of WES under the general supervision of Mr. F. A. Herrmann, Jr., Chief of the Hydraulics Laboratory, Mr. R. A. Sager, Assistant Chief of the Hydraulics Laboratory, Mr. W. H. McAnally, Chief of the Estuaries Division, and Mr. G. M. Fisackerly, Chief of the Estuarine Processes Branch (EPB). Mr. J. M. Keislich, SWG, was project coordinator. Work on the project began in December 1984 and was completed in December 1986.

Ms. T. M. Smith, EPB, was Project Engineer. Mr. A. M. Teeter, EPB, conducted the reconnaissance survey and provided consultation for the field program and the numerical modeling. Mr. H. A. Benson, EPB, supervised the field data collection program, and Ms. B. P. Donnell, Estuarine Simulation Branch (ESB), assisted with the field data analysis. Mr. D. P. Bach, ESB, and Dr. B. H. Johnson, Math Modeling Group, Hydraulic Analysis Division, provided advice and assistance with the numerical modeling. Ms. Smith, Mr. McAnally, and Mr. Teeter wrote the main text of this report. Mr. Teeter wrote Appendix A, Dr. Johnson wrote Appendix C, and staff of the Hydraulics Laboratory wrote Appendix B. Mrs. Marsha C. Gay, Information Products Division, Information Technology Laboratory, edited the report.

COL Dwayne G. Lee, CE, is the Commander and Director of WES. Dr. Robert W. Whalin is the Technical Director.

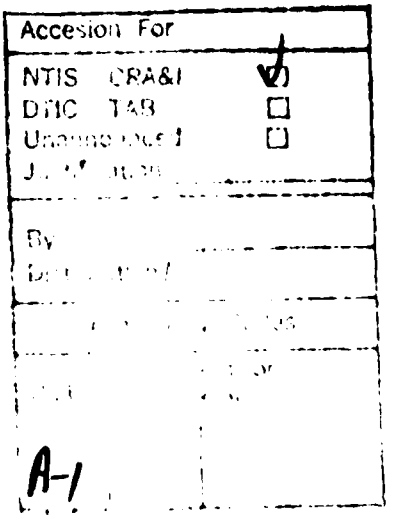

CONTENTS

CONVERSION FACTORS, NON-SI TO SI (METRIC)
UNITS OF MEASUREMENT

Non-SI units of measurement used in this report can be converted to SI (metric) units as follows:

Multiply	By	To Obtain
cubic feet	0.02831685	cubic metres
cubic yards	0.7645599	cubic metres
degrees (angle)	0.01745329	radians
feet	0.3048	metres
gallons (US liquid)	3.785412	cubic decimetres
inches	25.4	millimetres
knots (international)	0.514444	metres per second
miles (US nautical)	1.852	kilometres
miles (US statute)	1.609344	kilometres
ounces (US fluid)	0.02957353	cubic decimetres
pounds (force)-second per square foot	47.88026	pascals-second
pounds (mass)	0.4535924	kilograms

CORPUS CHRISTI INNER HARBOR SHOALING INVESTIGATION

PART I: INTRODUCTION

Background

1. Corpus Christi Bay is a shallow, wind-dominated system on the east coast of Texas and is sheltered from the open waters of the Gulf of Mexico by a low, narrow strip of land known as Mustang Island. Corpus Christi Harbor, located at the northwestern corner of the bay (Figure 1), experiences high shoaling rates in the harbor entrance area. A planned deepening project for the harbor is expected to increase shoaling rates and volumes.

2. The harbor forms a part of the Corpus Christi Ship Channel, a deep-draft project providing access from the gulf to several ports within the Corpus Christi Bay system. The channel extends from deep water in the gulf through a natural inlet at Aransas Pass, then across 21 miles* of open water to the harbor. The navigable channel then extends an additional 8.7 miles via five turning basins and connecting channels to a terminating point at Viola Turning Basin at the head of the project. The project has been completed to a depth of 45 ft mean low water, with the exception of the upper portion of the harbor which has an average depth of 40 ft.

3. The 8.7-mile-long portion of the waterway from the harbor entrance to the Viola Turning Basin (Figure 2) is bounded by land on three sides. The harbor project, isolating the waterway from Nueces Bay and the Nueces River to the north, was constructed by disposing of dredged material to create a protective embankment along the north side of the channel. Thus, with the exception of water from the surface drainage and the effluents from municipal and industrial use, all water in the inner harbor comes from the adjacent portions of Corpus Christi Bay and the navigation channel serving the harbor.

4. Historically, the first 2 miles of the inner harbor channel (from the breakwaters at the basin entrance through the basin itself) have had

---

* A table of factors for converting non-SI units of measurement to SI (metric) units is presented on page 4.

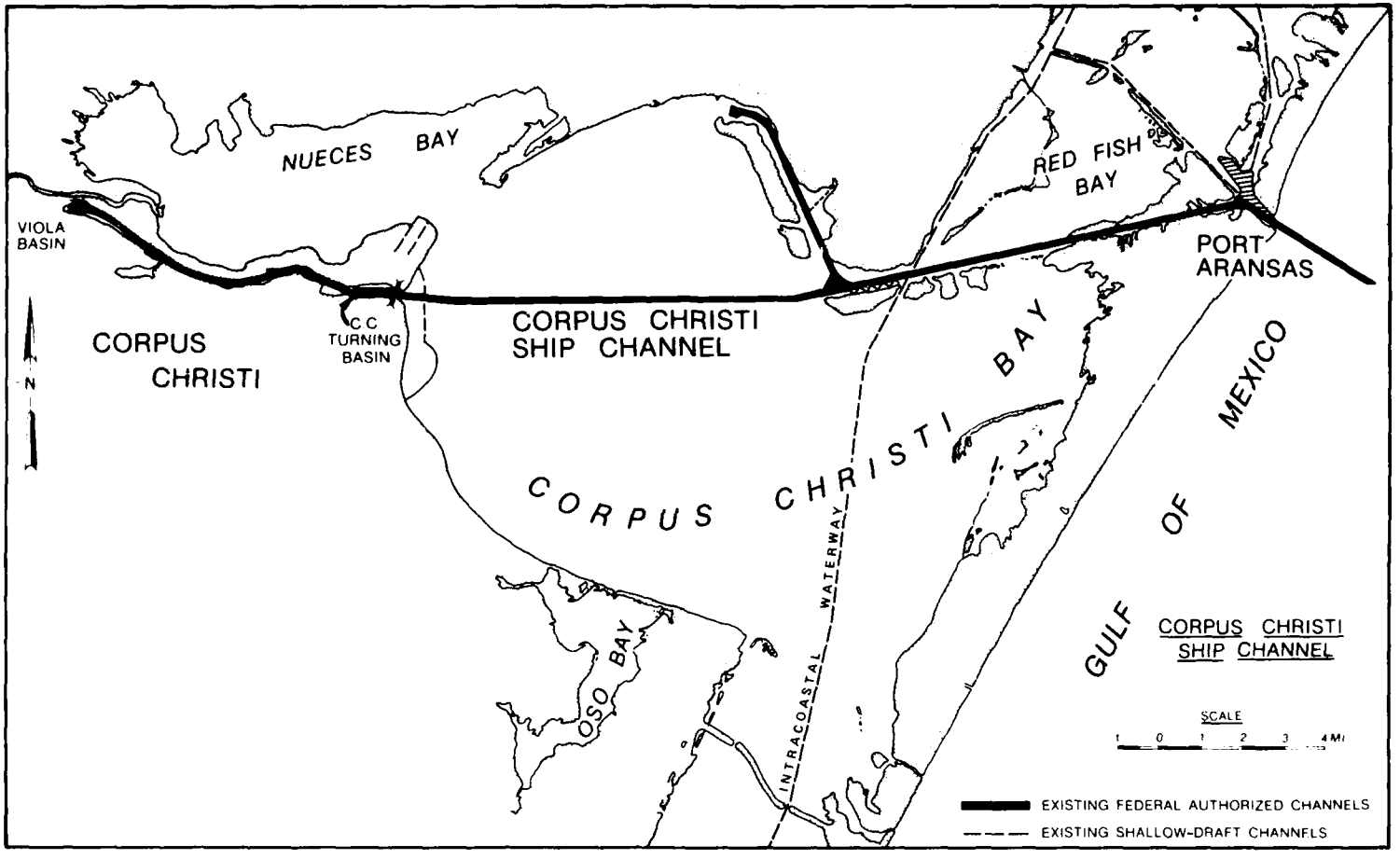

Figure 1. Corpus Christi Bay

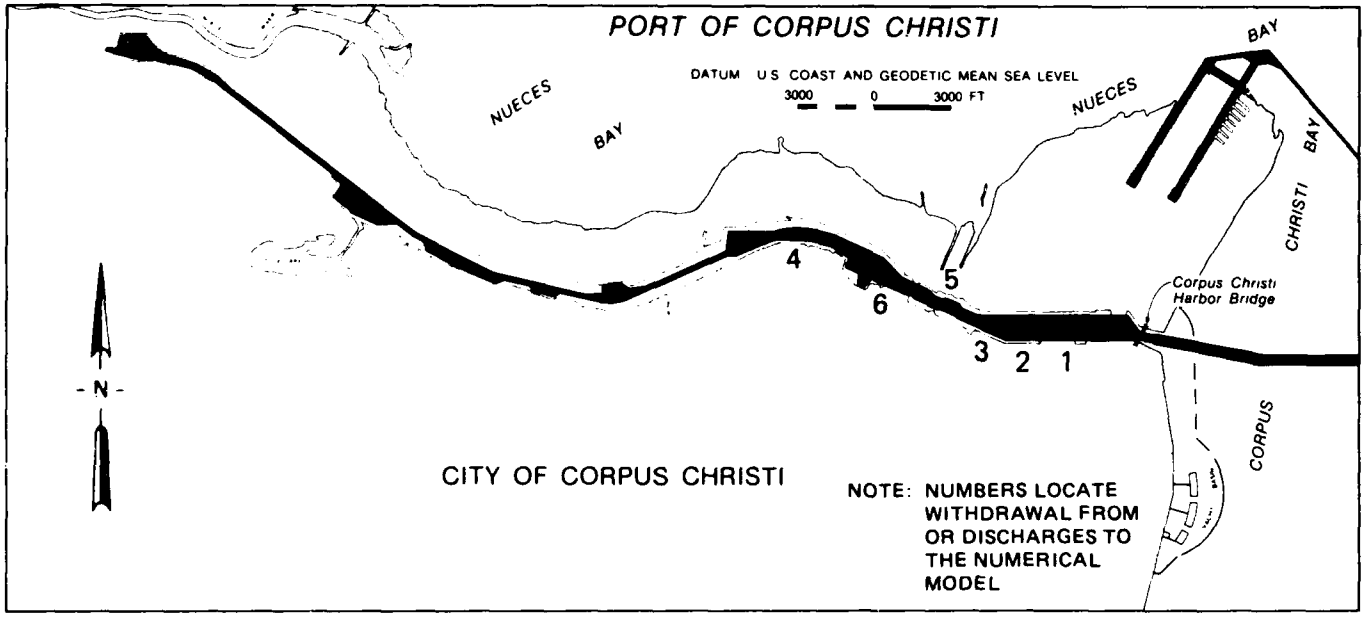

Figure 2. Corpus Christi Harbor

relatively high shoaling rates of about 700,000 cu yd per year. The deepening of the channel to its 45-ft project depth beginning in 1978 and still continuing has raised concerns that the shoaling rate in this area will increase. Concerns have also been expressed regarding the fate of dredged material under disposal plans for the authorized project. Extensive amounts of dredged material have been placed in bay and upland disposal areas. According to the Corpus Christi Port Authority (Nueces County Navigation Commission 1979), open water disposal of sediments dredged from the harbor is no longer considered acceptable by regulatory agencies, and land disposal sites are limited in size and number. Alternatives to reduce the shoaling quantity and thereby reduce the disposal requirements are needed. Therefore, the processes controlling sediment deposition in the inner harbor area need to be defined so that the alternatives can be evaluated.

5. The Committee on Tidal Hydraulics (CTH), Corps of Engineers, US Army, performed a study of this sedimentation problem in 1964 (CTH 1965). The primary finding of that study was the identification of a water circulation pattern similar to a density current phenomenon caused by one or both of the following: (a) the large industrial discharges to and withdrawals from the harbor and (b) a higher mean density of water in Corpus Christi Bay than in the inner harbor. CTH recommended additional comprehensive field studies to determine with more certainty the processes controlling the water circulation, sediment transport, and deposition patterns.

Purpose

6. The objectives of this study were to determine the sources and causes of shoaling occurring in the inner harbor and to evaluate alternative methods for reducing the high volume of maintenance dredging required near the harbor entrance. In addition, the schedule for the overall study required a rapid completion of the model tests.

Approach

7. This investigation was conducted in three phases. Phase I was a short-term reconnaissance survey to gather the hydraulic, salinity, temperature, and sediment data necessary to characterize the system and to identify

phenomena that contribute to the shoaling. That portion of the study was completed in August of 1984 and appears in this report as Appendix A. Phase II activities included monitoring harbor and bay hydraulics, salinities, and suspended sediment concentrations under a variety of conditions to define the factors that contribute significantly to harbor shoaling and to support the verification of numerical models. The purpose of the Phase III portion of the study was to numerically simulate the sedimentation process that occurs in the harbor to evaluate plans for the reduction of harbor shoaling.

8. Because of the time restriction, limited verification of the numerical models was determined to be sufficient for the purposes of this study.

9. A combination of models was used in the numerical simulations. The Phase I reconnaissance survey showed that the predominant shoaling mechanism is a density-driven current along the bay channel that brings fine-grained sediments into the harbor entrance area where the sediments deposit and accumulate. The vertical variation in velocities required a vertical model (one that reproduces the vertical velocity profiles accurately) to simulate sedimentation processes that occurred. LAEMSED (Laterally Averaged Estuarine Model with Sediment) was used to model the ship channel and harbor. Modeling the sediment contributions by sources in the bay required the use of a horizontal model (which is two-dimensional in the horizontal plane). The numerical modeling system, TABS-2, was used. Results from the TABS-2 (bay) model were used as input to the LAEMSED (harbor) model.

PART II: DESCRIPTION OF MODELS

Numerical Modeling

10. Numerical modeling employs special computational methods, such as iteration and approximation, to solve mathematical expressions that describe physical phenomena. Numerical models used in coastal hydraulic problems are of two principal types: finite difference and finite element. The finite difference method approximates derivatives by differences in the values of variables over finite intervals of space and time. This method requires discretization of space and time into regular grids of computation points. The finite element method employs piecewise approximations of mathematical expressions over a number of discrete elements. The assemblage of piecewise approximations is solved as a set of simultaneous equations to provide answers at points in space (nodes) and time.

11. Numerical models are classified by the number of spatial dimensions over which variables are permitted to change. Thus in a one-dimensional flow model, currents are averaged over two dimensions (usually width and depth) and vary only in one direction (usually longitudinally). Two-dimensional models average variables over one spatial dimension, either over depth (a horizontal model) or width (a vertical model). Three-dimensional models solve equations accounting for variation of the variables in all three spatial dimensions.

12. Numerical models are capable of simulating processes that cannot be handled in any other way. Once a numerical model has been formulated and verified for a given area, it can quickly provide results for different conditions.

The TABS-2 Modeling System

13. The TABS-2 system, developed by the Hydraulics Laboratory, US Army Engineer Waterways Experiment Station, is a set of generalized computer programs for two-dimensional numerical modeling of open-channel flow, transport processes, and sedimentation problems in rivers, reservoirs, bays, and estuaries (Thomas and McAnally 1985a). The two major components of the system used in this study were RMA-2V, the finite element model for hydrodynamics, and STUDH, the finite element sediment model.

14. RMA-2V solves the depth-integrated equations of conservation of mass and momentum in two horizontal directions. Friction is calculated with Manning's equation and eddy viscosity coefficients are used to define lateral turbulence exchanges. The sedimentation model, STUDH, solves the convection-diffusion equation with bed source terms. These terms are structured for either sand or cohesive sediments. Clay erosion is based on work by Partheniades (1962) and the deposition of clay utilizes Krone's (1962) equations. The hydrodynamics from RMA-2V are used as input to STUDH. A more detailed description of both models appears in Appendix B.

The LAEMSED Model

15. LAEMSED is the sediment version of the original estuarine model, LAEM (Laterally Averaged Estuarine Model), developed by Edinger and Buchak (1981). LAEM was developed for computing stratified flows in estuaries. Additions to LAEM for suspended sediment computations and to include a sediment bed model were made by Johnson (Johnson, Trawle, and Kee in preparation). These modifications were patterned after work by Thomas and McAnally (1985a) in the development of the two-dimensional sediment model, STUDH.

16. The basic flow and transport equations that are solved in LAEMSED are statements of the conservation of mass and momentum of the flow field plus the conservation of the heat, salt, and suspended sediment in the water body. Boussinesq's eddy coefficient concept is employed to account for effect of turbulence in the flow field. The routines that compute the exchange of sediment between the sediment bed and the water column are modifications of those found in STUDH. A more detailed description of the model is given in Appendix C.

PART III: FIELD INVESTIGATIONS

17. Field data obtained in Phases I and II of the study were used for limited model verification. The data collected in the Phase II portion consisted of long-term tidal, current, and water sample data and two intensive surveys. Long-term data collection began in December 1984 and was completed in October 1985. Ten months of tidal data, 9 months of velocity data, 7 months of wind data, and 4 months of suspended sediment and salinity data were collected. Long-term stations are shown in Figures 3 and 4. In addition, two intensive surveys were conducted in the inner harbor. The first, conducted in February 1985, measured velocities, salinities, and suspended sediment concentrations at nine stations over a 25-hr period. The second intensive survey was conducted in June 1985. Only 14 hr of data were collected during the second survey because of hazardous weather conditions. The field data collection and analysis are described by Smith (in preparation).

18. Because the current velocities measured during the February intensive survey were below the threshold of the current meters (approximately 0.1 ft/sec) a majority of the time, only the data from the June survey were used for model verification. Station locations for this survey are given in Figure 5.

19. A statistical analysis was performed on wind data collected at the Corpus Christi Area Office, US Army Engineer District, Galveston, and on current velocity data measured at sta V4 during May 1985, the longest period for which both wind and velocity data near the harbor entrance were available. Data were analyzed to determine the correlation between wind velocities and current velocities near the harbor entrance. Polar histograms of velocities and wind speeds are shown in Figure 6. Forty-one percent of the current velocities occurring at this station had direction headings in the northwestern quadrant (Q4) and thirty-six percent of the headings fell in the southwestern quadrant (Q3). Fifty-four percent of the wind headings were in the northwestern quadrant (from the southeast) and thirty-one percent occurred in the southwestern quadrant. Observations of the data from other times of the year show the same pattern. These data and the physical characteristics of the system (small tide range and wide shallow bay) suggest that currents near the channel at sta V4 are strongly influenced by wind.

20. It is reported that during most of the year, winds at Corpus

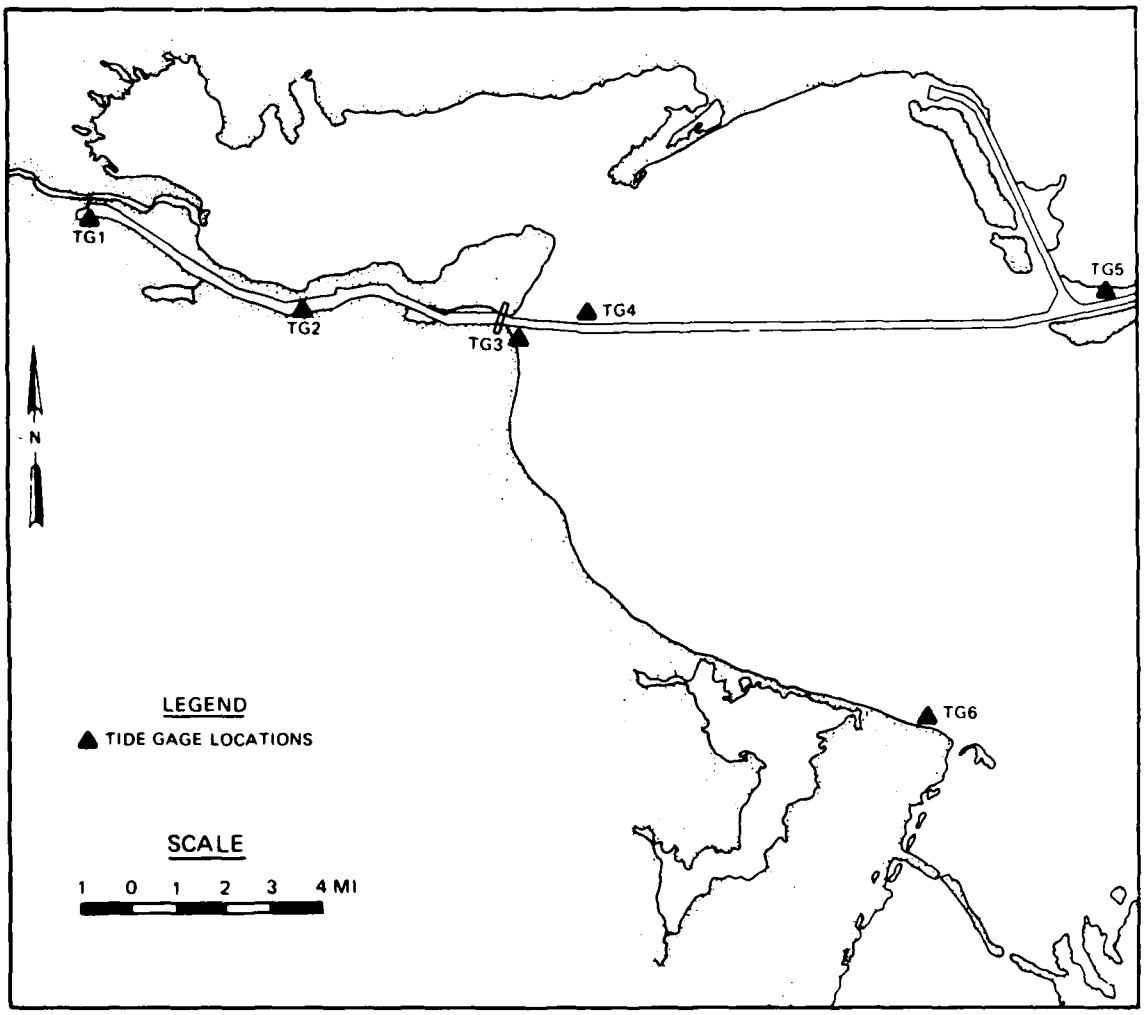

Figure 3. Long-term tide stations

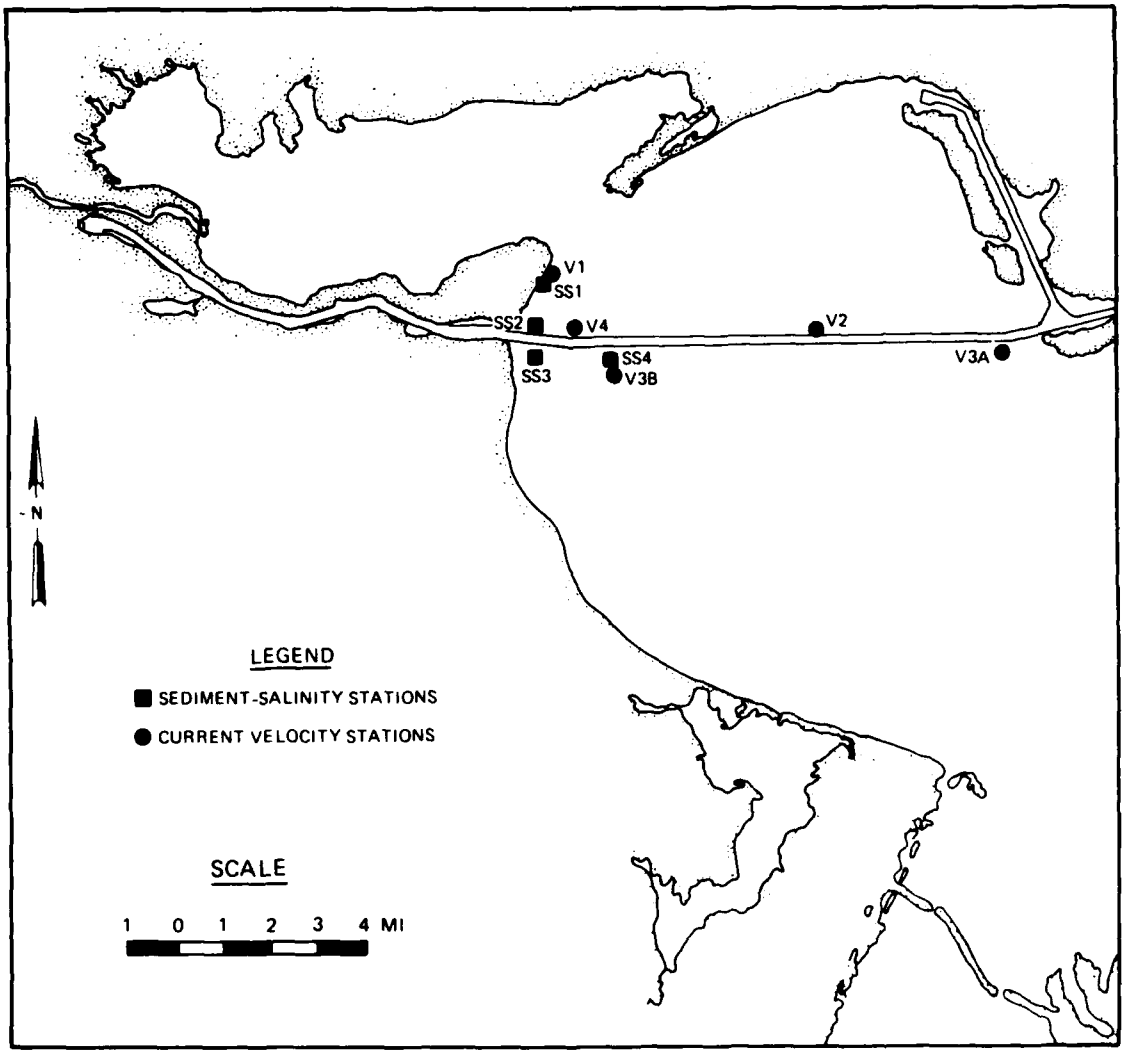

Figure 4. Long-term velocity and water sample stations

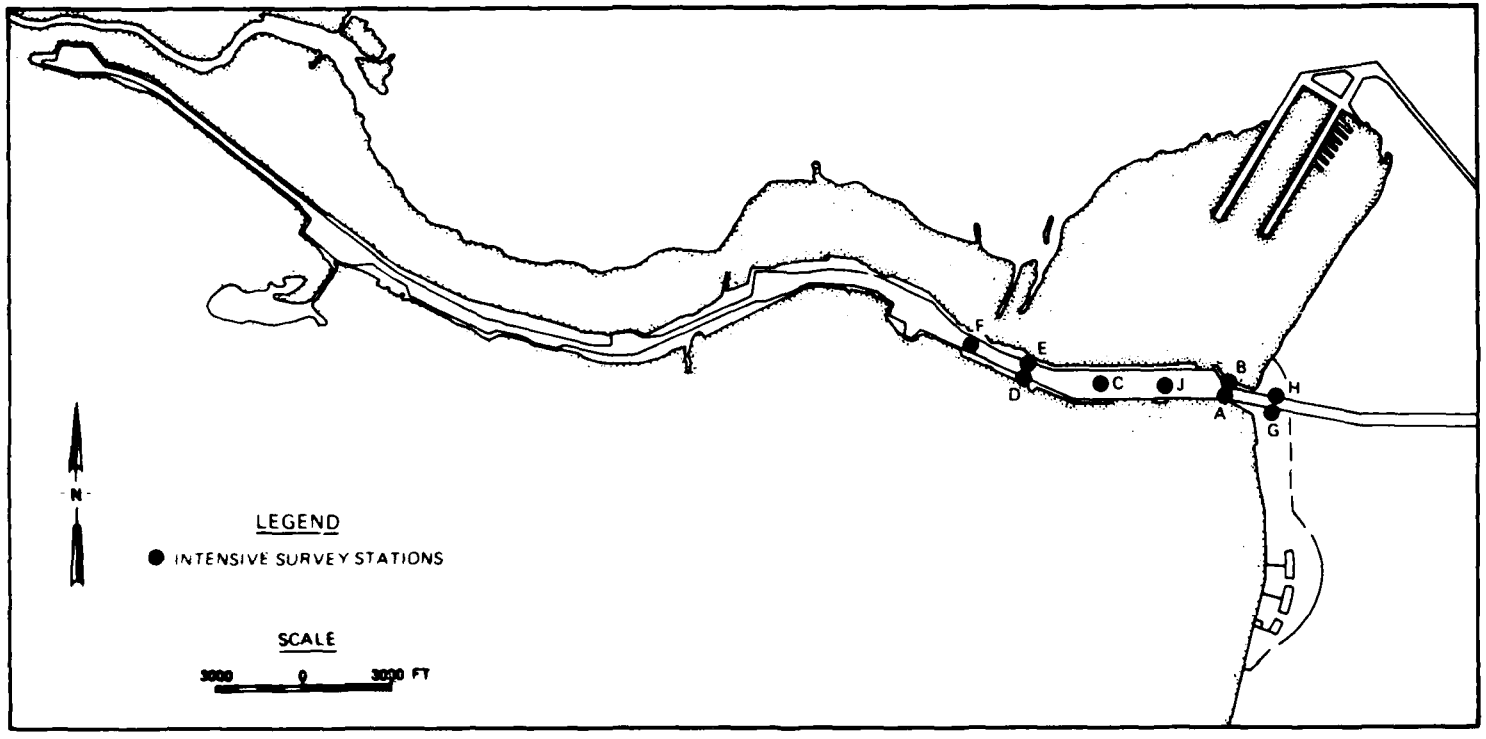

Figure 5. 18 June survey station locations

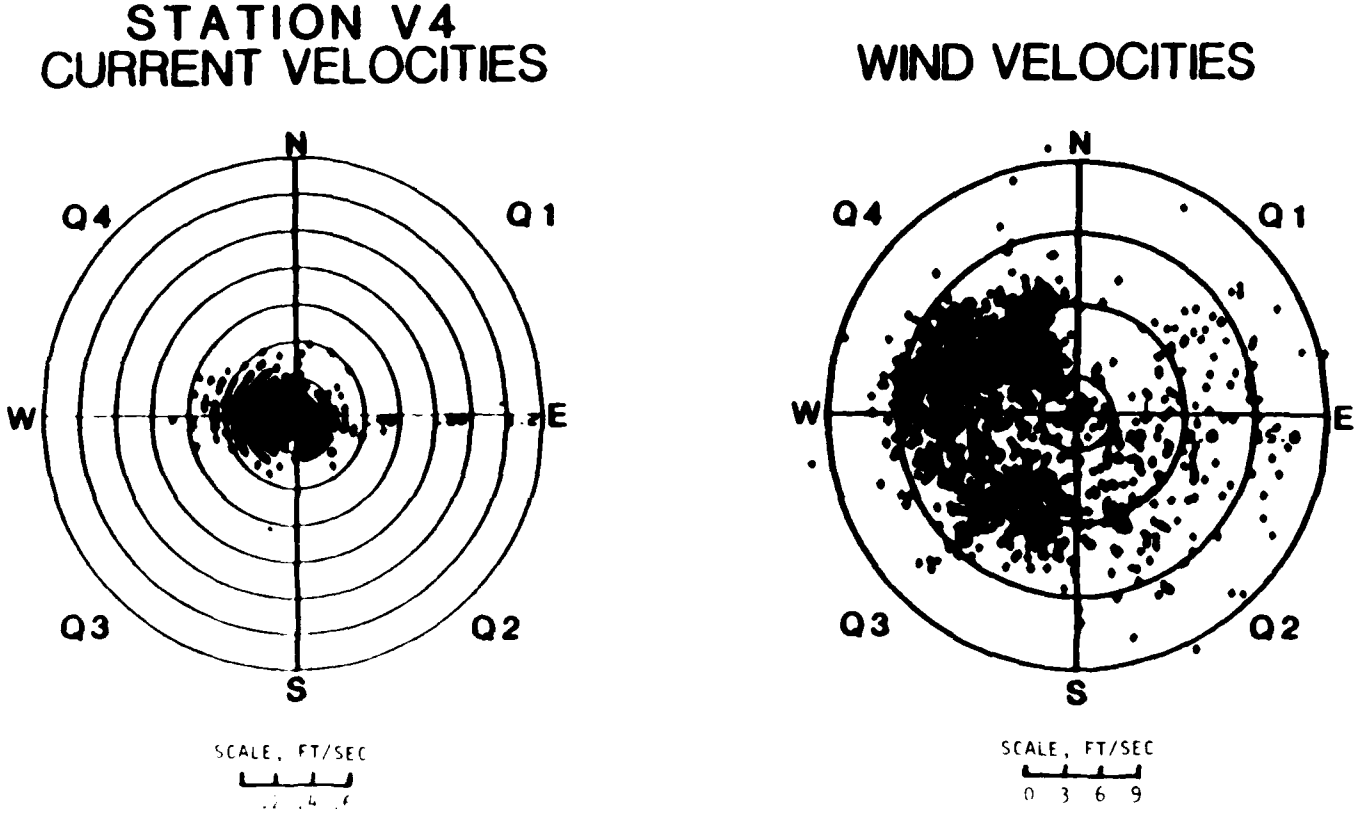

Figure 6. Polar histogram of current and wind data from May 1985, sta V4

Christi are generally from the southeast (Texas A&M Research Foundation 1973). Also, throughout the period of record (January-October 1985), a majority of the current velocities were toward the northwest. Therefore, it is reasonable to assume that a majority of the time, current directions in the bay near the channel are heavily influenced by winds and flow is predominantly toward the entrance.

21. Present dredging practices at the Corpus Christi Ship Channel were defined during field data collection. Material that is dredged in the bay channel is discharged in open water about 1,600 ft south of the channel. The mound from these point discharges has never been observed to reach the surface. This observation confirms a prediction stated in the Phase I report (Appendix A, paragraph 47) that the dredged material is spreading over a large surface area before mounding, becoming easily erodible.

22. Observations of suspended sediment concentrations measured from automatically withdrawn water samples (locations shown in Figure 4) show that in the earlier months of data collection (June-July 1985) the highest concentrations measured occurred near sta SS4 on the southern side of the channel. Concentrations at this station declined during the latter portion of the survey period. The probable reason for the elevated values in suspended sediment concentrations is the dredging of the bay channel taking place near the station location at that time. Concentrations at sta SS1 near Corpus Christi Beach remained relatively high (about 120 ppm) during the survey period.

23. Hydrographic surveys from 1965 to 1984 were obtained from the Corpus Christi Area Office. Shoaling rates were computed by comparing the postdredge survey with the following predredge survey, thus establishing the amount of material that had shoaled during that period. The following tabulation shows the results of that comparison. Shoaling rates from 0.7 to 2.0 ft

Region	Location	Station	Shoaling Period	Average Annual Infill ft	LAEMSED Predicted Infill ft
1	East of harbor entrance (bay channel)	1060+00-1100+00	Mar 74-Dec 78 Mar 80-Feb 84	2.6 2.0	2.4
2	Harbor entrance and first turning basin	1100+00-1150+00	Sep 71-Dec 78 Mar 80-Nov 83	0.7 2.0	0.9

per year were computed for the harbor entrance area and the Corpus Christi Turning Basin. The hydrographic surveys near the disposal areas did not reveal any significant accumulation of mounded sediment.

24. Corpus Christi Bay supports a productive shrimp fishery, and the use of weighted nets may make a significant contribution to the amount of suspended solids. Schubel et al. (1978) report that the amount of sediment resuspended each year by shrimpers is approximately 16 to 131 times that dredged for channel maintenance. During the reconnaissance survey and field data collection efforts it was noted that shrimping was particularly heavy near the harbor entrance.

PART IV: VERIFICATION OF THE MODELS

RMA-2V Verification

25. As previously stated, verification of the models was limited due to time constraints. The finite element mesh of the bay used as input to RMA-2V and STUDH is shown in Figure 7. The mesh was made up of elements (three- or four-sided figures) and nodes (corners and midside points of the elements). The final numerical mesh, consisting of 892 elements and 2,810 nodes, contained a detailed representation of the harbor entrance and the bay disposal areas. Elements of the various regions of the bay were assigned different types for specifying hydrodynamic and sediment parameters (such as Manning's n and diffusion coefficients). This network contained 34 different element types. Boundary conditions for the hydrodynamic model consisted of velocity specifications at the Nueces River (the primary source of fresh water to the system) and water-surface elevations at the ocean boundary.

26. RMA-2V verification was performed using data collected at the stations in the bay during 15-16 June 1985. Tidal data were filtered to remove meteorological effects and high-frequency oscillations. The mean water-surface elevation was obtained by filtering the 9 months of available tidal records. This elevation was assigned a value of 100.0 in RMA-2V so that all bed elevations and water-surface elevations would be positive. The tide range at the exit (Port Aransas) during this period was 1.2 ft. The Nueces River average discharge during June was 620 cfs. Hydrodynamic verification of RMA-2V was accomplished by adjusting bottom roughness and eddy viscosity coefficients, then comparing model water-surface elevations and velocities with prototype data. One-hour time-steps were used. Eddy viscosity coefficients ranged from 10 lb-sec/ft^2 for the very small elements to 400 lb-sec/ft^2 for the extremely large elements. The following tabulation provides a summary of the selected verification roughness values assigned to various regions:

Region	Manning's n
Ship Channel	0.012
Corpus Christi Bay	0.025-0.04
Nueces Bay	0.06

27. After sufficient time was allowed for model spin-up, a 25-hr test was conducted. Plates 1-3 show prototype-numerical model water-surface

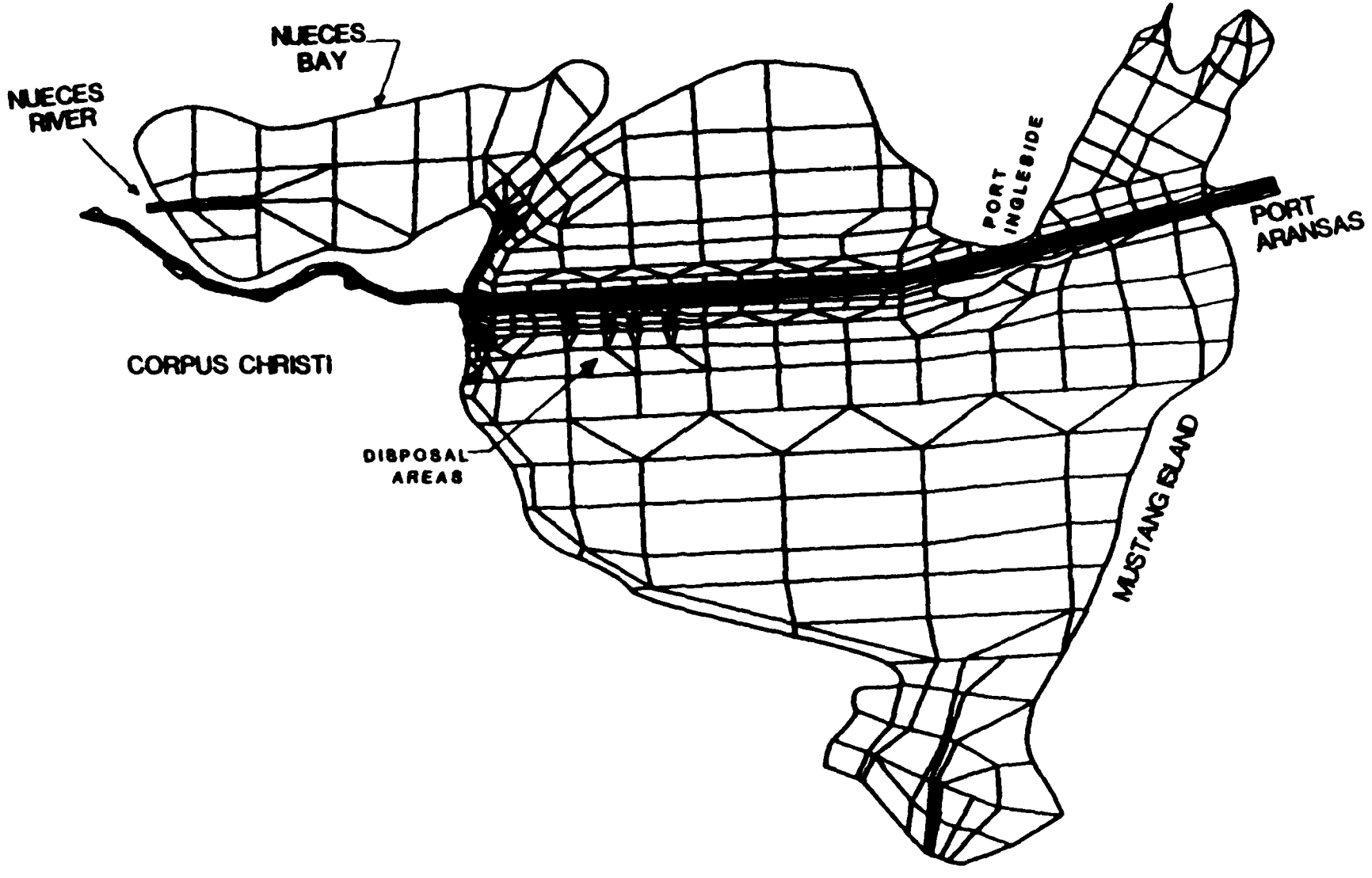

Figure 7. Finite element mesh for RMA-2V and STUDH

elevations at the six tide stations, and Plates 4-6 show prototype-numerical model velocity at three velocity stations. Phase and range agreement were good at the tide stations near the area of interest (sta TG1-TG4). With the exception of a few data points, good agreement was also obtained at the velocity stations. At lower velocities (those below 0.1 ft/sec) the magnitude of the current was below the threshold of the meter, and the field data tended to be inconsistent at some points.

28. After adjustment of the bay hydrodynamic model to the 15-16 June data, a test was conducted corresponding to the time of the harbor survey (17-18 June). The tide range at Port Aransas during this period was 1.3 ft. Plates 7-9 show prototype-numerical model water-surface elevation comparisons and Plate 10 shows prototype-numerical model velocity comparisons for stations where field data were available. Plots showing hourly current velocities throughout the tidal cycle are shown in Plates 11-17.

29. As stated in paragraph 19, bay currents are strongly dependent on wind, especially during periods of low tidal energy. The verification period was during a period of strong tidal energy, and running RMA-2V with wind did not improve the verification over the no-wind case. Resources and time for the feasibility study did not allow running the various seasonal wind conditions prevalent in the area; therefore, wind was not considered in the plan runs. Model runs with varying wind speeds and directions should be included in the design study.

STUDH Verification

30. Shoaling problems in the harbor result primarily from the deposition of fine-grained material. Thus the sediment was considered to be a clay. Because of the required study schedule, a very limited verification of STUDH was conducted. Since the objective of this portion of the study was to examine dredged material return to the channel, the sediment in the present disposal areas was allowed to erode while the remainder of the bay was assigned an inerodible bottom. Parameters such as critical shear stress for erosion, critical shear stress for deposition, and diffusion coefficients were varied until model concentrations at the three bay sediment stations matched those observed in the prototype. Table 1 provides the values used for the various sediment coefficients in the model.

31. During the intensive survey, suspended sediment concentrations remained relatively constant over the tidal cycle with the exception of the last few hours (storm event). The concentrations computed in STUDH at nodes corresponding to these prototype stations also remained fairly constant during the last half of the tidal cycle. These average concentrations for model and prototype at the four sediment stations are given in the following tabulation.

Station	Prototype Concentrations ppm	STUDH Concentrations ppm
SS1	51	91
SS2	33	35
SS3	16	30
SS4	83	73

At sta SS1 near Corpus Christi Beach, STUDH concentrations exceeded those measured in the field, but are still considered reasonable. Agreement was good at the other three stations.

LAEMSED Verification

Hydrodynamic verification

32. LAEMSED modeled the Corpus Christi Ship Channel from Viola Basin to approximately 8 miles east of the harbor entrance (near Port Ingleside). The grid boundaries from the Viola Basin to the harbor entrance were the land boundaries; and from the harbor entrance east to its right boundary, the grid encompassed only the ship channel. A schematic of a portion of the finite difference grid is shown in Figure 8. Associated with each grid cell is a width corresponding to the width of the channel in that area. Each cell had a length dx of 1,000 ft and a height dh of 3 ft. The entire grid contained 102 reaches (dx's) and 21 vertical layers (dh's). One-minute time-steps were required.

33. Lateral inflows into the channel from the bay were calculated from RMA-2V results. The flow across channel element sides was calculated, and these values served as input into LAEMSED. Associated with each inflow is a sediment concentration obtained from field data. Industrial inflows QIN and withdrawals QWD were also modeled in LAEMSED. Information concerning two withdrawals and four discharges from industries along the harbor were used as

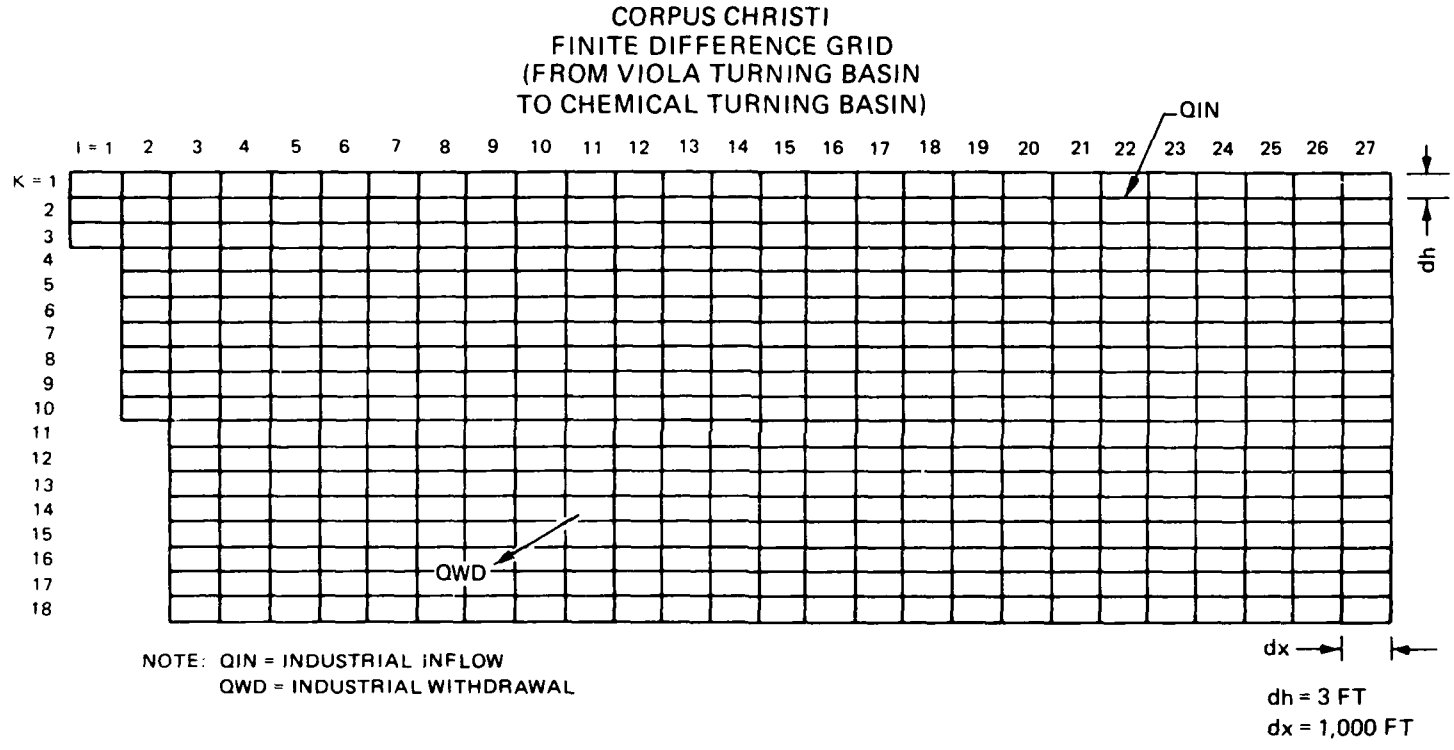

Figure 8. Portion of LAEMSED grid

input into the model. These are given in Table 2. Their locations are shown in Figure 2.

34. The flow computations in LAEMSED were verified through use of the field data collected 18 June 1985 and discussed in Part III. The tide range at the right boundary (gage TG5) for this period was 0.9 ft. Salinities varied during the observation from 33.5 to 36.8 ppt near the bottom and 28.2 to 33.5 ppt at the surface. A generally linear vertical distribution of salinity had been observed in the field and was used in the model. Sediment concentrations varied vertically from 10 g/ℓ near the surface to 30 g/ℓ near the bottom but did not vary significantly in time during the data collection. Recorded tides at five locations and velocity measurements at surface, middepth, and bottom at six locations were used for adjustment purposes. The eastern boundary of the grid extended across the bay to sta TG5 where water levels were recorded, providing water level boundary conditions for the model. Four tidal cycles were run as a spin-up period before computed results were compared with the field data. A comparison of computed and recorded tides at the other four tide stations is presented in Plates 18 and 19. Phase and range comparison at all stations was good for the first 15 hr. The last 10 hr corresponds to the storm that occurred on 18 June. The prevalent southeasterly wind shifted to a northern wind, causing the depression in water surface observed in the prototype data. The storm was not modeled.

35. Plots of computed and recorded velocities at surface, middepth, and bottom are shown in Plates 20-25. At most stations, both model and prototype data show a net flow into the harbor at the bottom (flood currents) and out of the harbor at the surface (ebb currents). Stations near the entrance show a net inflow at middepth as well. Phase agreement at most stations was generally good; however, prototype magnitudes were much greater than model, especially at stations near the harbor entrance. As noted in Appendix A, paragraph 39, these field data were so erratic as to be unreasonable. High winds during the survey period caused motion of the boats from which measurements were taken and may have induced short-period surges that contaminated the data. Velocities measured during the intensive survey in February were more on the order of those computed by the model. For these reasons and others, the discrepancies are not considered to reflect a poor verification.

Sediment verification

36. As in STUDH, only the sediment parameters for clays were used in

LAEMSED. Table 1 provides the values used for the various sediment coefficients in the model. The bed was assumed to be initially free of sediment. Initial sediment concentrations in each layer were interpolated from field data (paragraph 34). Sediment was introduced into the model by assigning a concentration to the lateral inflows that represent flow into the channel from the bay. These concentrations were also obtained from field data (paragraph 33).

37. The shoaling rates computed from hydrographic surveys (paragraph 21) were for two separate areas. Region 1 is the 4,000-ft-long section of channel just east of the entrance, and region 2 consists of the harbor entrance and the Corpus Christi Turning Basin. The tabulation in paragraph 23 shows the computed shoaling rates in these areas compared with those estimated from the hydrographic surveys. West of region 2, further into the harbor, both prototype and model shoaling rates were less than 0.25 ft per year. The only major discrepancy is in region 2 where the model value was close to the rate computed during the first period, but less than half of that of the most recent shoaling rates. During this period of time (1980 to 1983), more than the usual amount of dredging was being conducted in the bay channel. Many sections of the channel were being dredged to the new authorized depth of 45 ft. This activity generated more dredged material, which was placed in the open water disposal areas and could have gradually flowed back into the channel and from there into the harbor.

PART V: APPLICATION OF THE MODELS

38. A number of alternatives were identified that could reduce the annual maintenance dredging. Presented in the following paragraphs is a description of each of the tested alternatives and how the two models were used to evaluate their effectiveness in reducing maintenance dredging.

Modification of Industrial Discharges and Withdrawals

39. One of the factors believed to be contributing to the density current phenomenon observed in the inner harbor is the large amount of industrial discharges into and withdrawals from the project. Therefore, the effect of their removal on the circulation pattern and shoaling rate was tested. Information concerning two withdrawals and four discharges from industries along the harbor is given in Table 2. Their locations are shown in Figure 2.

40. The Central Power and Light Company (Nueces Plant) withdraws about 450 mgd for cooling purposes from the inner harbor and discharges this water into Nueces Bay. This diversion of water represents a sink within the harbor and must be replaced with waters from Corpus Christi Bay. Because of the mixing mechanisms and vertical density gradients at the harbor entrance, it is possible that the waters that are brought into the harbor to replenish the cooling water diversions are the saltier, denser, sediment-laden waters near the bottom of the channel. Modification of the cooling water diversion, either through a reduction of the volume removed or through discharging the cooling water back into the harbor following its use, would reduce or eliminate the need for bay waters to make up for the diversion.

41. In addition to the large withdrawal from the channel, historical records show that an average daily freshwater discharge of about 18 mgd is released into the upper harbor. The mechanisms of freshwater/saltwater mixing could be such that the freshwater discharges induce a flow into the harbor entrance from the saltier, denser, sediment-laden waters of the bay channel. As the bay channel waters enter the harbor entrance, the sediment particles could settle to form the harbor entrance shoals. These inflows and withdrawals were simulated in the LAEMSED model, and their effects on the circulation pattern in the harbor and on the sediment deposition were tested.

Advance Maintenance Dredging

42. Advance maintenance dredging is the practice of dredging channel dimensions beyond project requirements to provide additional area within the project limits for sediments to deposit and increase the time between dredging. If the additional channel dimensions result in reducing the costs and frequency of maintenance dredging, then this option is economically feasible. Using LAEMSED, the change in shoaling rates, and therefore the change in the required dredging frequency, as a result of the advance maintenance was tested. This alternative would not achieve the objective of reducing the total volume dredged, but could reduce dredging costs and provide flexibility in disposal.

Structural Modifications

43. Structural modifications near the harbor entrance is a possible alternative for diverting sediment-laden waters from the harbor entrance. A sill near the channel bottom might act to inhibit encroachment of saline and sediment-laden waters into the harbor along the channel bottom. Simulations of such a structure near the channel bottom in conjunction with advance maintenance were performed, using LAEMSED, to observe the effect that the restriction of the denser bottom layers would have on sedimentation.

Relocation of Dredged Material Disposal Areas

44. Disposal practices at Corpus Christi Harbor, discussed in Part III, are believed to contribute directly to the shoaling problem that occurs there. As mentioned in paragraph 23, surveys conducted at the disposal areas show little evidence of dredged material remaining at the disposal areas. Evidence was observed in the reconnaissance survey that these materials are possibly being returned to the channel by wind-generated currents and by the general circulation of the bay (Appendix A, paragraphs 50 and 53). Currents in shallow areas adjacent to the channel flow obliquely to the channel. As the sediments are introduced into the channel by this oblique current, density mechanisms can move them to the harbor entrance where they redeposit to form the recurring shoaling. Using the TABS-2 model, these sites were relocated to the north and changes in the amount of sediment entering the channel were noted.

PART VI: PLAN TESTING

Conditions Tested

45. To evaluate the impact of the alternatives discussed in Part V, five plan tests were performed. They are as follows:

a. Plan 1. Elimination of industrial withdrawals and discharges (LAEMSED).

b. Plan 2. Advance maintenance dredging (LAEMSED).

c. Plan 3. Advance maintenance dredging in combination with a sill (LAEMSED).

d. Plan 4. Relocation of bay disposal sites to 1,900 ft north of the channel (STUDH).

e. Plan 5. Relocation of bay disposal sites to 6,000 ft north of the channel (STUDH).

Boundary and initial conditions for plan tests were identical to those used in the verification.

Plan 1 Results

46. Locations of the cells for which sedimentation rates are shown are given in Figure 9. The shoaling rates from the LAEMSED base condition test of 17-18 June and those from a simulation with alternative 1 modifications (described in paragraphs 39-41) are compared in Figure 10. As can be seen

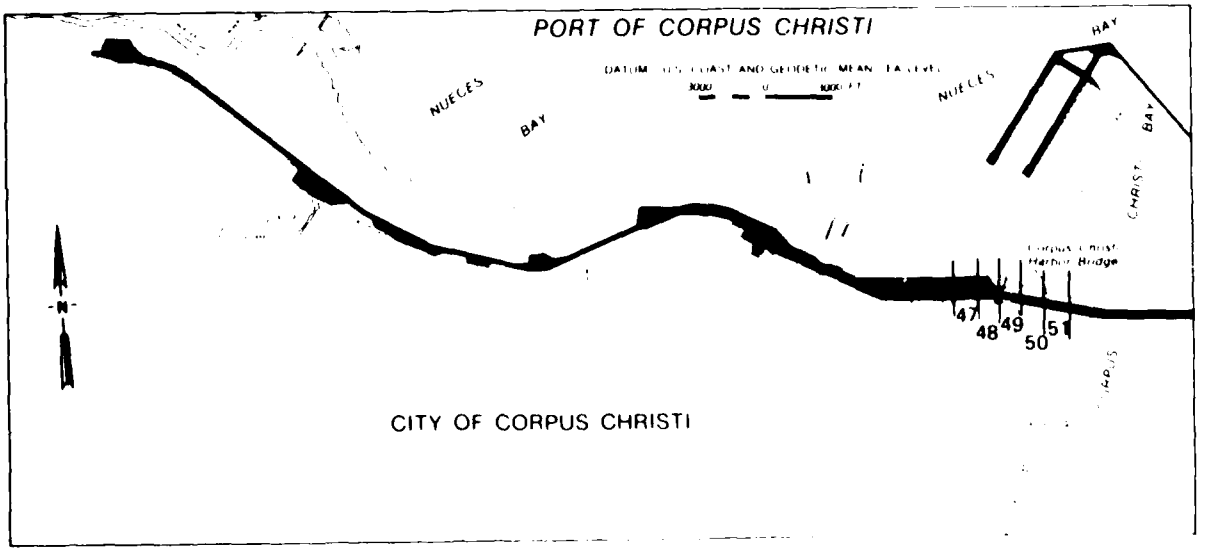

Figure 9. Location of LAEMSED computation cells near harbor entrance

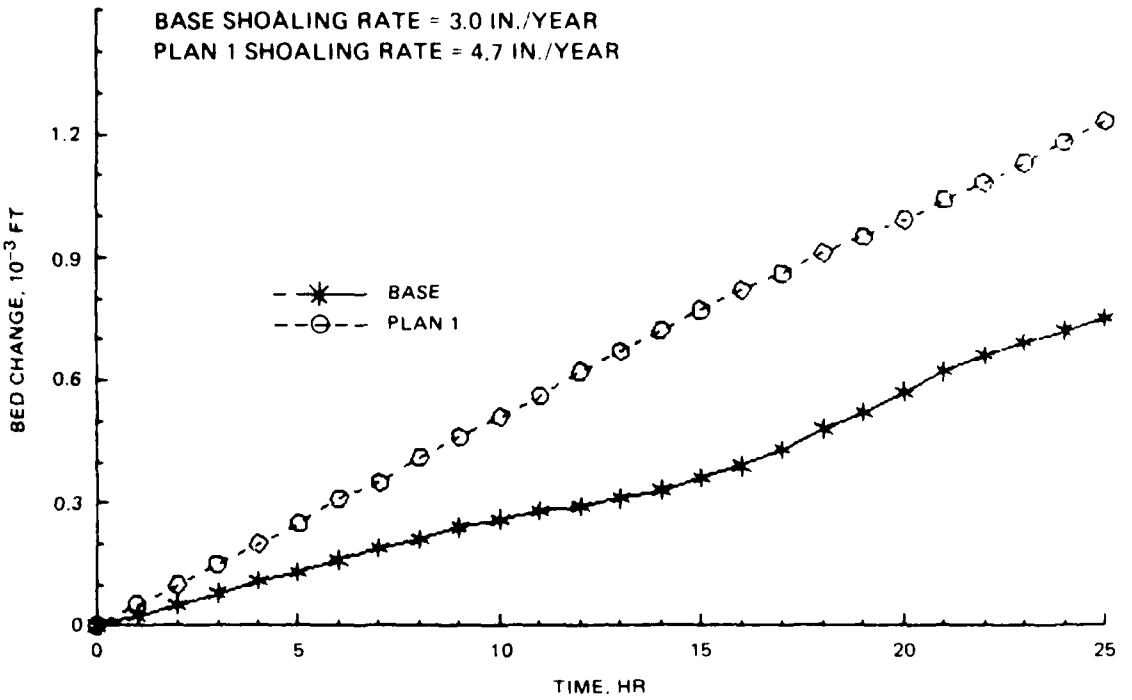

a. Cell 47

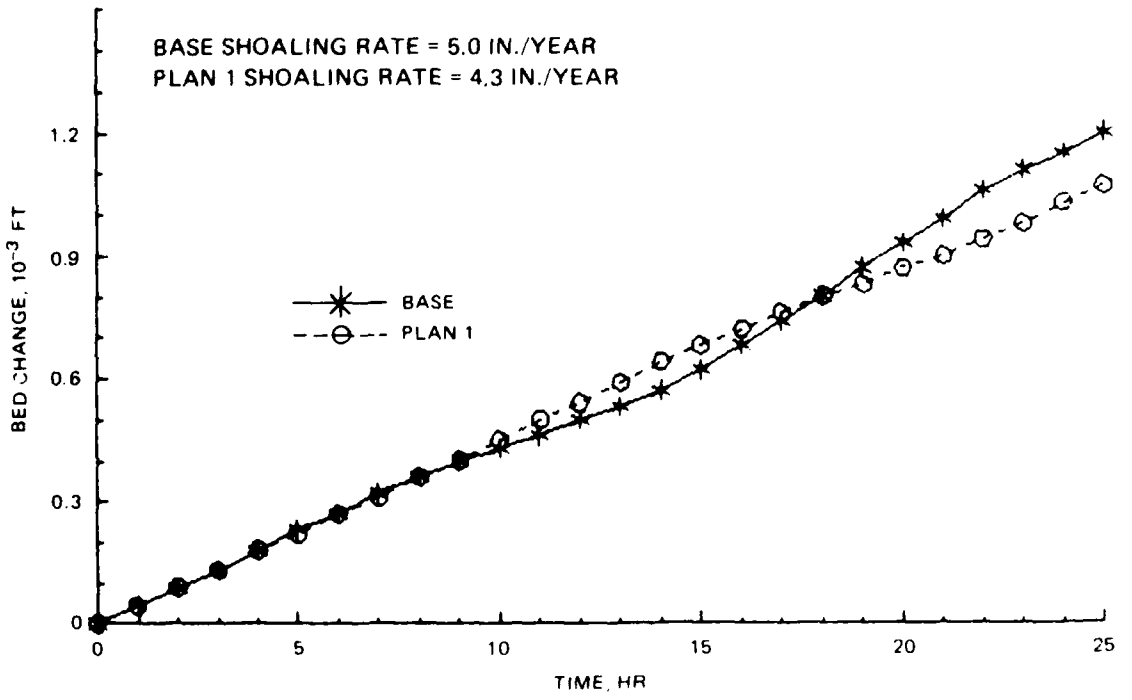

b. Cell 48

Figure 10. LAEMSED sedimentation results, base to Plan 1 (Continued)

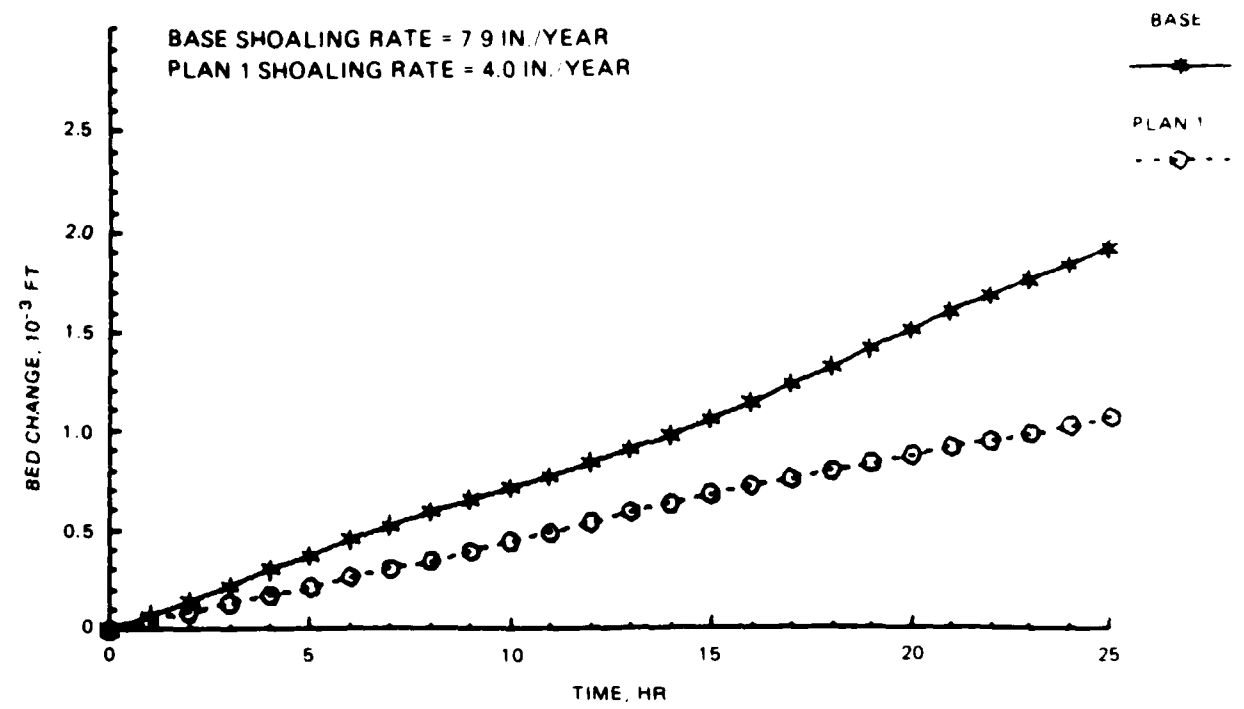

c. Cell 49

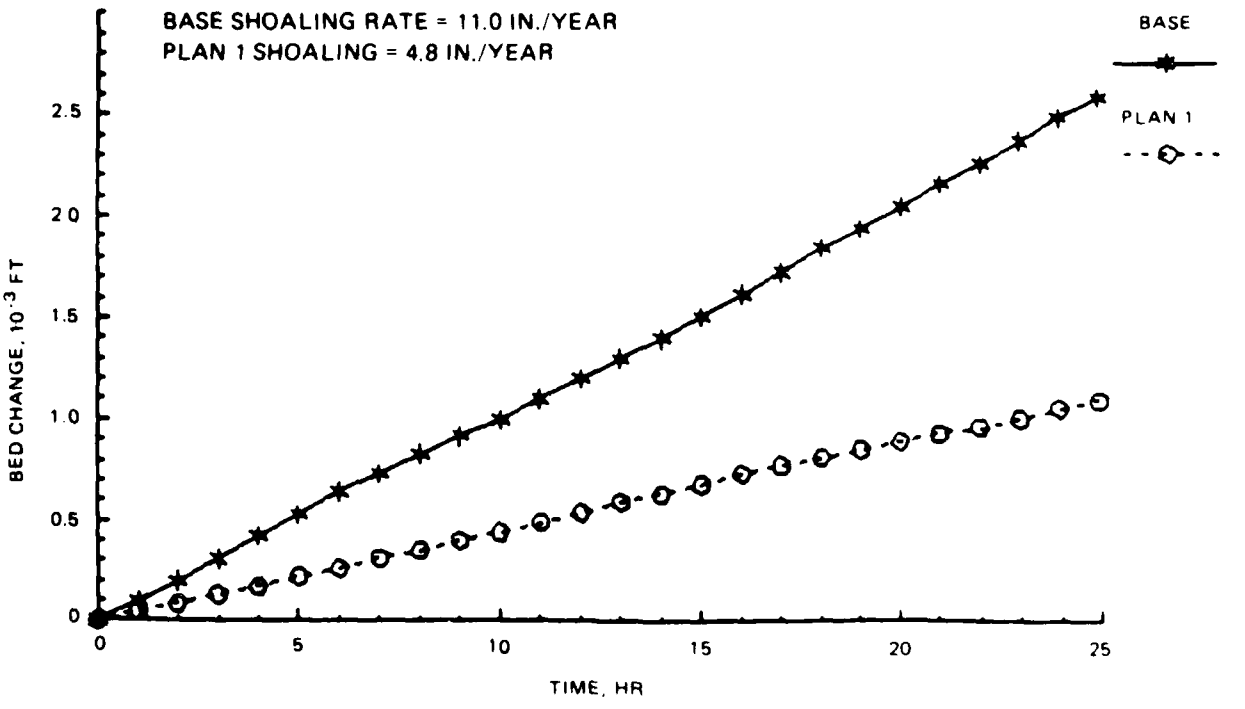

d. Cell 50

Figure 10. (Concluded)

from these graphs, Plan 1 decreased the shoaling rate at the harbor entrance and in the bay channel just east of the entrance. Just west of the entrance the shoaling stayed about the same, and in the Corpus Christi Turning Basin, shoaling rates increased.

47. The major difference Plan 1 made in the velocities was in the top half of the channel (since most of the discharges and withdrawals were at the surface). Base and Plan 1 surface velocities for sta A and D are shown in Figure 11. The flood predominance observed near the bottom at stations near the entrance in the base conditions was not affected. In the eastern end of the harbor and in the bay channel, the surface velocities became more ebb-dominated as seen in Figure 11a. Therefore, less sediment was drawn into the channel and shoaling decreased. However, in the western half of the first turning basin and further into the harbor, the surface velocities shifted more in the flood direction (see sta D, Figure 11b). The removal of the large surface withdrawal resulted in a reduction of vertical velocities, causing particle settling velocities to become less impeded. Slightly more sediment was allowed to deposit, leading to the small increase in shoaling observed in that area. From the western end of the turning basin to the breakwaters, the net change was a decrease in total shoaling volume of approximately 20 percent.

Plan 2 Results

48. Channel bottom elevations in the LAEMSED grid were deepened by 6 ft to reflect the result of advance maintenance dredging. Figures 12 and 13 show the resulting change in shoaling rates at cells located at the area of interest. Throughout the entrance and turning basin, shoaling rates increased slightly. The maximum increase observed was almost 1 in. per year, and this was in the turning basin. However, the bay channel east of the entrance, where base shoaling rates were the highest, experienced the smallest amount of increase (about 0.1 in. per year). An increase of less than 1 in. per year in an area where the base condition shoaling rates are already 9 in. per year may be small enough to make this plan economically attractive, and an economic analysis is appropriate. If the cost reduction can be obtained, the money saved could be used to revise disposal operations, as discussed later.

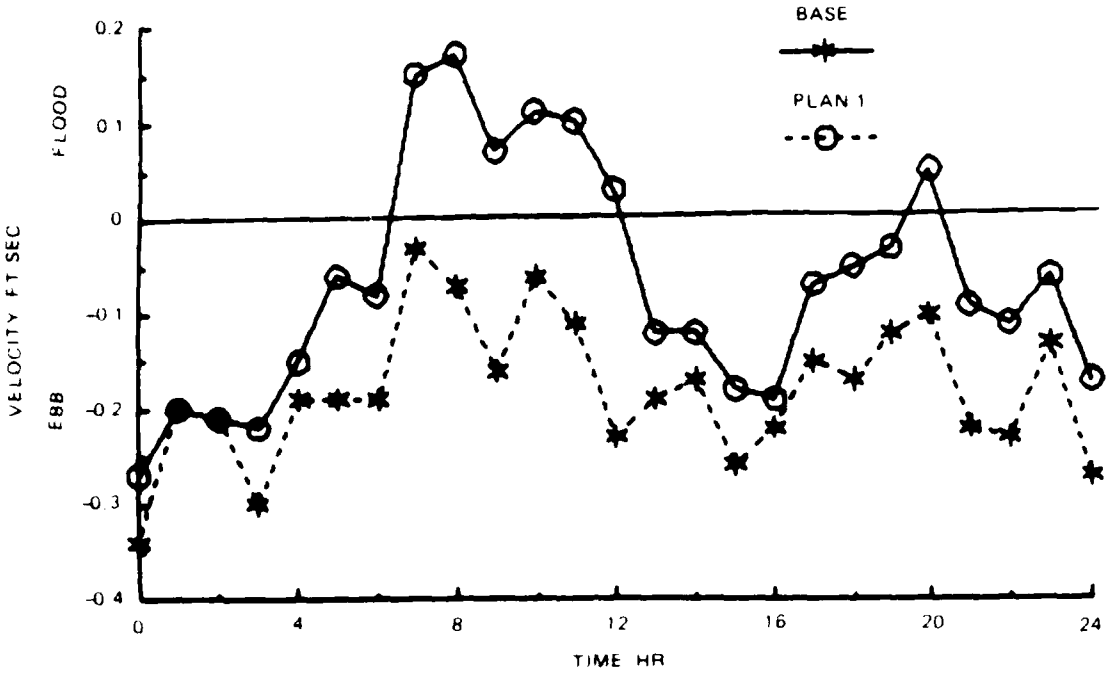

a. Sta A

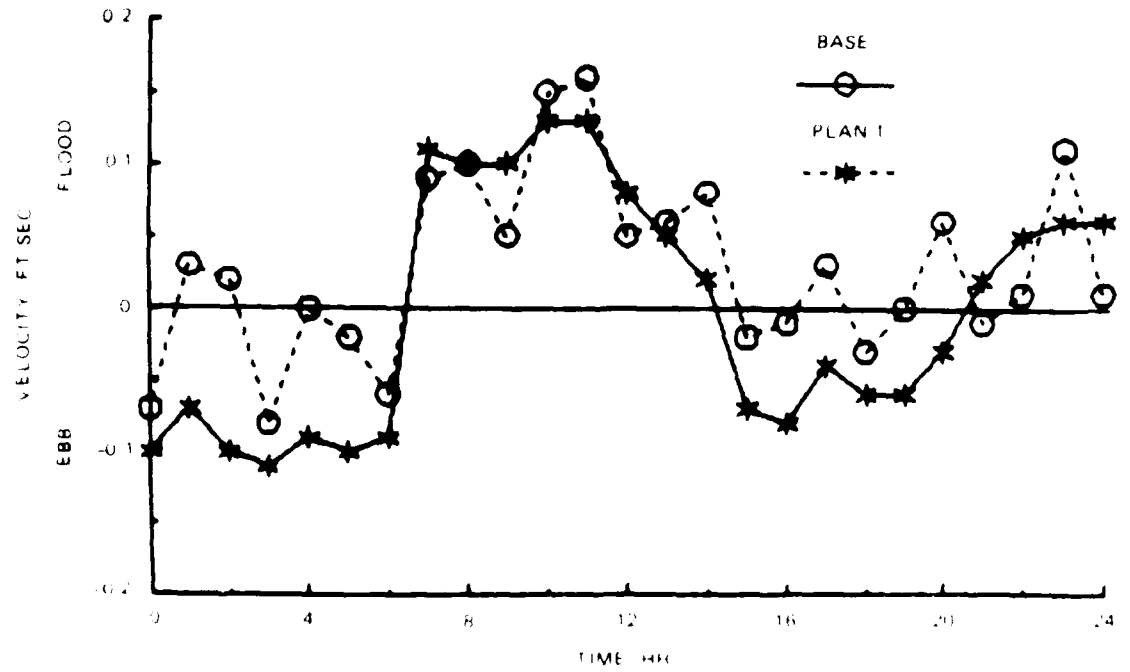

b. Sta D

Figure 11. Base and Plan 1 surface velocities from IAEMSED

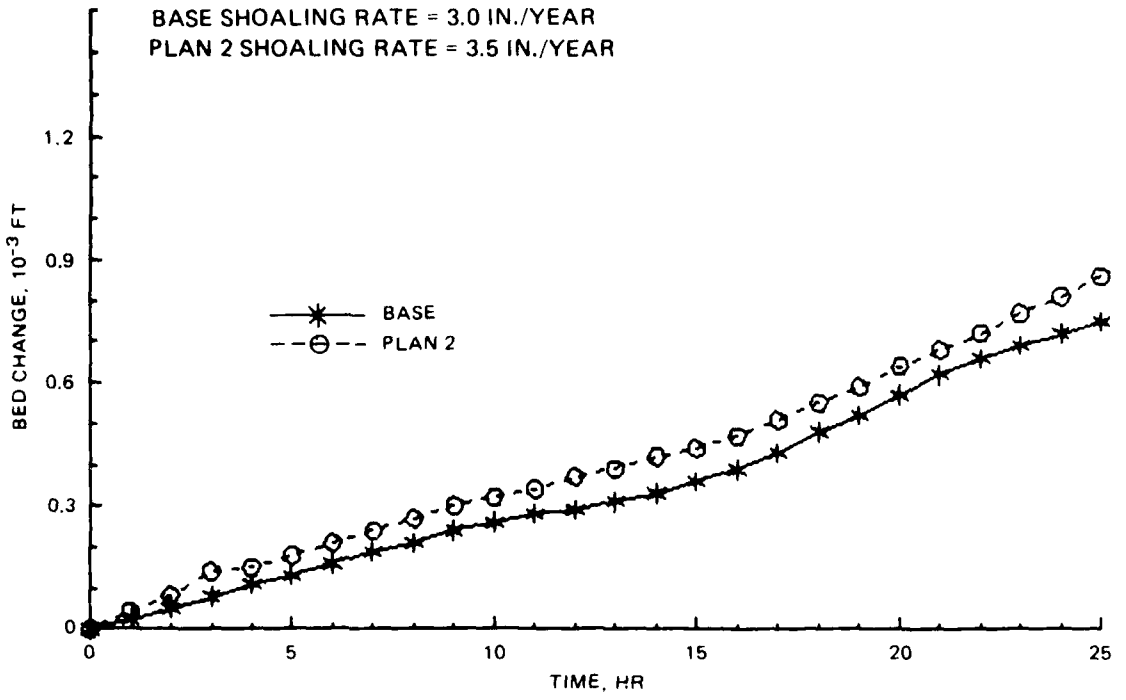

a. Cell 47

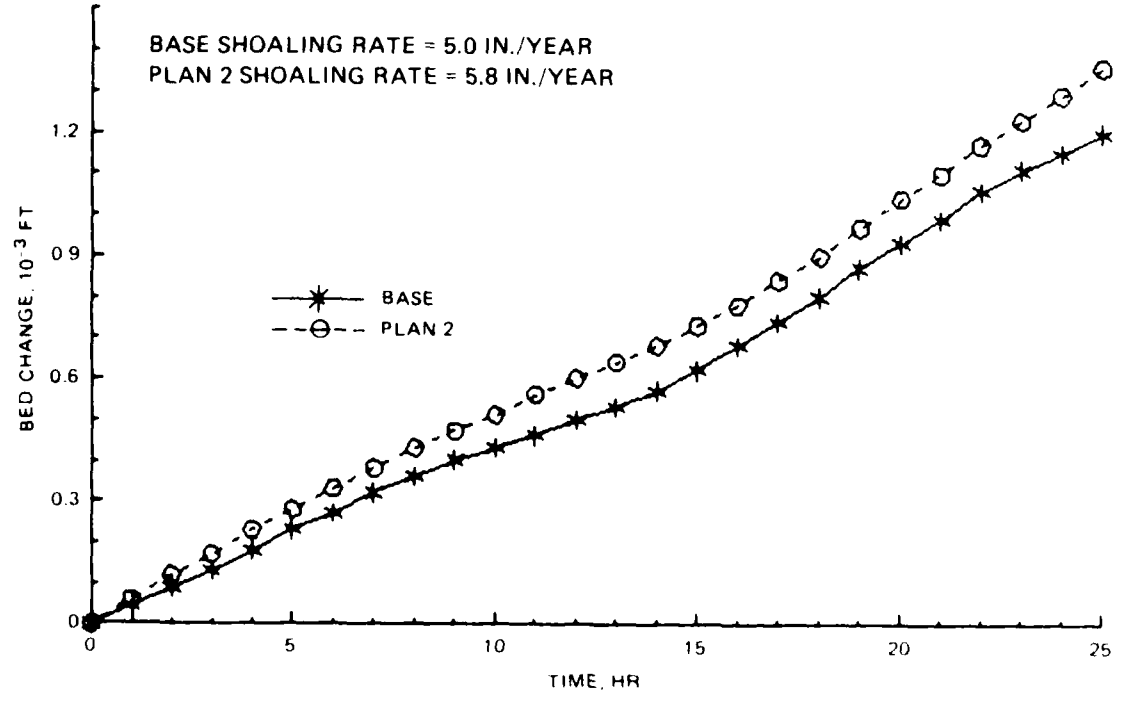

b. Cell 48

Figure 12. LAEMSED sedimentation results, base to Plan 2

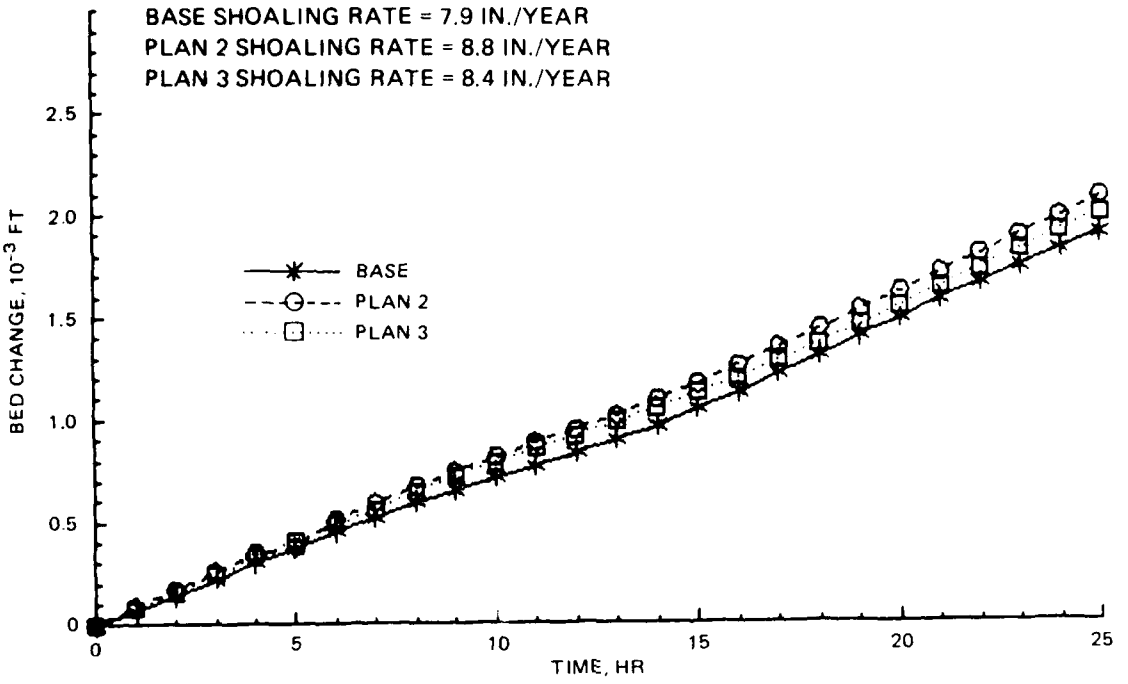

a. Cell 49

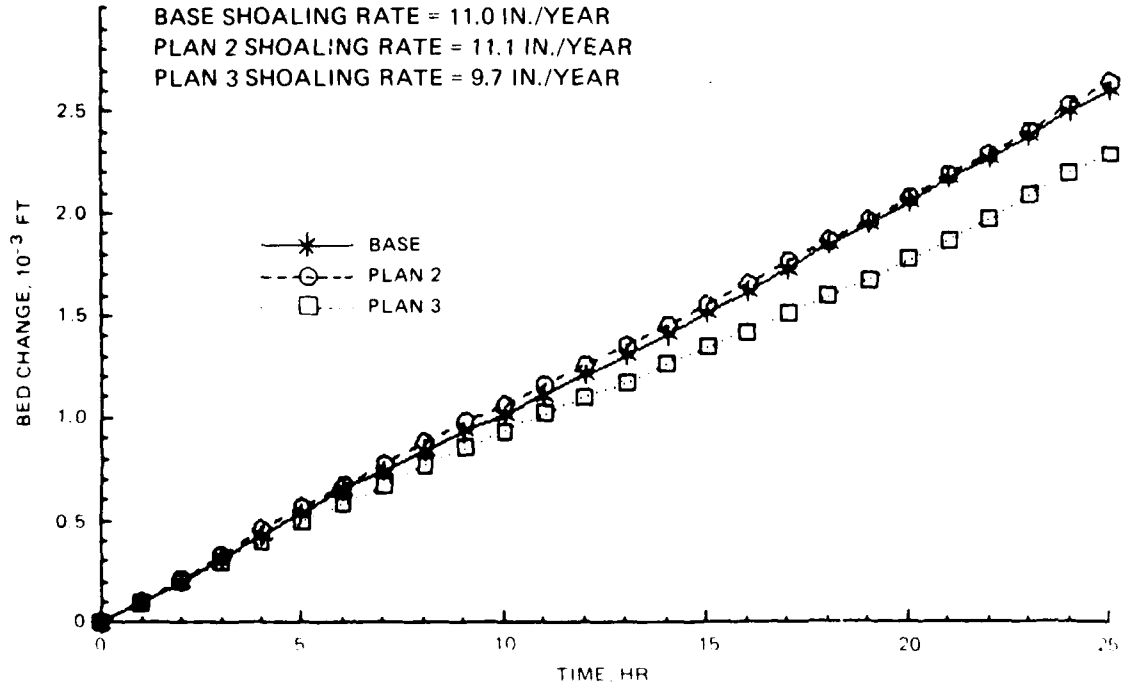

b. Cell 50

Figure 13. LAEMSED sedimentation results, base to Plan 2 and Plan 3

Plan 3 Results

49. In an attempt to offset the increased shoaling experienced in the Plan 2 test, a 3-ft-high sill was added in conjunction with the advance maintenance. The sill was added at the channel bottom just west of the entrance (cell 51). Since the sill was added in combination with advance maintenance dredging, a 50-ft controlling depth at mean low water was maintained. The resulting shoaling rates at cells 49 and 50 are shown in Figure 13. Just east of the sill, shoaling decreased from the Plan 2 alternative by almost 1.5 in. per year. Beyond this point further into the harbor, the effect became negligible.

Plan 4 Results

50. Results from RMA-2V showed that currents generally flowed from the existing disposal areas into the channel. Figure 14 shows peak ebb and flood velocities in the northwestern section of the bay. STUDH was used to observe the movement of sediment which was allowed to erode from the existing disposal areas as described in paragraph 30. The mass of eroded material flowing into the channel area from the disposal area was calculated by multiplying flow by sediment concentration at each time-step. The average flux of sediment into the channel was 35,000 kg/hr. Since LAEMSED results showed that much of the material entering the bay channel is pulled into the inner harbor, a means of reducing the amount of material entering the channel is needed. Based on observations of the circulation patterns and field sediment data, a probable solution seemed to be to relocate the disposal sites to the north of the channel at the same distance from the channel (2,000 ft). The finite element mesh was revised to reflect the new disposal areas in the model. The same sediment characteristics used in the base test were assigned to the plan disposal areas and a one-tidal-cycle simulation was made. Figure 15 shows base and plan disposal site locations. A graph of suspended sediment concentrations in the channel at sta R1 (shown in Figure 15) for base and Plan 4 conditions is shown in Figure 16. The concentrations computed in the Plan 4 simulation reached almost the same level as they did in the base during the ebb phase of the tide. Close inspection of the velocities in Figure 14 show that during ebb, the direction of flow is slightly toward the channel in the vicinity of the

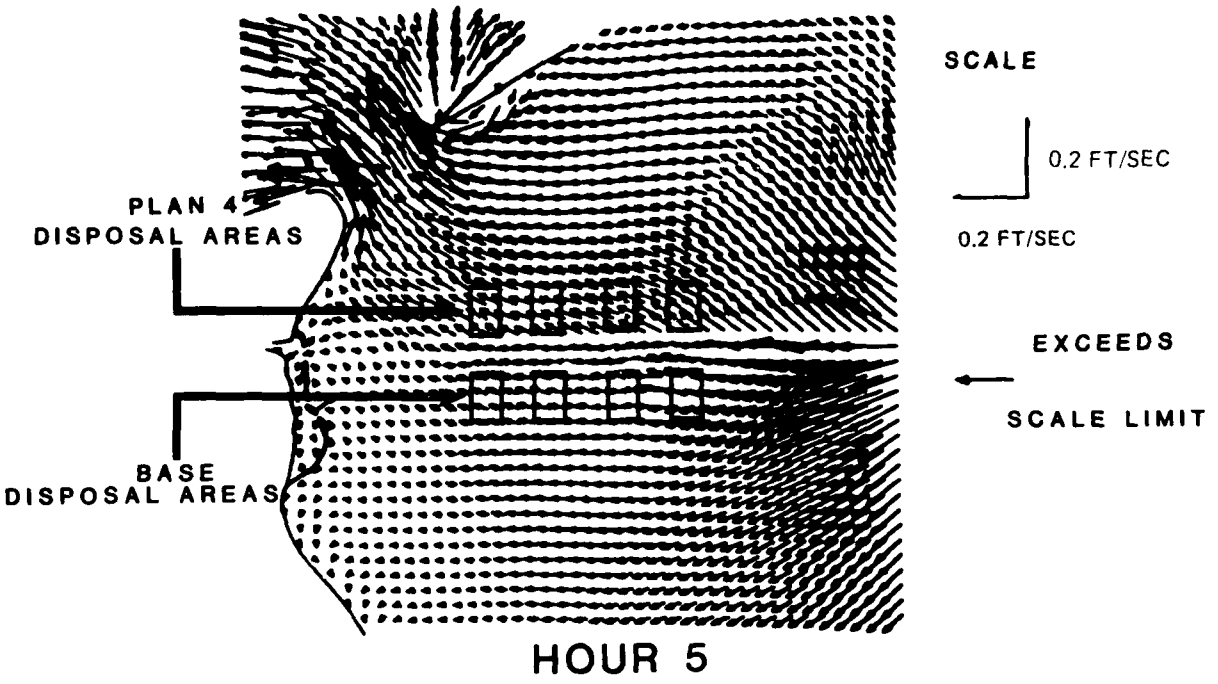

a. Peak flood velocities

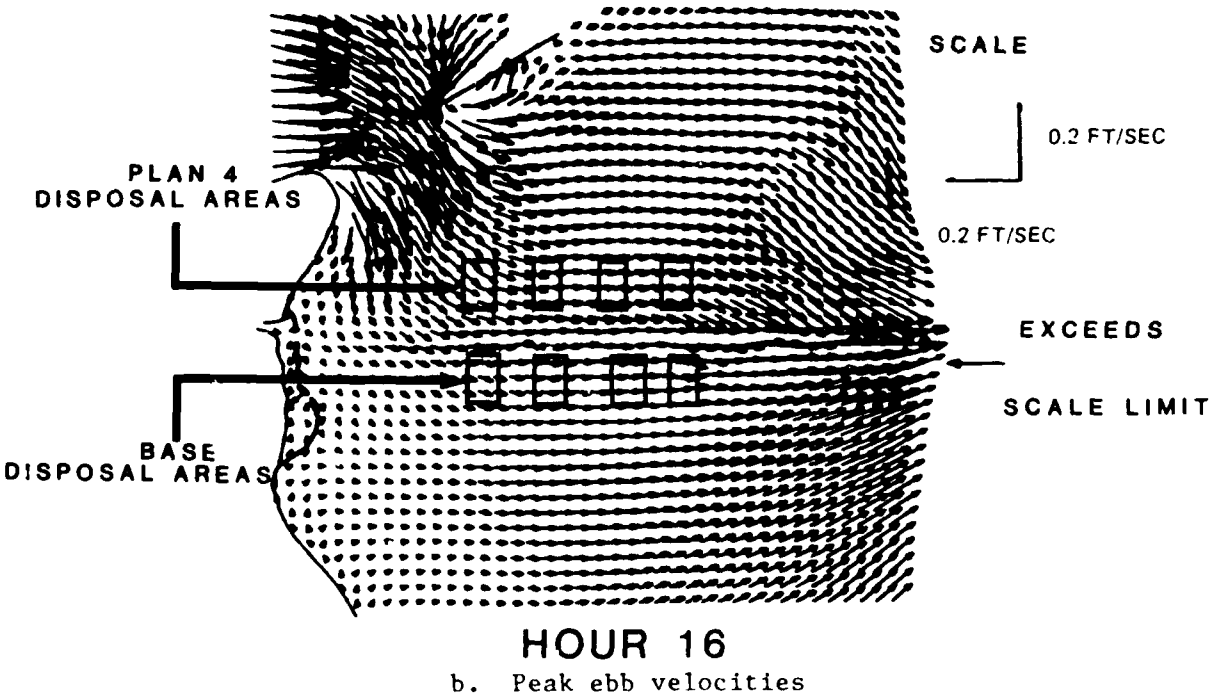

b. Peak ebb velocities

Figure 14. Flood and ebb velocities near base and Plan 4 disposal areas

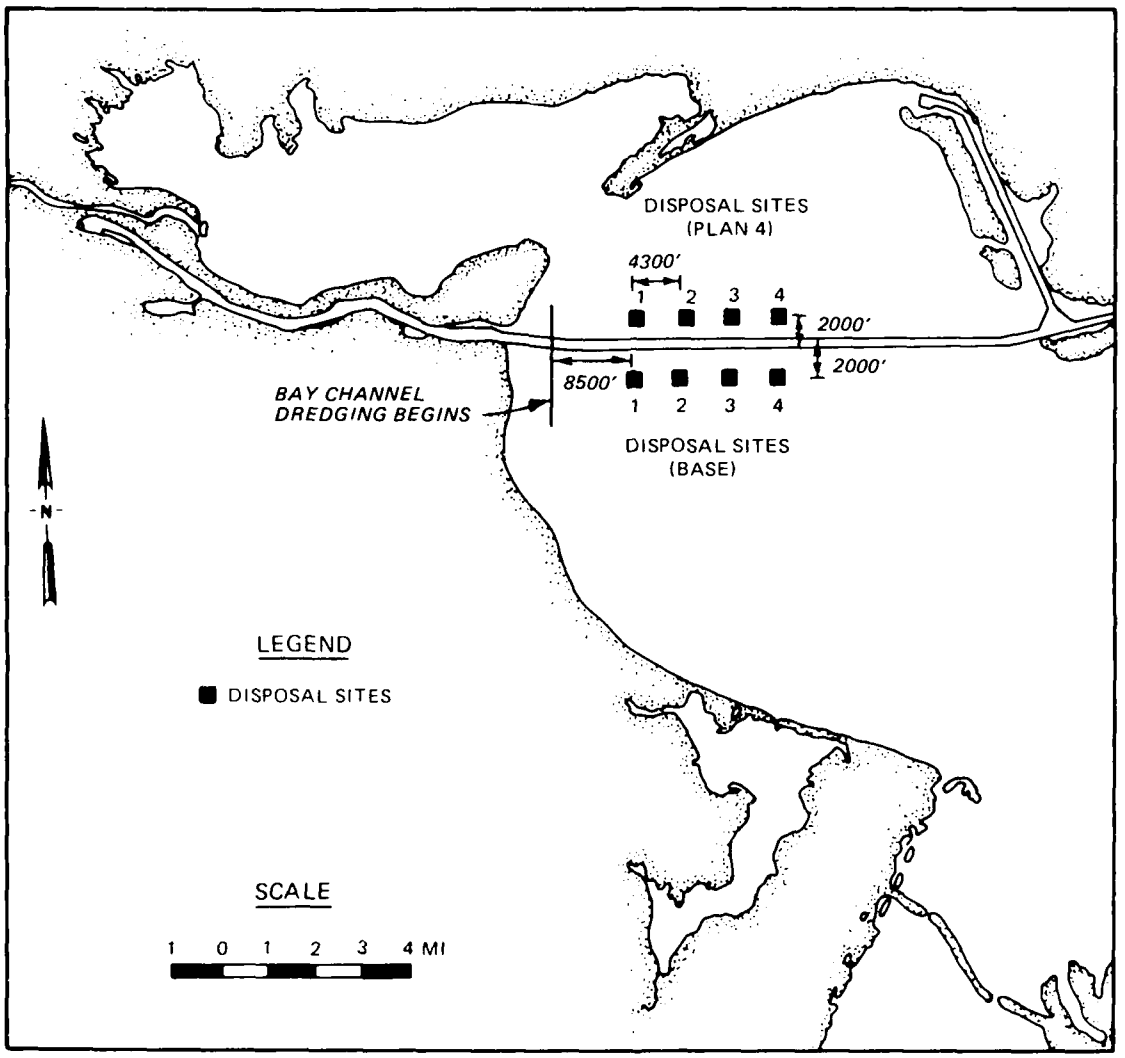

Figure 15. Base and Plan 4 disposal site locations

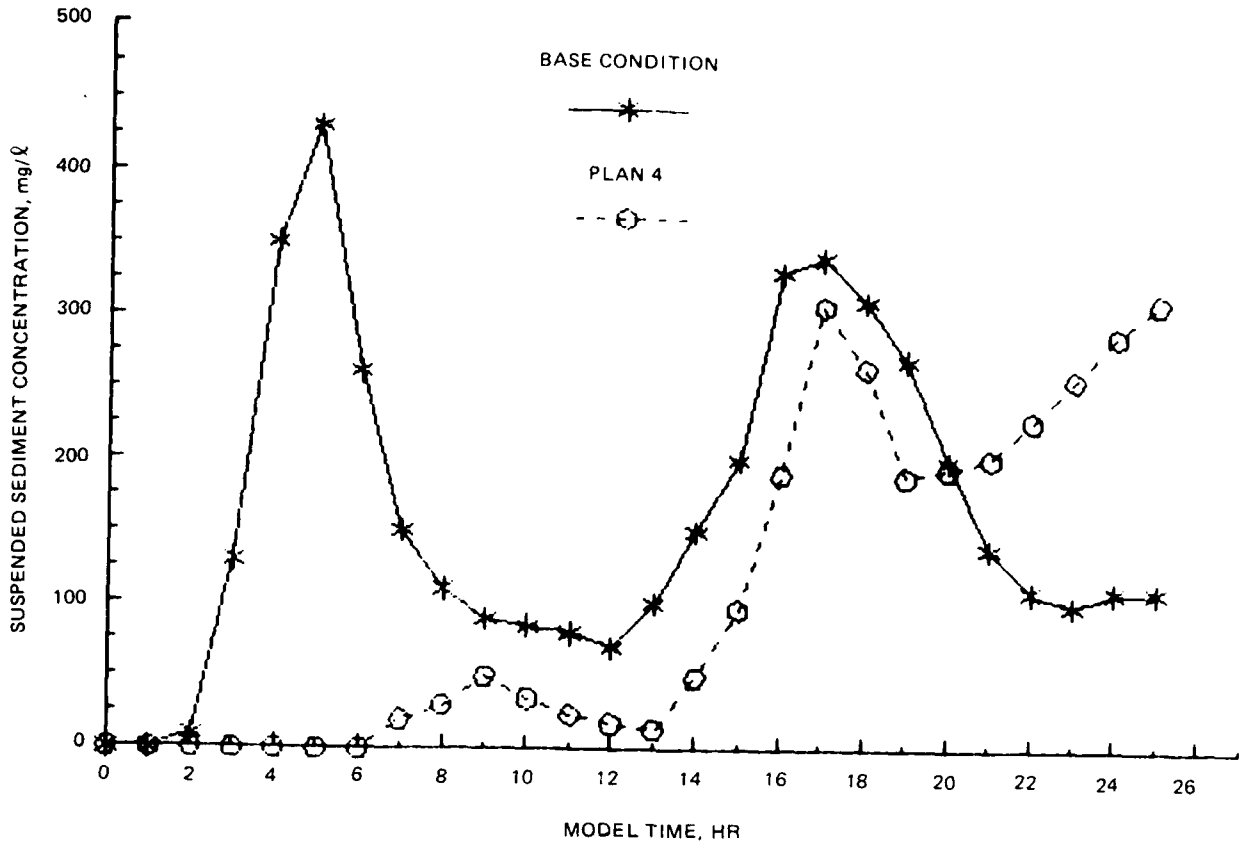

Figure 16. Sedimentation results, base to Plan 4, sta R1

plan disposal areas. Also, velocities are slightly larger north of the channel so more material is eroded. Therefore, there was not a significant decrease (less than 5 percent) in the amount of sediment flowing into the channel.

Plan 5 Results

51. Due to the results of the Plan 4 tests, it was decided to relocate the plan disposal areas further north for additional tests. The Plan 5 disposal sites are shown in Figure 17. Sites further north were chosen because RMA-2V results showed flow in this area to be almost always either parallel to or away from the channel. Their distance from the channel was limited to 6,000 ft for dredging cost purposes. Figure 18 shows Plan 5 disposal sites with RMA-2V velocity fields. As can be seen, the current velocities at the most western site (site 1) are much higher than at the other three sites due to the influence of the Nueces Bay tidal prism. A 6-hr STUDH simulation

showed that erosion of Plan 5 disposal site 1 was almost twice as much as that of any of the other base or plan sites. This created large suspended sediment concentrations which, even before the ebb phase of the tide, had begun to enter the channel as a result of diffusion. Therefore, Plan 5 was revised so that no material was placed in site 1 and more material was placed in sites 2-4. This was then labeled as Plan 5b. A 25-hr STUDH test allowing erosion of the Plan 5b disposal areas was conducted. Model concentrations at sta R1 after 25 hr were negligible. Figure 19 shows STUDH base and Plan 5b concentrations along the channel at hour 25. There was a resulting decrease of 75 percent sediment mass flux into the channel.

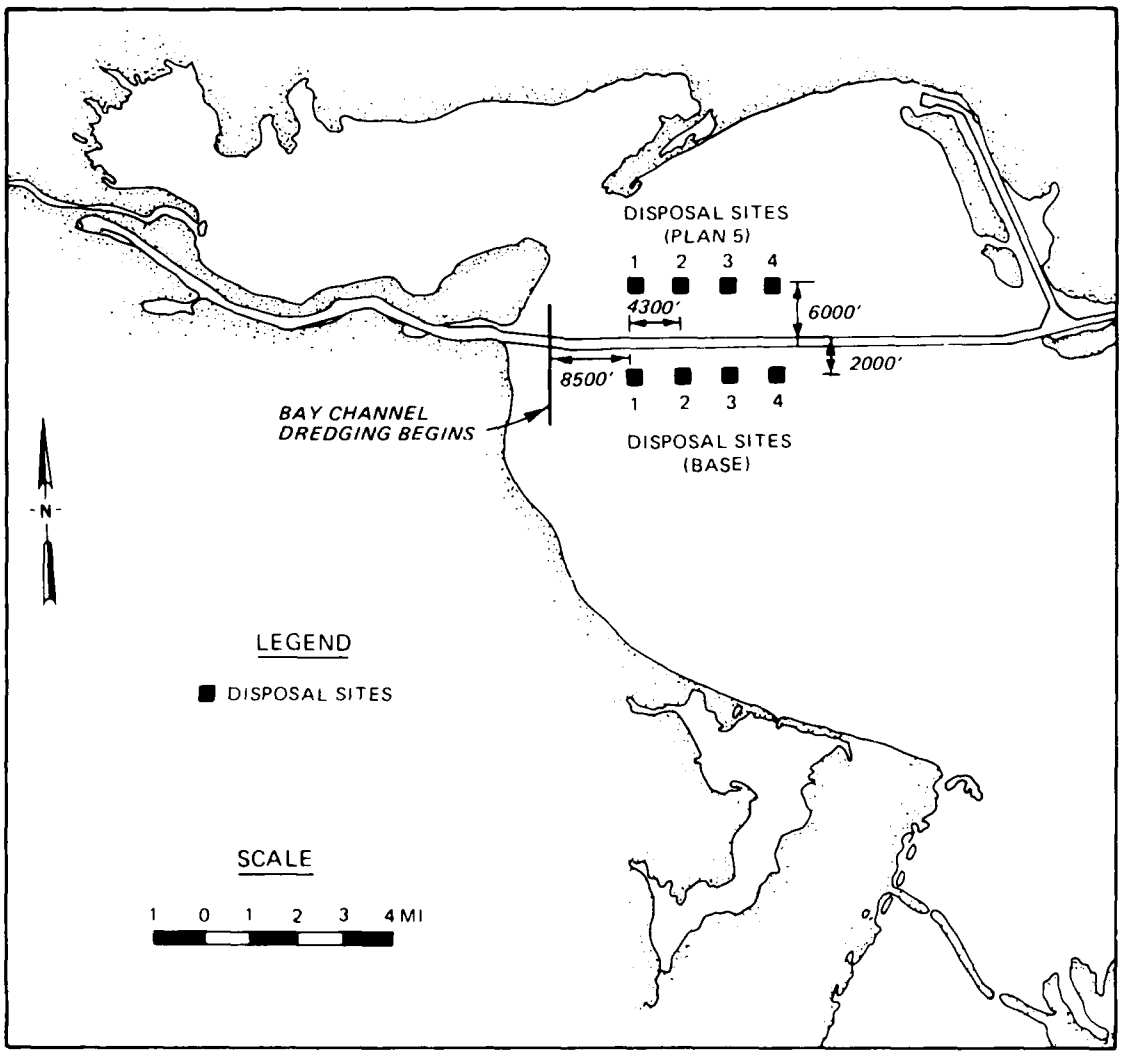

Figure 17. Base and Plan 5 disposal site locations

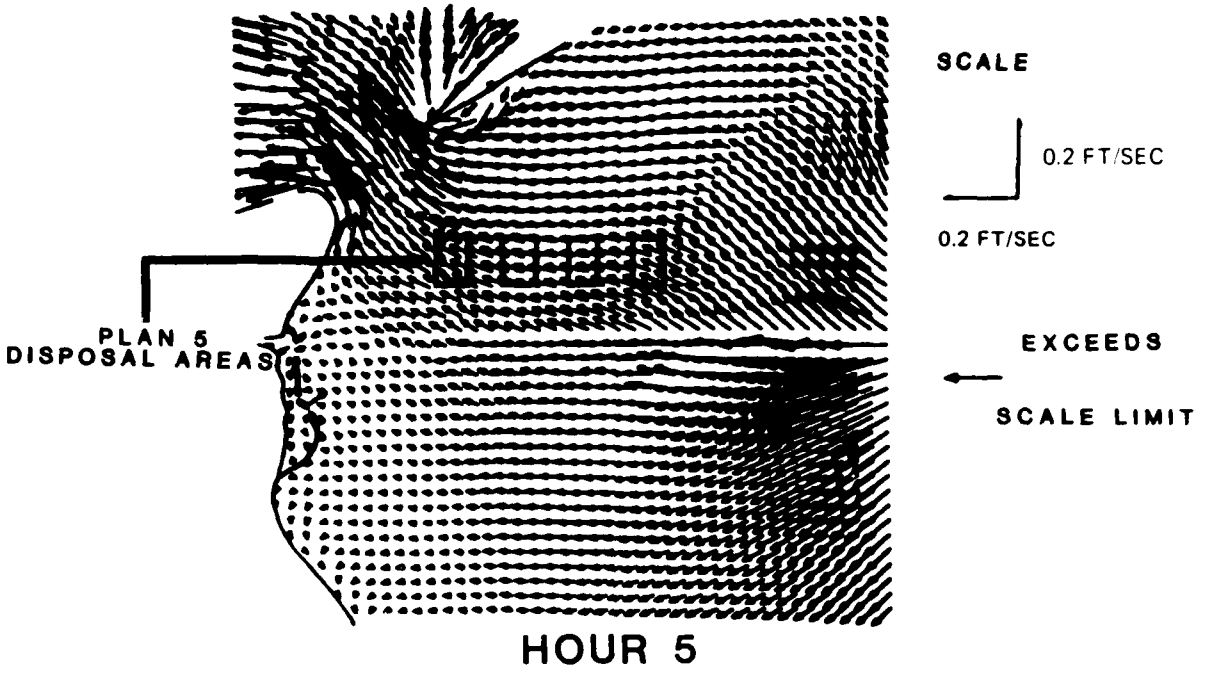

a. Peak flood velocities

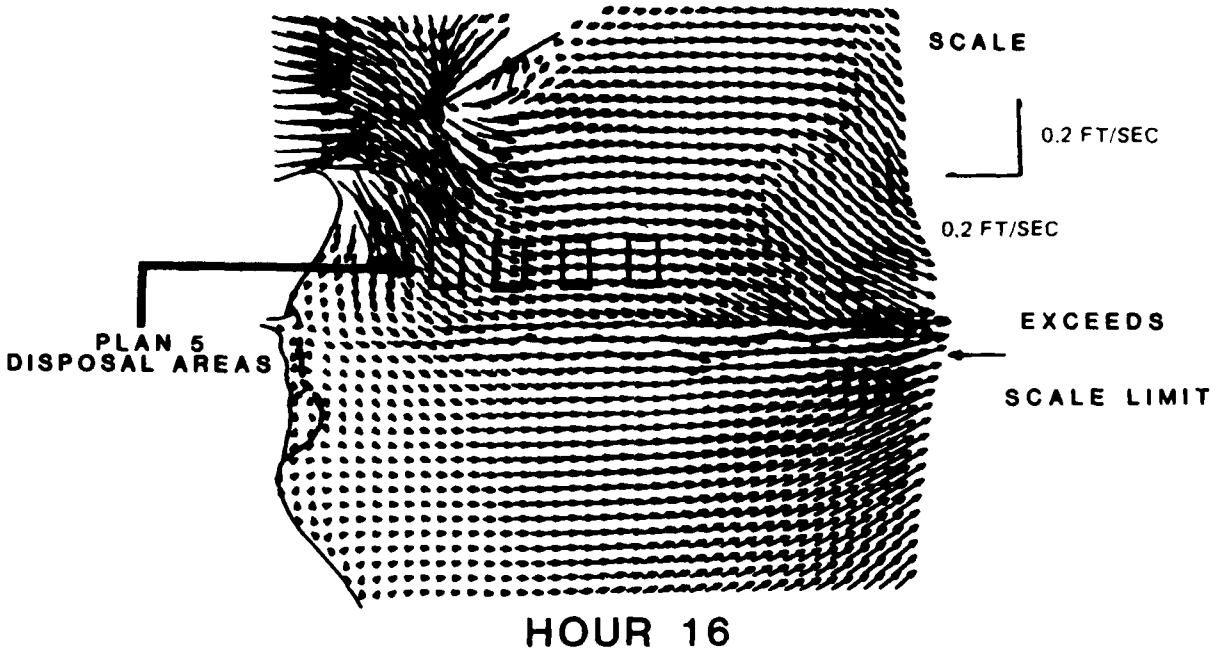

b. Peak ebb velocities

Figure 18. Flood and ebb velocities with Plan 5 disposal sites

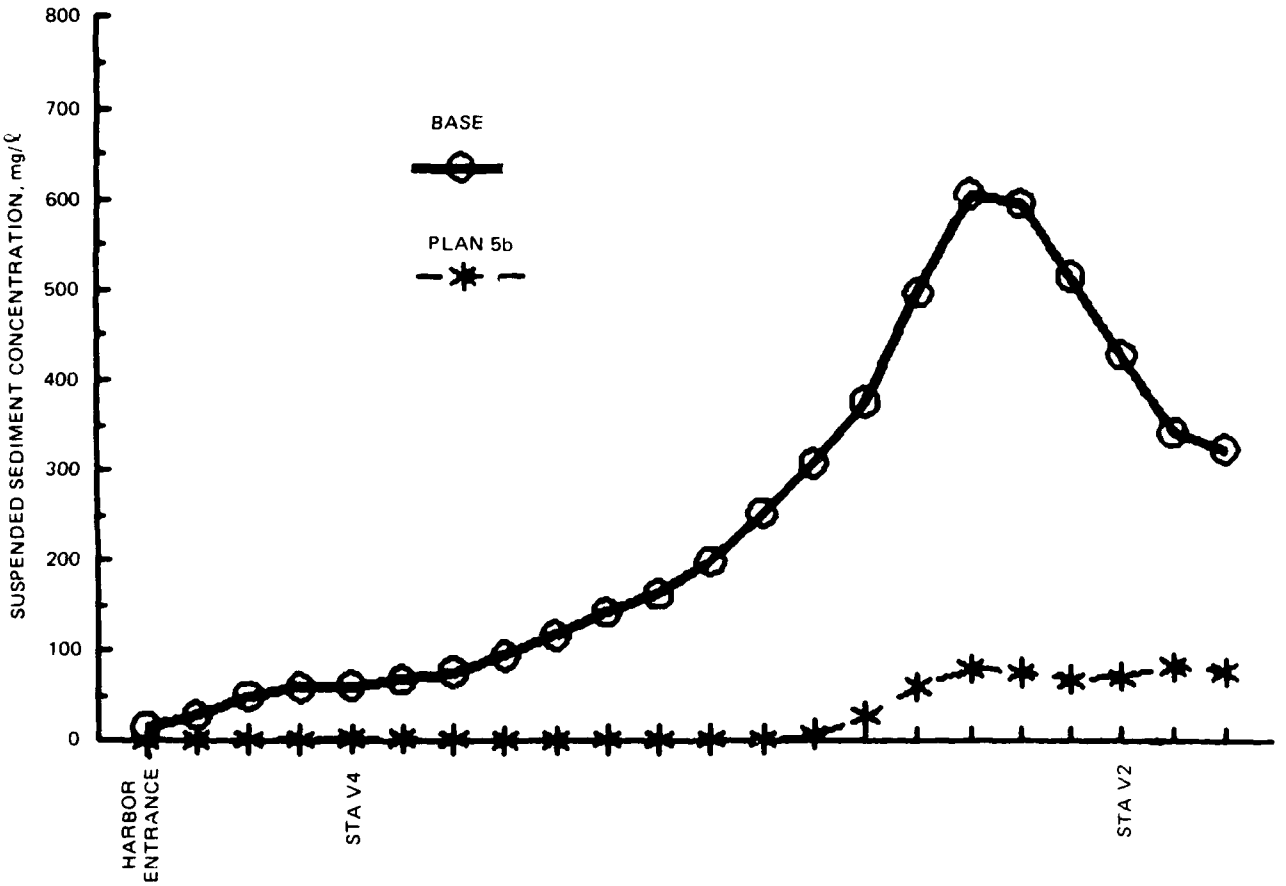

Figure 19. Sedimentation results, base to Plan 5b

PART VII: CONCLUSIONS AND RECOMMENDATIONS

52. Analysis of pre- and post-dredging surveys indicate that annual shoaling rates in the inner harbor area have been between 0.7-2.0 ft during 1978 to 1984.

53. Based on results from the LAEMSED numerical model, there would be about a 20 percent decrease in the shoaling rate associated with removal of the six major withdrawals and discharges in the harbor.

54. Advance maintenance of 6 ft during dredging in the harbor entrance and Corpus Christi Turning Basin would increase shoaling rates by a maximum of about 1 in. per year. In the areas with the greatest shoaling rate, no increase in shoaling was observed; therefore, advance maintenance would lessen the required dredging frequency. An addition of a sill in combination with advance maintenance did not decrease sedimentation in the inner harbor by a significant amount.

55. Results from the Phase I reconnaissance survey and the Phase II data collection appear to indicate that a primary source of shoaling is the dredged material disposal sites south of the channel closest to the harbor entrance. Field data and the TABS-2 hydrodynamic model have shown that currents generally flow from the disposal areas toward the channel most of the time. Due to the apparently high erodibility of the dredged material, it does not remain at the disposal site, but flows back into the channel and is pulled into the harbor by net inflow currents along the bottom. A disposal monitoring program is necessary to determine the rates of erosion of the material at these sites. It is recommended that periodic surveys of the disposal sites be performed, especially following a dredging operation, to determine the rate of erosion and/or consolidation of the dredged material.

56. Tests using the TABS-2 models have shown that relocation of the disposal sites to 6,000 ft north of the channel and moving them slightly eastward reduces the amount of sediment entering the bay channel by 75 percent. All indications suggest that moving the disposal areas to north of the channel and limiting agitation of sediments (e.g., by shrimping activity) in the area will reduce the amount of material reentering the channel and thus entering the inner harbor.

57. Model results and field data analyses (Appendix A) suggest that the shoaling mechanism consists of the following processes: Bay sediments,

including resuspended dredged material, are resuspended and travel across the channel where they settle into the deeper water. Circulations in the channel, driven by tides, density currents (due to hypersaline water, sediment concentration, and possibly freshwater discharges), and harbor discharges and withdrawals draw sediment-laden water into the harbor, where the sediment deposits.

58. The model results indirectly suggest that one of the following untested remedies might reduce sedimentation in the harbor:

a. Protection of the dredged material disposal area from wave action and tidal currents by construction of sills along two sides.

b. Trapping of sediment by a dredged trap adjacent to the harbor channel.

c. Disruption of the density current by

(1) A physical barrier (flap or curtain).

(2) A water or bubble curtain.

d. Mechanical dredging instead of hydraulic dredging of harbor.

e. Modification of channel geometry at bridge to alter deposition patterns.

This evaluation does not consider the economics of such solutions, but poses them only as possible technical solutions.

59. Due to the limited time available to conduct the study, the impact of wind fields was not evaluated. Additional tests to evaluate the impact of various wind conditions on the alternative plans should be conducted during the detailed design of improvements.

REFERENCES

Ackers, P., and White, W. R. 1973 (Nov). "Sediment Transport: New Approach and Analysis," Journal, Hydraulics Division, American Society of Civil Engineers, No. HY11.

Ariathurai, R., MacArthur, R. A., and Krone, R. B. 1977 (Oct). "Mathematical Model of Estuarial Sediment Transport," Technical Report D-77-12, US Army Engineer Waterways Experiment Station, Vicksburg, Miss.

Bennett, A. S. 1976. "Conversion of In Situ Measurements of Conductivity to Salinity," Deep Sea Research, Vol 23, pp 157-165.

Committee on Tidal Hydraulics, Corps of Engineers, US Army. 1965. "Sedimentation Problems in Entrance of Turning Basin, Corpus Christi, Texas," Vicksburg, Miss.

Edinger, J. E., and Buchak, E. M. 1979. "A Hydrodynamic Two-Dimensional Reservoir Model: Development and Test Application to Sutton Reservoir, Elk River, West River," prepared for US Army Engineer Division, Ohio River, Cincinnati, Ohio.

_____. 1981 (Nov). "Estuarine Laterally Averaged Numerical Dynamics; The Development and Testing of Estuarine Boundary Conditions in the LARM Code," Miscellaneous Paper EL-81-9, US Army Engineer Waterways Experiment Station, Vicksburg, Miss.

Johnson, B. H., Boyd, M. B., and Keulegan, G. H. 1987 (Apr). "A Mathematical Study of the Impact on Salinity Intrusion of Deepening the Lower Mississippi River Navigation Channel," Technical Report HL-87-1, US Army Engineer Waterways Experiment Station, Vicksburg, Miss.

Johnson, B. H., Trawle, M. J., and Kee, P. "A Numerical Model Study of the Effect of Channel Deepening on Shoaling and Salinity Intrusion in the Savannah Estuary" (in preparation), US Army Engineer Waterways Experiment Station, Vicksburg, Miss.

Krone, R. B. 1962. "Flume Studies of Transport of Sediment in Estuarial Shoaling Processes," Final Report, Hydraulics Engineering Research Laboratory, University of California, Berkeley, Calif.

Norton, W. R., and King, I. P. 1977 (Feb). "Operating Instructions for the Computer Program RMA-2V," Resource Management Associates, Lafayette, Calif.

Nueces County Navigation Commission. 1979. "Port Book 1979-80," Corpus Christi, Tex.

Owen, M. W. 1970. "Properties of a Consolidating Mud," Report No. INT 83, Hydraulics Research Station, Wallingford, Berkshire, England.

Partheniades, E. 1962. "A Study of Erosion and Deposition of Cohesive Soils in Salt Water," Ph.D. Dissertation, University of California, Berkeley, Calif.

Schubel, J. R., Carter, H. H., Wilson, R. E., Wise, W. M., Heaton, N. G., and Gross, M. G. 1978 (Jul). "Field Investigations of the Nature, Degree, and Extent of Turbidity Generated by Open-Water Pipeline Disposal Operations," Technical Report D-78-30, US Army Engineer Waterways Experiment Station, Vicksburg, Miss.

Smith, T. M. "Field Data Collection at Corpus Christi Bay and Harbor" (in preparation), US Army Engineer Waterways Experiment Station, Vicksburg, Miss.

Swart, D. H. 1976 (Sep). "Coastal Sediment Transport, Computation of Longshore Transport," R968, Part 1, Delft Hydraulics Laboratory, The Netherlands.

Texas A&M Research Foundation. 1973. "A Field Investigation of the Hydraulics and Stability of Corpus Christi Water Exchange Pass, Texas," College Station, Tex.

Thomas, William A., and McAnally, William H., Jr. 1985a (Aug). "User's Manual for the Generalized Computer Program System: Open-Channel Flow and Sedimentation, TABS-2," Instruction Report HL-85-1, US Army Engineer Waterways Experiment Station, Vicksburg, Miss.

_____. 1985b (Aug). "User's Manual for the Generalized Computer Program System: Open-Channel Flow and Sedimentation, TABS-2; Appendix F, User Instructions for RMA-2V, a Two-Dimensional Model for Free-Surface Flows," Instruction Report HL-85-1, US Army Engineer Waterways Experiment Station, Vicksburg, Miss.

_____. 1985c (Aug). "User's Manual for the Generalized Computer Program System: Open-Channel Flow and Sedimentation, TABS-2; Appendix G, A User's Manual for the Generalized Computer Program, Sediment Transport in Unsteady, 2-Dimensional Flow, Horizontal Plane, STUDH," by William A. Thomas, William H. McAnally, Jr., and Stephen A. Adamec, Jr., Instruction Report HL-85-1, US Army Engineer Waterways Experiment Station, Vicksburg, Miss.

White, W. R., Milli, H., and Crabbe, A. D. 1975. "Sediment Transport Theories: An Appraisal of Available Methods," Report Int 119, Vols 1 and 2, Hydraulics Research Station, Wallingford, England.

Table 1

Cohesive Sedimentation Coefficients

Coefficient	STUDH	LAEMSED
Critical shear stress for deposition, N/sq m	0.0001	0.0001
Critical shear stress for particle erosion, N/sq m	0.0005	*
Dry weight density-freshly deposited layer, kg/cu m	*	400
Particle specific gravity	2.65	2.65
Particle settling velocity, m/sec	0.00015	0.00015
Effective diffusion, sq m/sec	15	*

* Not used.

Table 2

Industrial Activity Near Harbor Entrance

Industry	Amount mgd	Discharge or Withdrawal	Location on Figure 2
City of Corpus Christi (Municipal Waste) Discharge Point 1	4	Discharge	1
City of Corpus Christi Discharge Point 2	4	Discharge	2
Southwestern Refining	1	Discharge	3
American Chrome and Chemical	1	Discharge	4
Central Power and Light	450	Withdrawal	5
American Chrome and Chemical	4	Withdrawal	6

STATION TG1

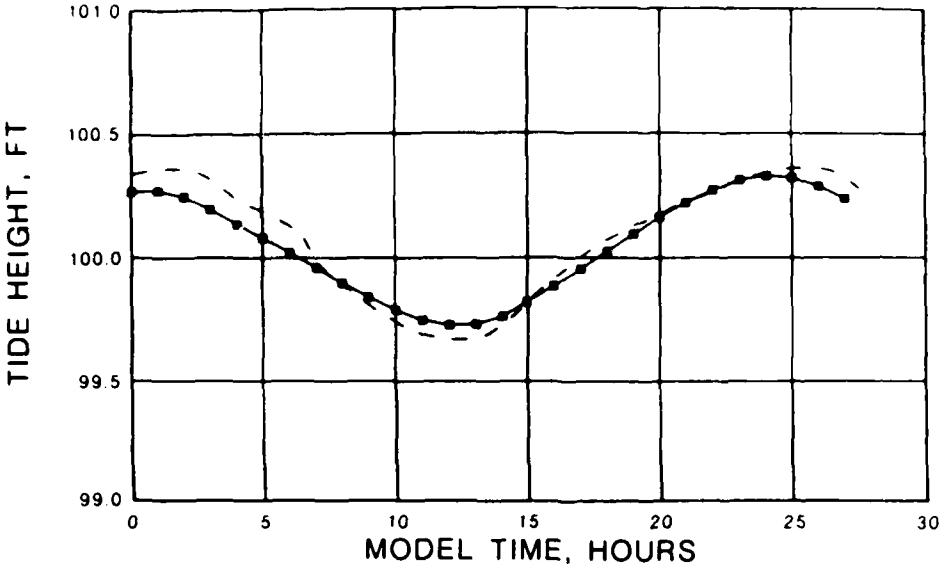

STATION TG2

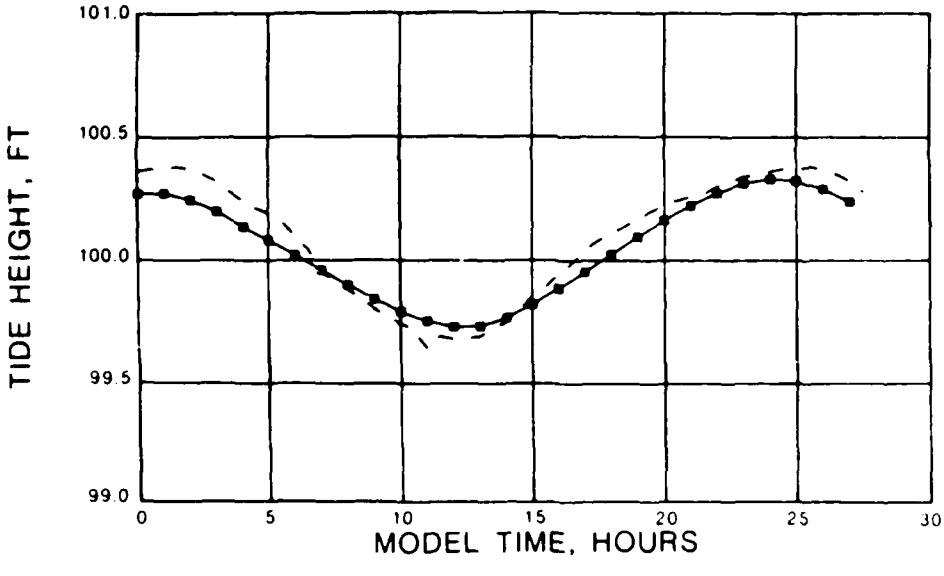

LEGEND

—●— MODEL

— – PROTOTYPE

RMA-2V VERIFICATION OF TIDAL HEIGHTS

15–16 JUNE 1985 **STATIONS TG1 AND TG2**

PLATE 1

STATION TG3

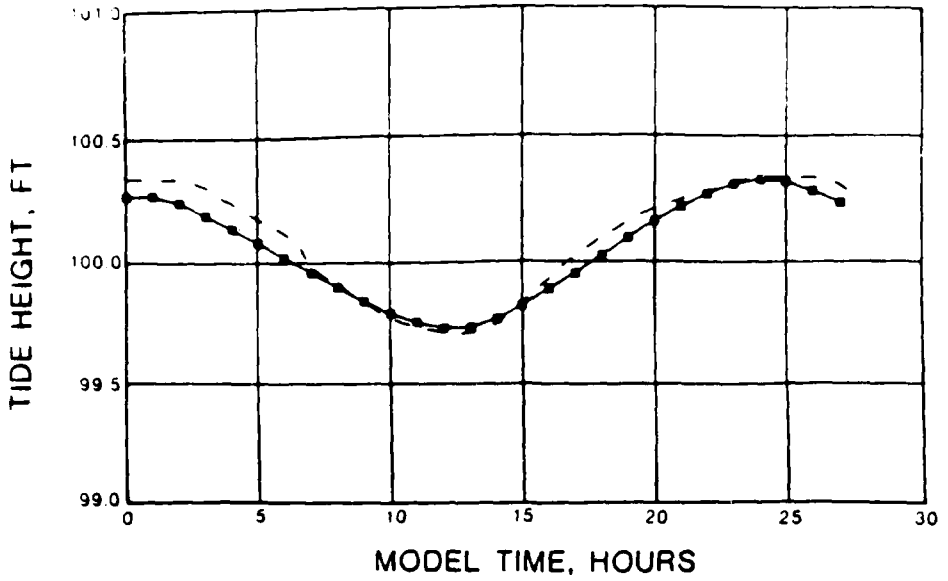

STATION TG4

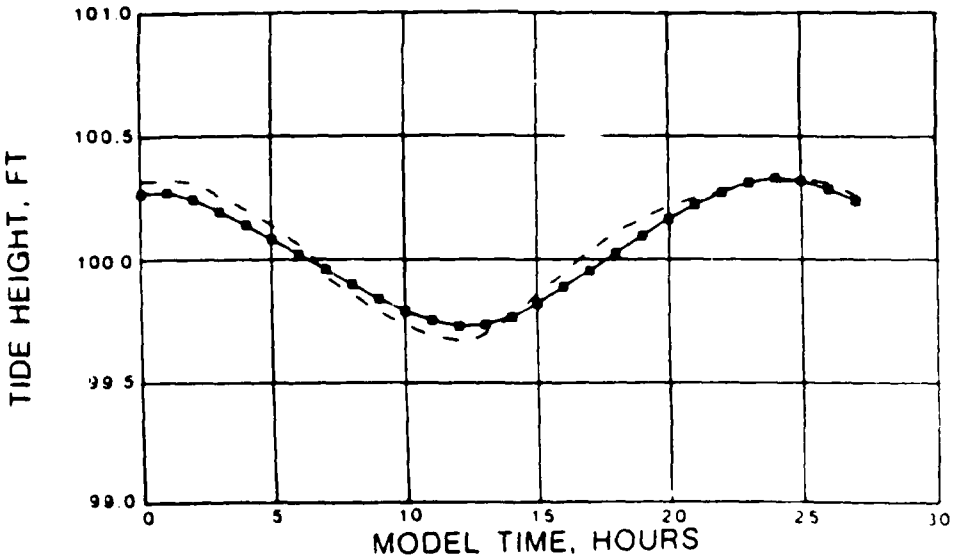

LEGEND

MODEL

PROTOTYPE

RMA-2V VERIFICATION OF TIDAL HEIGHTS

15-16 JUNE 1985 STATIONS TG3 AND TG4

PLATE 2

STATION TG5

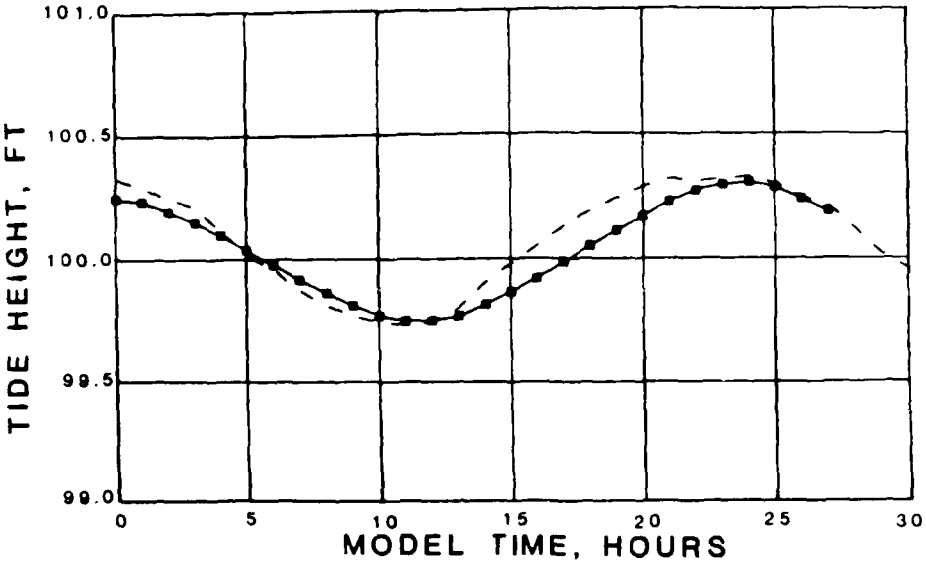

STATION TG6

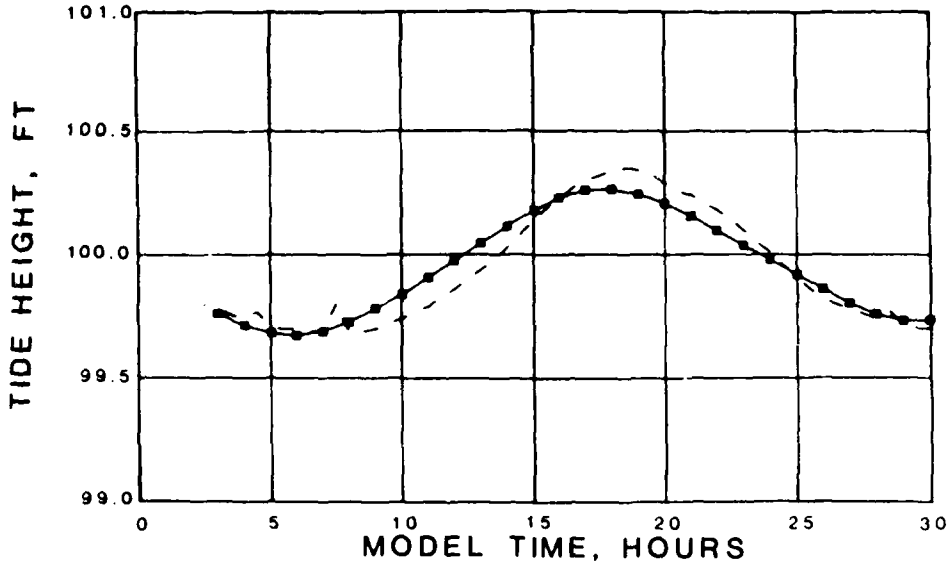

LEGEND

MODEL

PROTOTYPE

RMA-2V VERIFICATION OF TIDAL HEIGHTS

15-16 JUNE 1985 STATIONS TG5 AND TG6

PLATE 3

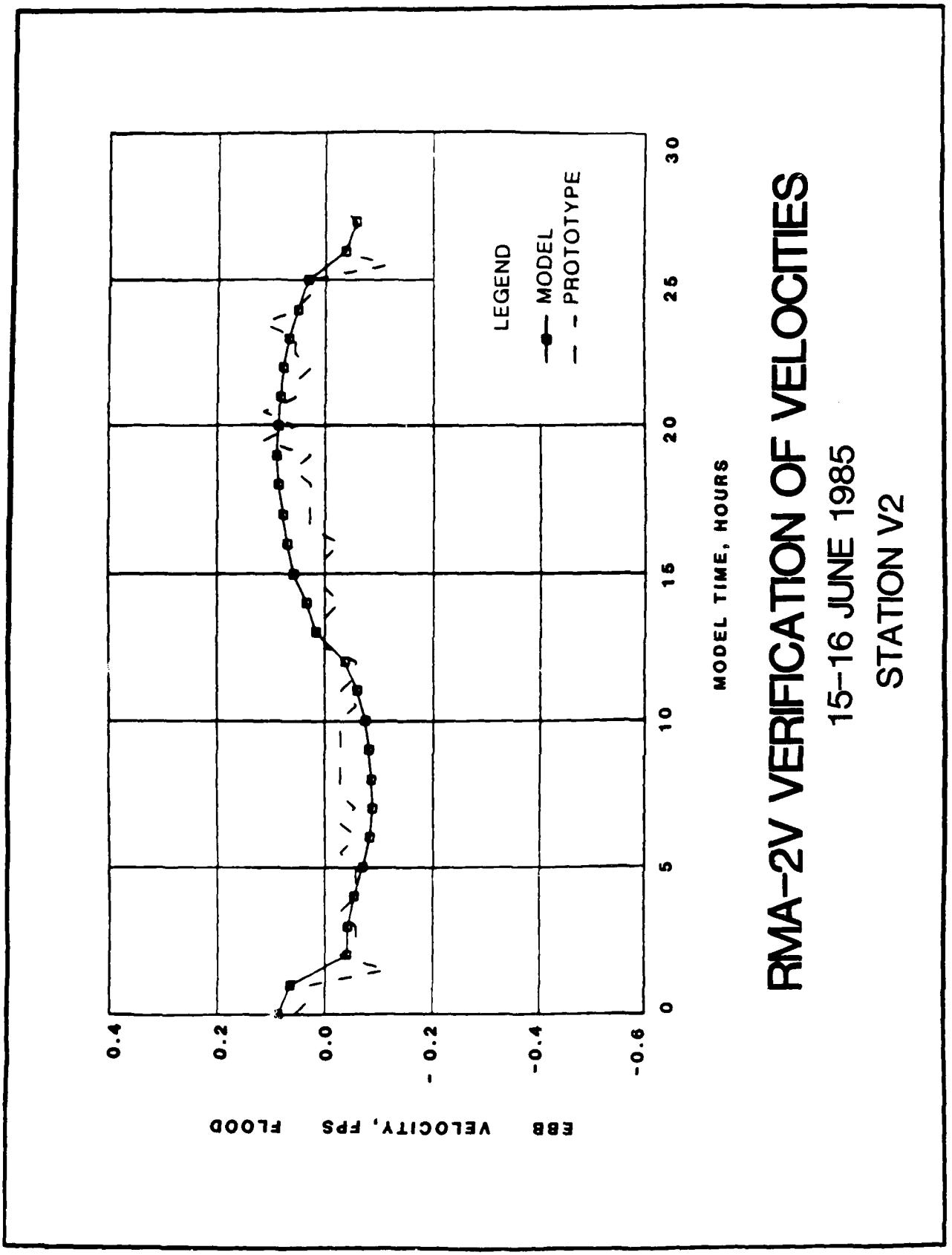
RMA-2V VERIFICATION OF VELOCITIES
15-16 JUNE 1985
STATION V2
LEGEND
MODEL
PROTOTYPE
MODEL TIME, HOURS
EBB VELOCITY, FPS FLOOD
0.4
0.2
0.0
- 0.2
-0.4
-0.6
0
5
10
15
20
25
30

PLATE 4

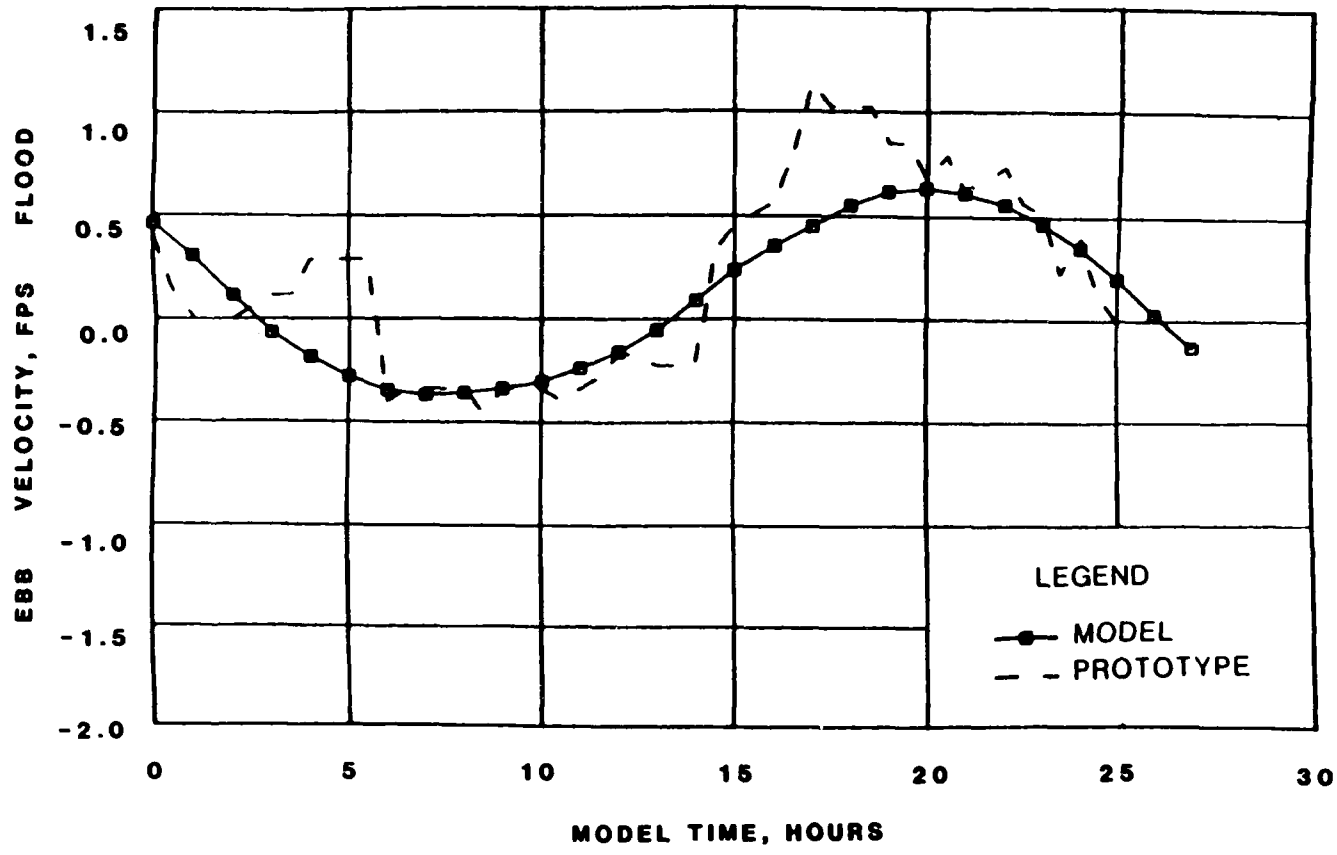

RMA-2V VERIFICATION OF VELOCITIES

15-16 JUNE 1985

STATION V3

PLATE 5

PLATE 6

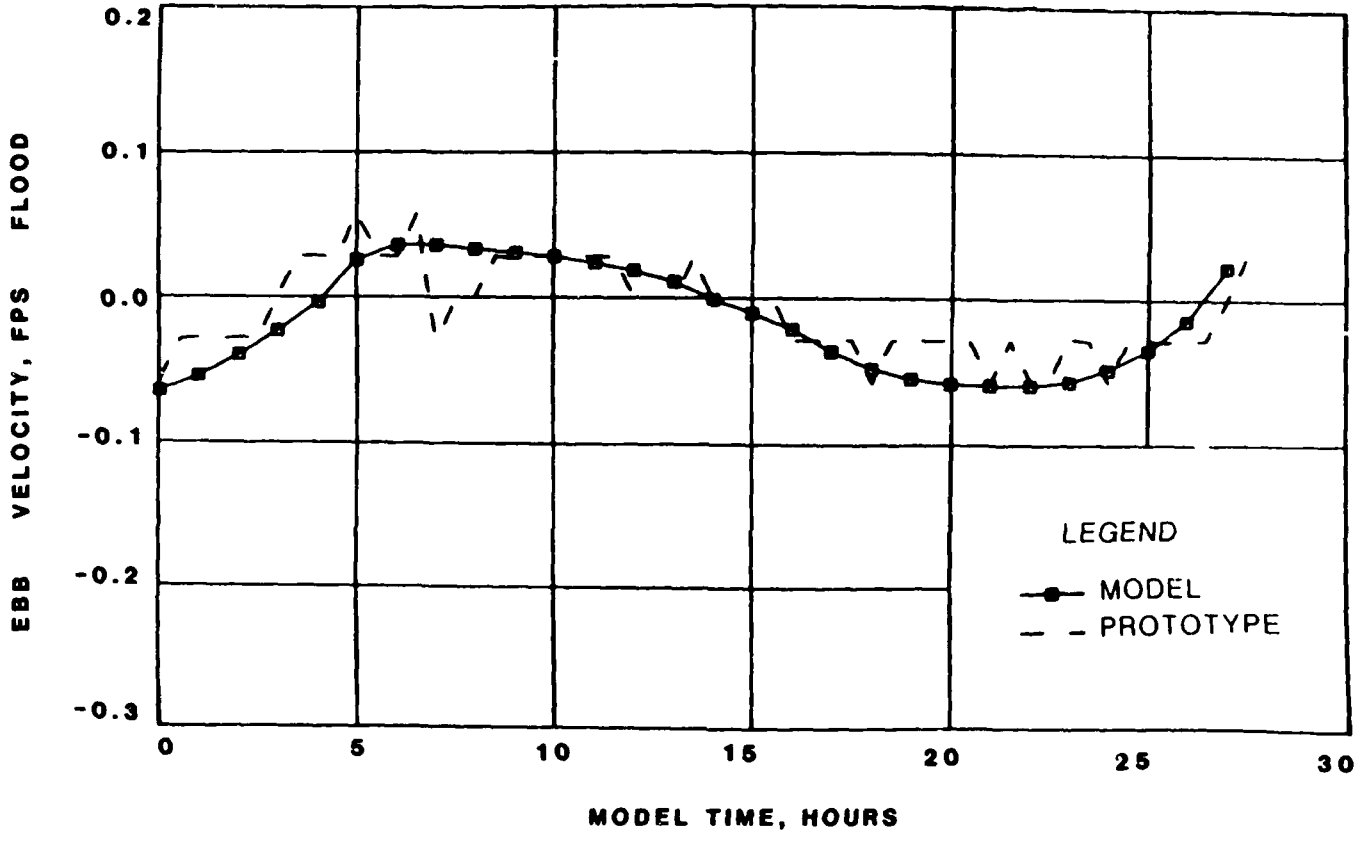

RMA-2V VERIFICATION OF VELOCITIES

15-16 JUNE 1985

STATION V4

STATION TG1

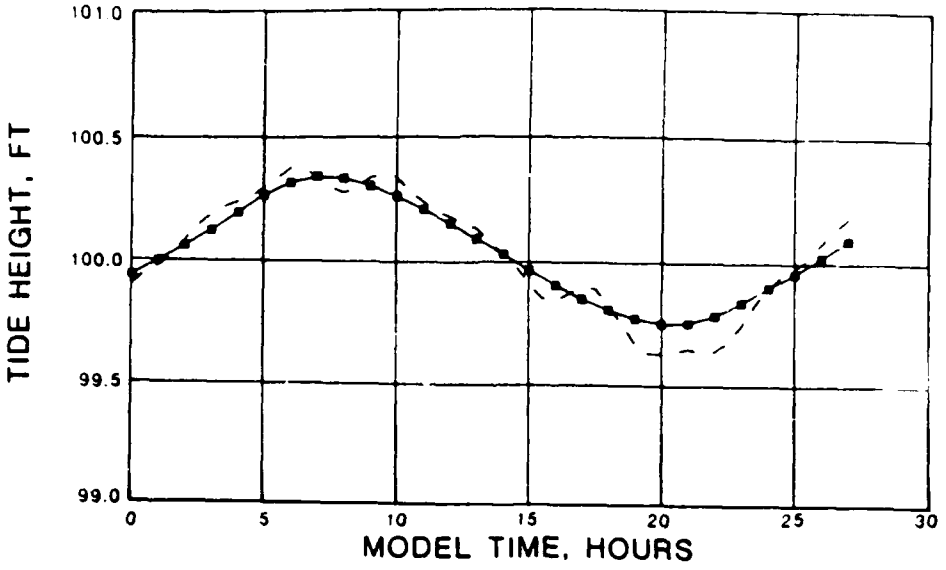

STATION TG2

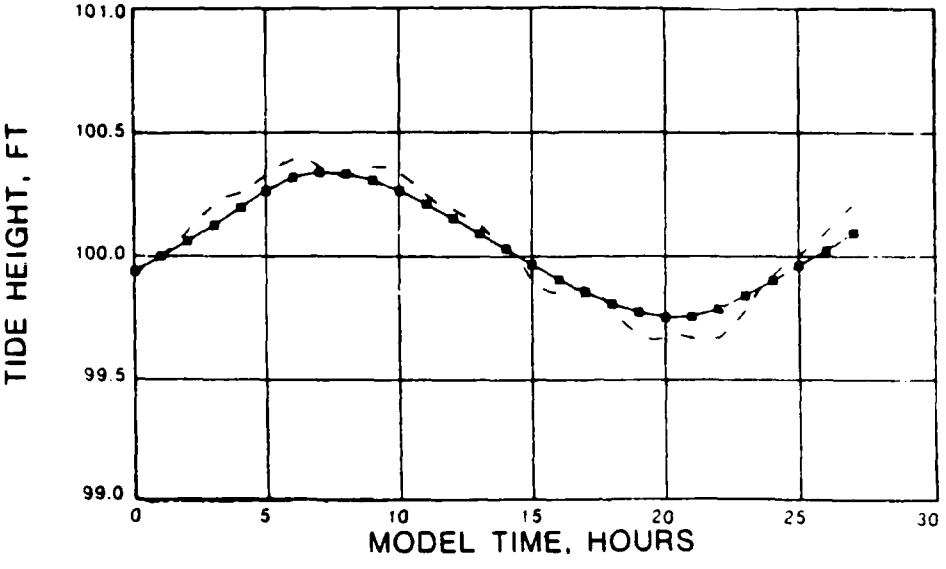

LEGEND

MODEL

PROTOTYPE

RMA-2V TIDAL HEIGHTS

17-18 JUNE 1985 STATIONS TG1 AND TG2

PLATE 7

STATION TG3

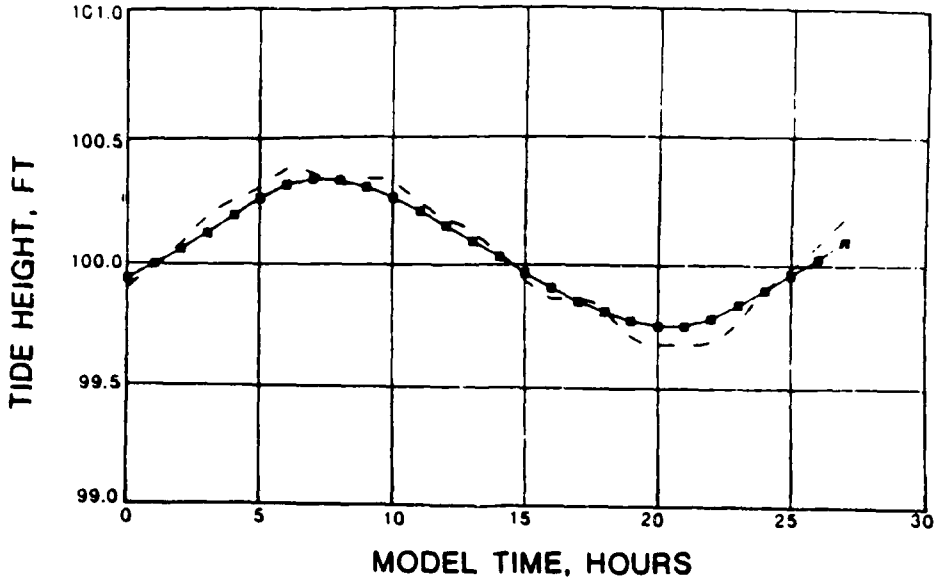

STATION TG4

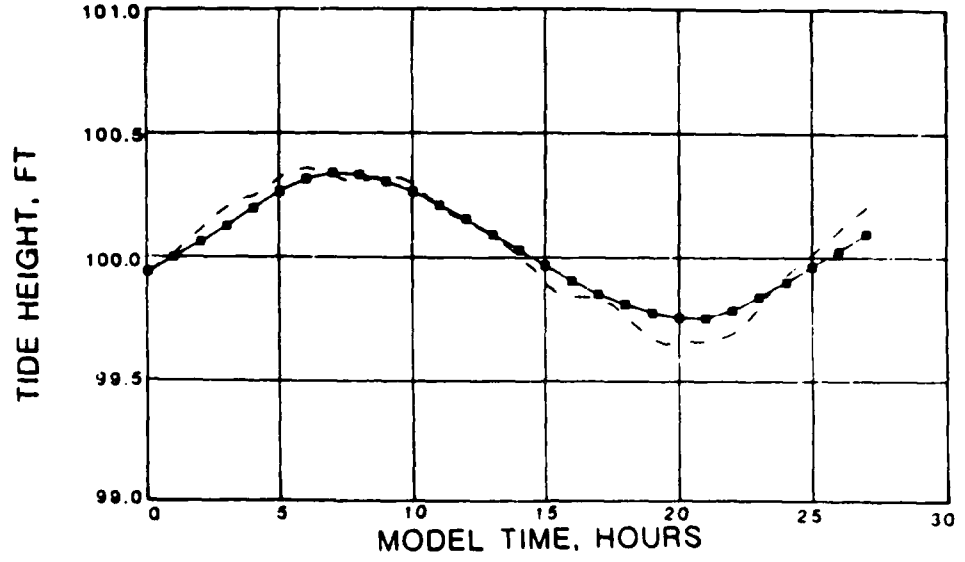

LEGEND

MODEL

PROTOTYPE

RMA-2V TIDAL HEIGHTS

17-18 JUNE 1985 STATIONS TG3 AND TG4

PLATE 8

STATION TG5

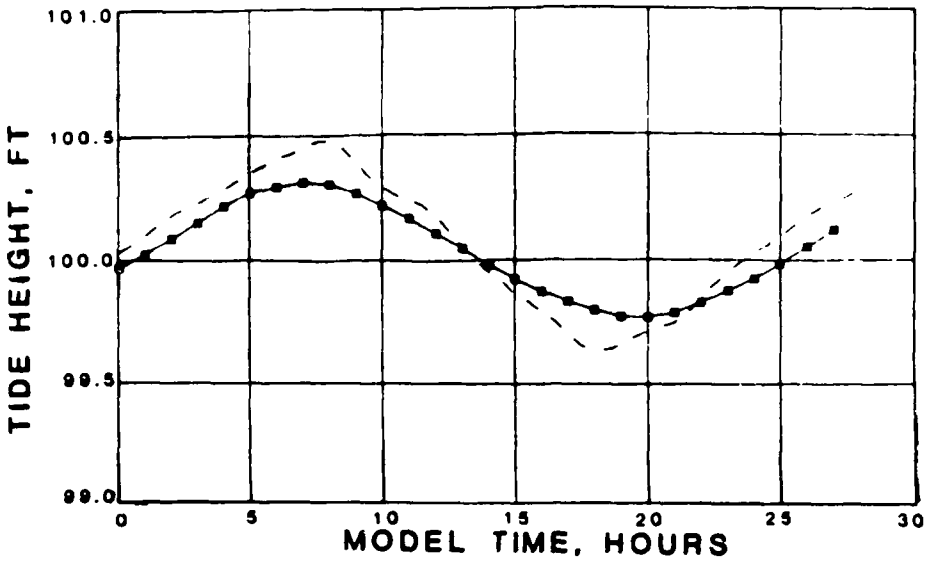

STATION TG6

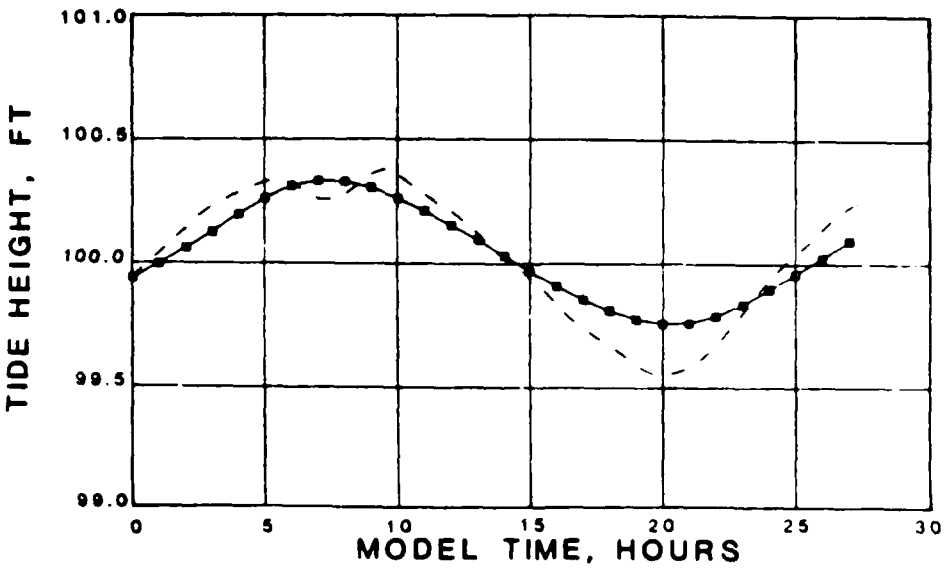

LEGEND

MODEL

PROTOTYPE

RMA-2V TIDAL HEIGHTS

17-18 JUNE 1985 STATIONS TG5 AND TG6

PLATE 9

PLATE 10

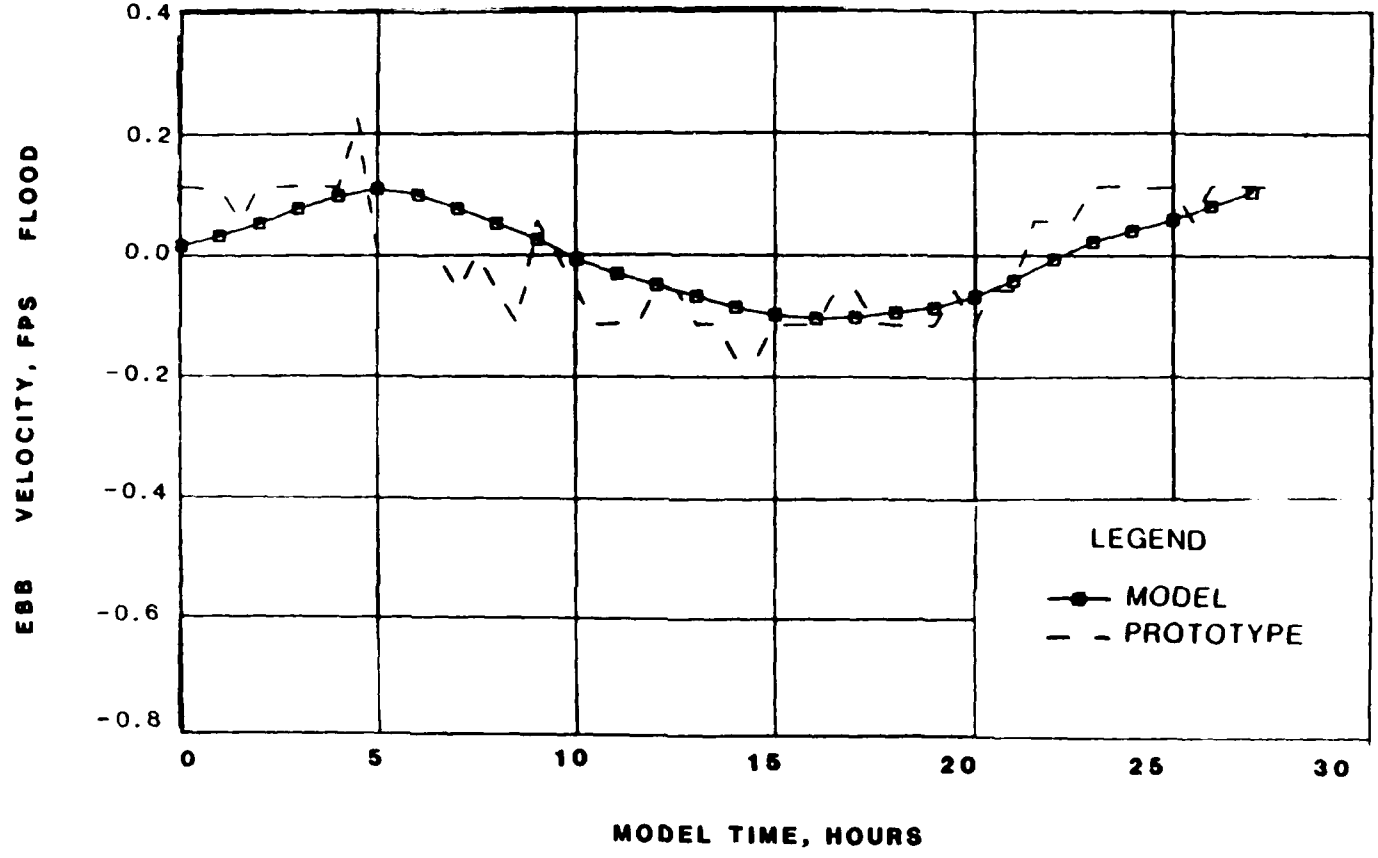

RMA-2V VELOCITIES

17-18 JUNE 1985

STATION V2

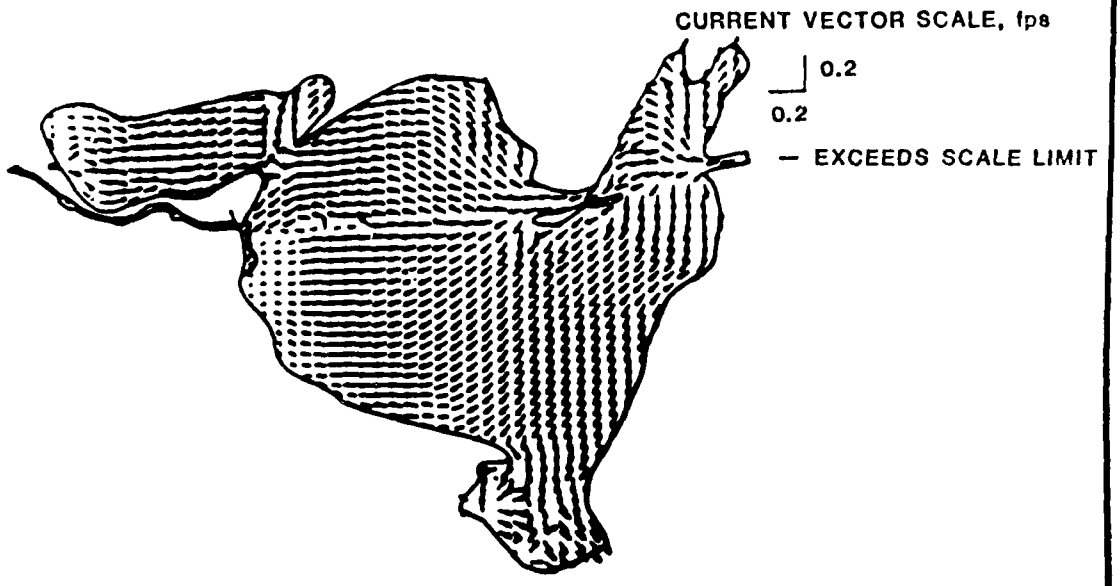

HOUR 1

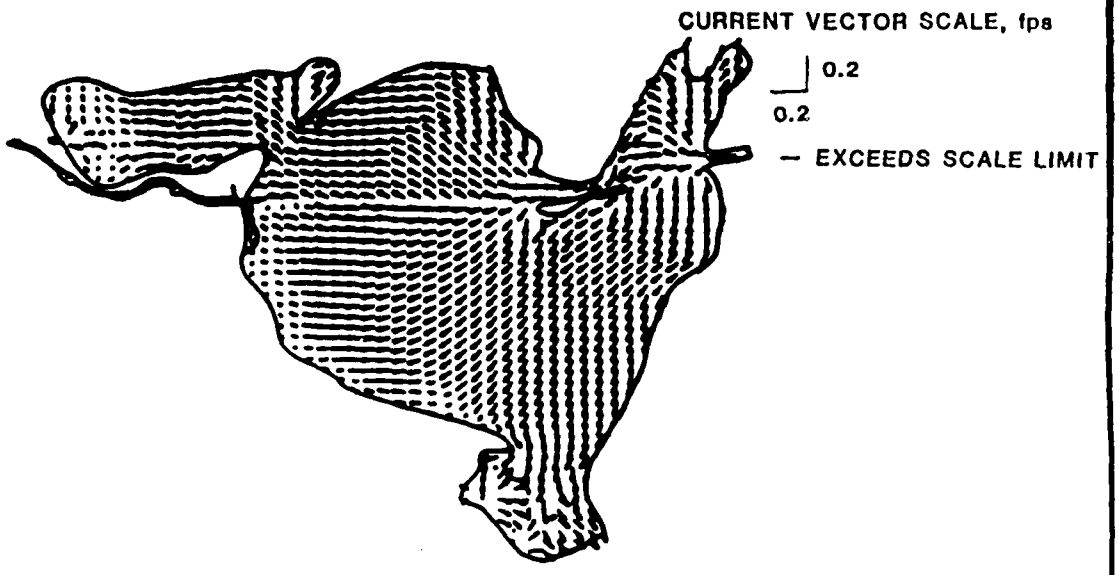

HOUR 3

RMA-2V CURRENT VECTORS

17-18 JUNE 1985

HOURS 1 AND 3

PLATE 11

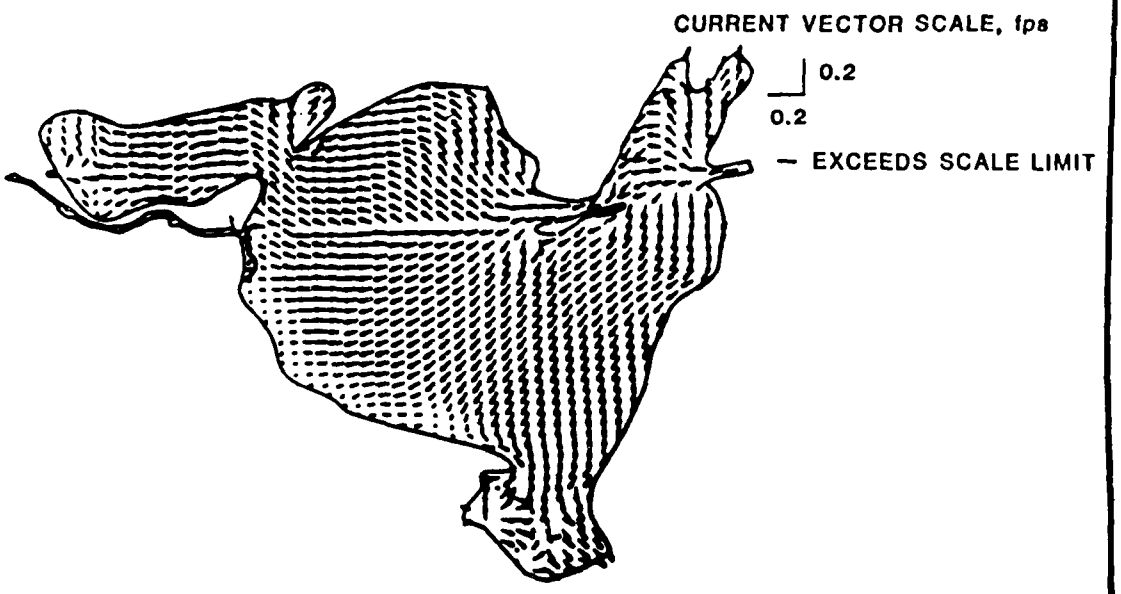

HOUR 5

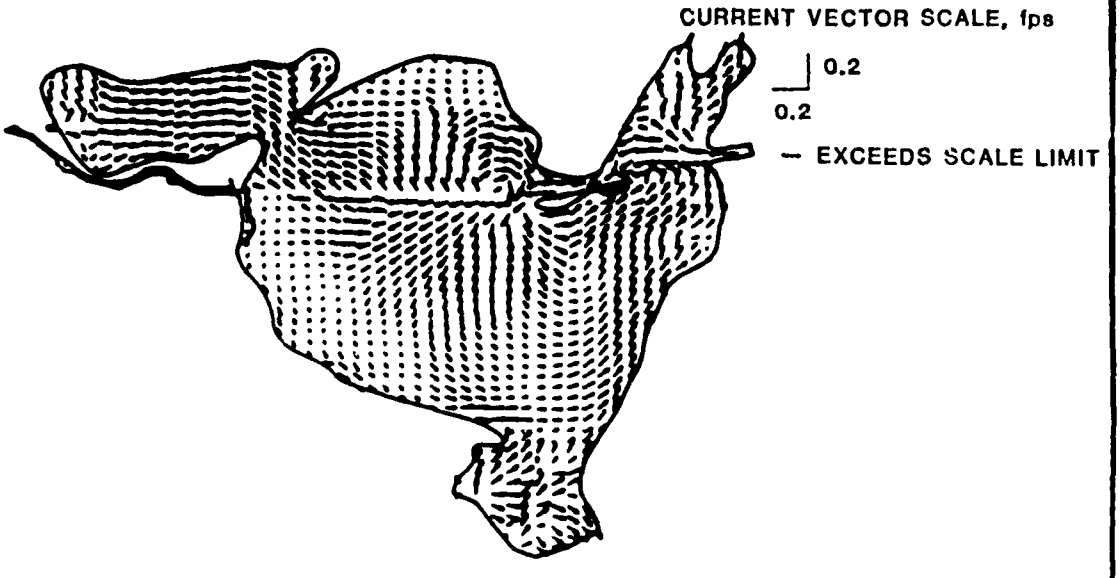

HOUR 7

RMA-2V CURRENT VECTORS

17-18 JUNE 1985
HOURS 5 AND 7

PLATE 12

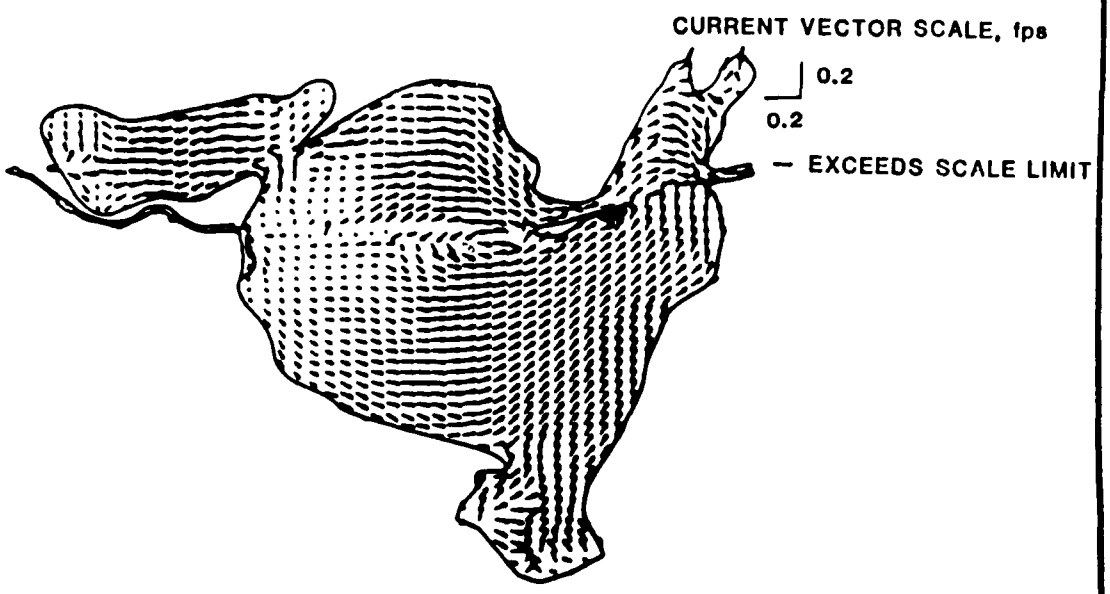

HOUR 9

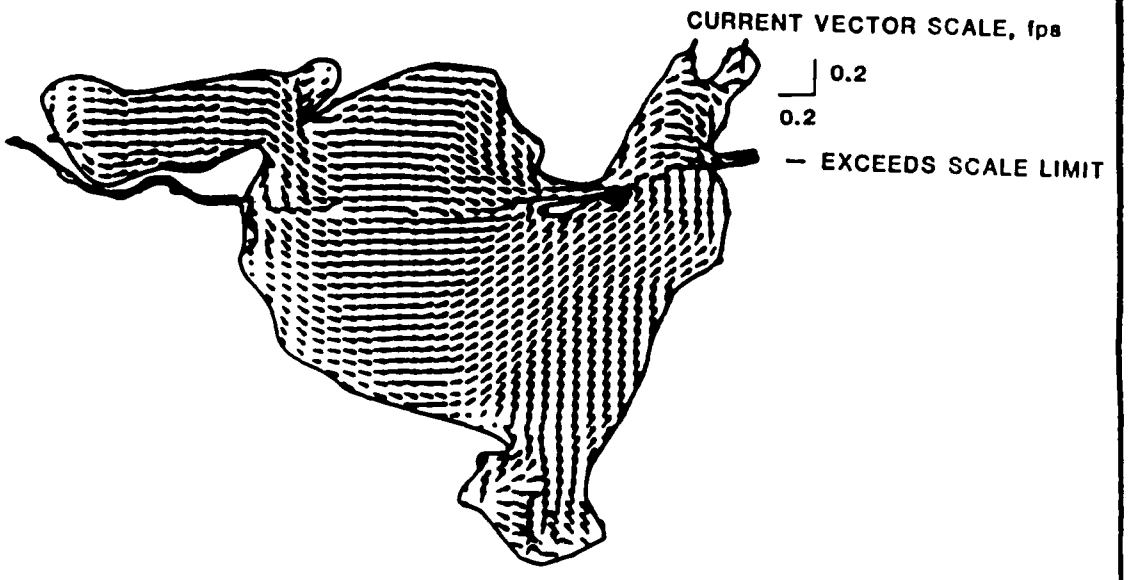

HOUR 11

RMA-2V CURRENT VECTORS

17-18 JUNE 1985
HOURS 9 AND 11

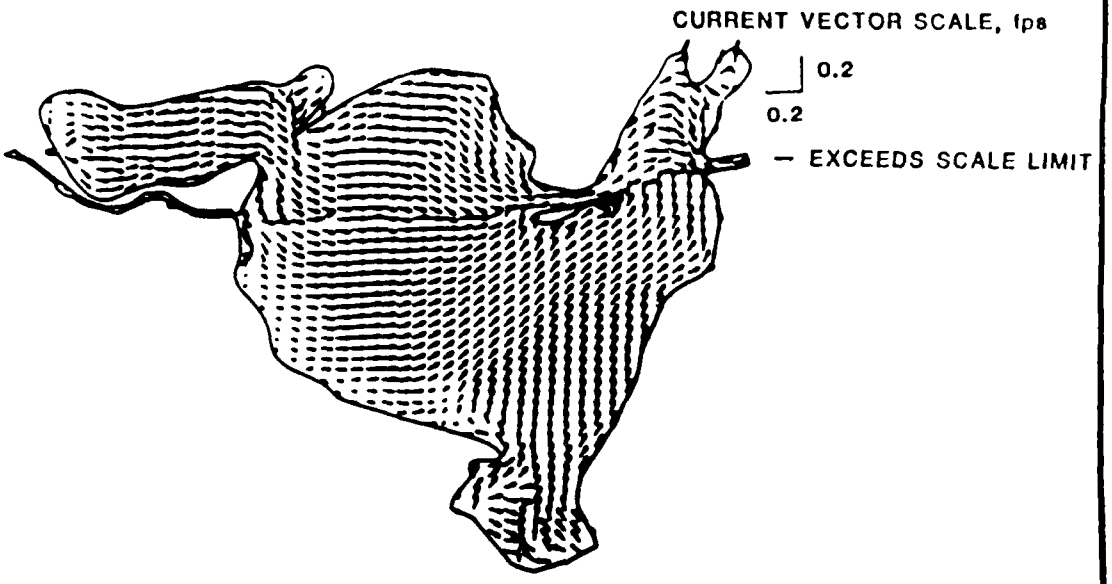

HOUR 13

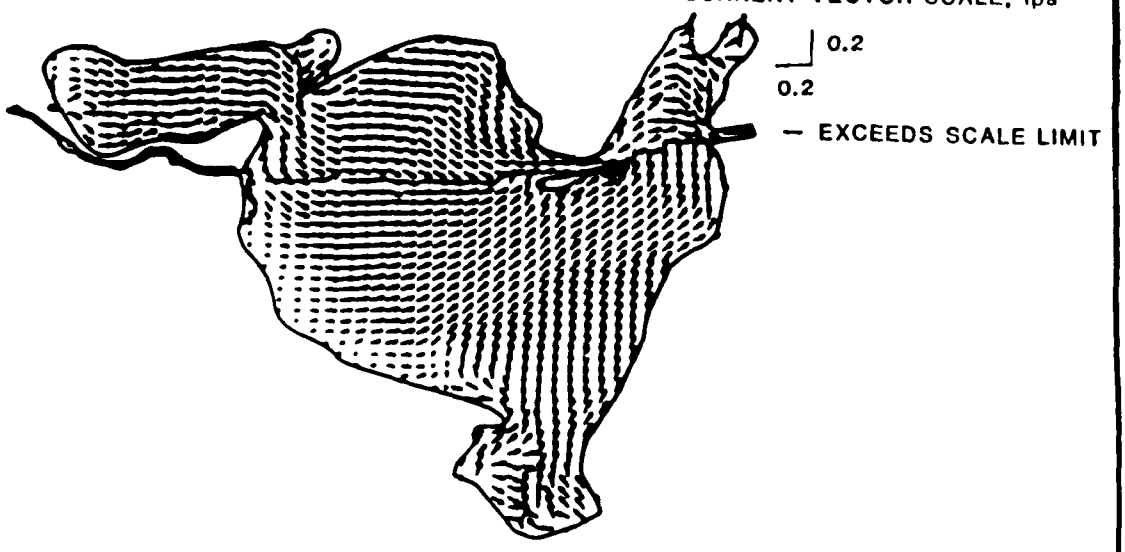

HOUR 15

RMA-2V CURRENT VECTORS
17-18 JUNE 1985
HOURS 13 AND 15

PLATE 14

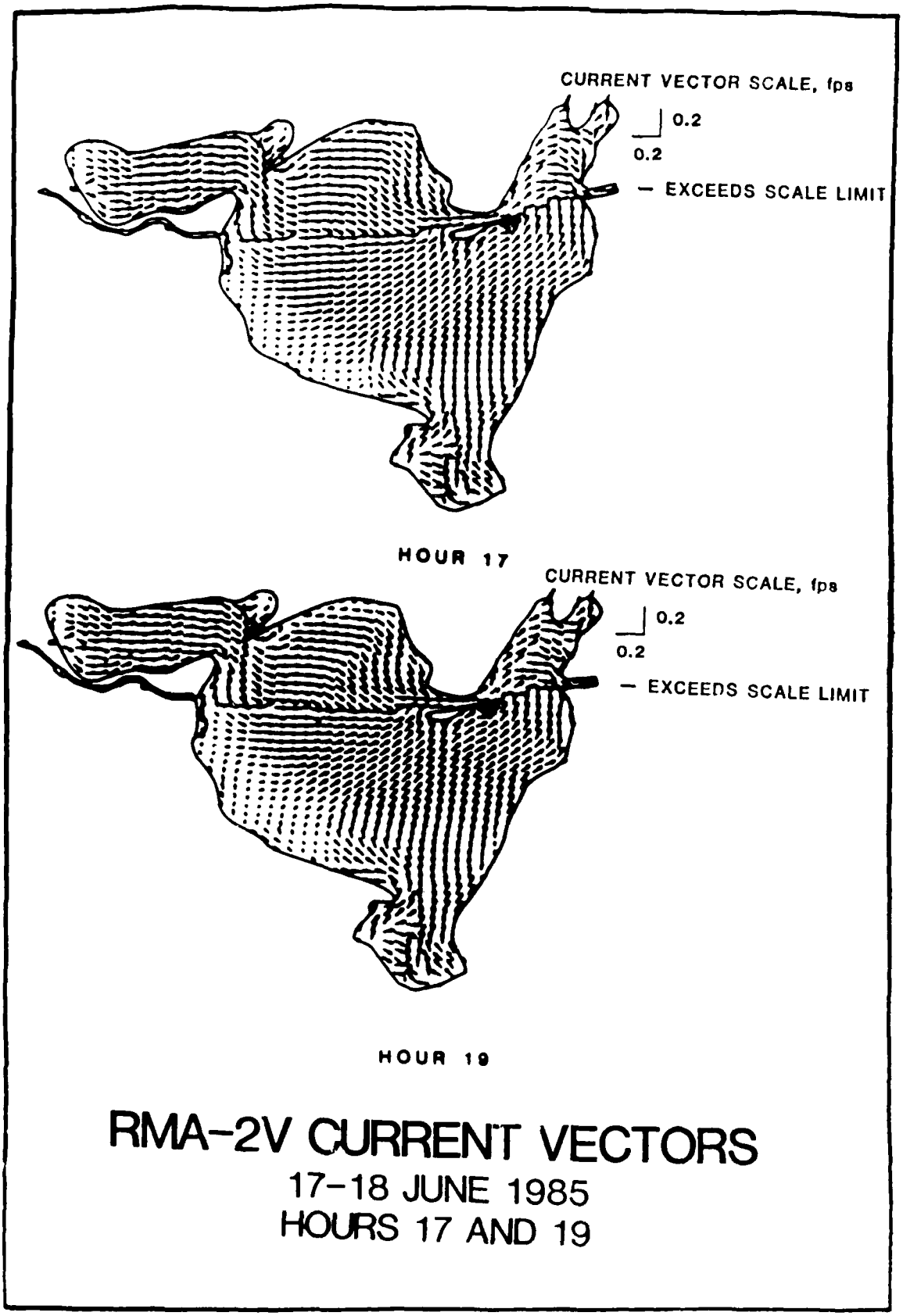

RMA-2V CURRENT VECTORS

17–18 JUNE 1985
HOURS 17 AND 19

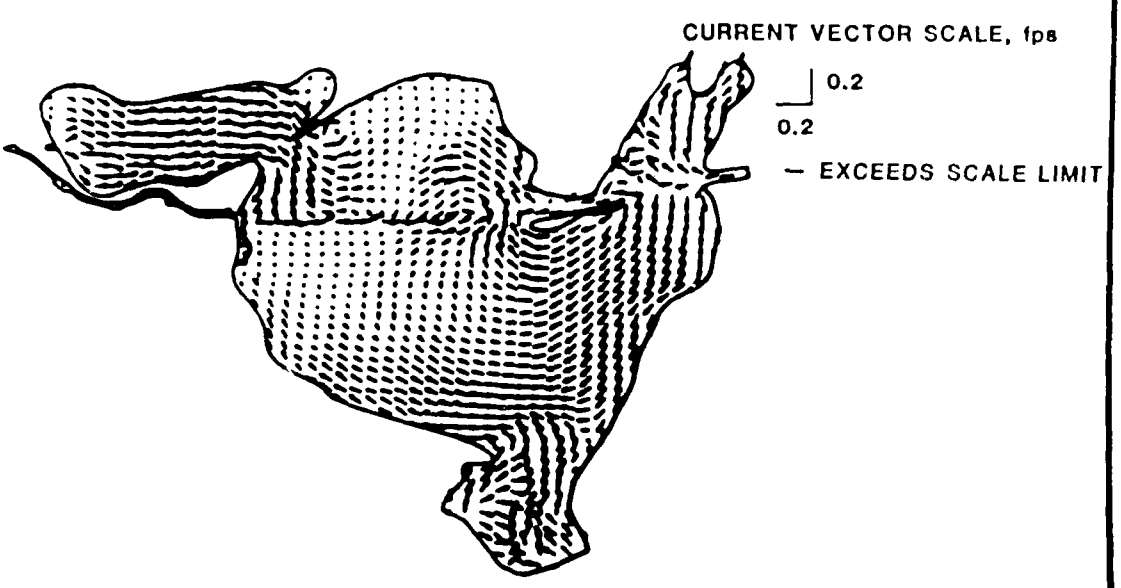

HOUR 21

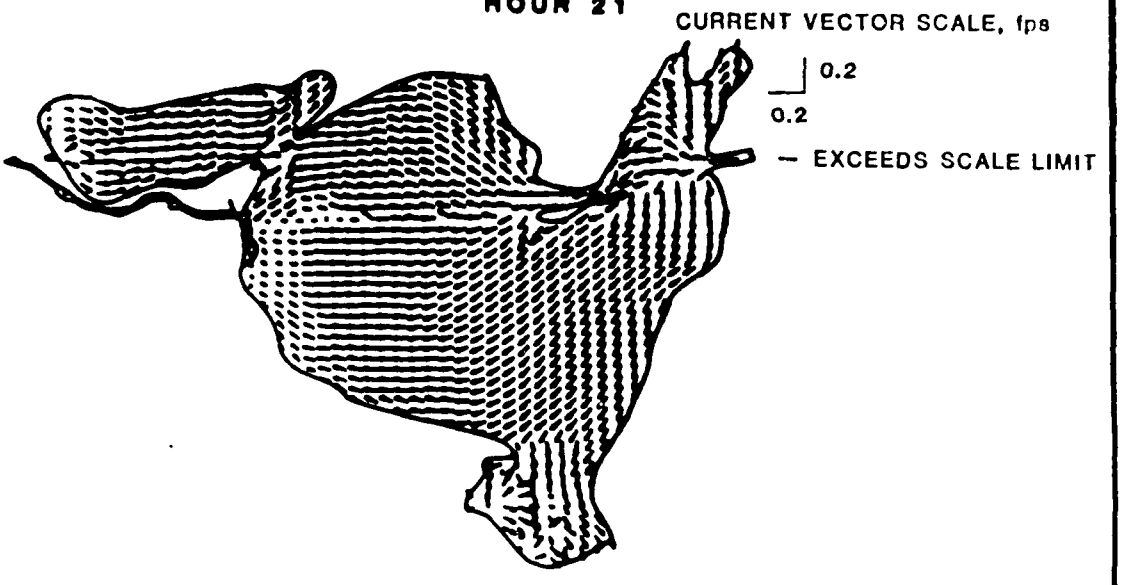

HOUR 23

RMA-2V CURRENT VECTORS

17-18 JUNE 1985
HOURS 21 AND 23

PLATE 16

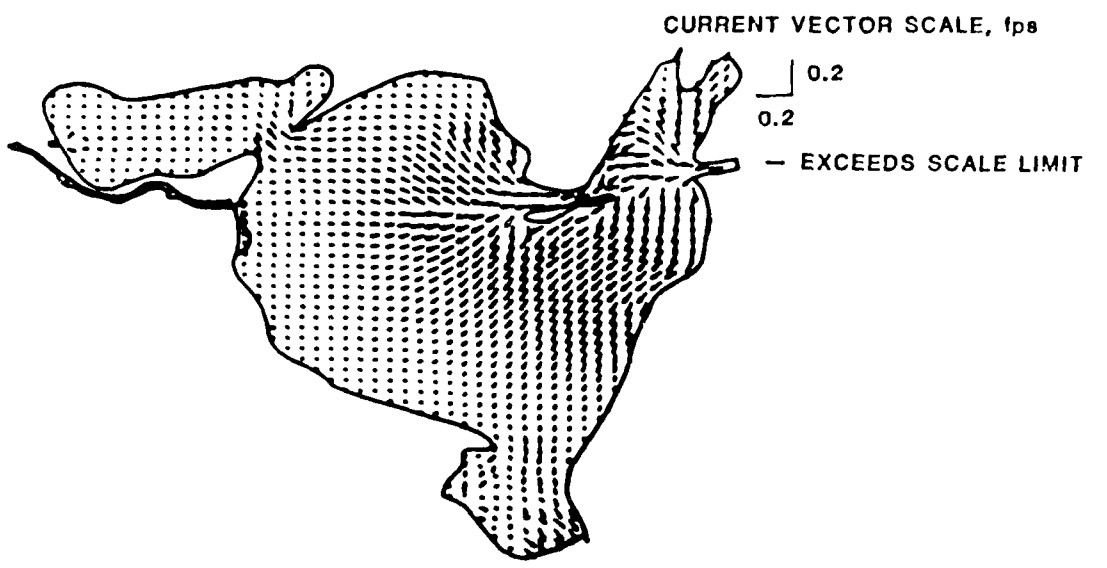

HOUR 25

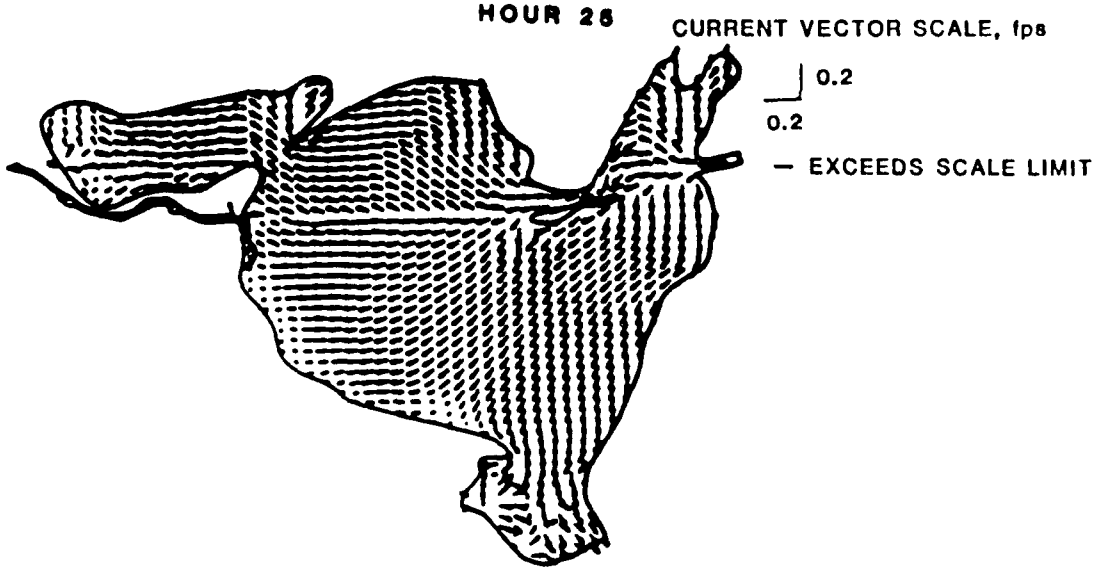

HOUR 27

RMA-2V CURRENT VECTORS

17-18 JUNE 1985
HOURS 25 AND 27

PLATE 17

STATION TG1

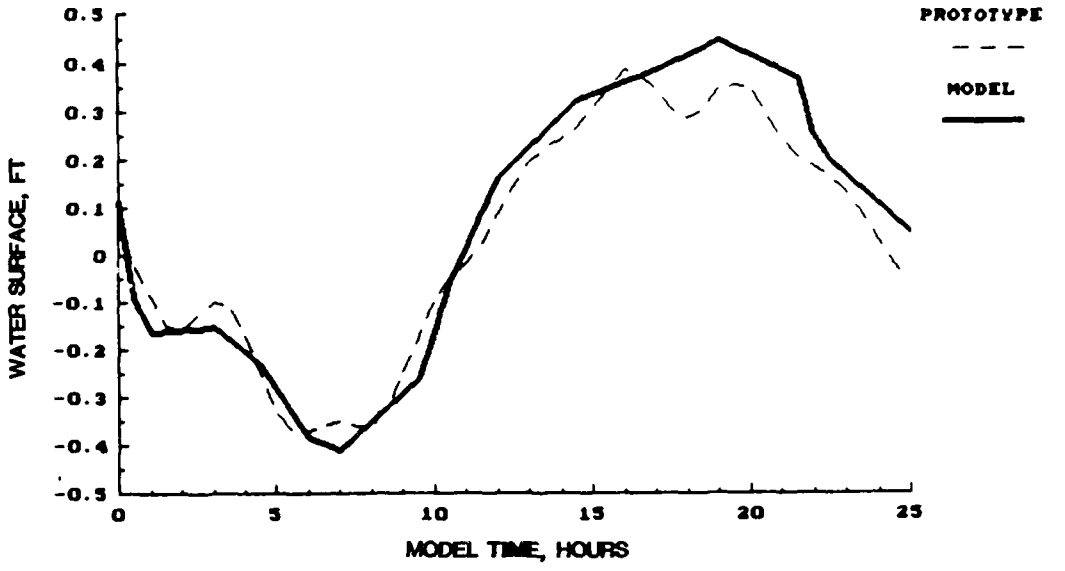

STATION TG2

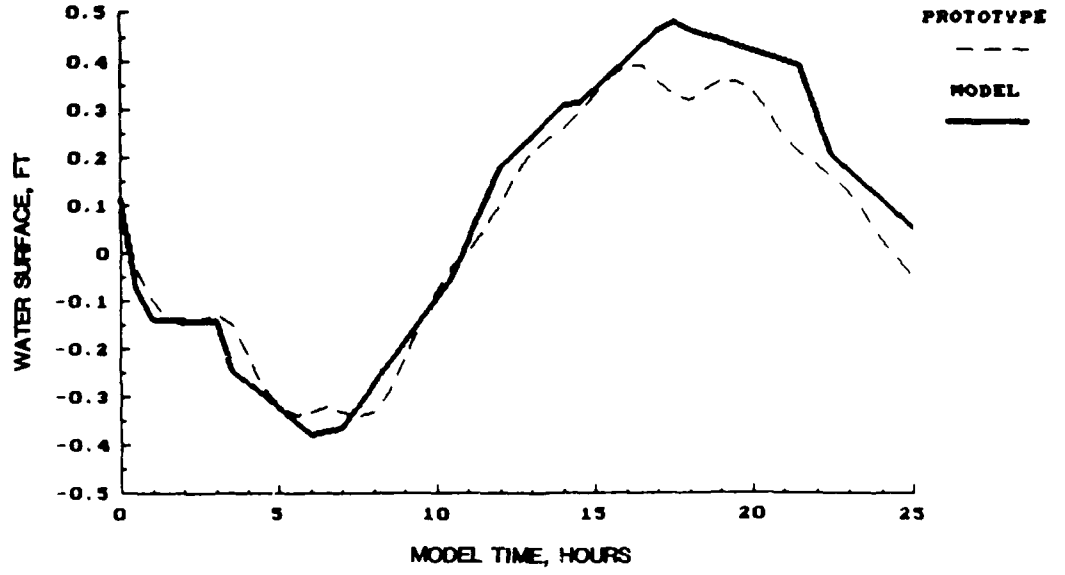

LAEMSED TIDAL VERIFICATION

17-18 JUNE 1985
STATIONS TG1 AND TG2

PLATE 18

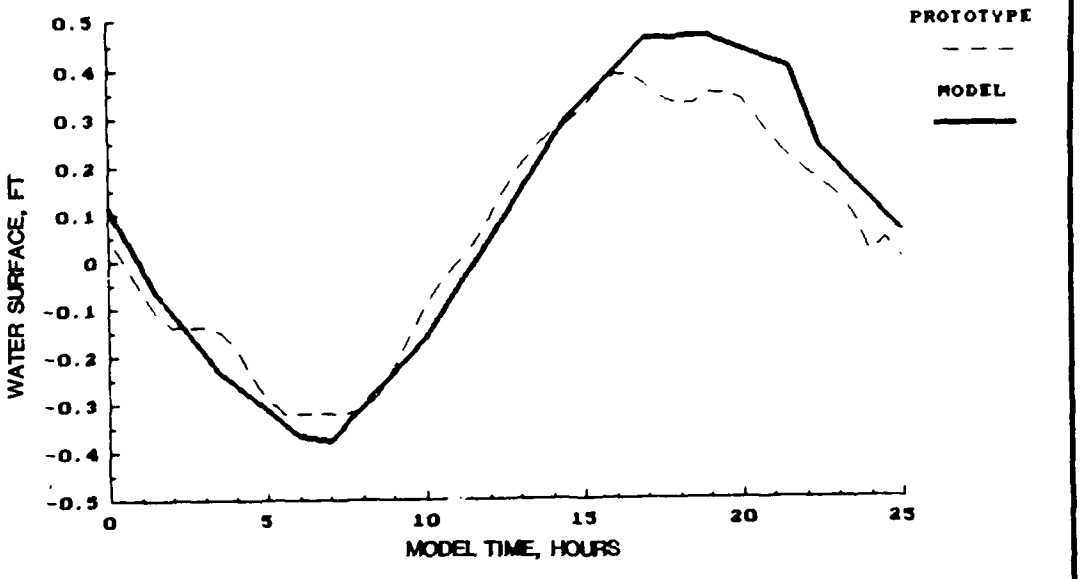

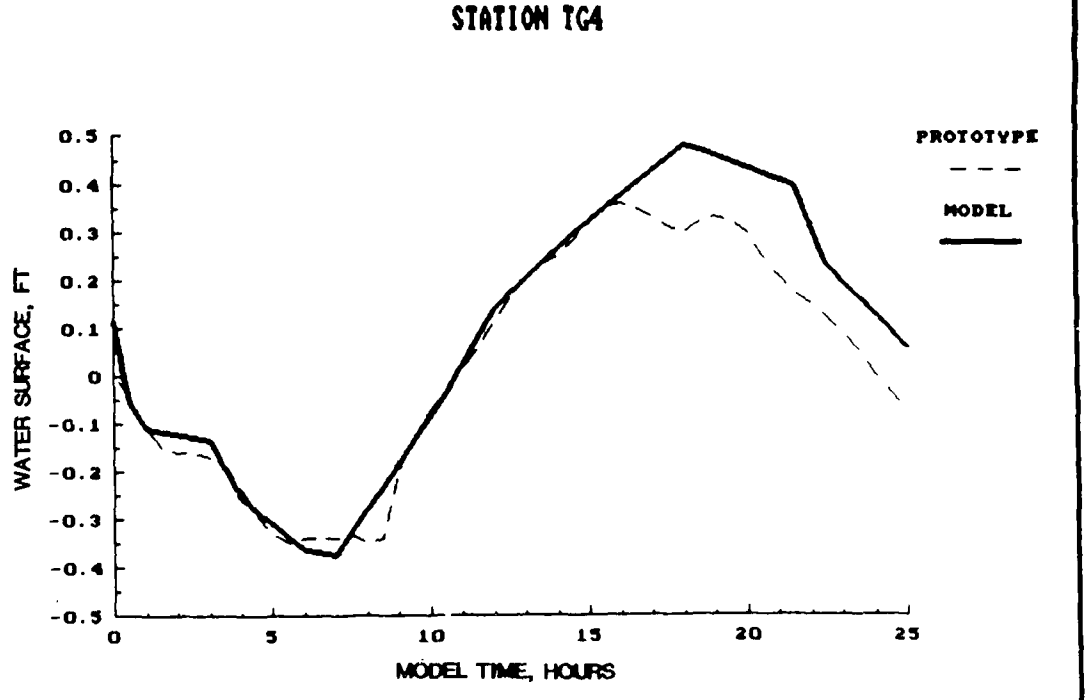

LAEMSED TIDAL VERIFICATION

17-18 JUNE 1985
STATIONS TG3 AND TG4

PLATE 19

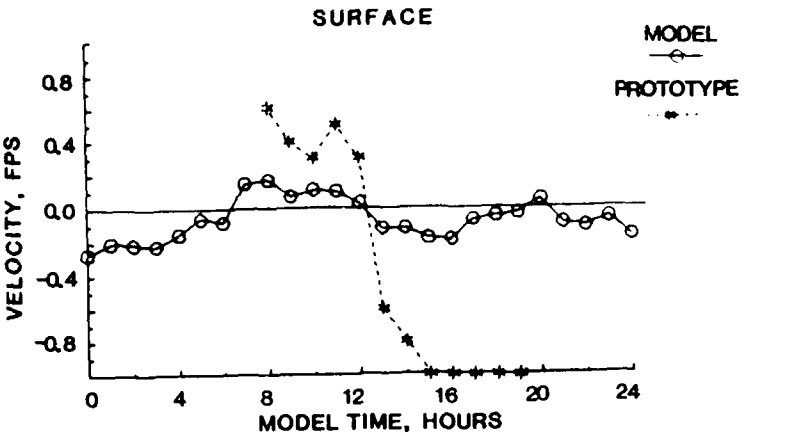

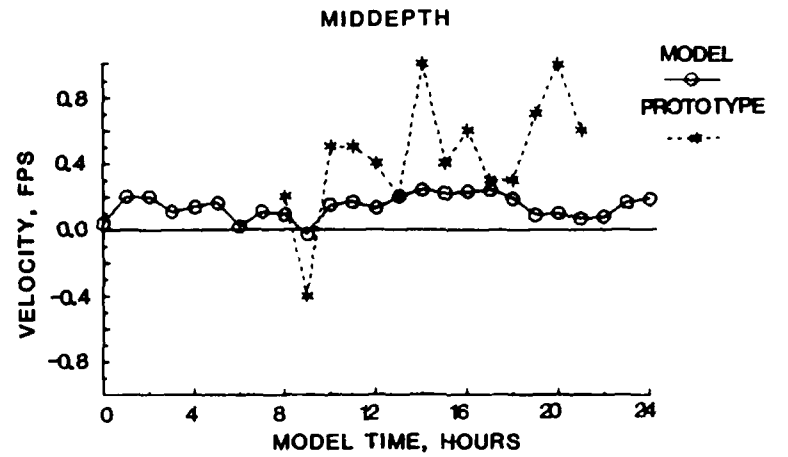

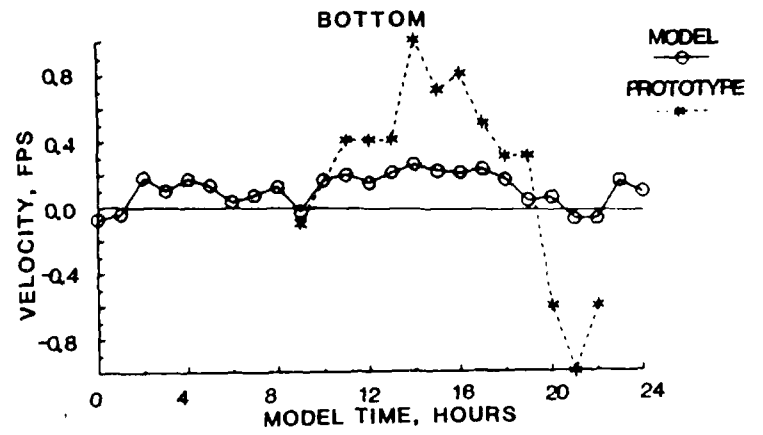

LAEMSED VELOCITY VERIFICATION

17-18 JUNE 1985

STATION A

PLATE 20

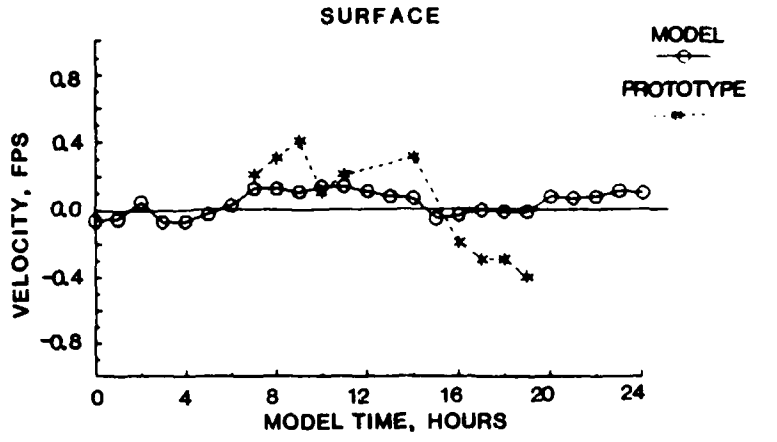

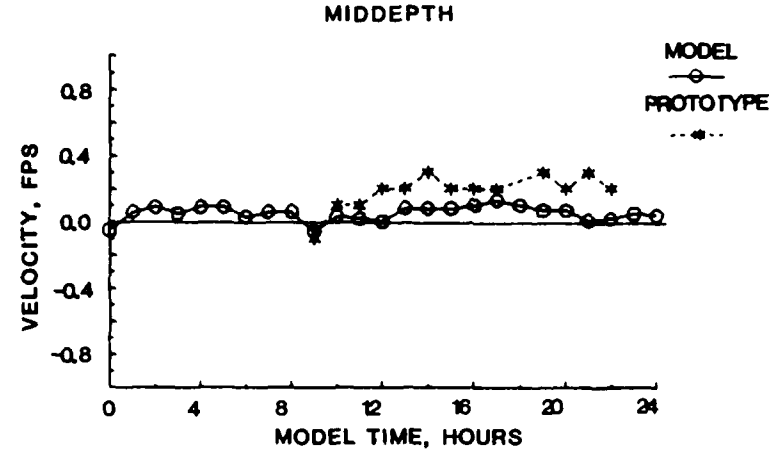

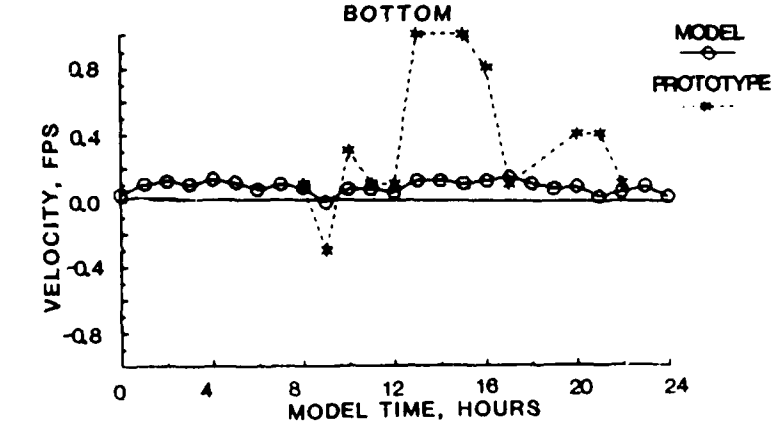

LAEMSED VELOCITY VERIFICATION

17-18 JUNE 1985

STATION C

PLATE 21

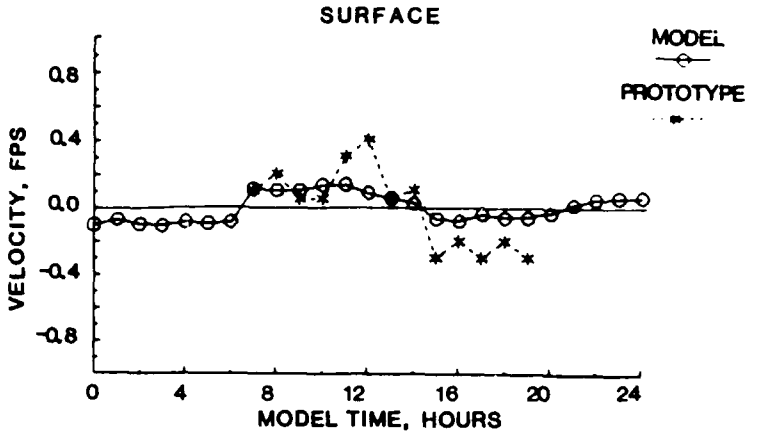

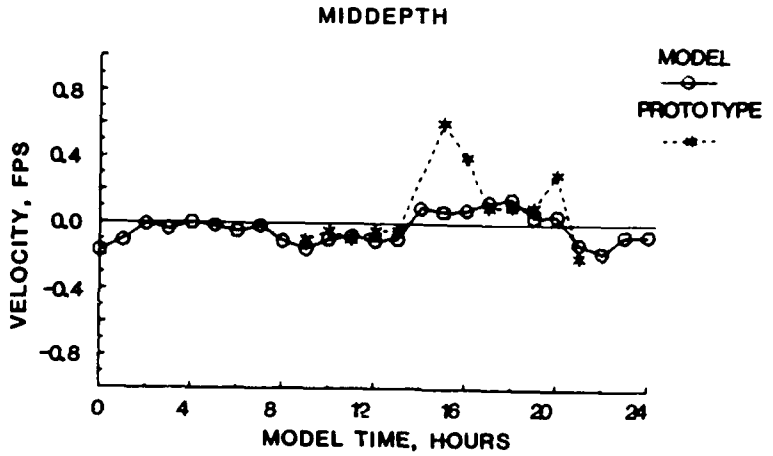

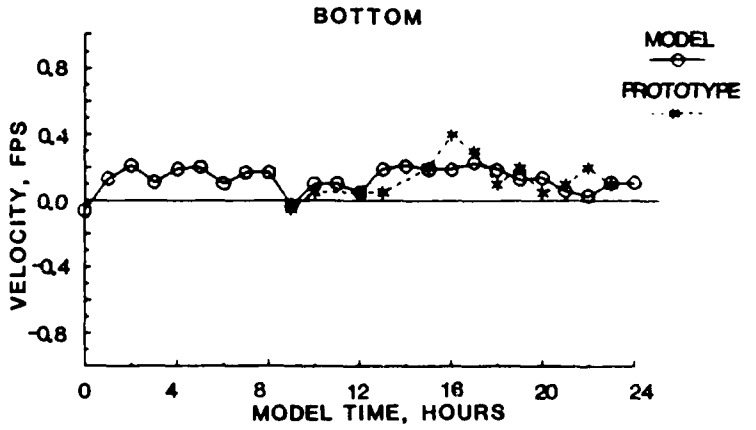

LAEMSED VELOCITY VERIFICATION
17-18 JUNE 1985
STATION D

PLATE 22

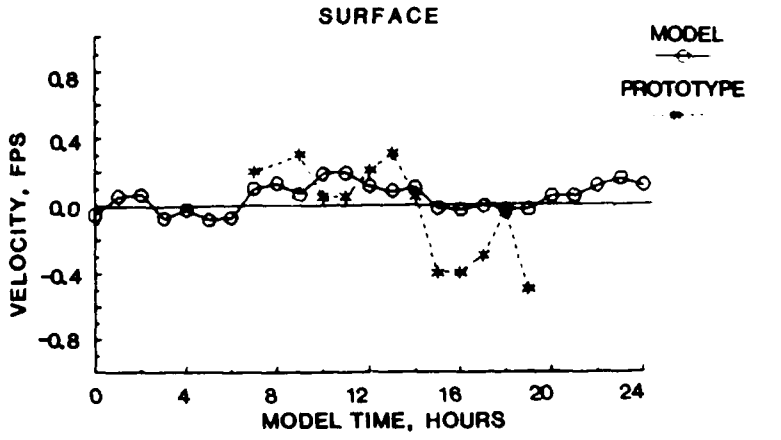

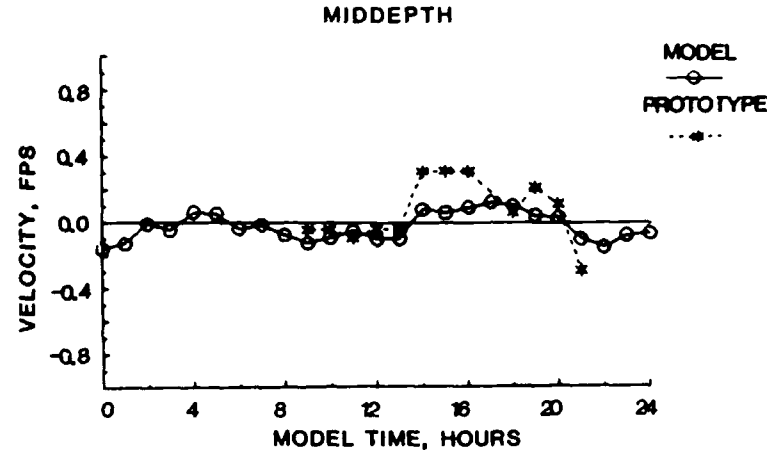

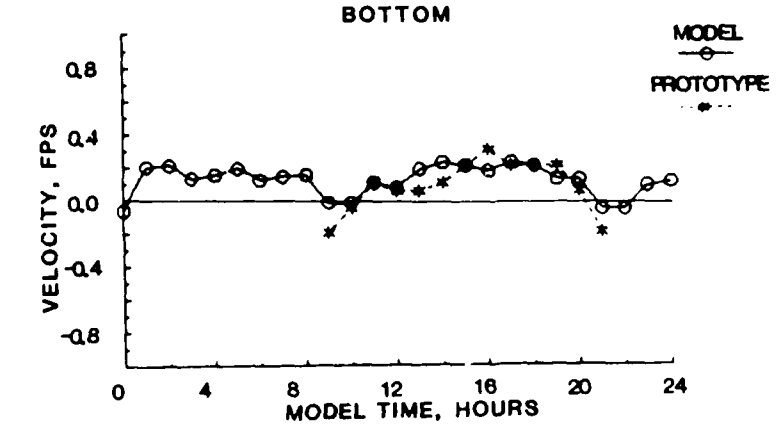

LAEMSED VELOCITY VERIFICATION

17-18 JUNE 1985

STATION F

PLATE 23

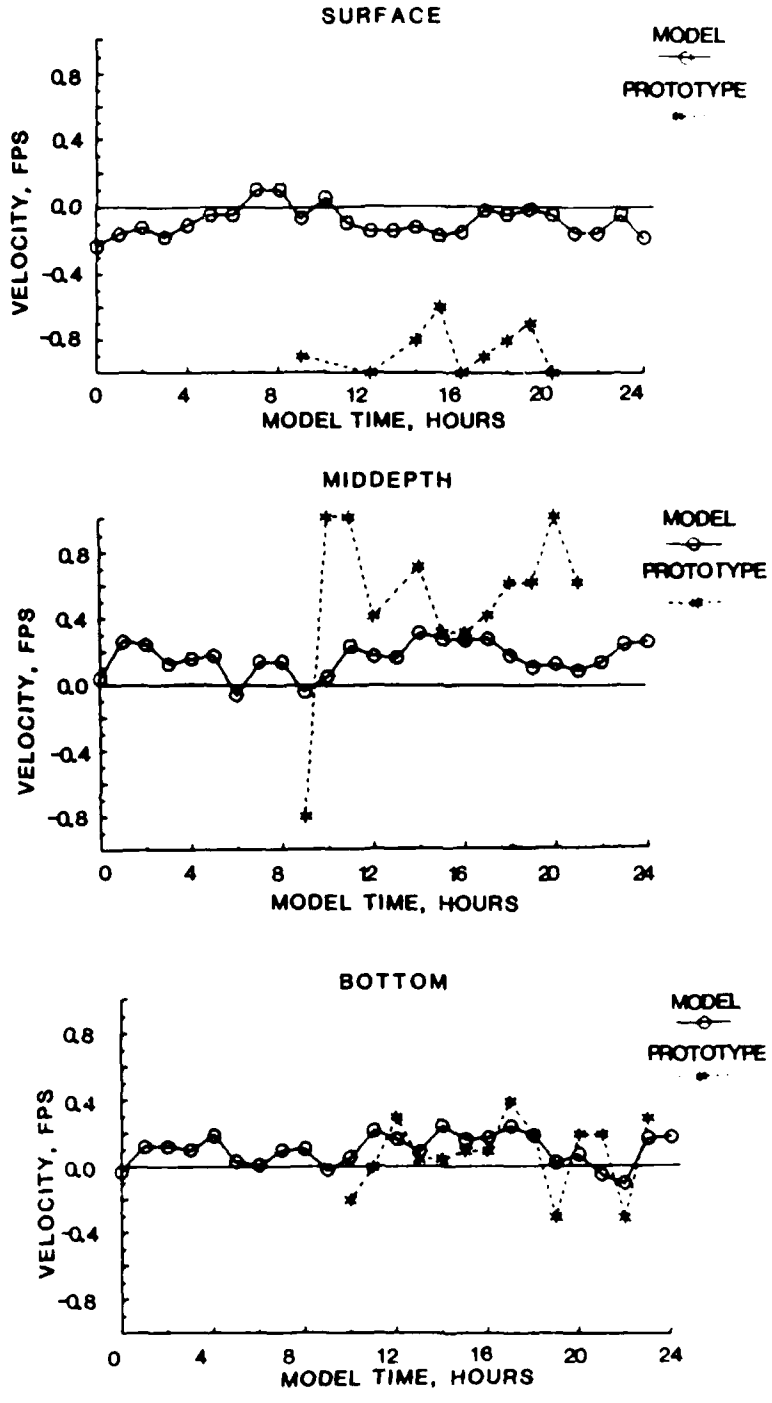

LAEMSED VELOCITY VERIFICATION

17-18 JUNE 1985

STATION G

PLATE 24

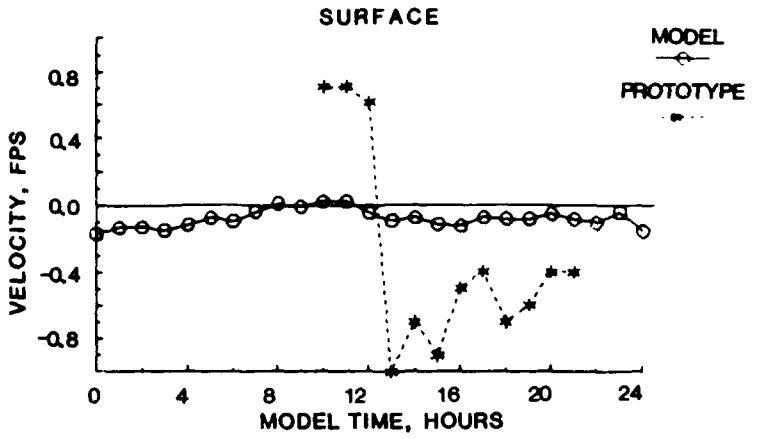

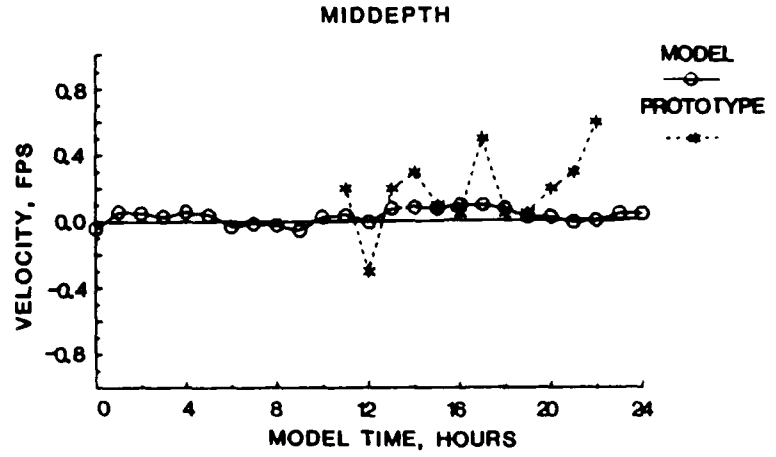

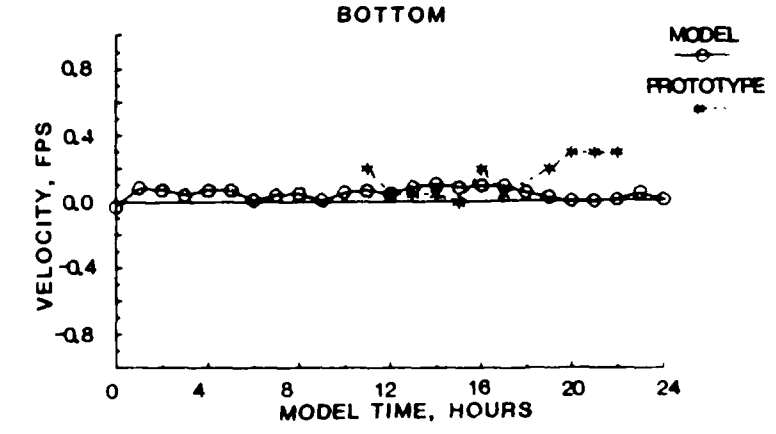

LAEMSED VELOCITY VERIFICATION
17-18 JUNE 1985
STATION J

PLATE 25

APPENDIX A: REPORT ON CONDITIONS AFFECTING SHOALING, CORPUS CHRISTI HARBOR, TEXAS, RECONNAISSANCE SURVEY, AUGUST 1984

Introduction

1. Shoaling rates between the Corpus Christi Harbor entrance and the Highway 181 bridge and in the turning basin of the harbor have been reported to be 360,000 and 550,000 cu yd annually, respectively. A reconnaissance survey was conducted in August 1984 to develop information on the causes of this shoaling, the characteristics and sources of the sediments, and circulations in the harbor and Corpus Christi Bay.

2. A previous study of this sedimentation problem was performed by the Committee on Tidal Hydraulics (CTH), Corps of Engineers, US Army (1965).* Figure A1 is a vicinity sketch of the harbor. That study concentrated on municipal/industrial withdrawals and discharges, and on chloride conditions in the harbor. The findings of that study were that large volumes of industrial withdrawals and relatively fresh discharges created a circulation between the harbor and the bay. The recommendations were to further define water usage in the harbor, to study circulation, and to measure suspended sediment loads.

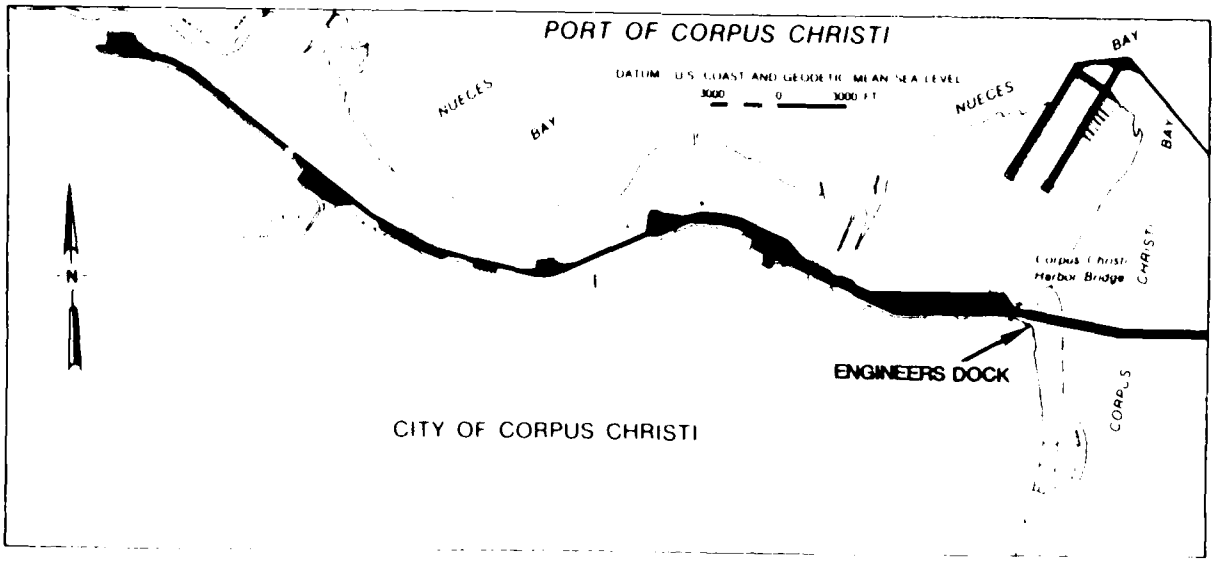

Figure A1. Corpus Christi harbor

* References in this Appendix are located in the References section of the main text.

Objectives

3. This report describes the results of salinity, temperature, suspended sediment concentration, settling velocity, and bed material property measurements. They are intended to more clearly define the sources, transport, and deposition of sediments in the harbor.

Approach

4. Salinity, temperature, and suspended sediment were measured to understand circulations and mixing. Suspended sediments and currents were used to estimate transport and settling rates. Since settling is such an important property, it was also determined from both field and laboratory tests. Bed material samples were taken from the bay to identify the nature of shoaling material and possible sources of material. Tests on these samples provided information on sediment characteristics during sedimentation and hindered-settling consolidation.

Description of Tests

Field procedures and equipment

5. The survey took place 20-23 August 1984. Conditions for the survey were about normal for the time of year. The weather was warm and dry. Afternoon winds were typically southeast 12-15 knots. Early morning winds were south 3-5 knots. Because of a prolonged dry spell, river flows were very low.

6. A 21-ft survey boat was used. Strong winds from the southeast made working in the bay in the afternoon impractical. Sampling, therefore, was done in the bay in the early morning and shifted to the harbor by afternoon.

7. A tide gage was established at the US Army Engineer District, Galveston, dock (Engineers dock, Figure A1) near the entrance to the harbor. A Fischer and Porter Model 1550 with a paper punch recorder was used. It was fitted with a stilling well and hydraulic damper to exclude short waves. No datum plane was established. Water-surface elevations were recorded every 15 min.

8. Two current meters were located off the Engineers dock. One was deployed at a depth of 6 ft below the water surface and the other 6 ft from

the bottom on a single string. The water depth was 24 ft. The deployment lasted about a day. Endeco Model 174 recording current meters with conductivity and temperature sensors were used. Currents were recorded at 2-min intervals. Threshold speed for these meters is 0.08 ft/sec and the manufacturer's stated accuracy is ±3 percent of full scale (5 ft/sec). Directional accuracy is ±7.5 deg when velocities are above threshold.

9. Water column measurements were repeatedly taken at a network of harbor and bay sampling stations. Table A1 gives the channel mile locations and description of the harbor/channel sampling stations from the Viola Turning Basin through the harbor and into Corpus Christi Bay channel to day marker 62. Table A2 gives a description of the bay stations. Figure A2 shows their approximate locations in the bay.

10. Conductivity, salinity, temperature, turbidity, and depth were measured in situ using an InterOceans Model 513 CSTD-Tr measuring device. The instrument consists of a sensor package and an onboard readout unit. The

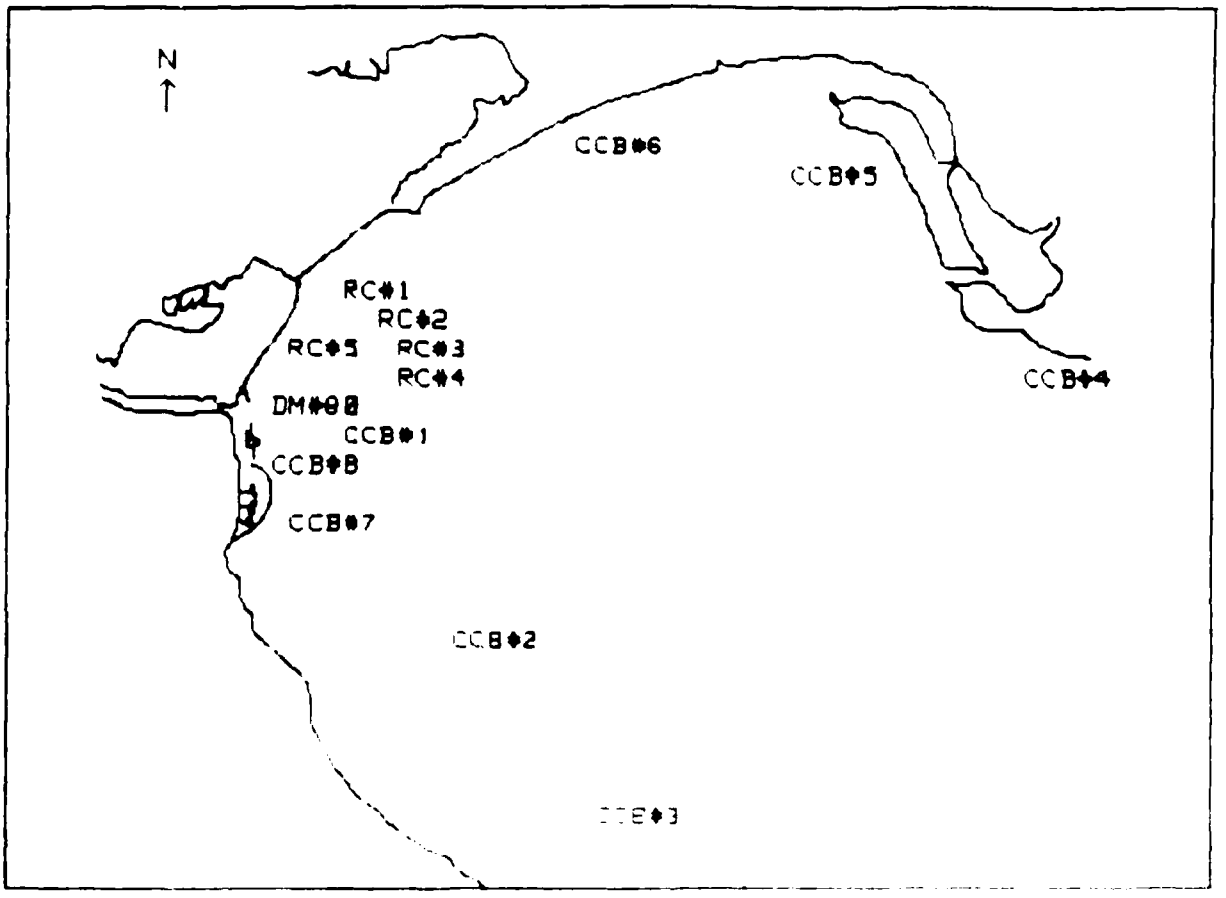

Figure A [illegible]

manufacturer gives its precision as follows: conductivity ±0.02 mmhos/cm; salinity ±0.05 ppt; temperature ±0.02° C; and depth ±0.15 m.

11. Suspended sediment samples were taken with either a pump or water bottle samplers. The former consists of a 12-v d-c pump and 100 ft of 1/4-in.-ID plastic tubing. The horizontal intake points into the flow. Pumped samples were stored in 8-oz bottles. A total of 222 samples were collected.

12. The water bottle sampler is a long polyvinyl chloride tube with closures at both ends. It is deployed from the survey boat suspended from a wire and sinker in the horizontal position. The sampler orients itself with the flow. A messenger weight is sent down the wire to close the device. This sampler was used to collect large-volume (5-gal) samples and for settling velocity determinations in the field.

13. Six field settling tests were performed using the water bottle samplers. After collection of a sample, the sampler was placed vertically in a rack. Subsamples were taken from the sampling tube at 0, 8, 15, 30, 60, 120, 180, and 240 min. These subsamples were analyzed for concentration of suspended material (CSM) and the data treated as laboratory settling test results.

14. Current velocities were also measured from the survey boat using over-the-side equipment. The current meter was a Gurly Model 665 which uses a vertical-axis cup-type impeller. Accuracy is ±0.1 ft/sec for current speeds less than 1 ft/sec and ±5 percent for current speeds greater than 1 ft/sec. Accuracy of the direction indicator is ±10 deg at current speeds greater than 0.5 ft/sec. Accuracy of the current measurements also depends on wave action and the motion of the survey vessel.

15. Current measurements were made while the survey boat was tied to a pile or other object. Attempts were made to use anchors to hold the boat stationary, but these were unsuccessful.

16. Bed sediment samples were taken with a Peterson-type grab sampler. Attempts were also made to use a gravity corer. These attempts failed as will be discussed later. Twenty-six bed sediment samples were collected. Their locations are given in Table A3.

Laboratory and data analyses

17. Water samples were analyzed for total suspended material and salinity or were used in settling tests. Determination of CSM was by filtration

and gravimetric analyses. Nuclepore polycarbonate filters with 0.45-μ pore size were used. Samples were drawn through the filters with a vacuum system. The filters and holders were then washed with distilled water to remove salts. The filters were dried at 105° C for 1 hr. CSM was calculated from the weight of material retained on the filters and the sample volume filtered.

18. Water column data consisting of CSM and current velocity with depth were fit to exponential and logarithmic curves, respectively. Depth-averaged CSM and current speed U , friction velocity U* , suspended sediment transport rate Q(sed) , and CSM stratification were then computed. CSM stratification is equal to the surface-to-bottom difference divided by the depth-averaged CSM and is related to the settling characteristics of the sediment and the turbulence characteristics of the flow.

19. Salinity and temperature data were used to compute water density using Bennett's function (Bennett 1976). The density parameter σ_{ST} was used for the density due to salinity and temperature, where σ_{ST} equals (density - 1) × 1,000. (If σ_{ST} equals 24.5, then density equals 1.0245 g/ml, for instance.) The density anomaly due to the presence of suspended sediment was also computed assuming the density of the sediment particles to be 2.65 g/ml. It was designated σ-C_{sm} and was used to evaluate the effect of suspended material on circulation. The total density parameter was then σ_{ST}-C_{sm} .

20. Settling tests were performed on three 5-gal samples in the laboratory. These samples were vigorously shaken for 5 min by hand prior to being introduced into a 4-in.-diam by 6-ft-high settling column. Samples were withdrawn from near the bottom of the tube with time, and these subsamples analyzed for CSM.

21. Settling tests were also performed on bed material resuspended into the supernatant of the 5-gal samples. The procedure used was the same as for the other settling tests. Resuspended samples were vigorously mixed and poured into the settling column. Samples were withdrawn with time and analyzed for CSM. The sediment used for these tests was a mixture from three stations (sediment locations 14, 15, and 16 described in Table A3) located in an area ranging from under the bridge to between the breakwaters. A series of nine tests was conducted with the initial CSM varied between 250 and 8,900 mg/l. These tests determined the dependence of settling velocity on CSM.

22. Observations were made in the laboratory of the thickness of deposited material with time during settling tests of initial CSM values of 1,250 mg/ℓ and above. These observations were used in conjunction with the results of the settling tests to compute the initial density of the bed formed by sediment settling from suspension.

23. Raw data from field and laboratory settling tests consisted of CSM at sampling times. A regression equation was fit to the data by the least squares method. Coefficients from this equation were then used to calculate the settling velocity distribution. Tests with initial CSM of 2,250 mg/ℓ and above exhibited interference among particles which made settling velocities almost uniform. For these tests, Owen's (1970) method of visually following the descent of the strong concentration gradient was used to estimate settling velocity.

24. Bed sediment samples were analyzed for bulk wet density (BWD), cation exchange capacity (CEC), loss on ignition, percent moisture, and grain size as well as settling velocity as noted earlier. BWD was determined using 25-ml wide-mouth pycnometers. CEC was determined (after air-drying samples) by a sodium saturation method. Loss on ignition was calculated from weight loss after heating samples for 1 hr at 550° C. Percent moisture was determined by evaporation at 105° C. Salts were not removed. Grain size was determined on dispersed samples using hydrometer and sieve analyses.

25. CEC was used as a measure of sediment cohesiveness: the higher the CEC, the more cohesive the sediment. Typical values in meq/100 g for mineralogical groups are as follows: kaolinite, 1-15; illite, 10-40; chlorite, 10-40; and montmorillonite, 50-150.

26. Consolidation or flocculant settling tests were performed on the same sediment used in the settling tests. Sediments were mixed with native water to concentrations ranging from 20 to 200 g/ℓ. They were poured into transparent cylinders about 1.2 ft high with diameters ranging from 2-1/8 to 8 in. depending on the test concentration. At these high concentrations, the suspension behaved as a mass and collapsed. A sharp interface formed between the sediment and a clear overlying layer. The rate of descent of this interface was equal to the hindered settling velocity for this sediment at this concentration.

Test Results

Water column measurements

27. A plot of the water levels at the Engineers dock is shown in Figure A3. Tides were diurnal with ranges of 0.5 to 0.8 ft.

28. Vertical profiles of concentration C and current speed U are grouped by location: bay and interior channel. The first group is the channel stations with results presented in Plates A1-A28. The velocity measurements for these profiles are suspect or were not attempted at all. Tests results for stations located in the bay are shown on Plates A29-A51. Profiles in Plates A1-A51 are shown in terms of normalized distance Z/H , where Z is the height above the bed and H is the total depth. Most of these profiles include velocity measurements. A method being developed under the "Fine-Grained Shoaling in Navigation Channels" work unit of the Improvement of Operations and Maintenance Techniques research program was applied to these data. Stratification of CSM and shear velocity estimates based on Manning's friction assumption were used to calculate settling velocity. The mean settling velocity for 25 data sets was 0.25 mm/sec.

29. Tables A4-A7 contain observed salinity, temperature, CSM, C_{ST} , $C-C_{sm}$, and $C_{ST}-C_{sm}$. Each table contains a transect either along the harbor channel or through the bay.

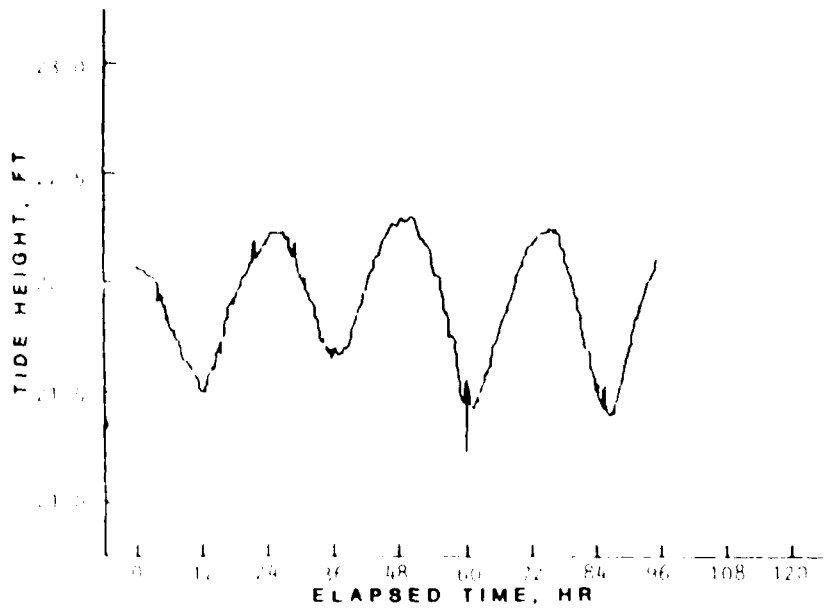

Figure A3. Water levels at Engineers dock starting 0830 20 August 1984

30. Current speed is shown with depth for the bay stations in Plates A29-A51. Plots of the direction and depth-averaged speed are shown in Figures A4, A5, and A6 for 21, 22, and 23 August, respectively. Plots showing depth-averaged CSM and σ_{ST}-C_{sm} densities for 22 August are presented in Figures A7 and A8, respectively.

31. Data from the current meter string at the Engineers dock indicated a very short ebb at both the surface and bottom, with speeds of 0.2 to 0.3 ft/sec lasting only about 1-2 hr. Currents during the flood were stronger (0.4 ft/sec) at the bottom than at the surface (0.3 ft/sec). Duration of the flood was 4-6 hr. Since the condition and position of these meters were uncertain during the deployment, detailed data are not presented.

32. Table A8 contains the results of four field settling tests. Cumulative settling velocity distribution in percent and a differential distribution by settling classes are shown. Some parameters for the settling velocity distribution are also given. The weighted average of the distribution is the most representative of these. Geometric mean and standard deviation, skewness, and kortosis are also shown. The mean average settling velocity of these four tests was 0.25 mm/sec.

Laboratory results

33. Table A9 contains the results of the laboratory tests on three 5-gal field samples. These samples were neither kept cool nor chemically preserved prior to analysis, and the results should be viewed with some caution.

34. Results of the laboratory tests on resuspended bed material are given in Table A10 for concentrations ranging from 250 to 1,840 mg/ℓ. On concentrations between 2,250 and 8,900 mg/ℓ, the tests were conducted by observing the rate of descent of the strong concentration gradient which occurs as settling velocities become more uniform. The results of those tests are presented in Table A11, which also gives the initial bed density results.

35. Results of settling tests on the dependence of settling velocity on CSM showed that, compared to other sediments, shoaling materials exhibited a rather small dependence. This could be because these materials are so highly cohesive (as indicated by CEC) that they form tight, rapidly settling aggregates, even at low concentrations. The range of settling velocities is typical. The standard deviation of the settling velocity distributions is generally small, indicating that aggregates are fairly uniform.

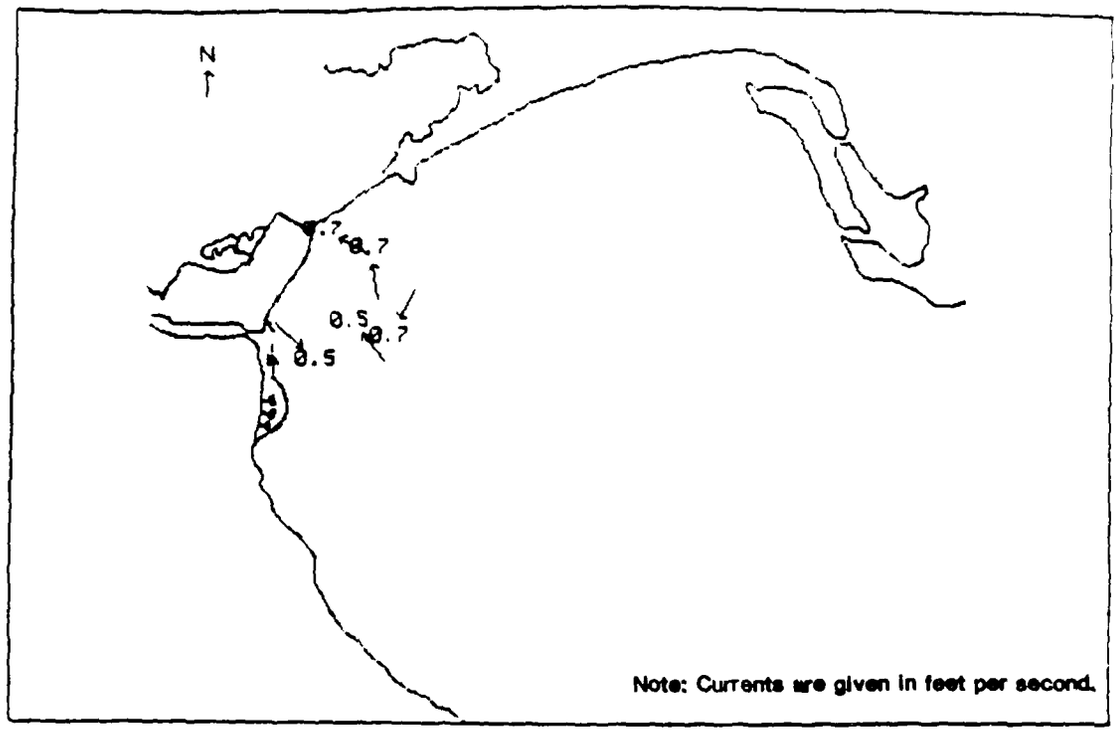

Figure A4. Depth-averaged velocities, 21 August 1984, flood tide

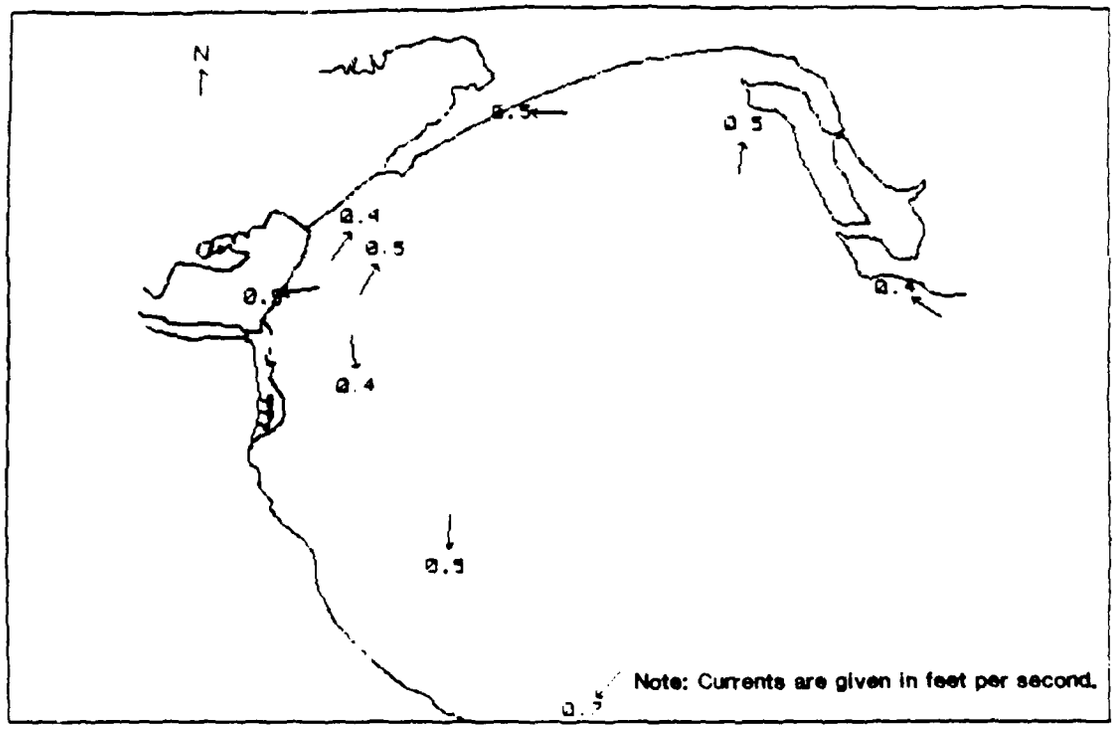

Figure A5. Depth-averaged velocities, 22 August 1984, near high water

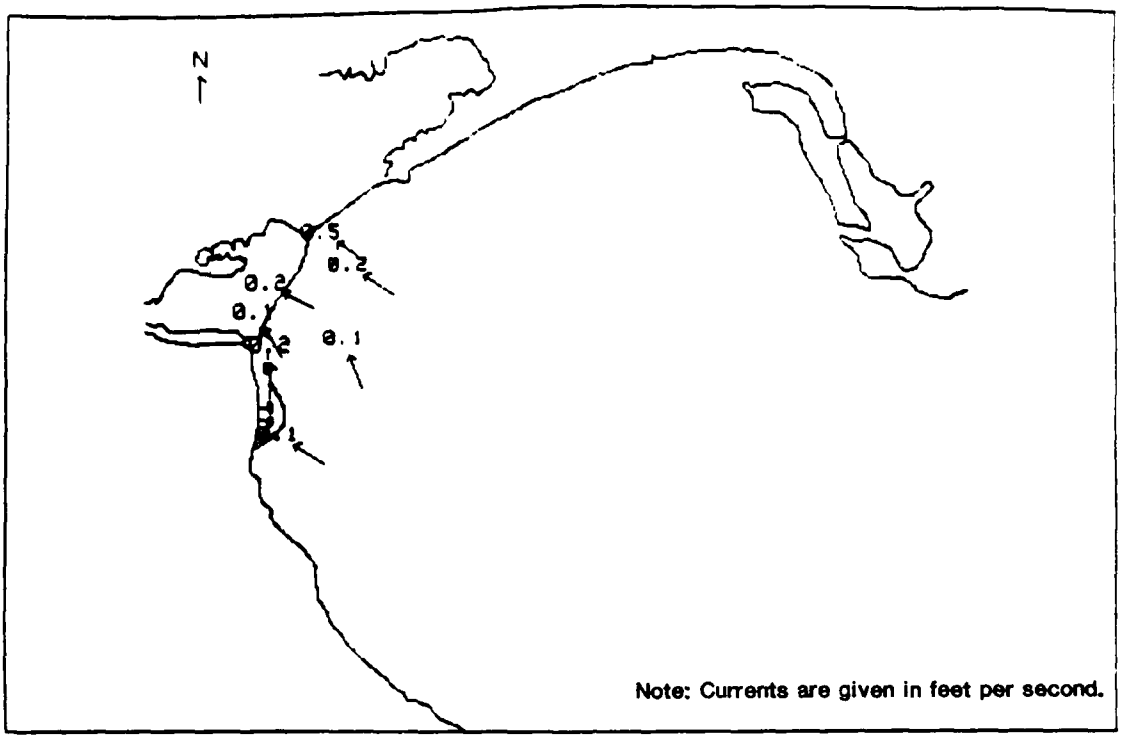

Figure A6. Depth-averaged velocities, 23 August 1984, flood tide

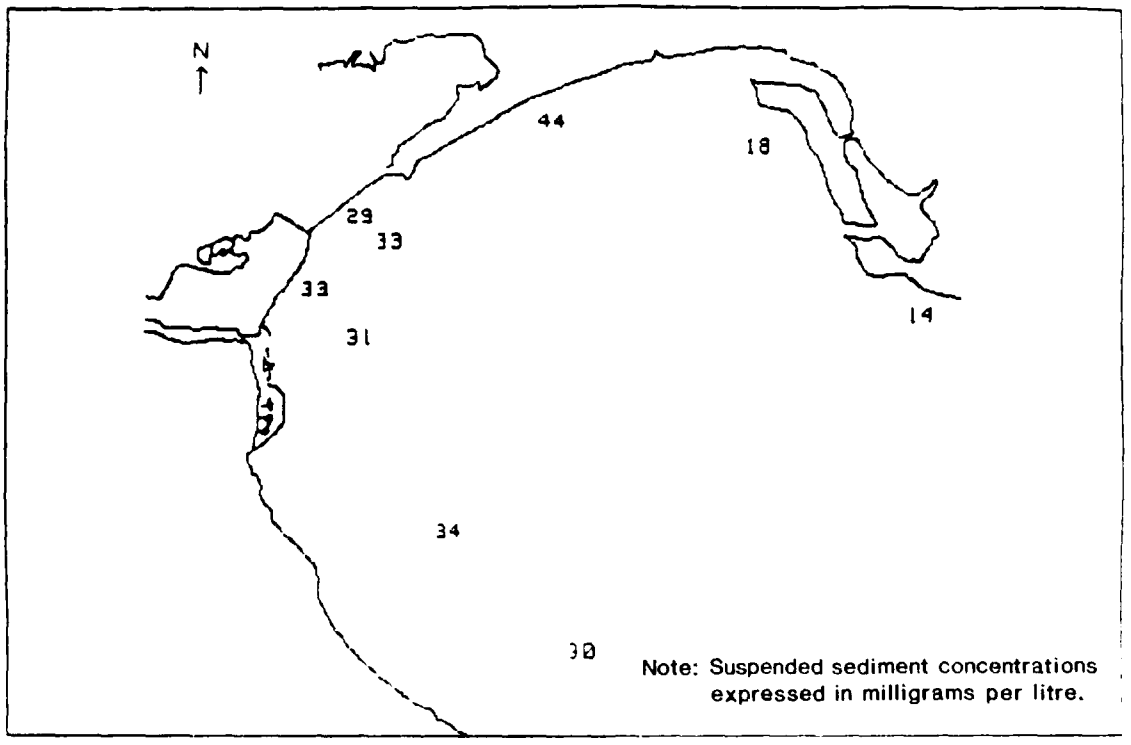

Figure A7. Depth-averaged CSM, 22 August 1984

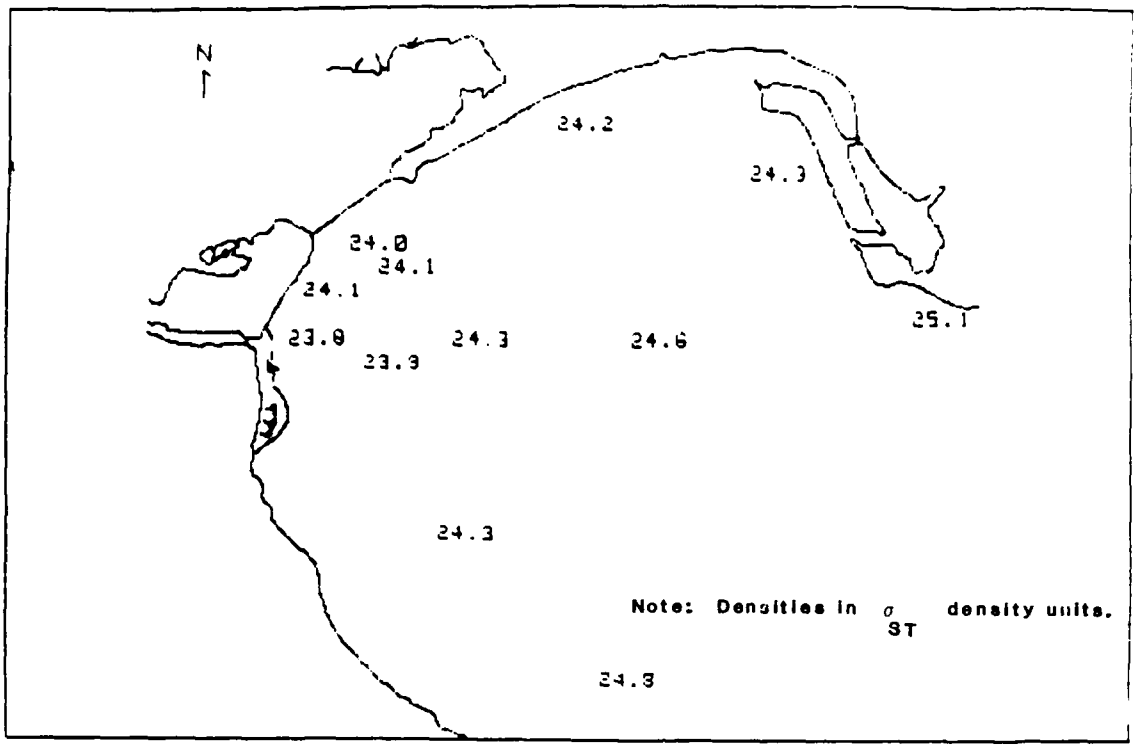

Figure A8. Depth-averaged σ_{ST}-C_{sm} densities, 22 August 1984

36. Initial bed densities were calculated from deposit thicknesses and sedimentation rates. The deposits grew essentially linearly during the tests, reached a maximum thickness, and then thinned. Table A11 shows estimated bed concentrations and densities for three times: when 50 percent of the material had settled (when available), when the peak bed thickness occurred, and at the end of the test.

37. Consolidation test results are summarized in Table A12. Initial and final concentrations and settling rates are given. Figure A9 summarizes the effect of concentration on settling rates from settling tube and consolidation tests. It can be seen that the rapid falloff in hindered settling velocity occurs between 0.1 and 0.2 g/cu cm. Hindered settling velocities at newly deposited concentrations are about 0.025 mm/sec. A characteristic time T for the newly deposited material to reach fully settled conditions can be approximated as $T = 8.5H_o$ where T is in hours and H_o is the initial height of the deposit in metres.

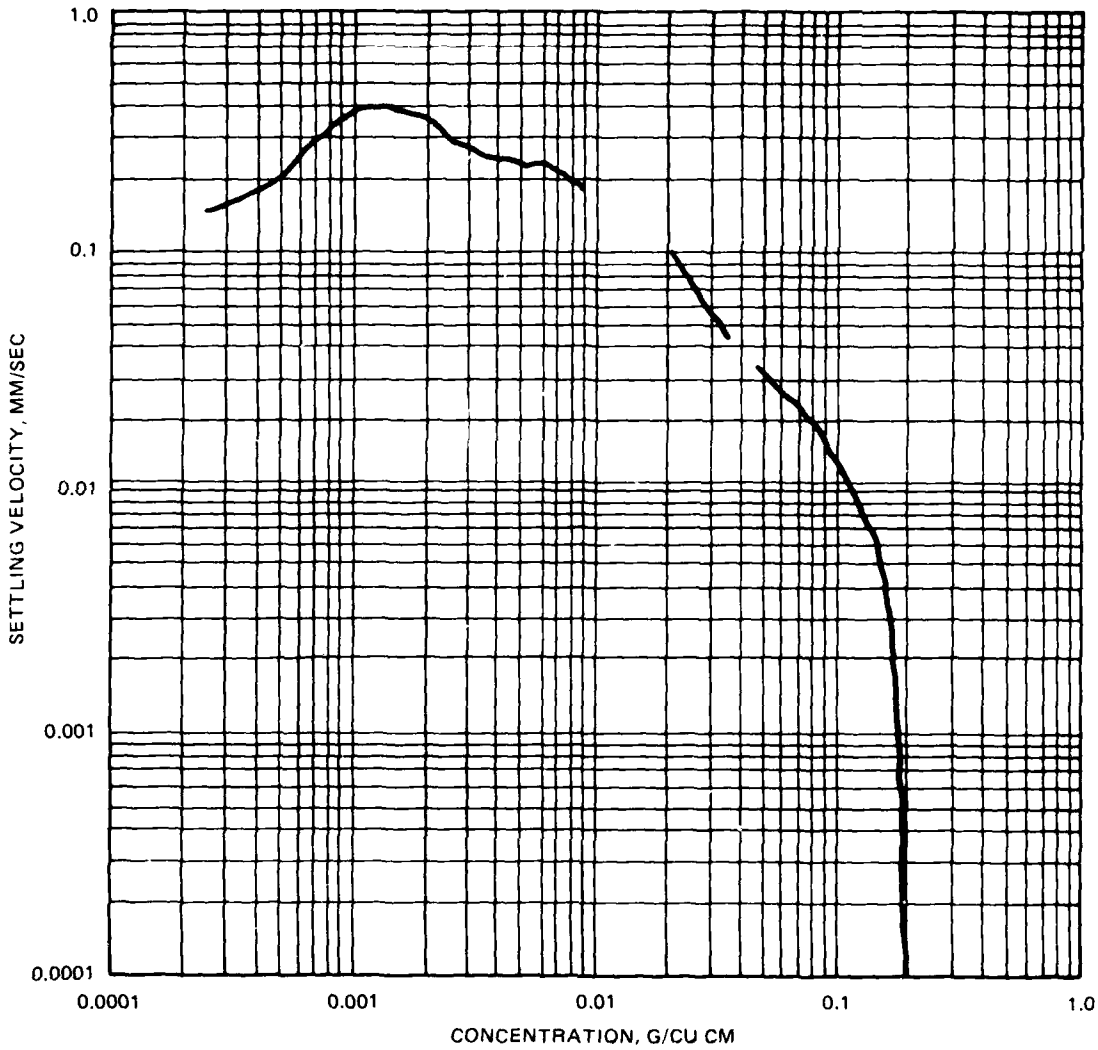

Figure A9. Effect of concentration on settling velocity from settling and consolidation tests

Discussion of Results

Critique of tests

38. The basic assumption of the reconnaissance survey was that conditions sampled were representative of conditions responsible for the shoaling. This implies that the shoaling is nearly continuous or constant and not dominated by extreme events such as storms or freshets. This assumption will be tested later by comparing calculated to observed shoaling rates.

39. Current speeds measured from the survey boat were found to be very

low in the harbor. As mentioned previously, attempts to make measurements from an anchored survey boat were not successful. The motion of the survey boat was apparently sufficient to contaminate the true current at the harbor stations. Even when the survey boat was moored tightly to piers, etc., the instrument readings were erratic and sometimes unreasonable. Currents were apparently at or below the threshold of the current meter. Results, therefore, are more qualitative than quantitative. Current measurements in the bay were not affected by this problem.

40. The current meter string was struck and dragged, presumably by a fishing boat. The string had been moved to shallower water when retrieved. Directions in the data were erratic, and therefore these data are also qualitative.

41. Because of the numbers of fishing boats in the bay and the relatively short periods spent in the bay during the survey, only one drogue deployment was carried out.

42. The settling tests relied on accurate CSM determination. Low CSM's made two of the field settling tests unreliable.

43. Core sampling of bed material was unsuccessful. A gravity corer of 100 lb was used on a handline. The device that retains the sample in the corer did not work properly.

44. Table A13 presents a summary of the CEC, loss on ignition, percent moisture, BWD, and clay-silt-sand distribution. Plates A52-A77 present dispersed particle size distribution plots for the samples.

Sources of sediments

45. CTH (1965) found that the Nueces River carried an average 300,000 cu yd of sediment annually. The material was much like the shoaling material in grain size. The reconnaissance survey also found some bed material in the bay similar to the shoaling material in grain size and other characteristics, but not in BWD. Some signs of bank erosion on the northern edge of Corpus Christi Bay were noted during the survey. It appears that there are multiple sources that supply fine-grained material to the bay.

46. Oso Bay Sewage Treatment Plant, which is similar in treatment level and magnitude to the effluent discharge to the harbor, discharges about 330,000 kg per year of waste solids. Because this is two orders of magnitude lower than the shoaling rate, waste solids do not seem to be contributing to shoaling directly.

47. The disposal of dredged material in the bay could have acted as a source of shoaling material. Hydraulically dredged fine-grained material has a concentration of roughly 0.075 g/ml. This material will assume a finite angle of repose only after it densifies to about 0.15 g/ml. Therefore the disposed material will spread over a large area before consolidating. The large surface area encourages the loss of material to erosion. Material which is consolidated from dense suspensions takes longer to reach a fully settled state than sediments which are settled from low concentration suspension. Even after 5 weeks of consolidation, sediments used in consolidation testing had reached concentrations of only 0.24 g/ml as opposed to their in-place concentrations of 0.36 g/ml. The shear strengths of these materials are very strongly dependent on concentration. Some studies have used a power law with an exponent of 2.5. Therefore, disposed dredged material probably remains more susceptible to erosion than the shoaled material from which it comes for a long period of time.

48. The highest CSM's found during the survey were in Corpus Christi Channel in the bay. The highest depth-averaged CSM was at DM#62 and the highest point sample CSM was at the breakwaters. These high CSM's were associated with the channel rather than the shallow areas of the bay. The channel is deep enough that wind-wave action did not disturb bed sediments. The characteristic settling time for the channel is about 16 hr based on settling velocities.

49. CSM's in the shallow parts of the bay were moderate. Although the afternoon wind conditions probably increased CSM's somewhat, it is unlikely that CSM in the bay would have compared to those in the channel. Currents in the shallow portions of the bay were strong enough to have kept most of the fine-grained material suspended. As mentioned in paragraph 47, fine-grained bed sediments of the shallow bay area are partially consolidated, with BWD's greater than 1.2. No repositories of newly deposited fine-grained material as fluid mud were discovered.

50. Fine-grained materials entering the bay from the Nueces system or by erosion of bed material could have been concentrated in the deep channel areas by several processes. Tidal currents in the channel were observed by drogues to be aligned with the channel. Currents in the shallow areas adjacent to the channel flowed obliquely to the channel. The surface layer of the channel, therefore, may be supplied with an advective source of suspended

material. Sediments which settled out of the surface layer could have been trapped in the channel. Also hypersaline waters formed by evaporation would tend to sink into the depths of the channel and may have carried sediments with them. Salinities associated with high CSM in the bay channel were the highest found on the survey.

51. Figure A10 shows a three-dimensional plot of CSM along the channel and with depth. It shows graphically the relative concentrations observed in the channel. The data collected during the reconnaissance survey indicate that sediments in suspension in the bay channel periodically intrude into the outer harbor. These suspended sediments, therefore, form the source with the most direct transport route to the harbor.

52. Figures A11-A14 show concentration probability plots for all channel stations, inner harbors, outer harbor, and bay channel, respectively. The ordinate is an exponential probability function. The distributions can be seen to be generally lognormal, although large surface-to-bottom differences may have distorted the distributions for the outer harbor and bay channel. Note the CSM's were generally lowest in the inner harbor, between Avery Point and Viola turning basins shown in Figure A14, and that there is a change in scale for this figure.

Transport of sediment

53. Sediments responsible for the shoaling in Corpus Christi Harbor are transported by circulations in the harbor and in the bay.

54. The circulation in the harbor is surprisingly strong. CTH (1965) indicated that while the tidal prism was 120 mgd during its survey, the flow into the harbor was 3,000 mgd. The 38-ft depth was dominated by flows entering the harbor during the entire tidal cycle, and the 30-ft depth was dominated by flows entering the harbor 88 percent of the time. The 3- and 12-ft depths were dominated by flows exiting the harbor.

55. The density-driven flows out of the harbor are equal to the freshwater (waste) discharges times their dilution. The vertical profiles of salinity from the reconnaissance survey were used to estimate the dilution of freshwater inflows to the harbor. Dilution can be estimated by $(S_e - S_a)/S_o - S_a)$ where S_e is the salinity of the effluent discharged into the harbor (assumed to be 3 ppt), S_a is the inflow salinity at the bottom of the channel, and S_o is the outflow salinity at the surface. Based on eight

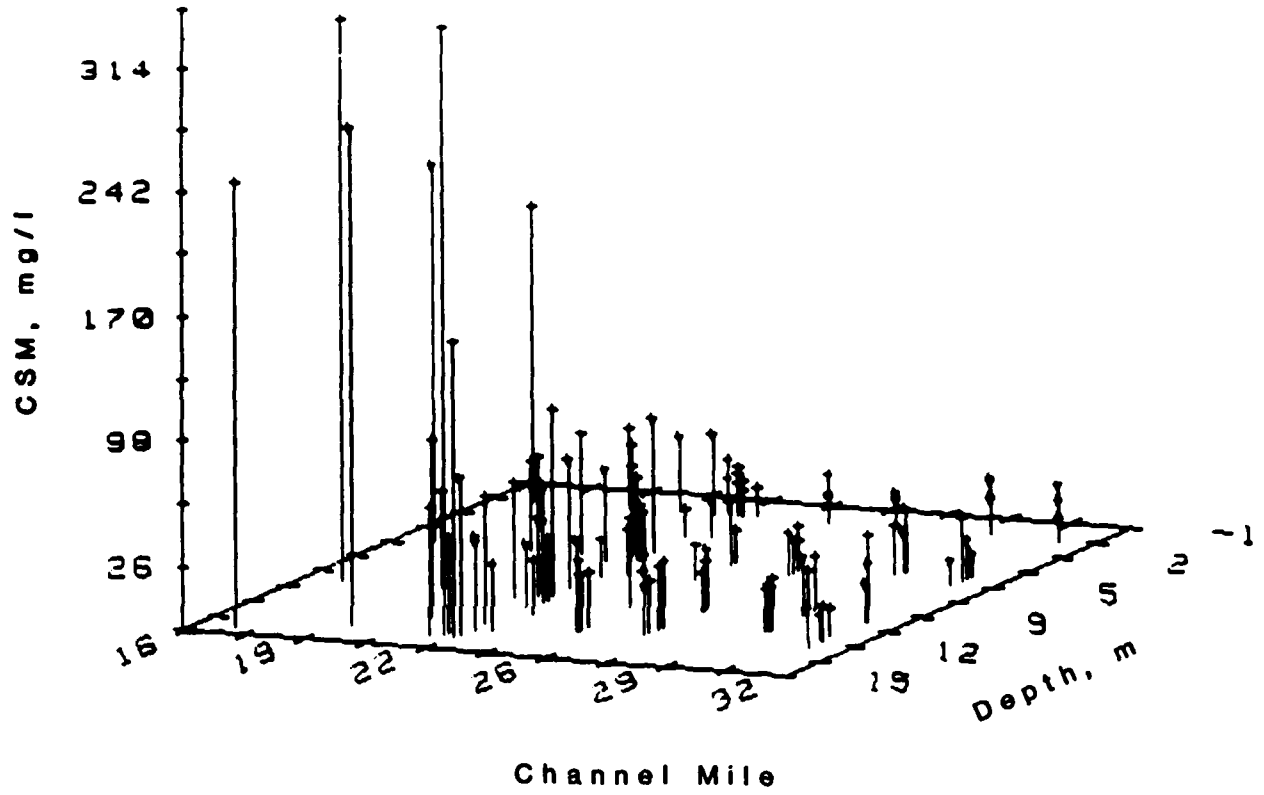

Figure A10. Three-dimensional plot of CSM with depth and channel mile

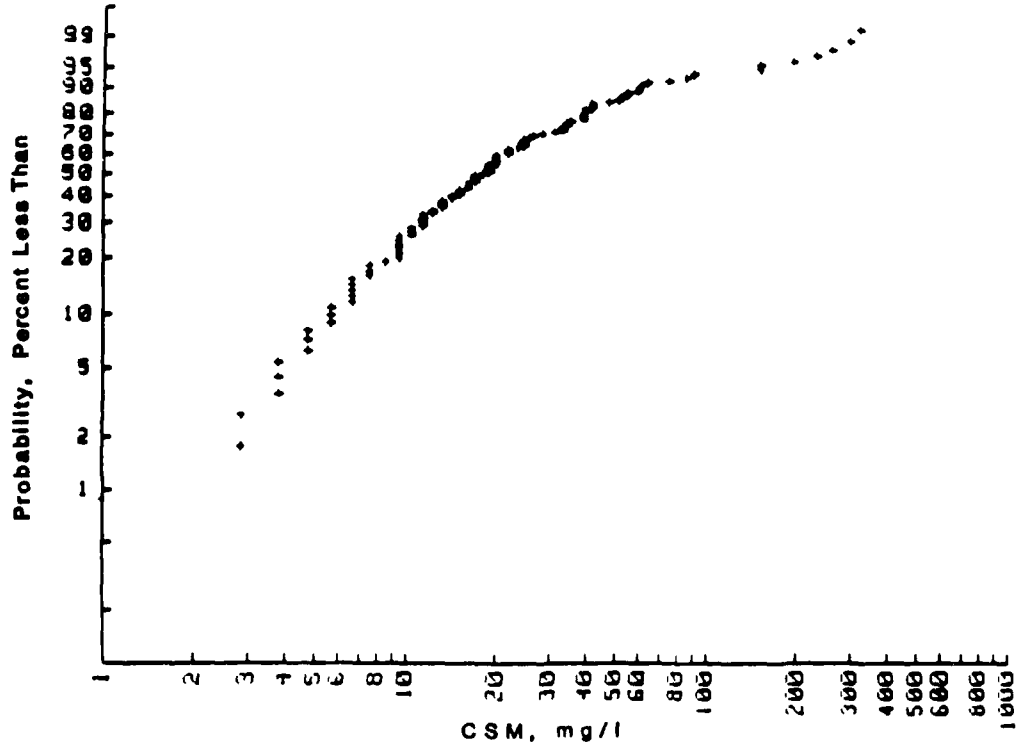

Figure A11. Weibull probability plot of all channel samples

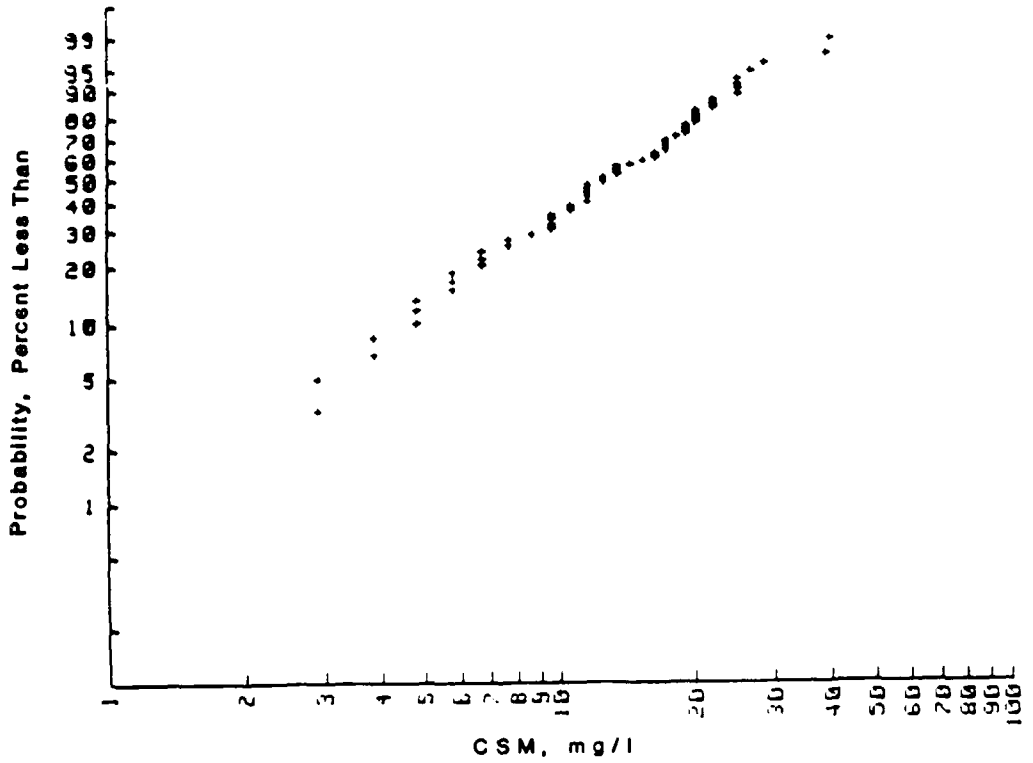

Figure A12. Weibull probability plot of harbor samples beyond Avery Point

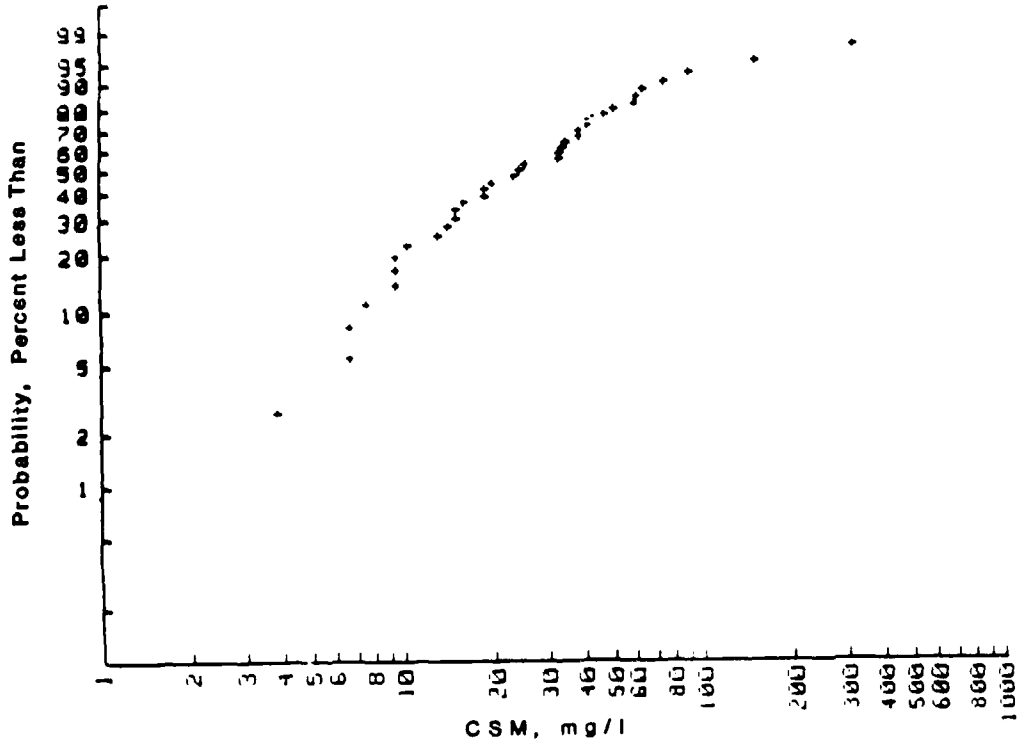

Figure A13. Weibull probability plot of harbor samples taken between the jetties and Avery Point

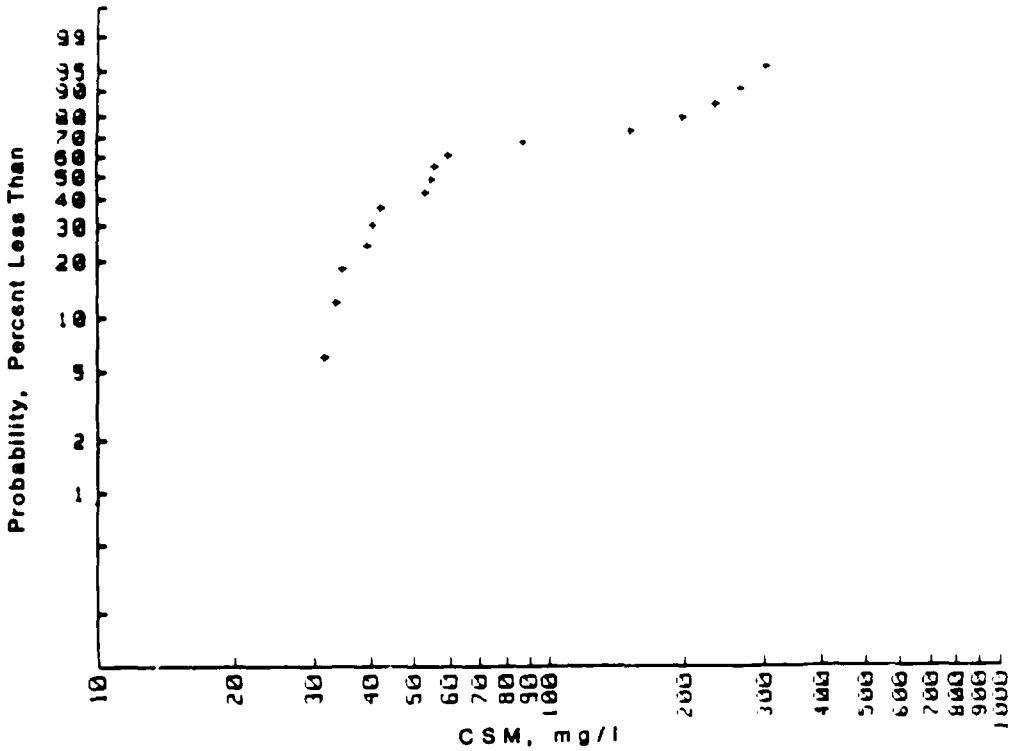

Figure A14. Weibull probability plot of Corpus Christi Bay-Channel samples

profiles from between the breakwaters, the Engineers dock, and the bridge, the average dilution was estimated as 43.

56. A flow budget was constructed assuming that the tide floods at the bottom and ebbs at the surface, that the freshwater discharges leave the harbor at the surface, and that withdrawals are made up of bottom water. The assumptions about the discharges and withdrawals follow from the dilution argument given earlier. Therefore, if only about 2 percent of the harbor water was composed of fresh discharges, only about 2 mgd of the fresh discharges would have been withdrawn from the harbor. Using the industrial withdrawals and discharges compiled in the CTH (1965) report, the following flow budget was constructed:

Source	Flows, mgd	
	Surface	Bottom
Tidal prism	-284	284
Dilution water	-645	645
Fresh discharges	-15	--
Withdrawals	--	80
Total	-944	1,009

The net flow into the harbor was assumed to be 65 mgd as indicated in the CTH report. The tidal prism is based on the average tide range.

57. The largest component of this budget can be seen to be the dilution water flow. Its magnitude is sensitive to the estimated dilution factor applied to the freshwater discharges. This flow was induced as a direct result of the freshwater discharges into the harbor.

58. The geometry of the system also contributes to the distribution of net flows in the harbor. The channel is 400 ft wide in the bay, and the breakwaters are 630 ft apart. At the bridge the channel narrows to 300 ft and then opens to about 1,000 ft in the turning basin. Constrictions in width have been found to produce converging near-bottom net currents in other tidal flows, and have been associated with shoaling areas. The shoaling area is centered about this constriction, with little shoaling occurring in the western end of the turning basin. In addition to producing a near-bottom convergence zone, the constriction also probably enhances mixing in the harbor and thus increases dilution water flows.

59. Circulation in the bay can be inferred from the σ_{ST}-C_{sm} distribution for 22 August (Figure A8). It appears that circulation is radially outward from the harbor entrance. Isopleths of density run generally north-south. The spot measurements of currents in the bay are for flood (21 and 23 August) (Figures A4 and A6, respectively) and near high water (22 August) (Figure A5). They indicate that typical bay current speeds are on the order of 0.5 ft/sec and generally counterclockwise during flood. In the Rincon channel area (RC#1-4, Figure A2), currents were strongly influenced by the Nueces Bay system. Drogues launched at CCB#1, shown in Figure A2, adjacent to the channel, closely paralleled the channel for 3.5 hr.

60. The contribution of CSM to density-driven flows was normally very small. When concentrations reached about 200 mg/ℓ, however, CSM did appear to contribute to both longitudinal gradients in the channel and to vertical gradients. Intrusion of bay-channel waters into the harbor may be enhanced by the presence in the bay channel of high concentrations of suspended material.

Deposition of sediment

61. Two methods were used to estimate shoaling rates in the harbor. Estimates were made to test the hypothesis that the reconnaissance survey represents important shoaling conditions.

62. One method of estimating shoaling uses a sediment budget, the

approach taken in the CTH (1965) report. The CTH approach used point measurements of CSM and currents at a single station on the eastern edge of the turning basin over a cycle. This method accounted for 158,000 cu yd annual shoaling rate as opposed to a rate of 550,000 cu yd established from dredging records.

63. A flow budget was presented previously. When that budget is combined with eight CSM profiles (three flood, three ebb, and two slack water), the mass of sediment settling can be estimated by $(CSM*Q)_{in} - (CSM*Q)_{out}$ where Q is the inflow is at the bottom and the outflow at the surface. With a conversion for a specific weight of 361 kg/cu m (22.5 lb dry weight/cu ft) obtained from laboratory analyses of BWD, the estimated annual shoaling volume was 445,000 cu yd total for the harbor. The total harbor shoaling was estimated to be 910,000 cu yd per year by dredging records in the CTH (1965) report.

64. The second estimate of shoaling was obtained by calculating settling flux. The mass rate of deposition was assumed to be equal to the bottom CSM times the settling velocity (0.25 mm/sec). It was assumed that all sediment particles which settle stick to the bed.

65. For the outer channel between the breakwaters and the bridge, the average near-bottom concentration was 99.5 mg/ℓ. The estimated average shoaling was 7.2 ft per year or an average shoaling rate of 1,000,000 cu yd per year.

66. The turning basin had an average near-bottom CSM of 28.2 mg/ℓ. This yielded a shoaling thickness of 2 ft per year or 239,000 cu yd per year. The combined shoaling for the outer channel and turning basin was 1,239,000 cu yd per year.

67. The two estimates of shoaling rates bracket the rates reported in the CTH report (1965). The spread of these estimates is not unusual and is due to their assumptions, and to the data on which they are based.

68. The conditions found during the reconnaissance survey appear to be representative of those responsible for shoaling, although episodic events may also be important.

Conclusions

69. It appears that the shoaling problem is caused by high

concentrations of suspended material in the bay channel which are transported along that channel and drawn into the harbor by a strong density current. Low bottom velocities and relatively high settling rates allow the particles to settle and consolidate near the channel convergence of the outer harbor.

AD-A189 323 CORPUS CHRISTI INNER HARBOR SHOALING INVESTIGATION(U) 2/3
CAVER (TROY V) DOVER NJ T M SMITH ET AL. SEP 87
WES/TR/HL-87-13

UNCLASSIFIED F/G 13/2 NL

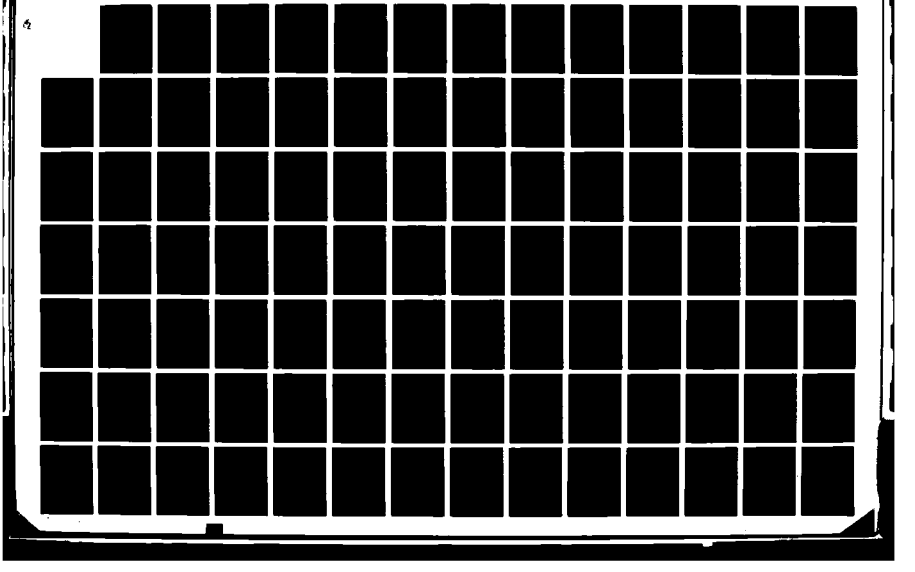

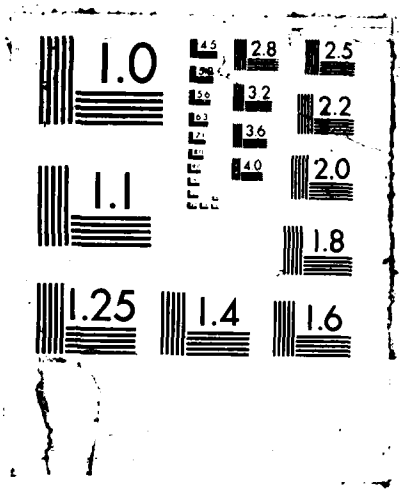
1.0
1.1
1.25
1.4
1.6
1.8
2.0
2.2
2.5
2.8
3.2
3.6
4.0

Table A1

Location and Nomenclature of Water Column Sampling Stations in the Channel

Channel Mile	Location	Abbreviation
31.0	Viola Turning Basin	Viola
29.2	Tule Lake Turning Basin day marker	DM#2
26.7	Tule Lake near bulk materials dock (day marker)	DM#9
24.9	Avery Point Turning Basin	AP
23.0	Corpus Christi Harbor Turning Basin	TB
22.6	Highway 181 Bridge overpass	Brdg
22.5	Engineers dock	Eng Dk
22.2	Between breakwaters at harbor entrance	Jetty
21.8	Corpus Christi Channel day marker	DM#82
20.9	Corpus Christi Channel day marker	DM#80
19.6	Corpus Christi Channel day marker	DM#74
17.0	Corpus Christi Channel day marker	DM#62

Table A2

Location and Nomenclature of Water Column Sampling Stations in the Bay

Description	Abbreviation
Rincon Channel	
Rincon Channel near causeway (pile)	RC#1
Rincon Channel day marker 10	RC#2
Rincon Channel day marker 6	RC#3
Halfway between RC#3 and DM#80	RC#4
Destroyed pier 0.6 miles north of breakwater	RC#5
Corpus Christi Bay	
Range marker south of DM#80	CCB#1
Sun Oil platform	CCB#2
Cities Service platform	CCB#3
Destroyed range marker to old harbor city entrance	CCB#4
Gas wellhead	CCB#5
Portland	CCB#6
Day marker south and east of Corpus Christi Small Boat Harbor	CCB#7
Breakwater opening (day marker 1)	CCB#8
Adjacent to Channel	
Day marker	DM#80B
Day marker	DM#82B
Day marker	DM#86

Table A3

Bed Sample Locations

Sample No.	Location/Station	Channel Mile
1	Corpus Christi Turning Basin/TB	22.8
2	Corpus Christi Turning Basin	23.2
3	Avery Point Turning Basin/AP	24.9
4	Chemical Turning Basin	25.8
5	Tule Lake Turning Basin	29.1
6	Viola Turning Basin	31.2
7	Viola Turning Basin/Viola	31.0
8	Viola Channel	29.8
9	Tule Lake Channel	27.3
10	Tule Lake Channel - North Flank	27.1
11	Tule Lake Channel Bulk Materials Dock/DM#9	26.7
12	Chemical Turning Basin	25.7
13	Chemical Turning Basin - North Flank	25.7
14	Under 181 Bridge/Bridge	22.6
15	Engineers Dock	22.5
16	Between breakwaters/jetties	22.2
17	Rincon Channel/RC#1	--
18	Rincon Channel/RC#2	--
19	Rincon Channel/RC#3	--
20	Between Rincon Channel and DM#80/RC#4	--
21	Corpus Christi Channel DM#80/DM#80B	20.9
22	Corpus Christi Channel DM#80 center line/DM#80	20.9
23	Corpus Christi Channel DM#82/DM#82B	21.8
24	Corpus Christi Channel center line at DM#82/DM#82	21.8
25	Between breakwaters/jetties	22.2
26	Off north breakwater at DM#86	--

Table A4

Sample Data for 20 August 1984

Station	Time CST	Depth m	Salinity ppt	Temperature °C	σ_{ST}	CSM mg/ℓ	$\sigma - C_{sm}$	$\sigma_{ST} - C_{sm}$
Eng Dk	1340	10.5	37.4	29.6	23.7	26	0.0	23.7
		7.0	37.1	29.7	23.4	10	0.0	23.4
		3.1	36.7	29.9	23.1	7	0.0	23.1
AP	1415	11.7	37.0	29.0	23.6	21	0.0	23.6
		6.3	36.2	29.2	22.9	5	0.0	22.9
		0.6	36.3	29.9	22.8	5	0.0	22.8
DM#9	1440	11.4	36.7	28.8	23.4	28	0.0	23.4
		5.6	36.2	29.3	22.9	13	0.0	22.9
		0.6	36.0	30.1	22.5	7	0.0	22.5
DM#2	1503	10.8	36.5	28.9	23.2	14	0.0	23.3
		6.2	36.0	29.8	22.6	20	0.0	22.6
		0.6	36.9	29.9	22.5	10	0.0	22.5
Viola	1525	11.1	36.7	28.8	23.4	6	0.0	23.4
		5.6	35.9	30.4	22.3	4	0.0	22.3
		0.6	35.9	30.7	22.2	3	0.0	22.2

Table A5

Sample Data for 21 August 1984

Station	Time CST	Depth m	Salinity ppt	Temperature °C	σ_{ST}	CSM mg/ℓ	σ-C_{sm}	σ_{ST}-C_{sm}
RC#1	0615	1.0	37.8	28.8	24.3	32	0.0	24.3
		0.3	37.6	28.9	24.1	33	0.0	24.1
RC#2	0635	2.4	37.6	29.1	24.0	81	0.1	24.1
		0.6	38.0	28.9	24.4	65	0.0	24.4
RC#3	0645	3.5	37.4	29.0	23.9	45	0.0	23.9
		2.1	37.4	29.0	23.9	45	0.0	23.9
		0.6	37.6	29.0	24.0	46	0.0	24.1
RC#4	0710	3.5	37.4	29.0	23.9	41	0.0	23.9
		2.0	37.4	29.0	23.9	35	0.0	23.9
		0.6	37.5	28.9	24.0	19	0.0	24.0
DM#80B	0725	4.0	37.3	29.1	23.8	41	0.0	23.8
		2.9	37.3	29.2	23.8	44	0.0	23.8
		0.6	37.4	29.1	23.8	28	0.0	23.9
DM#80	0730	12.0	37.3	29.2	23.8	91	0.1	23.8
		7.1	37.3	29.3	23.8	55	0.0	23.8
		5.1	37.3	29.3	23.7	58	0.0	23.8
		0.6	37.4	29.2	23.8	33	0.0	23.8
DM#82B	0750	4.1	38.0	29.1	24.3	96	0.1	24.3
		2.8	37.3	29.1	23.8	28	0.0	23.8
		0.6	37.5	29.3	23.9	31	0.0	23.9
DM#82	0815	13.7	37.5	29.1	24.0	62	0.0	24.0
		9.8	37.7	29.2	24.0	57	0.0	24.1
		5.6	37.4	29.2	23.9	42	0.0	23.9
		0.6	37.6	29.3	23.9	35	0.0	24.0
Jetty	0835	13.5	37.7	29.2	24.0	44	0.0	24.1
		9.4	37.6	29.3	24.0	35	0.0	24.0
		5.0	37.2	29.4	23.6	54	0.0	23.7
		0.6	36.9	29.5	23.4	10	0.0	23.4
Brdg	0920	13.0	37.7	29.3	24.0	41	0.0	24.0
		9.9	37.6	29.3	24.0	36	0.0	24.0
		5.4	37.0	29.6	23.4	16	0.0	23.4
		0.6	36.8	29.6	23.3	4	0.0	23.3

(Continued)

Table A5 (Concluded)

Station	Time CST	Depth m	Salinity ppt	Temperature °C	σ_{ST}	CSM mg/ℓ	σ-C_{sm}	σ_{ST}-C_{sm}
Viola	1130	11.6	36.1	29.4	22.8	5	0.0	22.8
		9.4	36.0	29.8	22.6	23	0.0	22.6
		5.0	35.8	30.1	22.3	26	0.0	22.3
		0.6	34.5	31.1	21.0	21	0.0	21.1
DM#2	1200	10.7	36.1	29.3	22.8	19	0.0	22.8
		9.3	36.1	29.4	22.8	23	0.0	22.8
		4.5	36.1	29.4	22.7	26	0.0	22.8
		0.6	36.0	29.5	22.6	21	0.0	22.7
DM#9	1215	11.6	36.5	29.1	23.2	26	0.0	23.2
		9.5	36.3	29.2	23.0	18	0.0	23.0
		5.1	36.2	29.3	22.9	19	0.0	22.9
		0.6	36.1	29.4	22.8	6	0.0	22.8
AP	1235	12.1	37.3	29.4	23.7	21	0.0	23.7
		9.2	37.2	29.3	23.7	7	0.0	23.7
		4.9	36.4	29.4	23.0	8	0.0	23.0
		0.6	36.4	29.5	23.0	4	0.0	23.0
Eng Dk	1253	12.3	37.5	29.2	23.9	63	0.0	24.0
		9.7	37.5	29.3	23.8	35	0.0	23.9
		5.2	36.9	29.7	23.3	20	0.0	23.3
		0.6	36.9	29.9	23.2	8	0.0	23.2

Table A6

Sample Data for 22 August 1984

Station	Time CST	Depth m	Salinity ppt	Temperature °C	σ_{ST}	CSM mg/ℓ	σ-C_{sm}	σ_{ST}-C_{sm}
Eng Dk	0605	13.5	37.6	29.3	23.9	79	0.0	24.0
		8.5	37.5	29.4	23.8	64	0.0	23.9
		5.3	37.5	29.4	23.8	37	0.0	23.8
		0.6	37.1	29.1	23.6	14	0.0	23.6
CCB#1	0620	3.3	37.5	29.4	23.8	31	0.0	23.8
		0.6	37.6	29.3	23.9	32	0.0	23.9
CCB#2	0645	4.0	37.6	29.0	24.1	42	0.0	24.1
		2.1	37.8	28.9	24.2	23	0.0	24.2
		0.6	38.1	28.7	24.5	41	0.0	24.5
CCB#3	0700	4.0	38.8	29.1	24.9	42	0.0	25.0
		1.9	38.8	29.2	24.7	35	0.0	24.8
		0.6	38.7	29.2	24.8	14	0.0	24.8
CCB#4	0730	1.1	38.7	28.7	25.0	14	0.0	25.0
		0.3	38.9	28.7	25.1	13	0.0	25.1
CCB#5	0800	2.5	38.0	29.2	24.3	17	0.0	24.3
		0.6	37.9	29.2	24.2	19	0.0	24.2
CCB#6	0815	2.4	37.6	28.8	24.1	55	0.0	24.2
		0.6	37.7	28.9	24.1	32	0.0	24.1
RC#1	0835	1.0	37.7	29.3	24.0	31	0.0	24.0
		0.3	37.7	29.3	24.0	27	0.0	24.0
RC#5	0850	3.0	37.8	29.2	24.2	39	0.0	24.2
		0.6	37.7	29.4	24.0	28	0.0	24.0
RC#2	0900	2.6	37.7	29.3	24.0	58	0.0	24.1
		0.6	37.7	29.4	24.0	49	0.0	24.0
DM#62	0921	14.3	39.1	29.4	25.1	244	0.2	25.2
		9.4	38.7	29.3	24.8	315	0.2	25.0
		5.2	37.6	29.1	24.0	206	0.1	24.1
		0.6	37.4	29.3	23.8	158	0.1	23.9
DM#74	0940	13.5	38.9	29.3	24.9	276	0.2	25.1
		9.3	38.1	29.3	24.3	44	0.0	24.4
		5.2	37.5	29.3	23.9	41	0.0	23.9
		0.6	37.5	29.5	23.8	36	0.0	23.8

(Continued)

Table A6 (Concluded)

Station	Time CST	Depth m	Salinity ppt	Temperature °C	σ_{ST}	CSM mg/ℓ	σ-C_{sm}	σ_{ST}-C_{sm}
Jetty	1000	13.7	37.8	29.4	24.0	340	0.2	24.3
		9.2	37.7	29.4	24.0	50	0.0	24.0
		5.0	37.2	29.3	23.6	41	0.0	23.7
		0.6	36.9	29.7	23.3	21	0.0	23.3
Eng Dk	1222	13.8	37.8	29.4	24.1	159	0.1	24.2
		9.2	37.7	29.3	24.0	96	0.1	24.0
		4.6	37.2	29.5	23.6	67	0.0	23.6
		0.6	36.8	30.0	23.1	17	0.0	23.1
AP	1240	12.3	37.1	29.4	23.5	42	0.0	23.5
		9.8	36.9	29.4	23.3	41	0.0	23.4
		5.2	36.7	29.4	23.2	26	0.0	23.2
		0.6	36.6	30.0	22.9	18	0.0	23.0
DM#9	1255	12.0	36.3	29.2	23.0	20	0.0	23.0
		9.4	36.3	29.3	22.9	17	0.0	22.9
		5.1	36.1	29.4	22.8	15	0.0	22.8
		0.6	36.2	30.0	22.6	10	0.0	22.7
DM#2	1310	11.0	36.0	29.4	22.7	14	0.0	22.7
		9.0	35.9	29.5	22.6	14	0.0	22.6
		5.0	36.0	29.9	22.6	18	0.0	22.6
		0.6	36.1	30.1	22.5	23	0.0	22.5
Viola	1325	11.5	36.1	29.4	22.8	10	0.0	22.8
		9.0	35.3	29.7	22.1	11	0.0	22.1
		4.8	35.9	30.1	22.4	12	0.0	22.4
		0.6	36.1	30.4	22.4	12	0.0	22.4

Table A7

Sample Data for 23 August 1984

Station	Time CST	Depth m	Salinity ppt	Temperature °C	σ_{ST}	CSM mg/ℓ	σ-C_{sm}	σ_{ST}-C_{sm}
CCB#1	0650	3.1	37.5	29.5	23.8	36	0.0	23.8
		1.4	37.5	29.5	23.8	27	0.0	23.8
		0.6	37.5	29.5	23.8	25	0.0	23.8
CCB#7	0700	2.5	37.4	29.1	23.9	25	0.0	23.9
		0.6	37.4	29.1	23.9	24	0.0	23.9
CCB#8	0710	1.3	37.3	28.8	23.9	28	0.0	23.9
		0.6	37.4	28.8	23.9	29	0.0	23.9
DM#82B	0720	1.5	37.0	29.1	23.6	13	0.0	23.6
		0.6	37.1	29.2	23.6	8	0.0	23.6
DM#86	0730	3.1	37.4	29.6	23.7	19	0.0	23.7
		0.6	37.1	29.5	23.5	16	0.0	23.5
Brdg	0832	13.0	37.9	29.6	24.1	44	0.0	24.1
		9.6	37.8	29.6	24.0	25	0.0	24.0
		5.2	37.4	29.6	23.7	16	0.0	23.7
		0.6	36.9	29.5	23.3	10	0.0	23.3
TB	0850	12.9	37.5	29.4	23.9	27	0.0	23.9
		11.0	37.5	29.5	23.8	20	0.0	23.8
		6.6	37.6	29.6	23.8	15	0.0	23.8
		2.8	36.9	29.6	23.3	11	0.0	23.3
		0.6	36.8	29.6	23.3	7	0.0	23.3
AP	0905	12.9	37.5	29.4	23.8	30	0.0	23.8
		9.2	37.0	29.4	23.5	17	0.0	23.5
		6.8	36.8	29.3	23.3	9	0.0	23.3
		0.6	36.7	29.4	23.2	7	0.0	23.2
DM#9	0925	12.3	36.8	29.4	23.3	18	0.0	23.3
		9.6	36.5	29.3	23.1	11	0.0	23.1
		5.4	36.3	29.3	23.0	10	0.0	23.0
		0.6	36.3	29.2	23.0	8	0.0	23.0
DM#2	0950	10.9	36.1	29.4	22.8	16	0.0	22.8
		8.7	36.0	29.4	22.7	20	0.0	22.8
		4.6	36.1	29.4	22.7	12	0.0	22.7
		0.6	36.1	29.4	22.8	12	0.0	22.8
Viola	1010	12.2	36.1	29.7	22.6	12	0.0	22.6
		9.5	36.1	29.8	22.6	13	0.0	22.6
		4.6	36.1	30.0	22.6	3	0.0	22.6
		0.6	36.1	30.2	22.5	1	0.0	22.5

Table A8

Field Settling Tests

Salinity ppt	Weighted Average Distribution mm/sec	Standard Deviation	Concentration mg/ℓ	Geometric Mean mm/sec	Skewness	Settling Height, m	Kortosis	Cumulative Percent >	Cumulative Settling Velocity mm/sec	Differential Settling Velocity mm/sec	Differential Concentration mg/ℓ
				Station Rincon 3, 21 August 1984							
37.4	0.191	4.6	41	0.063	0.18	0.85	0.43	10	4.609E-01	1.9683-0.6561	2.6
								20	2.203E-01	0.6561-0.2187	5.7
								30	1.231E-01	0.2187-0.0729	8.4
								40	7.490E-02	0.0729-0.0243	11.1
								50	4.822E-02	0.0243-0.0081	13.3
								60	3.233E-02	0.0081-0.0027	0.0
								70	2.236E-02	0.0027-0.0009	0.0
								80	1.586E-02	0.0009-0.0003	0.0
								90	1.147E-02	Total classes	41.1
				Station 181 Bridge, 21 August 1984							
37.5	0.463	5.6	26	0.264	0.19	0.85	0.45	10	2.561E+00	1.9683-0.6561	6.1
								20	1.074E+00	0.6561-0.2187	5.2
								30	5.510E-01	0.2187-0.0729	6.6
								40	3.138E-01	0.0729-0.0243	7.1
								50	1.911E-01	0.0243-0.0081	0.0
								60	1.220E-01	0.0081-0.0027	0.0
								70	8.080E-02	0.0027-0.0009	0.0
								80	5.504E-02	0.0009-0.0003	0.0
								90	3.837E-02	Total classes	25.0
				Station 181 Bridge, 22 August 1984							
37.5	0.199	16.2	45	0.022	0.18	0.85	0.43	10	8.292E-01	1.9683-0.6561	4.7
								20	2.159E-01	0.6561-0.2187	3.8
								30	7.426E-02	0.2187-0.0729	4.6
								40	2.982E-02	0.0729-0.0243	5.5
								50	1.327E-02	0.0243-0.0081	6.4
								60	6.357E-03	0.0081-0.0027	7.3
								70	3.224E-03	0.0027-0.0009	8.1
								80	1.711E-03	0.0009-0.0003	4.1
								90	9.424E-04	Total classes	44.5

(Continued)

Table A8 (Concluded)

Salinity ppt	Weighted Average Distribution mm/sec	Standard Deviation	Concentration mg/ℓ	Geometric Mean mm/sec	Skewness	Settling Height, m	Kortosis	Cumulative Percent >	Cumulative Settling Velocity mm/sec	Differential Settling Velocity mm/sec	Differential Concentration mg/ℓ
Station 181 Bridge, 23 August 1984											
37.6	0.146	3.1	20	0.101	0.21	0.85	0.57	10	4.778E-01	1.9683-0.6561	0.0
								20	2.513E-01	0.6561-0.2187	3.2
								30	1.596E-01	0.2187-0.0729	6.0
								40	1.101E-01	0.0729-0.0243	8.9
								50	7.975E-02	0.0243-0.0081	0.5
								60	5.975E-02	0.0081-0.0027	0.0
								70	4.589E-02	0.0027-0.0009	0.0
								80	3.594E-02	0.0009-0.0003	0.0
								90	2.859E-02	Total classes	18.6

Table A9

Laboratory Settling Tests on Field Samples

Salinity ppt	Weighted Average Distribution mm/sec	Standard Deviation	Concentration mg/ℓ	Geometric Mean mm/sec	Skewness	Settling Height, m	Kortosis	Cumulative Percent >	Cumulative Settling Velocity mm/sec	Differential Settling Velocity mm/sec	Differential Concentration mg/ℓ
Station Avery Point - Corpus Christi Harbor Turning Basin, 22 August 1984											
36.8	1.054	7.1	46	2.231	0.15	1.80	0.39	10	2.038E+01	1.9683-0.6561	34.3
								20	1.318E+01	0.6561-0.2187	6.3
								30	8.311E+00	0.2187-0.0729	4.8
								40	5.087E+00	0.0729-0.0243	0.6
								50	3.002E+00	0.0243-0.0081	0.0
								60	1.692E+00	0.0081-0.0027	0.0
								70	8.970E-01	0.0027-0.0009	0.0
								80	4.364E-01	0.0009-0.0003	0.0
								90	1.856E-01	Total classes	46.0
Station Engineers Dock, 22 August 1984											
37.6	0.395	6.9	35	0.154	0.20	1.80	0.48	10	2.060E+00	1.9683-0.6561	7.5
								20	7.446E-01	0.6561-0.2187	5.5
								30	3.475E-01	0.2187-0.0729	7.0
								40	1.838E-01	0.0729-0.0243	8.6
								50	1.052E-01	0.0243-0.0081	6.4
								60	6.361E-02	0.0081-0.0027	0.0
								70	4.009E-02	0.0027-0.0009	0.0
								80	2.610E-02	0.0009-0.0003	0.0
								90	1.745E-02	Total classes	35.0
Station 181 Bridge, 23 August 1984											
37.6	0.156	17.3	28	0.010	0.19	1.80	0.44	10	4.138E-01	1.9683-0.6561	2.1
								20	9.998E-02	0.6561-0.2187	1.9
								30	3.316E-02	0.2187-0.0729	2.4
								40	1.302E-02	0.0729-0.0243	2.9
								50	5.699E-03	0.0243-0.0081	3.5
								60	2.697E-03	0.0081-0.0027	4.0
								70	1.354E-03	0.0027-0.0009	4.6
								80	7.129E-04	0.0009-0.0003	5.1
								90	3.900E-04	Total classes	26.5

Table A10

Laboratory Settling Tests on Resuspended Sediment

Salinity ppt	Weighted Average Distribution mm/sec	Standard Deviation	Concentration mg/l	Geometric Mean mm/sec	Skewness	Settling Height, m	Kortosis	Cumulative Percent >	Cumulative Settling Velocity mm/sec	Differential Settling Velocity mm/sec	Differential Concentration mg/l
32.5	0.271	2.1	250	0.172	0.19	1.80	0.47	10	4.680E-01	1.9683-0.6561	10.8
								20	3.167E-01	0.6561-0.2187	71.4
								30	2.359E-01	0.2187-0.0729	144.6
								40	1.843E-01	0.0729-0.0243	23.1
								50	1.483E-01	0.0243-0.0081	0.0
								60	1.220E-01	0.0081-0.0027	0.0
								70	1.019E-01	0.0027-0.0009	0.0
								80	8.625E-02	0.0009-0.0003	0.0
								90	7.374E-02	Total classes	249.9
32.5	0.309	2.0	507	0.228	0.17	1.80	0.42	10	5.741E-01	1.9683-0.6561	19.4
								20	4.104E-01	0.6561-0.2187	198.7
								30	3.132E-01	0.2187-0.0729	274.0
								40	2.481E-01	0.0729-0.0243	0.0
								50	2.016E-01	0.0243-0.0081	0.0
								60	1.669E-01	0.0081-0.0027	0.0
								70	1.401E-01	0.0027-0.0009	0.0
								80	1.190E-01	0.0009-0.0003	0.0
								90	1.020E-01	Total classes	492.1
32.5	0.388	1.5	742	0.291	0.20	1.80	0.48	10	4.625E-01	1.9683-0.6561	0.0
								20	4.245E-01	0.6561-0.2187	572.7
								30	3.875E-01	0.2187-0.0729	115.6
								40	3.513E-01	0.0729-0.0243	0.0
								50	3.156E-01	0.0243-0.0081	0.0
								60	2.803E-01	0.0081-0.0027	0.0
								70	2.448E-01	0.0027-0.0009	0.0
								80	2.082E-01	0.0009-0.0003	0.0
								90	1.677E-01	Total classes	688.3

(Continued)

Table A10 (Concluded)

Salinity ppt	Weighted Average Distribution mm/sec	Standard Deviation	Concentration mg/ℓ	Geometric Mean mm/sec	Skewness	Settling Height, m	Kortosis	Cumulative Percent >	Cumulative Settling Velocity mm/sec	Differential Settling Velocity mm/sec	Differential Concentration mg/ℓ
37.5	0.563	1.9	1,250	0.374	0.07	1.80	0.33	10	7.966E-01	1.9683-0.6561	268.6
								20	6.731E-01	0.6561-0.2187	714.9
								30	5.655E-01	0.2187-0.0729	266.5
								40	4.723E-01	0.0729-0.0243	0.0
								50	3.917E-01	0.0243-0.0081	0.0
								60	3.224E-01	0.0081-0.0027	0.0
								70	2.631E-01	0.0027-0.0009	0.0
								80	2.125E-01	0.0009-0.0003	0.0
								90	1.697E-01	Total classes	1,250.0
37.5	0.485	1.7	1,840	0.370	0.11	1.80	0.35	10	7.124E-01	1.9683-0.6561	198.1
								20	5.816E-01	0.6561-0.2187	1,278.5
								30	4.839E-01	0.2187-0.0729	305.3
								40	4.085E-01	0.0729-0.0243	0.0
								50	3.488E-01	0.0243-0.0081	0.0
								60	3.007E-01	0.0081-0.0027	0.0
								70	2.613E-01	0.0027-0.0009	0.0
								80	2.286E-01	0.0009-0.0003	0.0
								90	2.012E-01	Total classes	1,781.9

Table A11

Density of Settled Deposits

Test No.	Suspension: Initial CSM, g/ℓ	Suspension: Ws_{50}* mm/sec	Deposited Sediments: 50% Settled: Time min	50% Settled: Concentration of Bed, dry, g/cu cm	50% Settled: BWD g/cu cm	Peak Bed Thickness: Time min	Peak Bed Thickness: Concentration of Bed, dry, g/cu cm	Peak Bed Thickness: BWD g/cu cm	End of Test: Time min	End of Test: Concentration of Bed, dry, g/cu cm	End of Test: BWD g/cu cm
4	1.25	0.392	--	--	--	140	0.0564	1.0593	240	0.0842	1.0764
5	1.8	0.348	--	--	--	110	0.0389	1.0486	135	0.0590	1.0609
6	2.25	10.294	63	0.0414	1.0500	130	0.0505	1.0556	145	0.0569	1.0596
7	3.0	0.263	70	0.0357	1.0466	120	0.0412	1.0499	145	0.0479	1.0540
8	6.0	0.217	77	0.0492	1.0548	160	0.0524	1.0568	210	0.0714	1.0680
9	8.9	0.172	95	0.0355	1.0465	150	0.0346	1.0459	190	0.0522	1.0567
		Mean	76	0.0405	1.0495	135	0.0457	1.0527	178	0.0619	1.0626

* Ws_{50} = Median settling velocity.

Table A12

Consolidation Rates

Initial			Final		
Concentration, Dry, g/cu cm	BWD g/cu cm	Settling Rate mm/sec	Time hr	Concentration, Dry, g/cu cm	BWD g/cu cm
0.0203	1.0372	0.1000	2.1	0.0738	1.0700
0.0290	1.0423	0.0508	98.3	0.1835	1.1372
0.0339	1.0455	0.0419	98.1	0.1803	1.1353
0.0460	1.0529	0.0328	72.1	0.1658	1.1264
0.0576	1.060	0.0284	69.0	0.1623	1.1242
0.0742	1.0702	0.0236	68.4	0.1746	1.1318
0.0804	1.0740	0.0229	234.5	0.2144	1.1562
0.1997	1.1472	0.00009	168.0	0.2336	1.1680

Table A13

Corpus Christi Bed Sample Properties

Sample No.	BWD g/cu cm	Specific Weight, Dry, g/cu cm	Percent Moisture	Percent Volatile	CEC, meq/ 100 g	Percent Clay	Silt	Sand
1	1.411	0.630	60	2.0	43.1	60.9	16.3	22.8
2	1.202	0.289	72	4.5	61.5	73.9	23.6	2.5
3	1.332	0.502	62	1.9	42.6	61.3	18.7	20.0
4	1.341	0.515	59	1.9	39.6	52.8	18.0	29.2
5	1.343	0.519	56	1.7	32.2	47.8	8.6	43.6
6	1.709	1.116	21	2.8	8.4	14.2	5.8	80.0
7	1.267	0.394	61	2.3	35.5	53.4	19.2	27.4
8	1.181	0.254	71	3.2	51.8	63.1	30.6	6.2
9	1.339	0.513	58	2.2	36.8	48.8	7.3	43.9
10	1.948	1.505	18	0.6	4.7	8.2	3.1	88.7
11	1.280	0.417	60	2.6	38.5	51.1	20.2	28.7
12	1.805	1.272	32	2.9	43.1	25.5	11.7	62.8
13	2.008	1.603	19	0.7	1.0	4.4	0.6	95.0
14	1.344	0.521	60	3.3	42.6	67.0	20.5	12.5
15	1.210	0.302	69	4.4	55.7	76.8	20.9	2.3
16	1.235	0.344	68	5.2	55.1	76.5	20.8	2.7
17	1.925	1.469	20	0.6	1.0	--	3.1	96.9
18	1.927	1.471	23	1.3	6.0	13.6	3.1	83.3
19	1.436	0.671	50	3.5	34.1	52.2	24.0	23.8
20	1.392	0.598	55	3.2	44.2	65.3	29.0	5.7
21	1.358	0.544	58	3.9	42.0	52.5	16.4	31.1
22	1.216	0.313	71	3.3	60.0	74.9	24.2	30.9
23	1.405	0.620	55	3.8	31.4	51.6	20.1	28.3
24	1.256	0.377	66	3.6	55.9	70.7	27.6	1.7
25	1.205	0.293	71	3.2	59.5	79.4	19.4	1.2
26	1.509	0.789	43	2.3	25.9	39.8	21.1	39.1

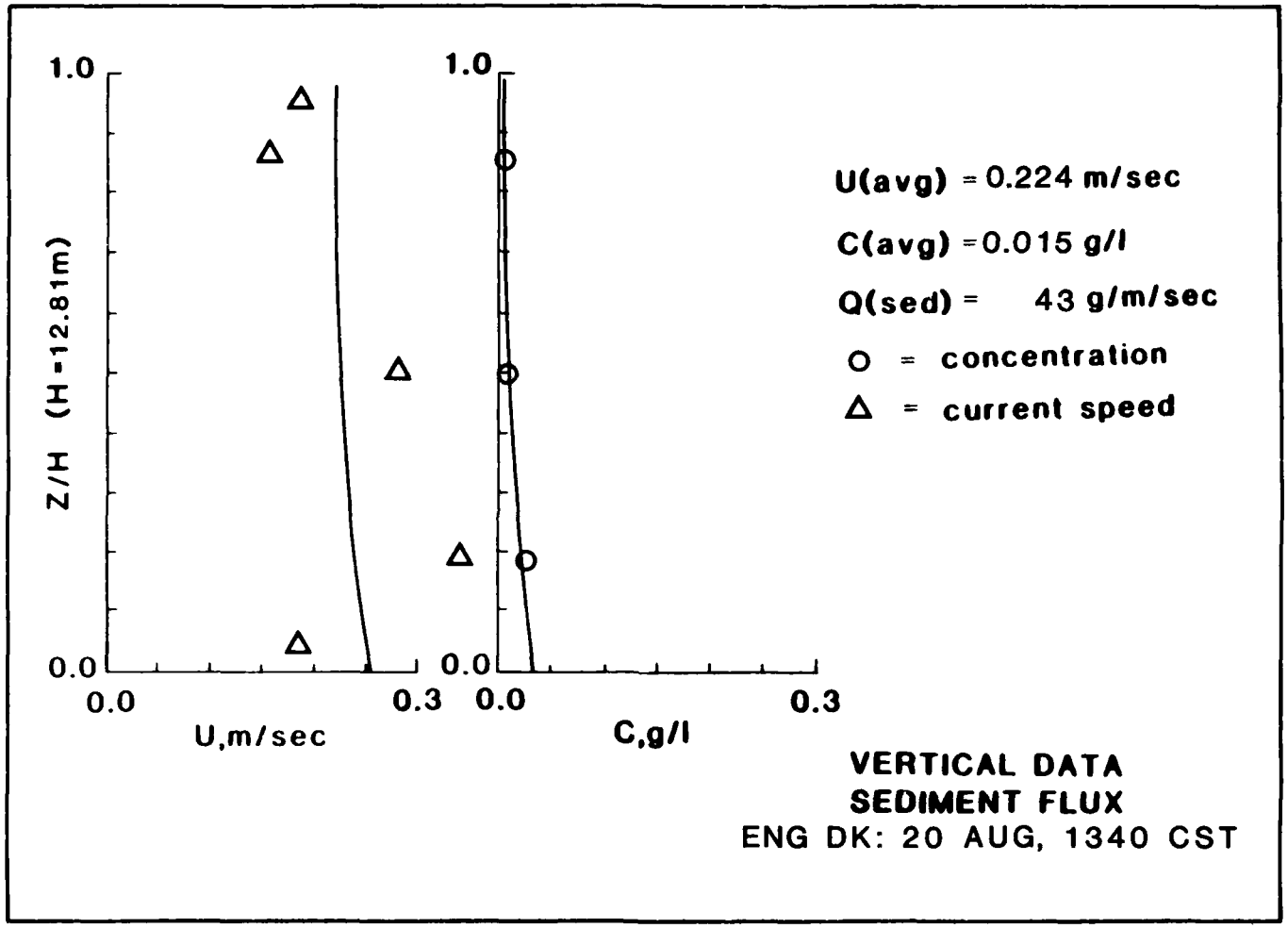
1.0
0.0
Z/H (H=12.81m)
0.0
0.3
U,m/sec
1.0
0.0
0.0
0.3
C,g/l
U(avg) = 0.224 m/sec
C(avg) = 0.015 g/l
Q(sed) = 43 g/m/sec
O = concentration
Δ = current speed
VERTICAL DATA
SEDIMENT FLUX
ENG DK: 20 AUG, 1340 CST

PLATE A1

PLATE A2

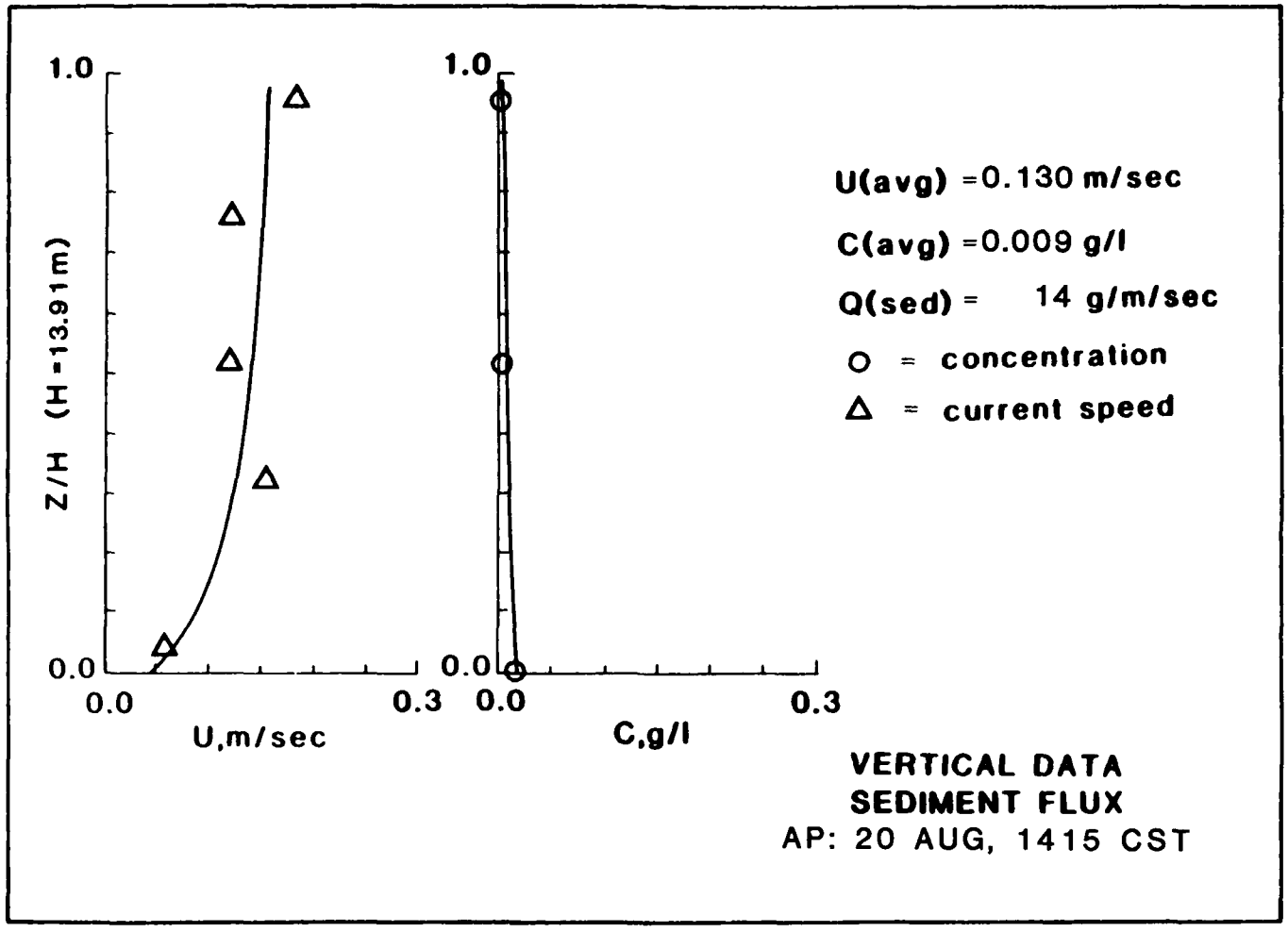
1.0
Z/H (H=13.91m)
0.0
0.0
0.3
U,m/sec
1.0
0.0
0.0
0.3
C,g/l
U(avg) =0.130 m/sec
C(avg) =0.009 g/l
Q(sed) = 14 g/m/sec
O = concentration
Δ = current speed
VERTICAL DATA
SEDIMENT FLUX
AP: 20 AUG, 1415 CST

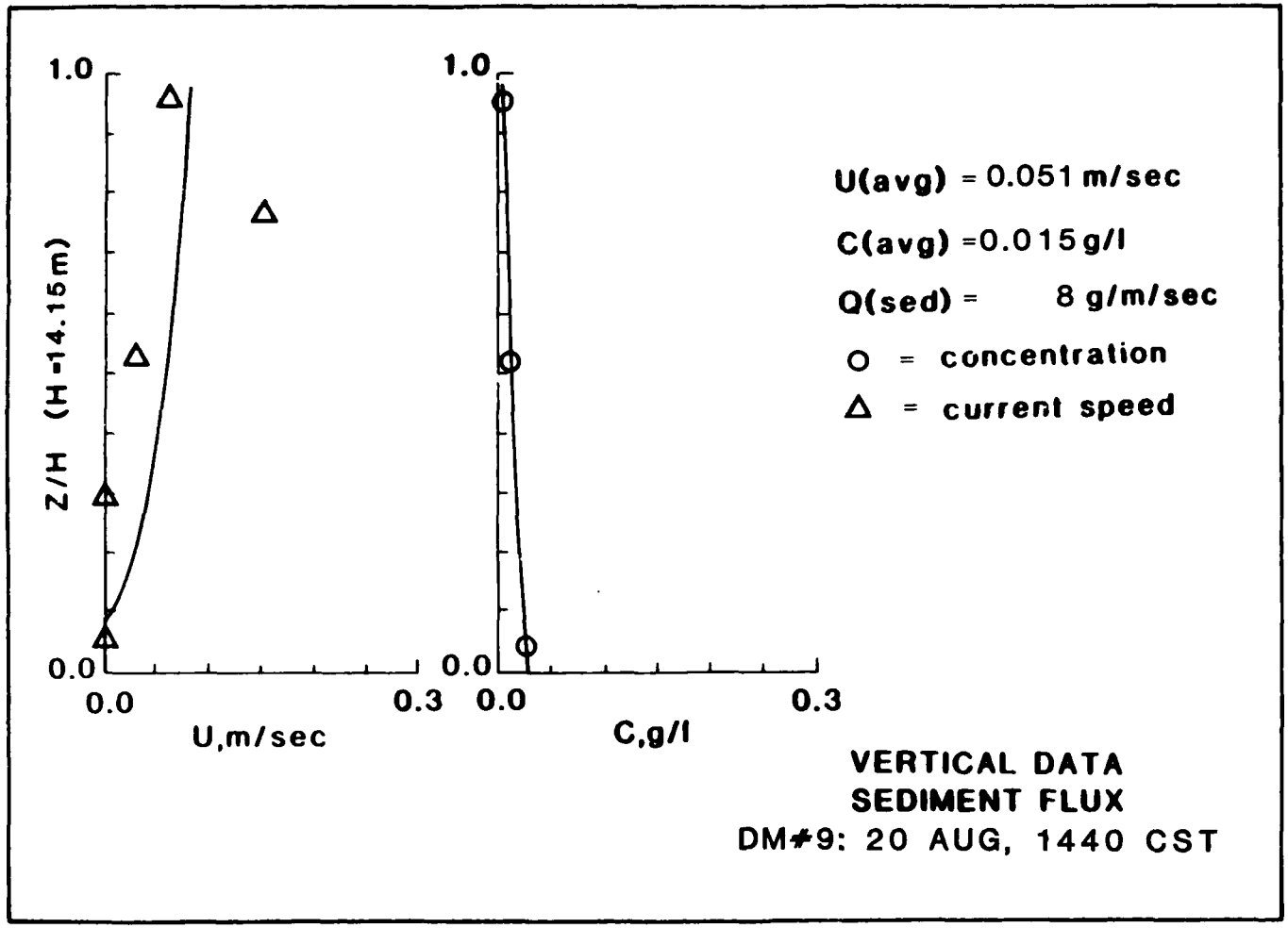
1.0
Z/H (H=14.15m)
0.0
0.0
0.3
U,m/sec
1.0
0.0
0.0
0.3
C,g/l
U(avg) = 0.051 m/sec
C(avg) =0.015 g/l
Q(sed) = 8 g/m/sec
O = concentration
Δ = current speed
VERTICAL DATA
SEDIMENT FLUX
DM#9: 20 AUG, 1440 CST

PLATE A3

PLATE A4

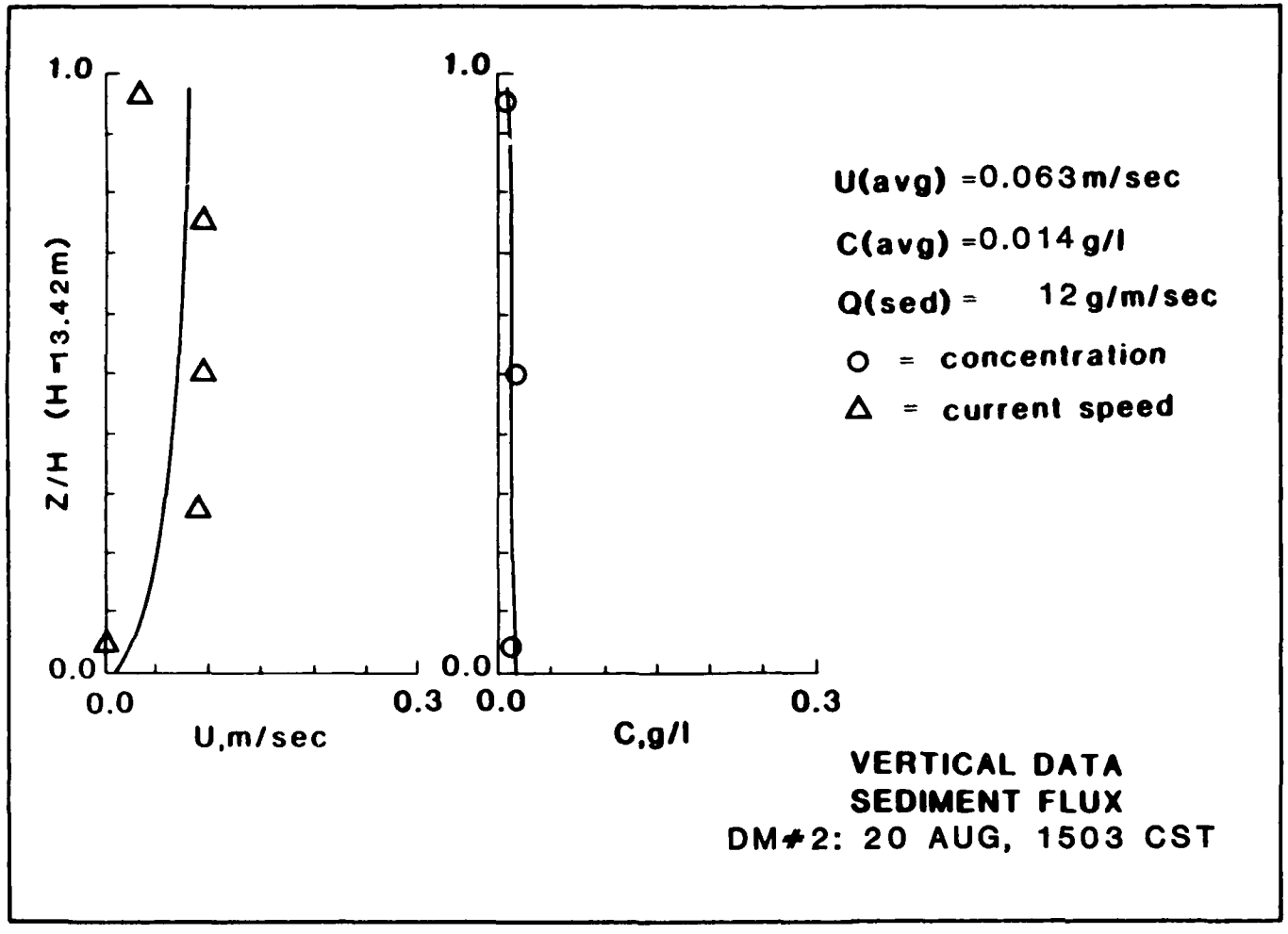
1.0
Z/H (H=13.42m)
0.0
0.0
0.3
U,m/sec
1.0
0.0
0.0
0.3
C,g/l
U(avg) =0.063m/sec
C(avg) =0.014 g/l
Q(sed) = 12 g/m/sec
○ = concentration
△ = current speed
VERTICAL DATA
SEDIMENT FLUX
DM#2: 20 AUG, 1503 CST

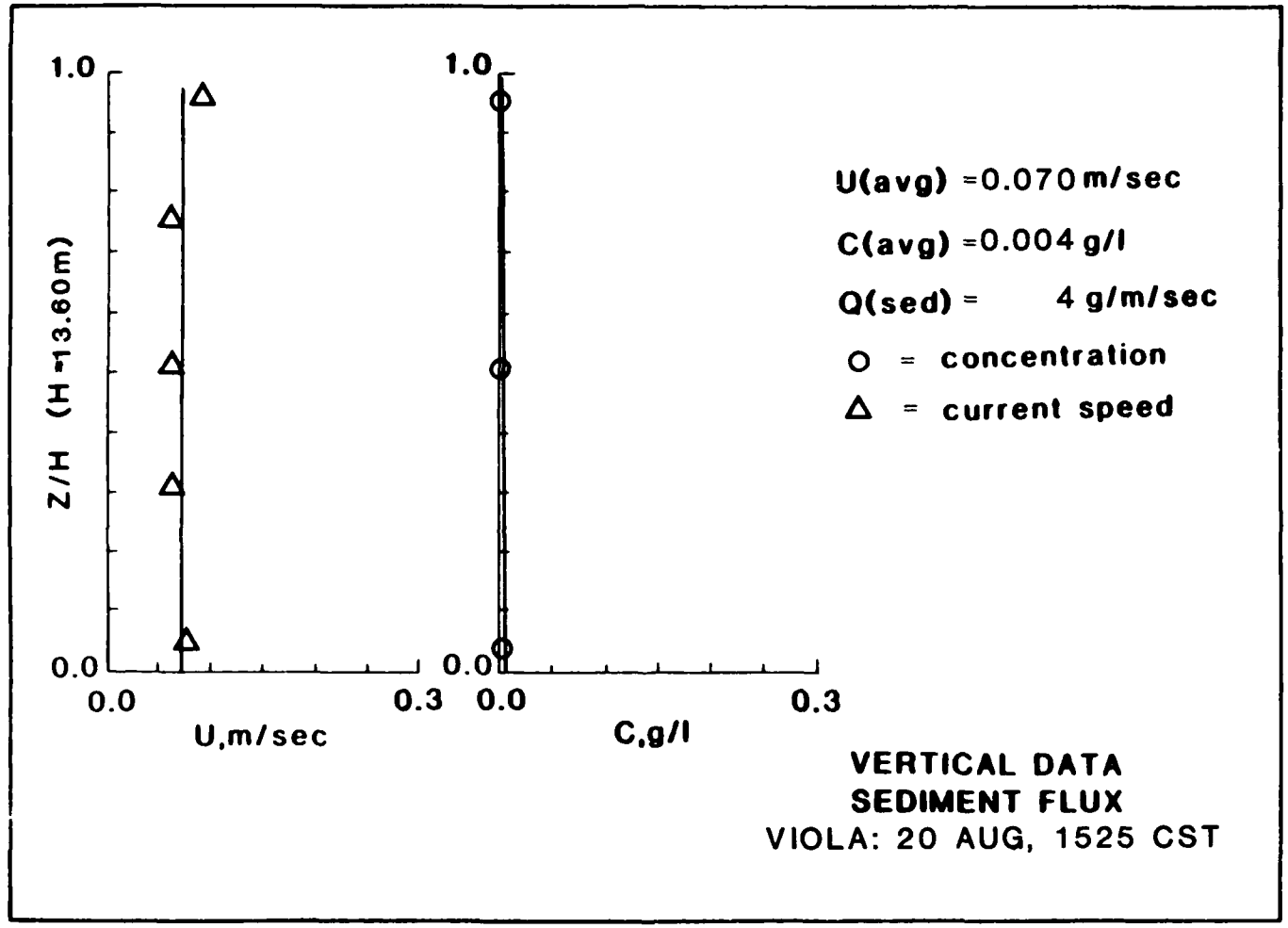
1.0
1.0
Z/H (H=13.60m)
0.0
0.0
0.0
0.3
0.0
0.3
U,m/sec
C,g/l
U(avg) =0.070 m/sec
C(avg) =0.004 g/l
Q(sed) = 4 g/m/sec
O = concentration
Δ = current speed
VERTICAL DATA
SEDIMENT FLUX
VIOLA: 20 AUG, 1525 CST

PLATE A5

PLATE A6

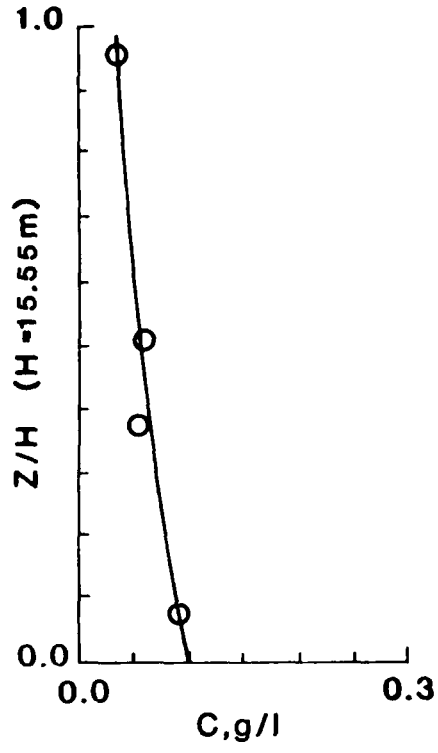

U(avg) =0.000 m/sec

C(avg) =0.057 g/l

Q(sed) = 0 g/m/sec

O = concentration

VERTICAL DATA
SEDIMENT FLUX
DM#80: 21 AUG, 0730 CST

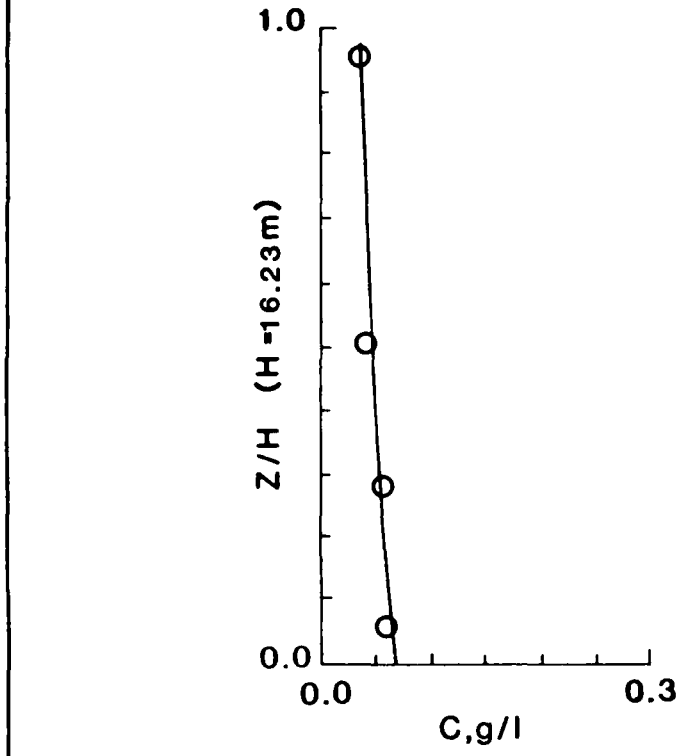

U(avg) =0.143 m/sec

C(avg) =0.047 g/l

Q(sed) = 102 g/m/sec

O = concentration

VERTICAL DATA
SEDIMENT FLUX
DM#82: 21 AUG, 0815 CST

PLATE A7

PLATE A8

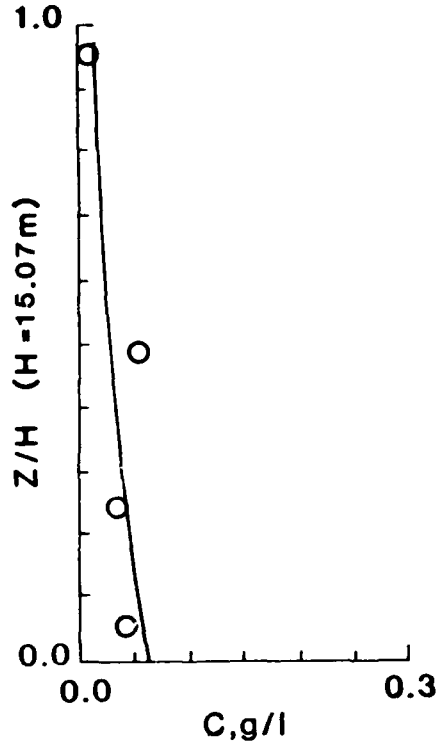

U(avg) =0.143 m/sec

C(avg) =0.030 g/l

Q(sed) = 56 g/m/sec

O = concentration

VERTICAL DATA
SEDIMENT FLUX
JETTIES: 21 AUG, 0845 CST

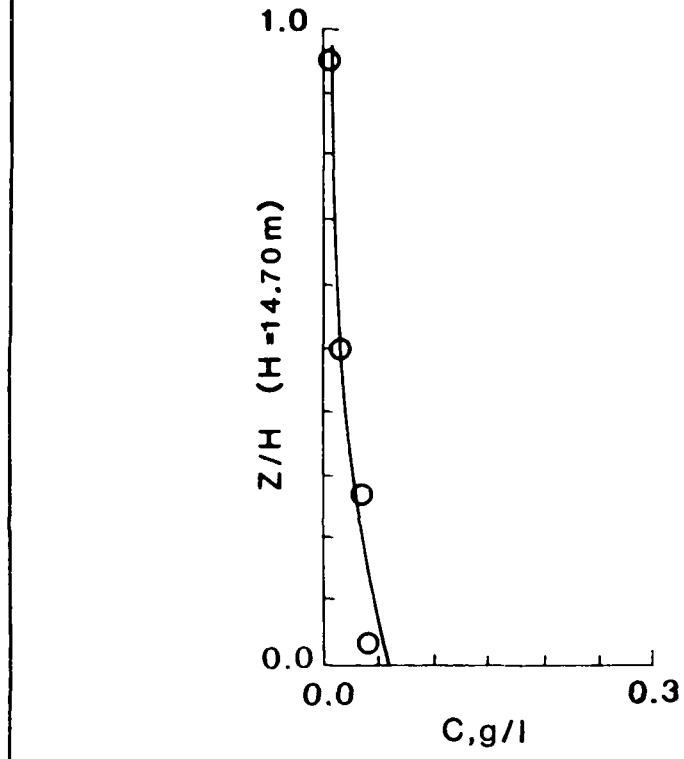

U(avg) =0.143 m/sec

C(avg) =0.020 g/l

Q(sed) = 32 g/m/sec

O = concentration

VERTICAL DATA
SEDIMENT FLUX
BRDG: 21 AUG, 0925 CST

PLATE A9

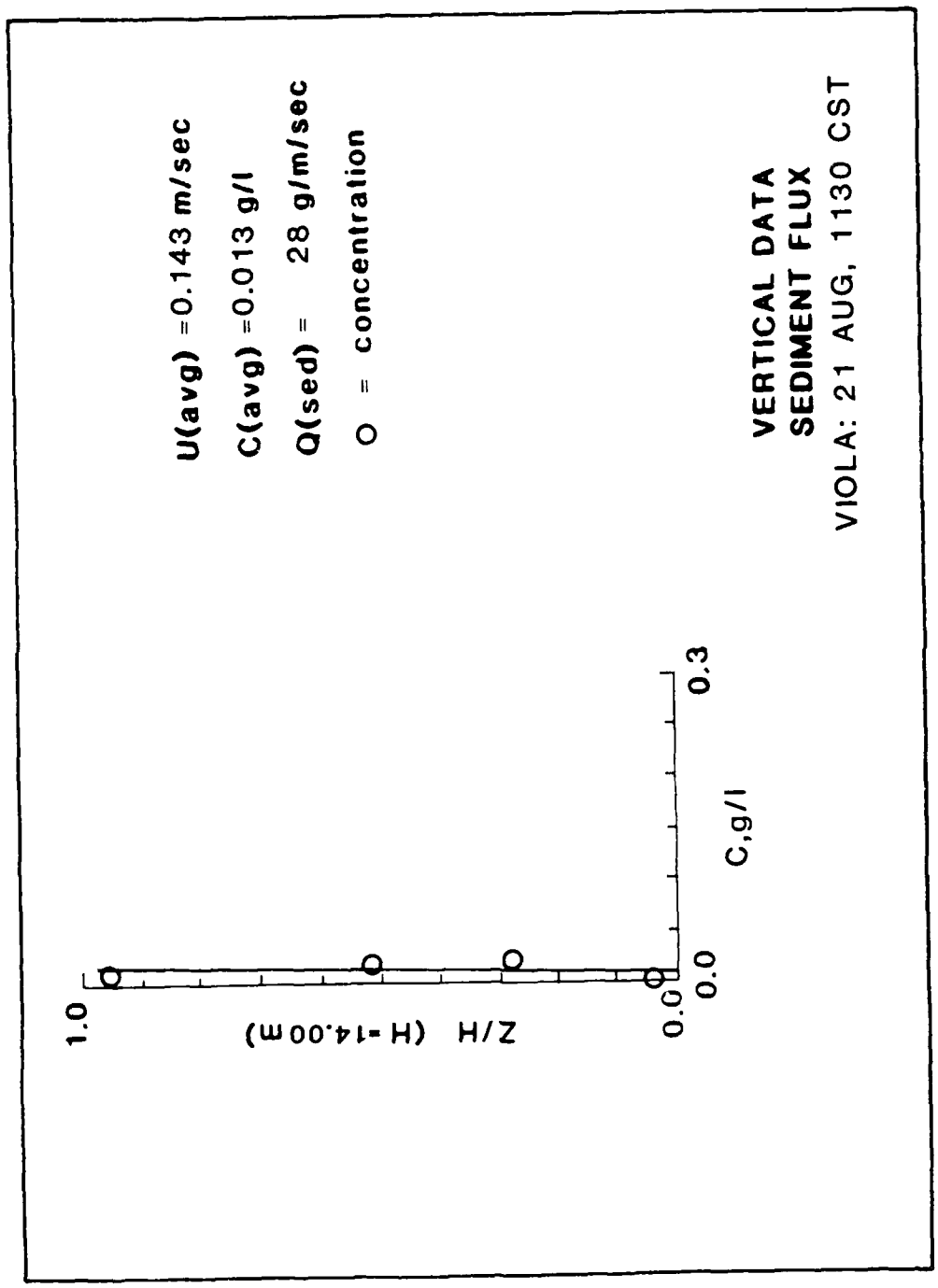
U(avg) =0.143 m/sec
C(avg) =0.013 g/l
Q(sed) = 28 g/m/sec
O = concentration
VERTICAL DATA
SEDIMENT FLUX
VIOLA: 21 AUG, 1130 CST
1.0
Z/H (H =14.00 m)
0.0
0.0
0.3
C,g/l

PLATE A10

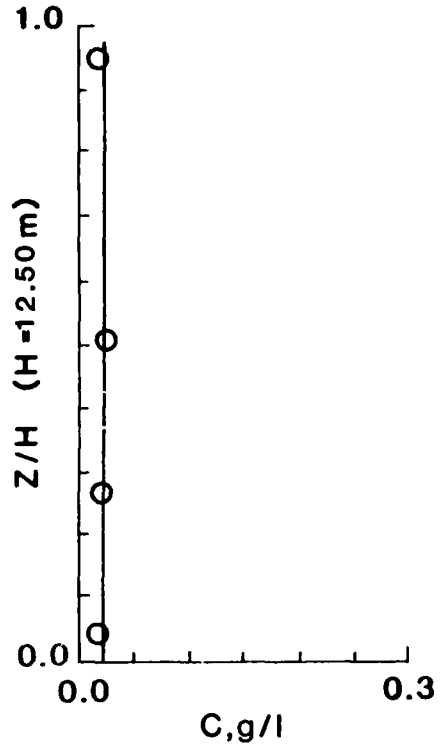

U(avg) =0.143 m/sec

C(avg) =0.022 g/l

Q(sed) = 40 g/m/sec

O = concentration

VERTICAL DATA
SEDIMENT FLUX
DM#2: 21 AUG, 1258 CST

PLATE A11

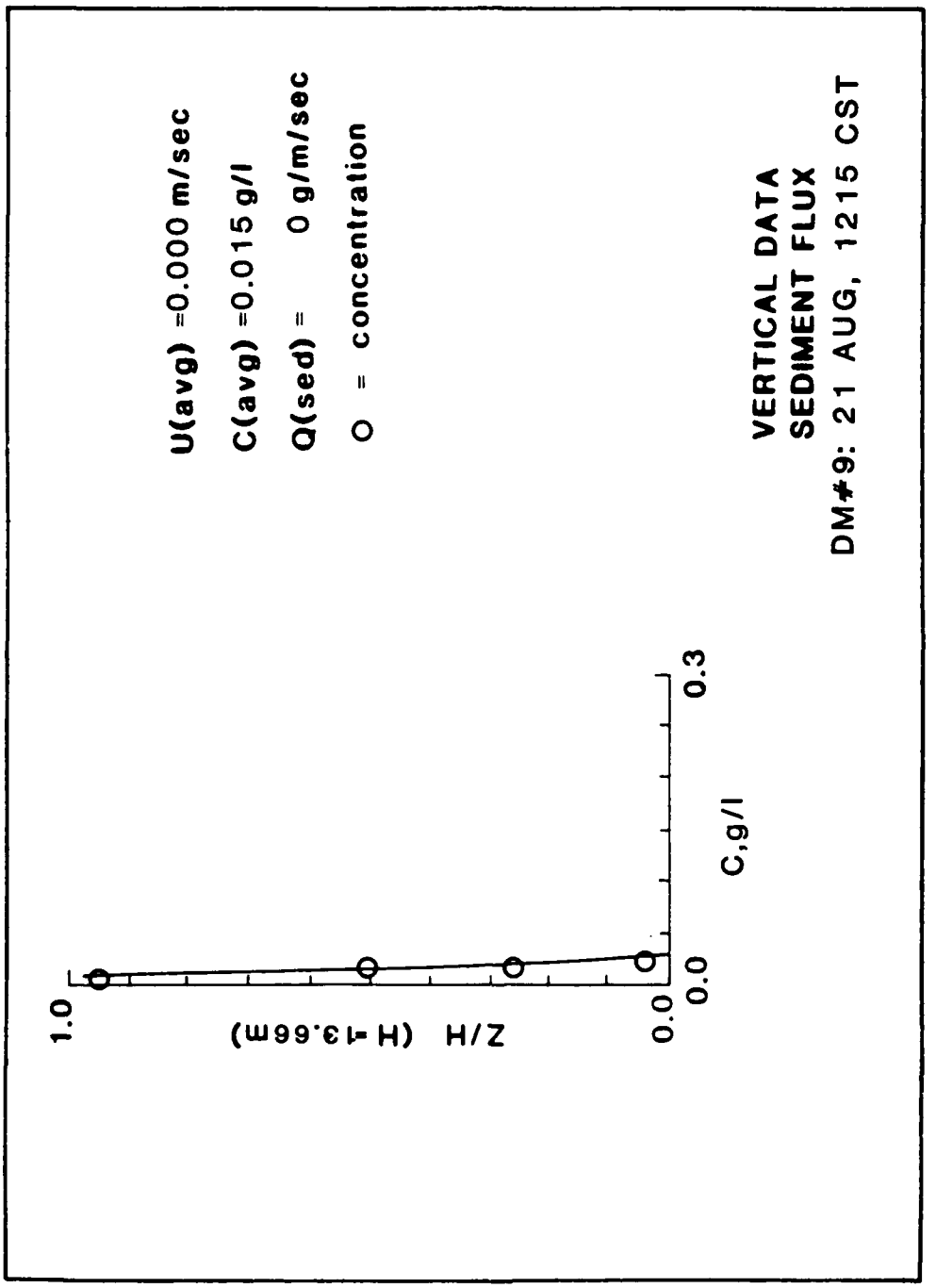
U(avg) =0.000 m/sec
C(avg) =0.015 g/l
Q(sed) = 0 g/m/sec
O = concentration
VERTICAL DATA
SEDIMENT FLUX
DM#9: 21 AUG, 1215 CST
1.0
0.0
Z/H (H =13.66m)
0.0
0.3
C,g/l

PLATE A12

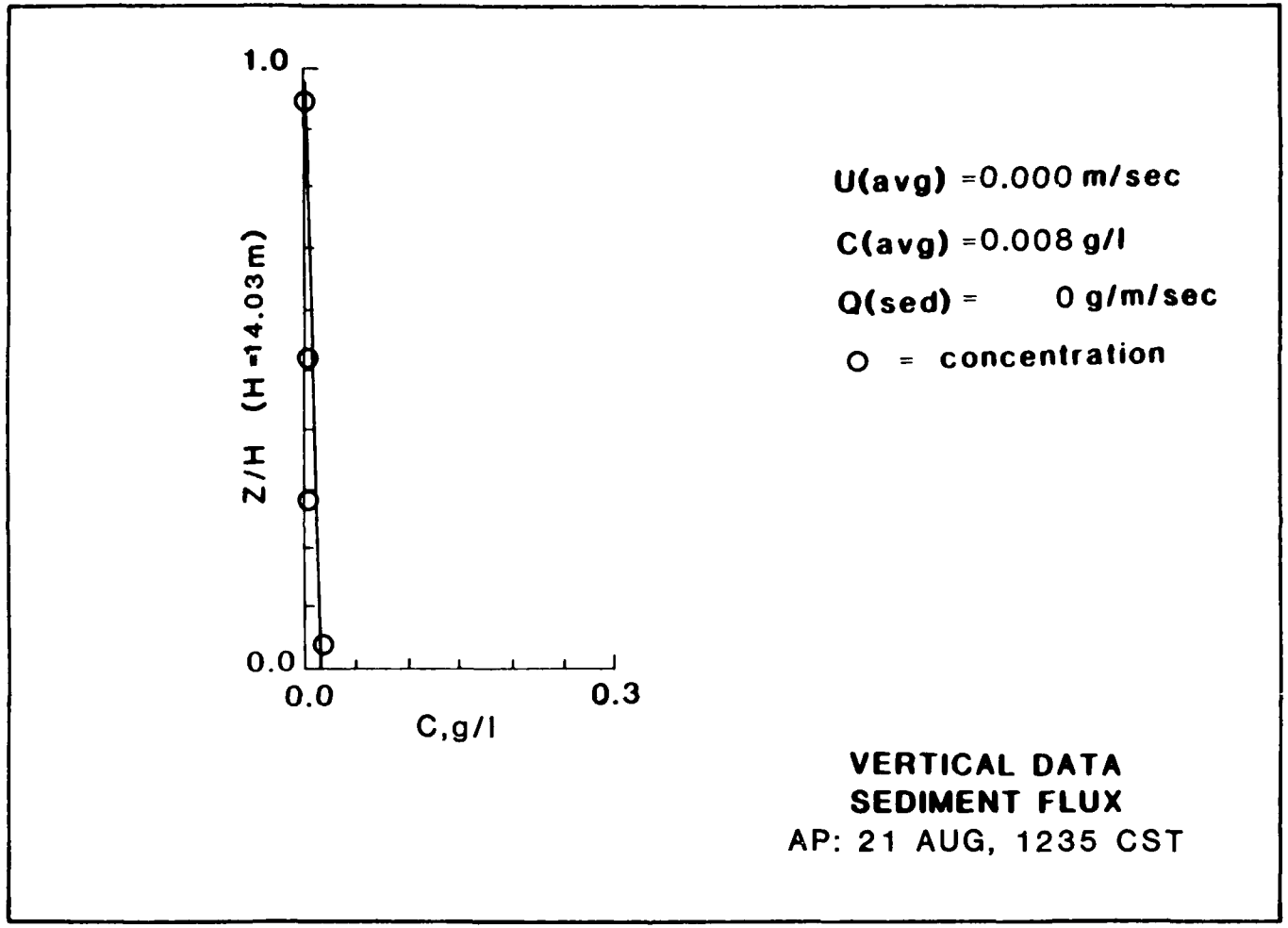
1.0
Z/H (H=14.03m)
0.0
0.0
0.3
C,g/l
U(avg) =0.000 m/sec
C(avg) =0.008 g/l
Q(sed) = 0 g/m/sec
O = concentration
VERTICAL DATA
SEDIMENT FLUX
AP: 21 AUG, 1235 CST

PLATE A13

PLATE A14

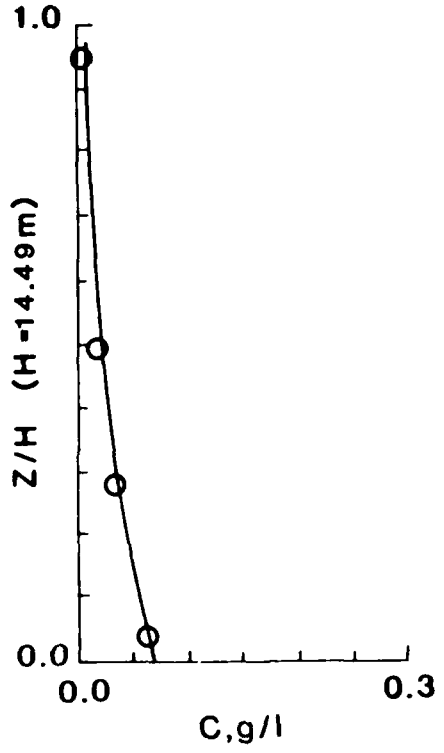

U(avg) =0.000 m/sec

C(avg) =0.026 g/l

Q(sed) = 0 g/m/sec

O = concentration

VERTICAL DATA
SEDIMENT FLUX
ENG DK: 21 AUG, 1253 CST

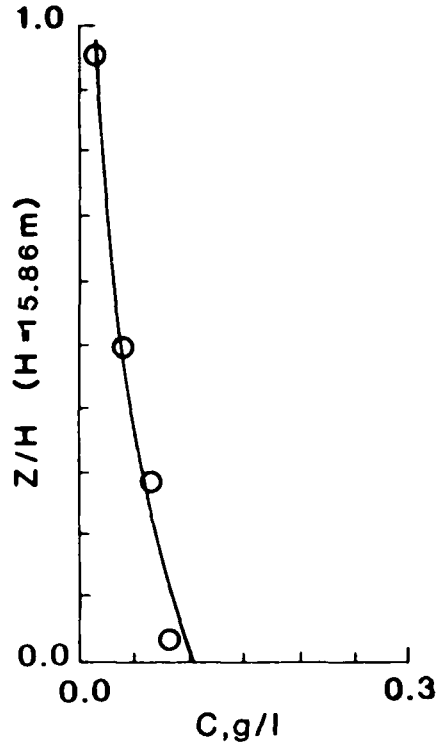

U(avg) =0.000 m/sec

C(avg) =0.042 g/l

Q(sed) = 0 g/m/sec

O = concentration

VERTICAL DATA
SEDIMENT FLUX
ENG DK: 22 AUG, 0605 CST

PLATE A15

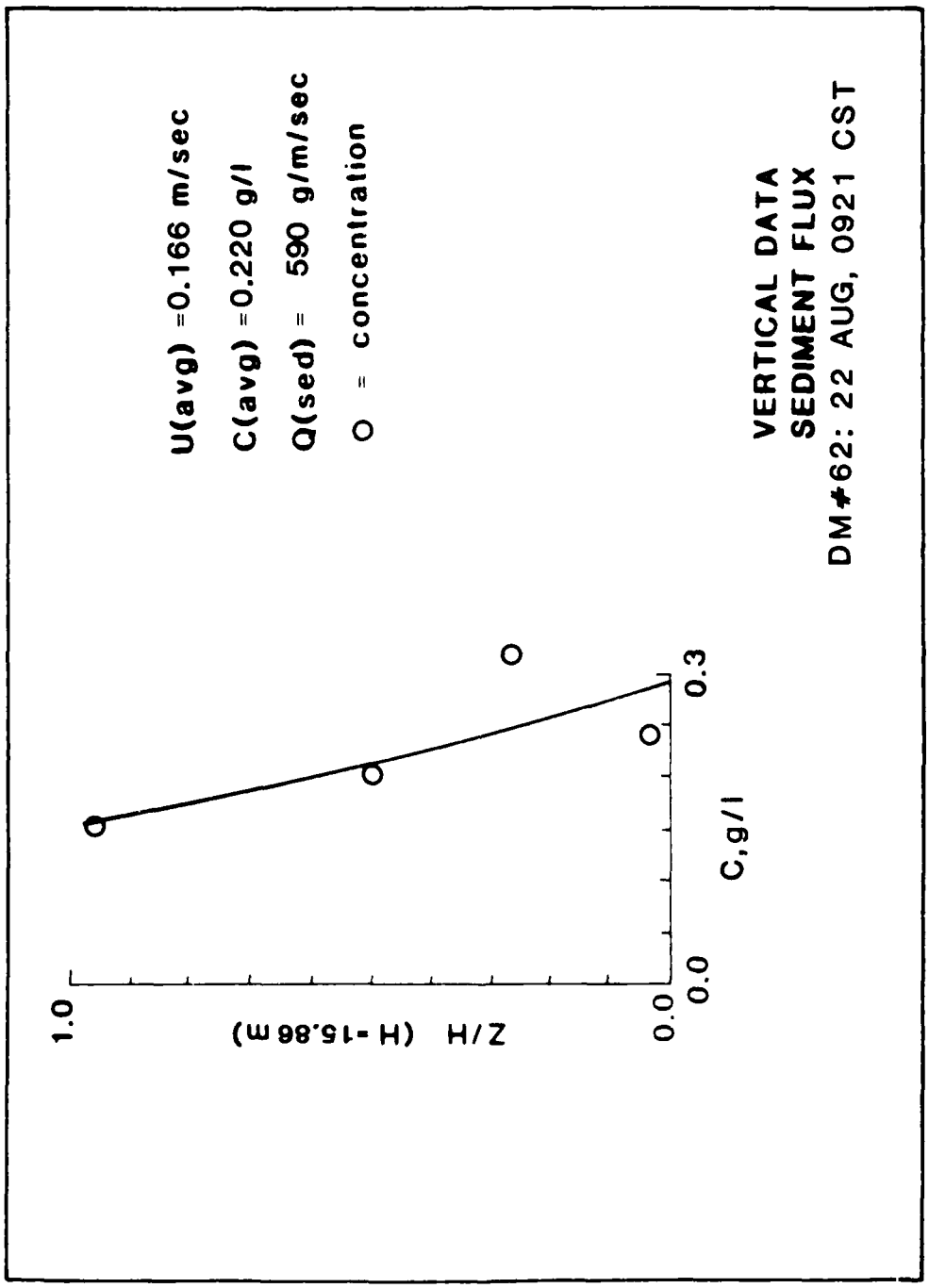
U(avg) =0.166 m/sec
C(avg) =0.220 g/l
Q(sed) = 590 g/m/sec
O = concentration
VERTICAL DATA
SEDIMENT FLUX
DM#62: 22 AUG, 0921 CST
1.0
Z/H (H=15.86 m)
0.0
0.0
0.3
C,g/l

PLATE A16

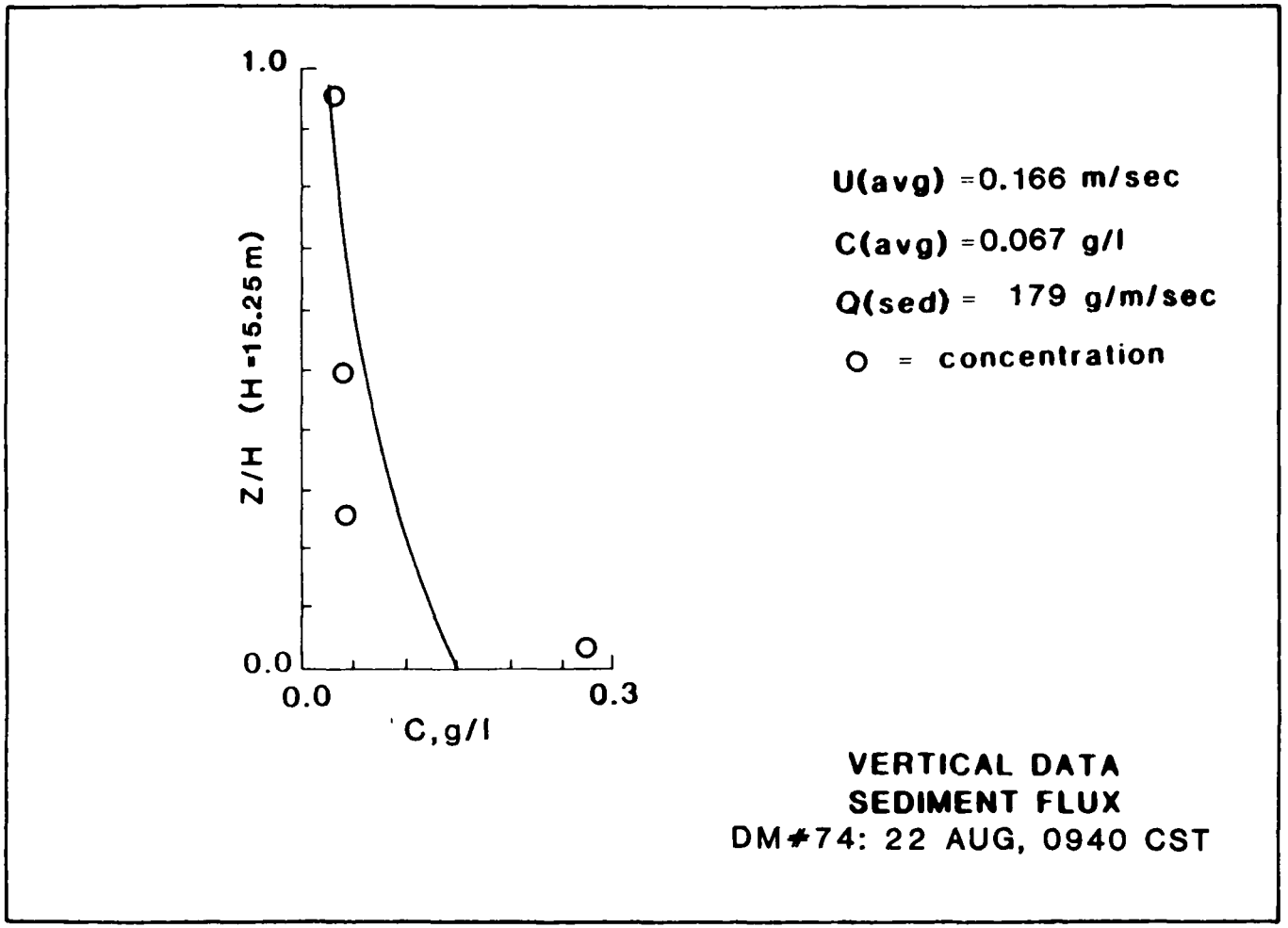
1.0
Z/H (H=15.25m)
0.0
0.0
0.3
C, g/l
U(avg) =0.166 m/sec
C(avg) =0.067 g/l
Q(sed) = 179 g/m/sec
O = concentration
VERTICAL DATA
SEDIMENT FLUX
DM#74: 22 AUG, 0940 CST

PLATE A17

PLATE A18

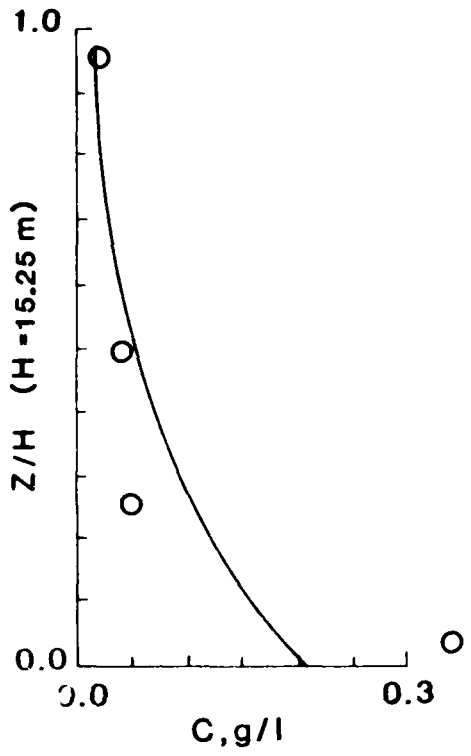

U(avg) =C.166 m/sec

C(avg) =0.069 g/l

Q(sed) = 192 g/m/sec

O = concentration

VERTICAL DATA
SEDIMENT FLUX
JETTIES: 22 AUG, 1000 CST

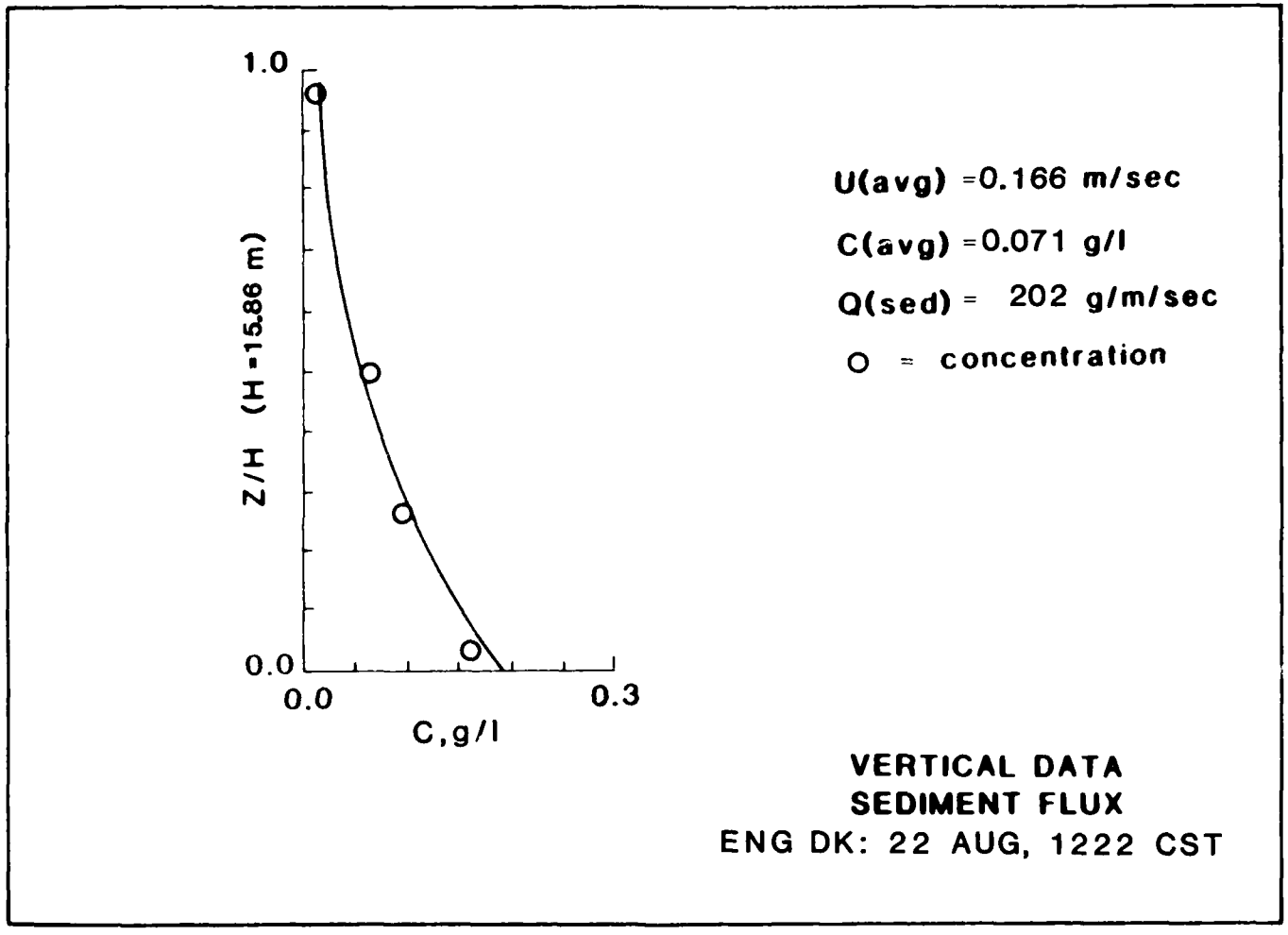
1.0
Z/H (H = 15.86 m)
0.0
0.0
0.3
C, g/l
U(avg) = 0.166 m/sec
C(avg) = 0.071 g/l
Q(sed) = 202 g/m/sec
O = concentration
VERTICAL DATA
SEDIMENT FLUX
ENG DK: 22 AUG, 1222 CST

PLATE A19

PLATE A20

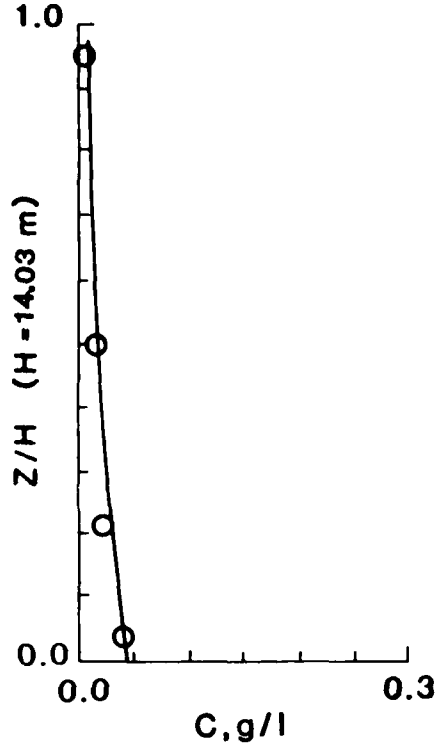

U(avg) = 0.166 m/sec

C(avg) = 0.020 g/l

Q(sed) = 49 g/m/sec

O = concentration

VERTICAL DATA
SEDIMENT FLUX
AP: 22 AUG, 1255 CST

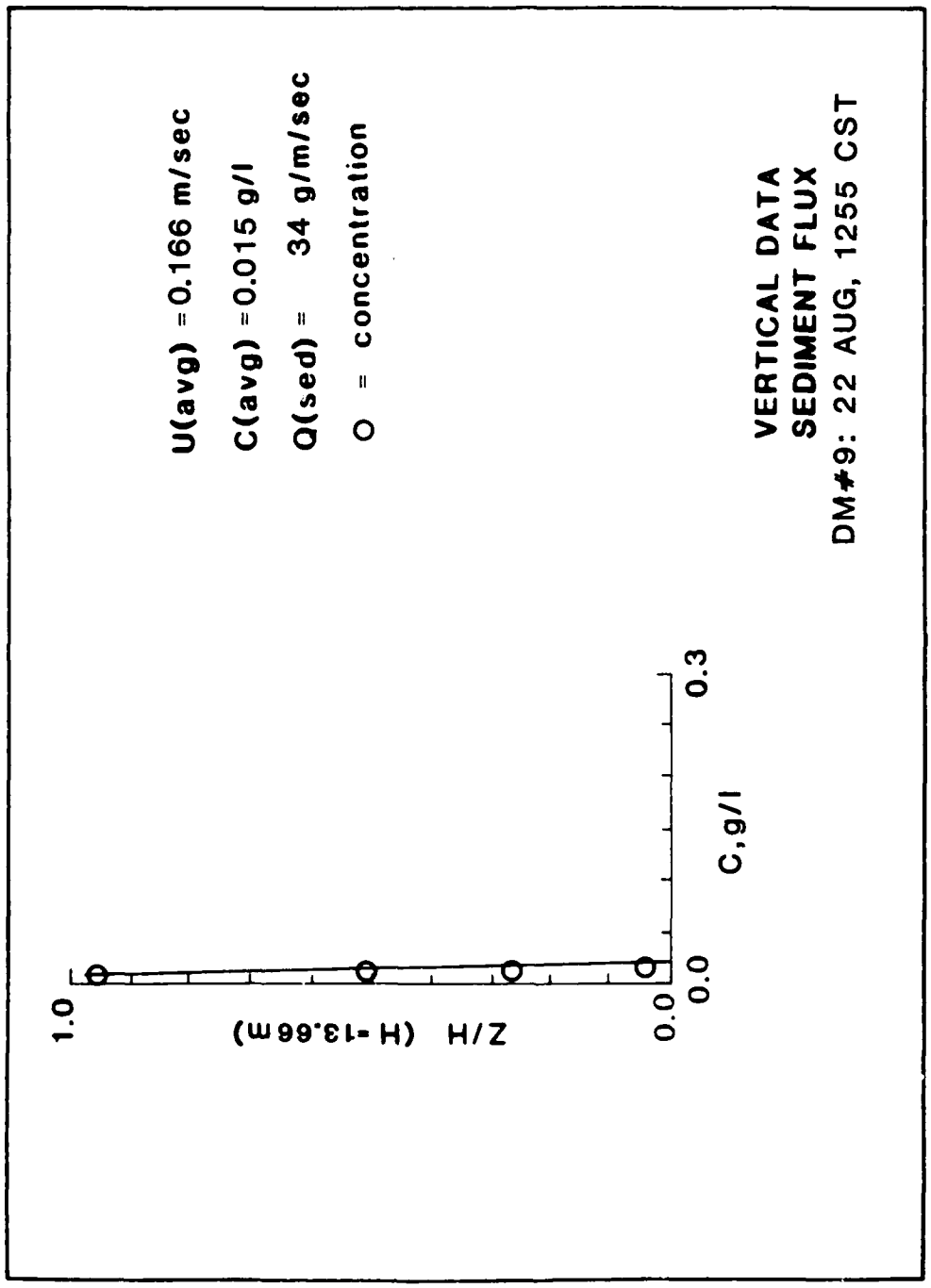
U(avg) = 0.166 m/sec
C(avg) = 0.015 g/l
Q(sed) = 34 g/m/sec
O = concentration
VERTICAL DATA
SEDIMENT FLUX
DM#9: 22 AUG, 1255 CST
1.0
Z/H (H=13.66m)
0.0
0.0
C,g/l
0.3

PLATE A21

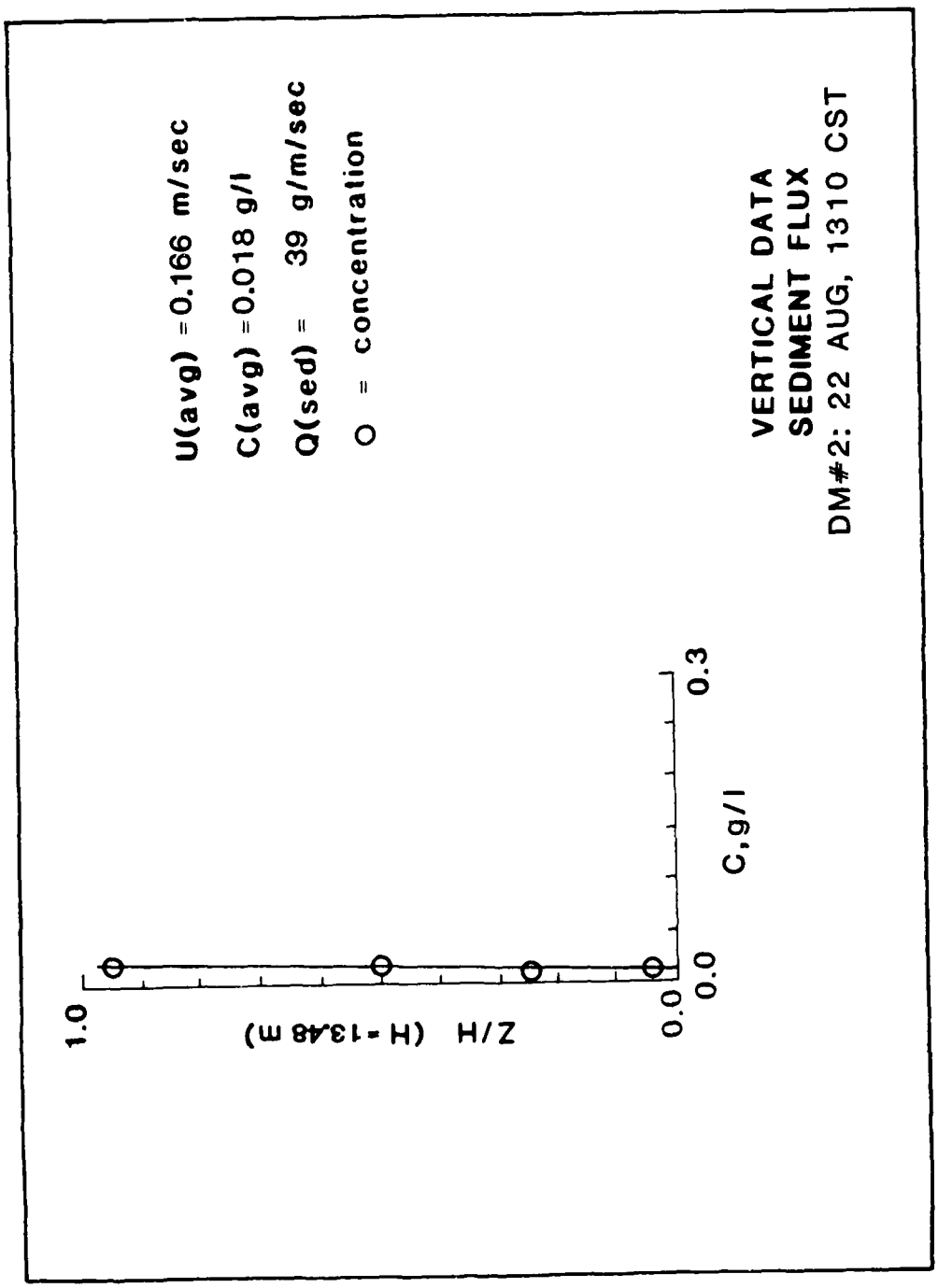
U(avg) = 0.166 m/sec
C(avg) = 0.018 g/l
Q(sed) = 39 g/m/sec
O = concentration
VERTICAL DATA
SEDIMENT FLUX
DM#2: 22 AUG, 1310 CST
1.0
Z/H (H = 13.48 m)
0.0
0.0
0.3
C, g/l

PLATE A22

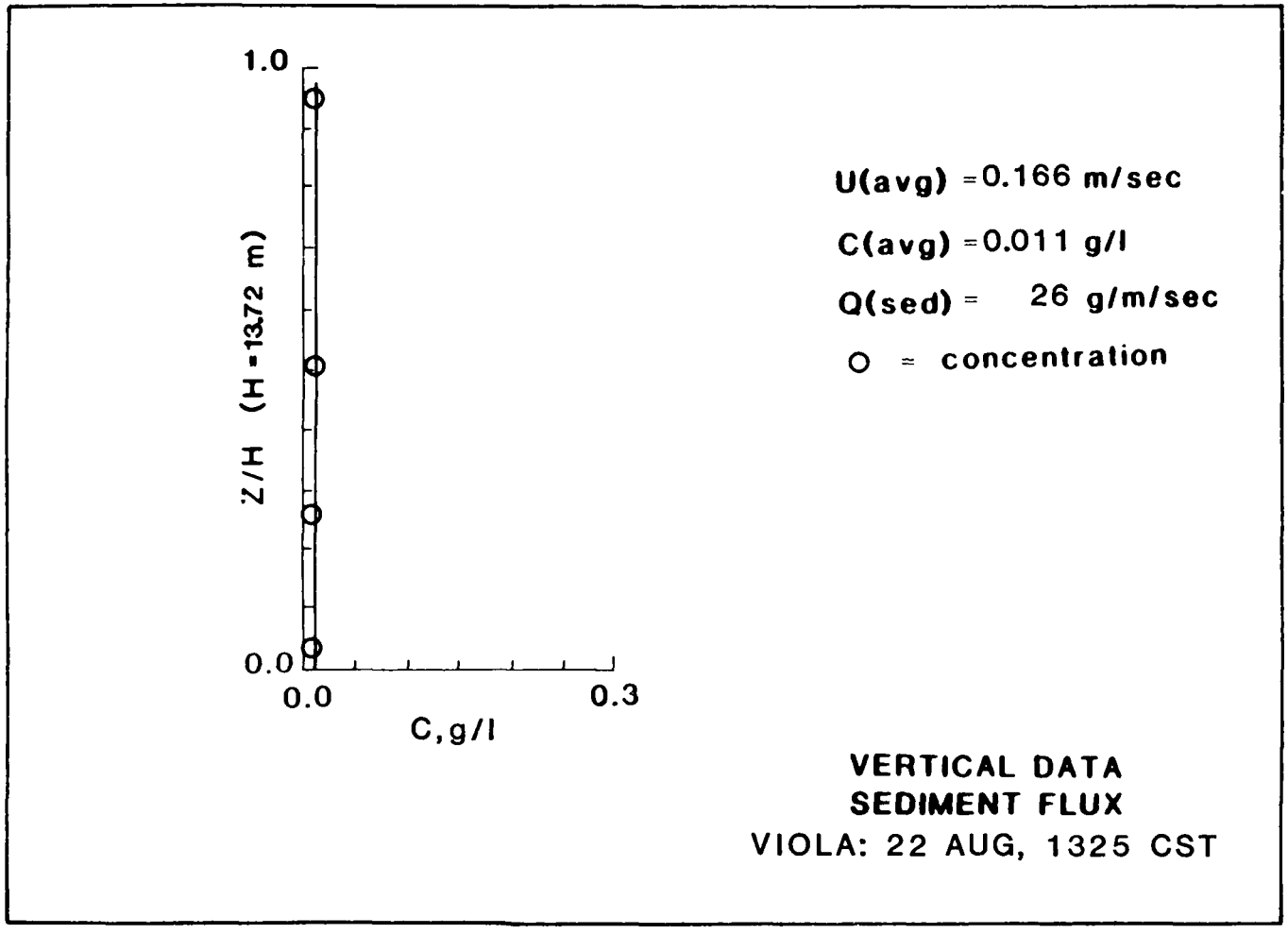
1.0
Z/H (H = 13.72 m)
0.0
0.0
0.3
C, g/l
U(avg) = 0.166 m/sec
C(avg) = 0.011 g/l
Q(sed) = 26 g/m/sec
O = concentration
VERTICAL DATA
SEDIMENT FLUX
VIOLA: 22 AUG, 1325 CST

PLATE A23

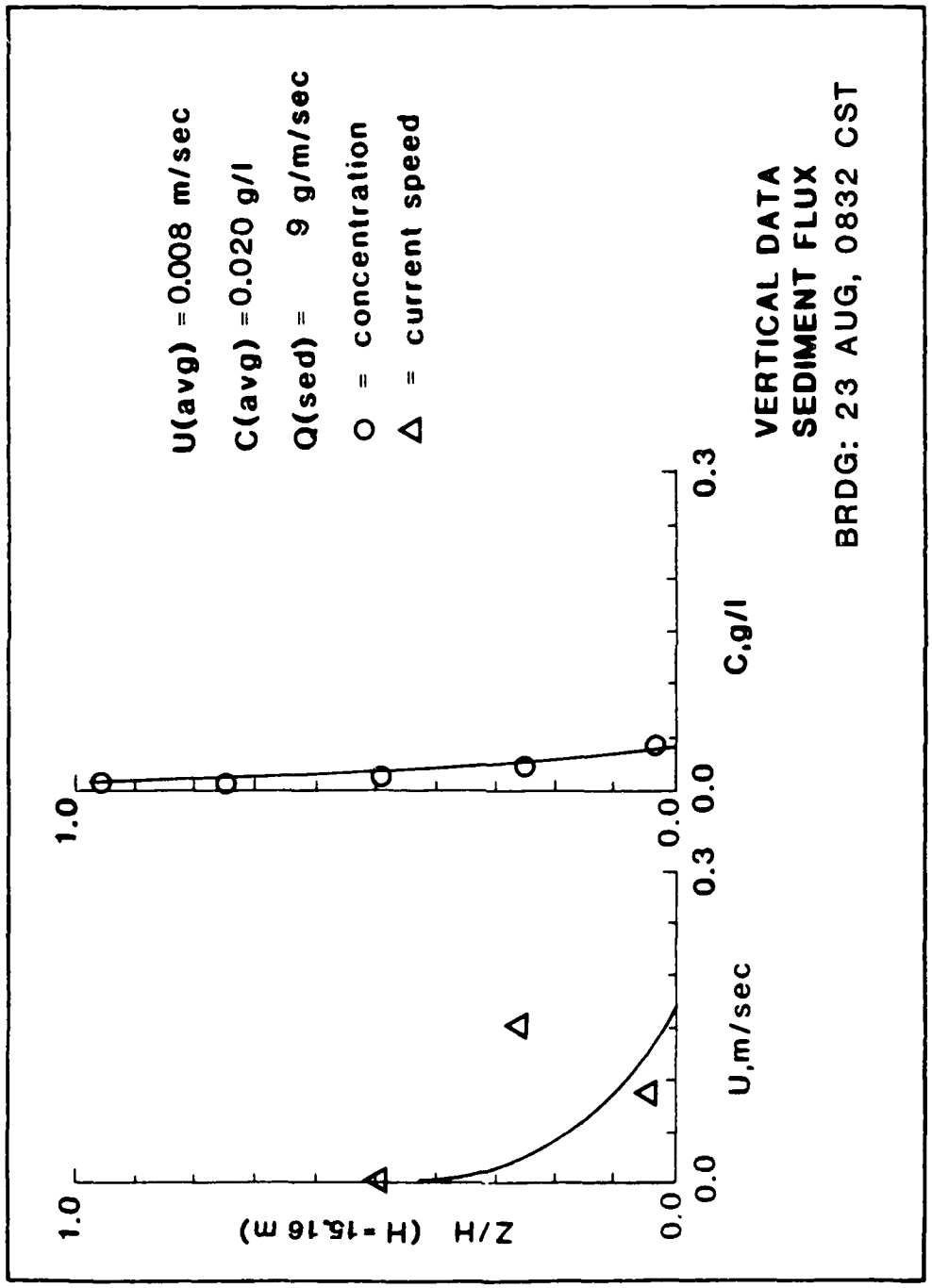
U(avg) = 0.008 m/sec
C(avg) = 0.020 g/l
Q(sed) = 9 g/m/sec
O = concentration
Δ = current speed
VERTICAL DATA
SEDIMENT FLUX
BRDG: 23 AUG, 0832 CST
Z/H (H = 15.16 m)
1.0
0.0
U,m/sec
0.0
0.3
C,g/l
0.0
0.3

PLATE A24

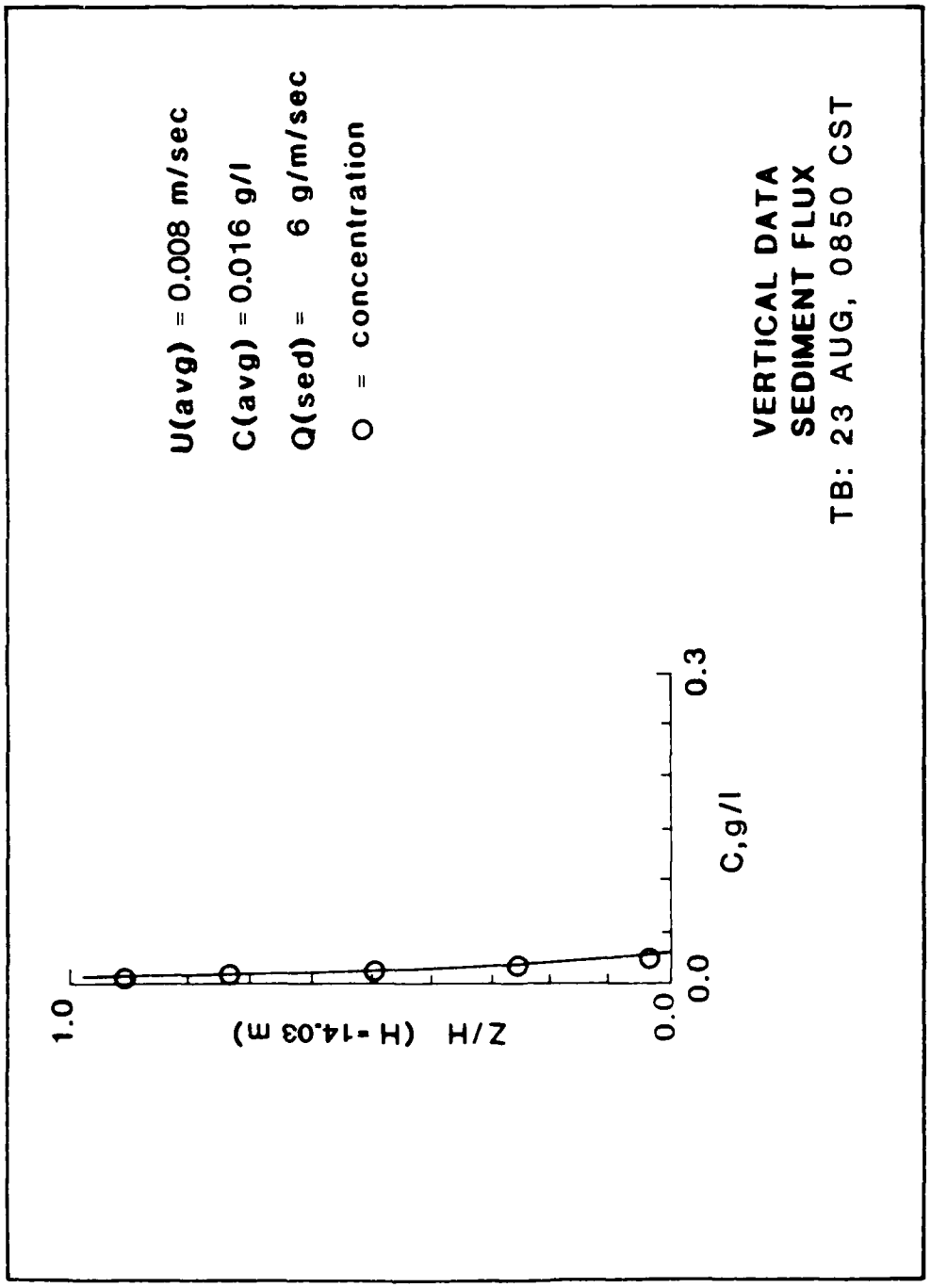
U(avg) = 0.008 m/sec
C(avg) = 0.016 g/l
Q(sed) = 6 g/m/sec
O = concentration
VERTICAL DATA
SEDIMENT FLUX
TB: 23 AUG, 0850 CST
1.0
Z/H (H = 14.03 m)
0.0
0.0
0.3
C,g/l

PLATE A25

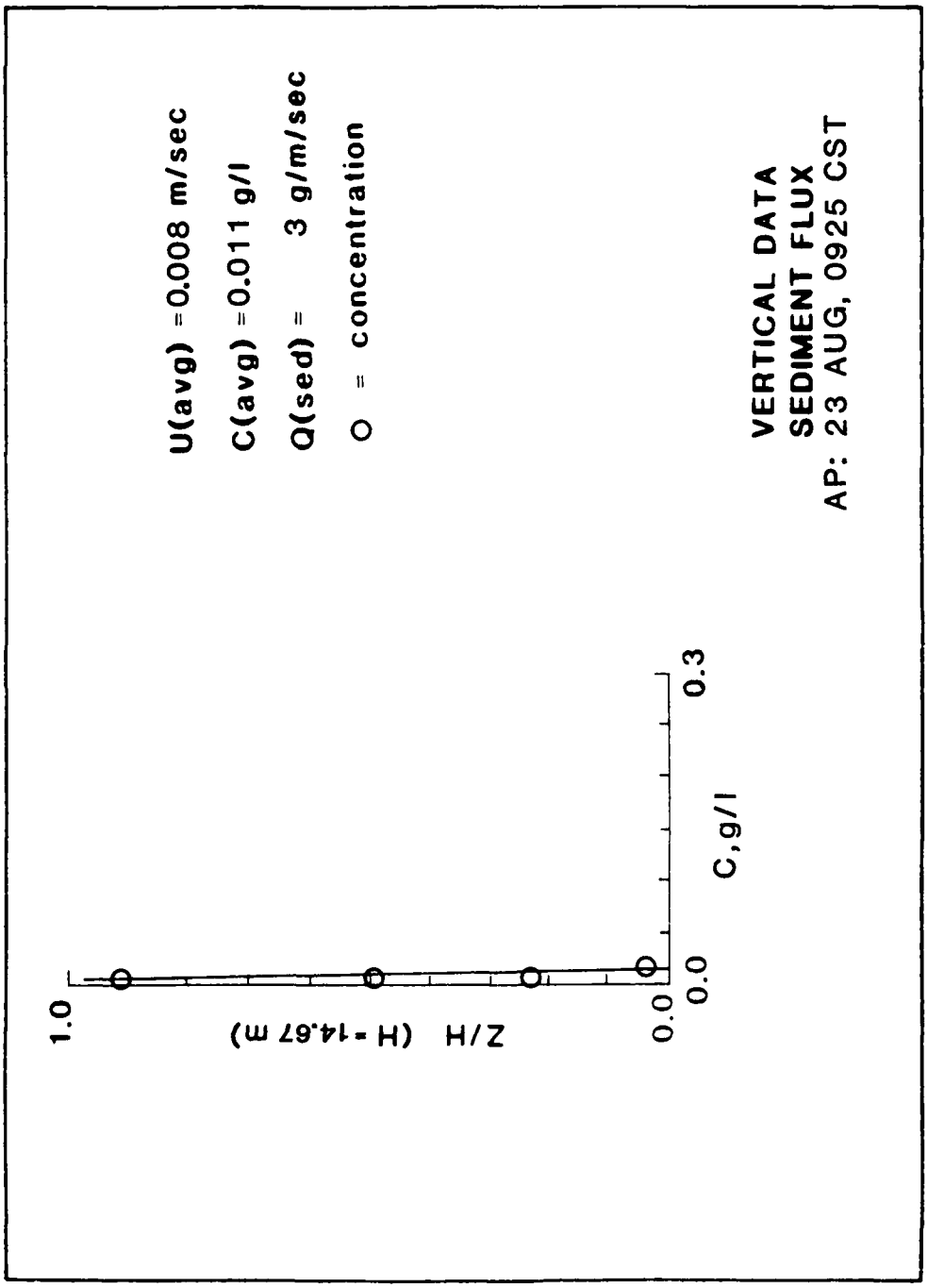
U(avg) =0.008 m/sec
C(avg) =0.011 g/l
Q(sed) = 3 g/m/sec
O = concentration
VERTICAL DATA
SEDIMENT FLUX
AP: 23 AUG, 0925 CST
1.0
Z/H (H = 14.67 m)
0.0
0.0
0.3
C,g/l

PLATE A26

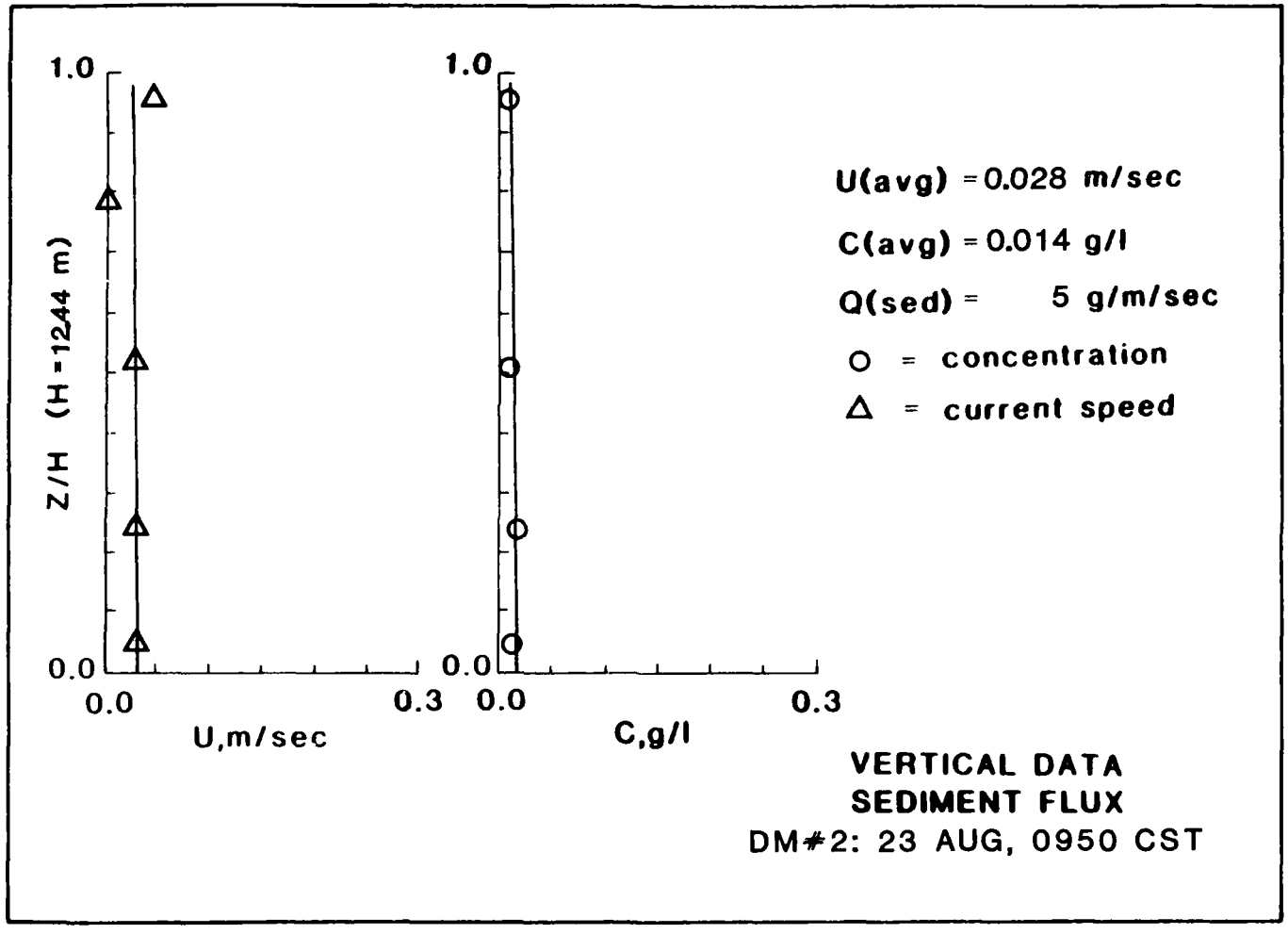
1.0
Z/H (H = 1244 m)
0.0
0.0
0.3
U,m/sec
1.0
0.0
0.0
0.3
C,g/l
U(avg) = 0.028 m/sec
C(avg) = 0.014 g/l
Q(sed) = 5 g/m/sec
○ = concentration
△ = current speed
VERTICAL DATA
SEDIMENT FLUX
DM#2: 23 AUG, 0950 CST

PLATE A27

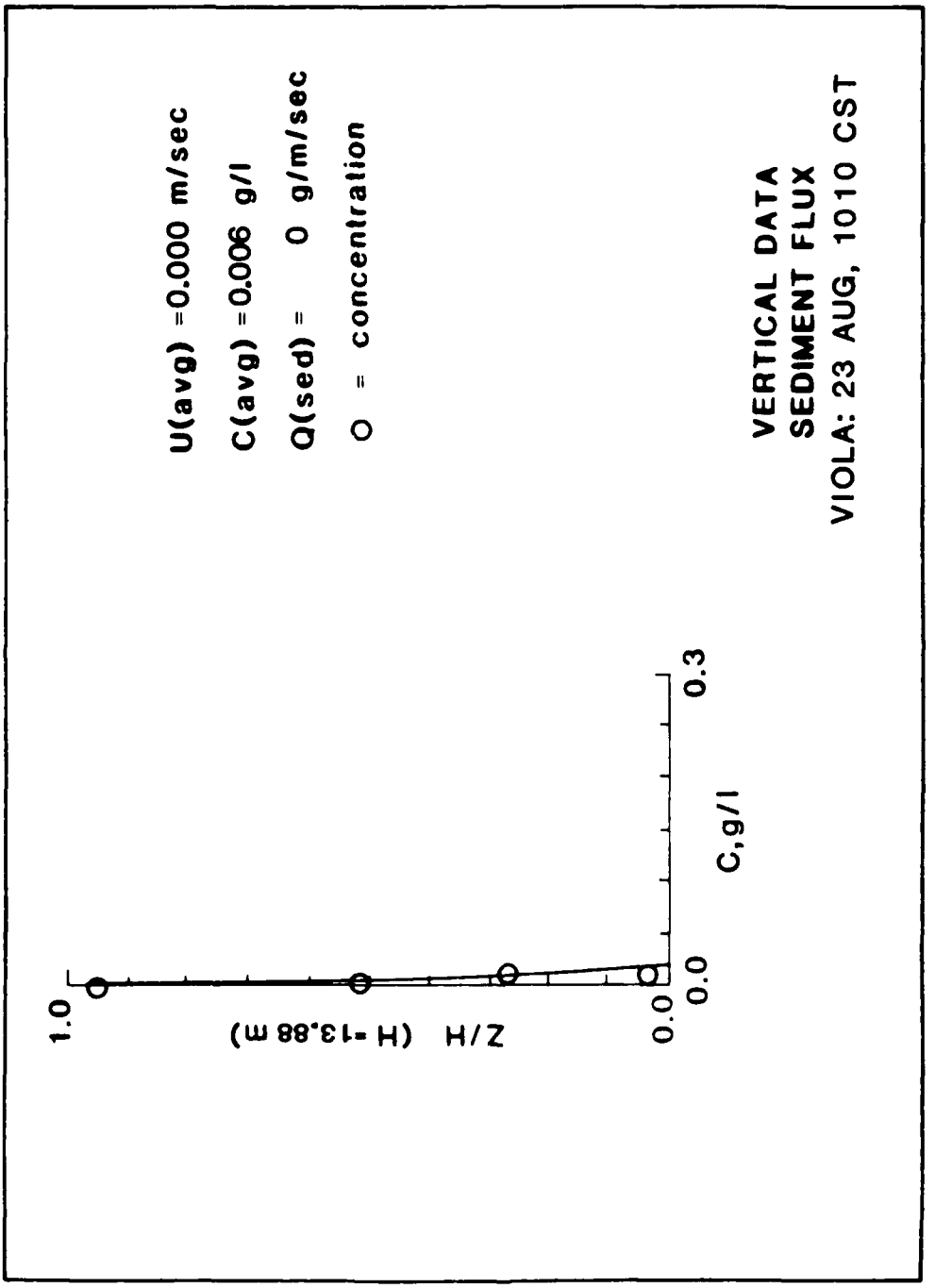
VERTICAL DATA
SEDIMENT FLUX
VIOLA: 23 AUG, 1010 CST
U(avg) =0.000 m/sec
C(avg) =0.006 g/l
Q(sed) = 0 g/m/sec
O = concentration
C,g/l
0.0
0.3
Z/H (H =13.88 m)
1.0
0.0

PLATE A28

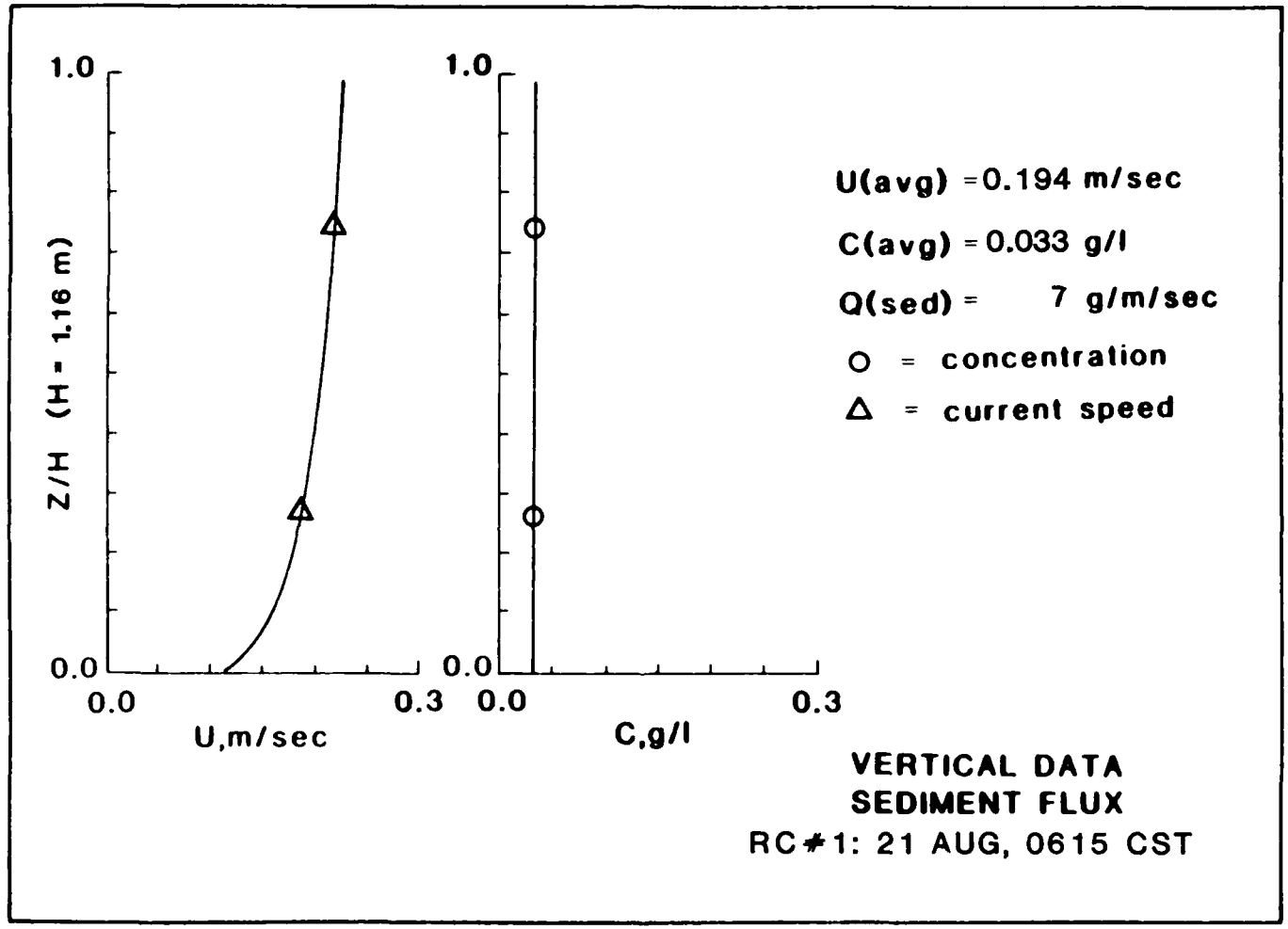
1.0
Z/H (H - 1.16 m)
0.0
0.0
0.3
U,m/sec
1.0
0.0
0.0
0.3
C,g/l
U(avg) = 0.194 m/sec
C(avg) = 0.033 g/l
Q(sed) = 7 g/m/sec
○ = concentration
△ = current speed
VERTICAL DATA
SEDIMENT FLUX
RC#1: 21 AUG, 0615 CST

PLATE A29

PLATE A30

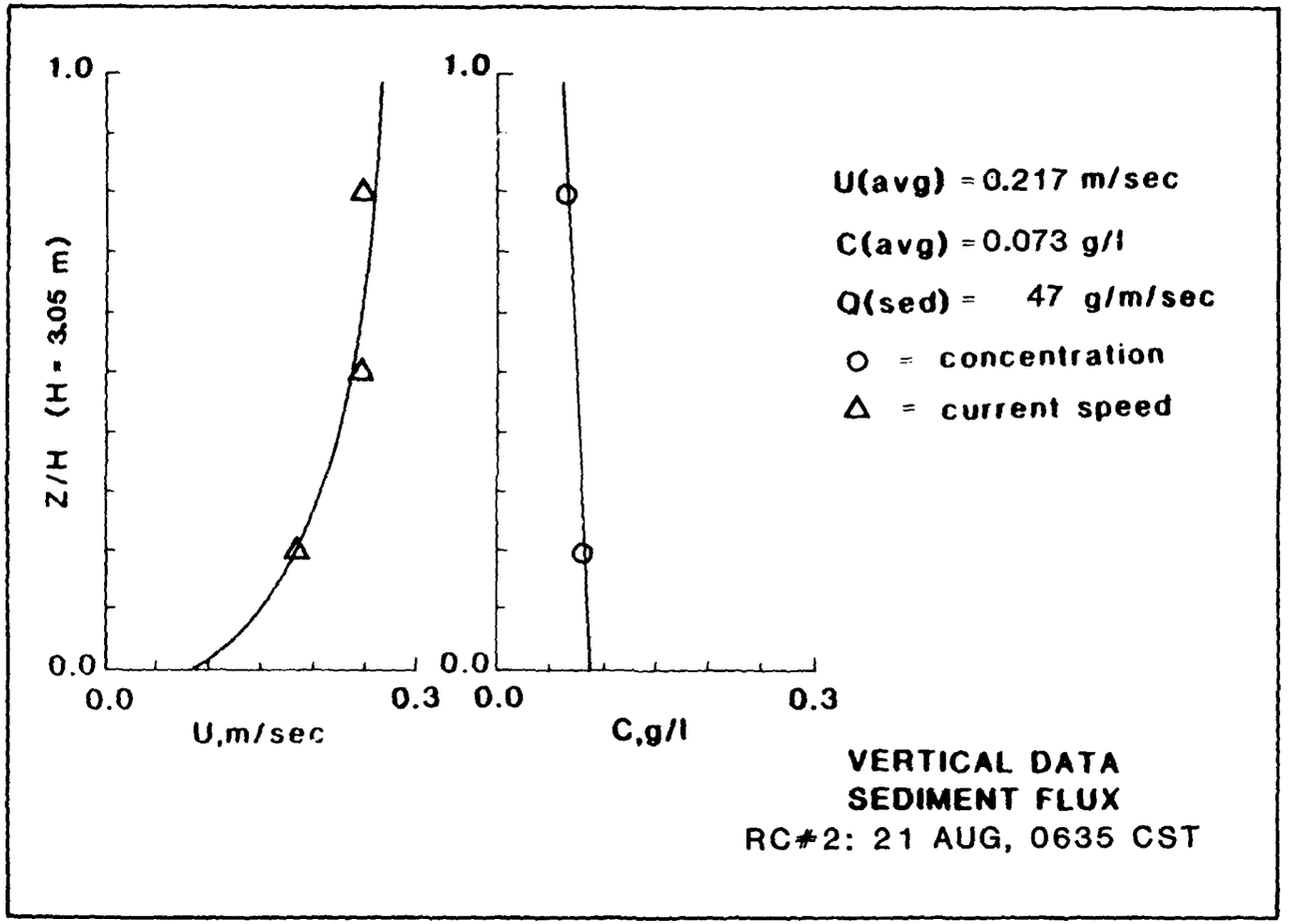

VERTICAL DATA
SEDIMENT FLUX
RC#2: 21 AUG, 0635 CST

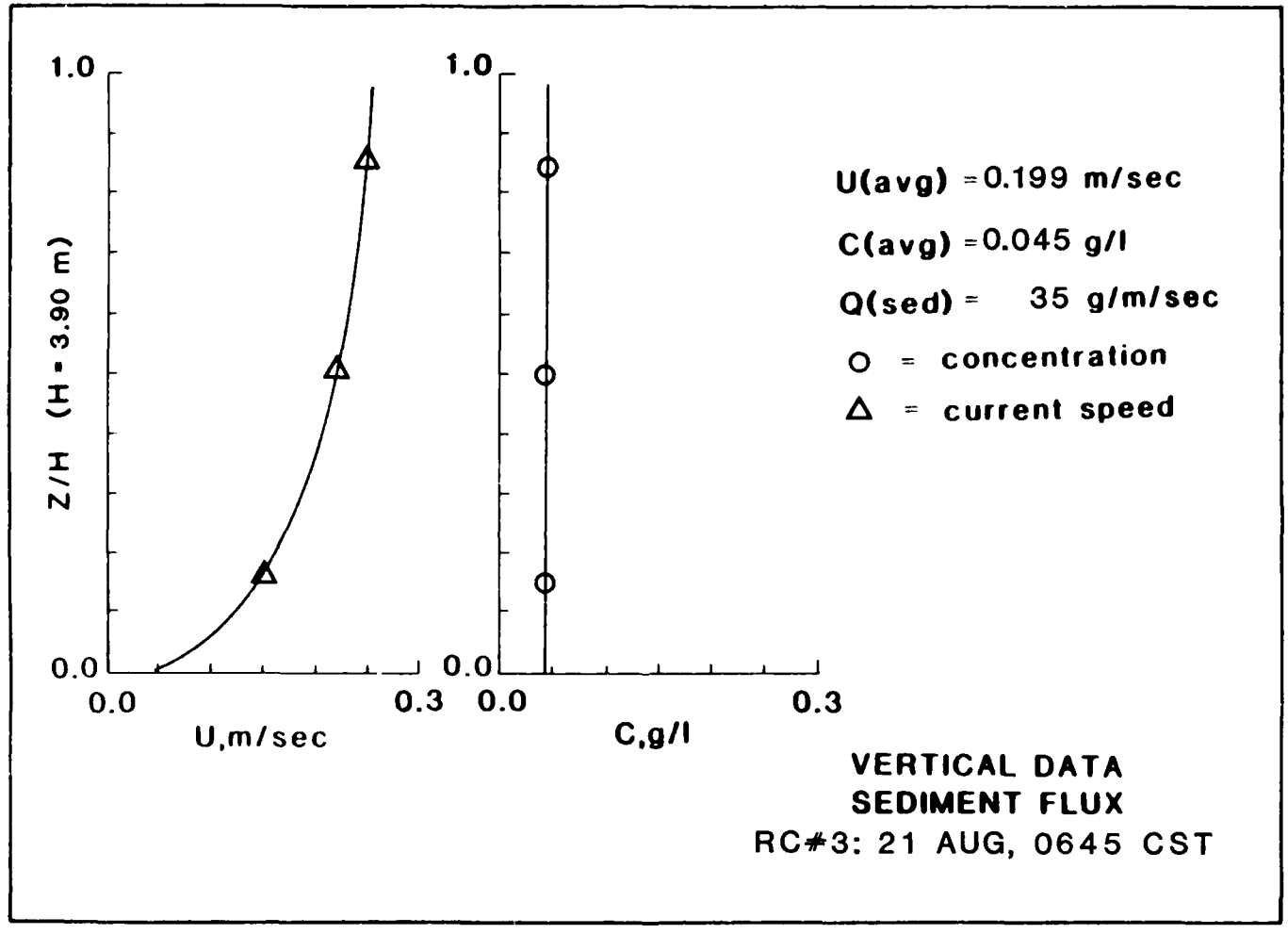
1.0
Z/H (H = 3.90 m)
0.0
0.0
0.3
U,m/sec
1.0
0.0
0.0
0.3
C,g/l
U(avg) = 0.199 m/sec
C(avg) = 0.045 g/l
Q(sed) = 35 g/m/sec
○ = concentration
△ = current speed
VERTICAL DATA
SEDIMENT FLUX
RC#3: 21 AUG, 0645 CST

PLATE A31

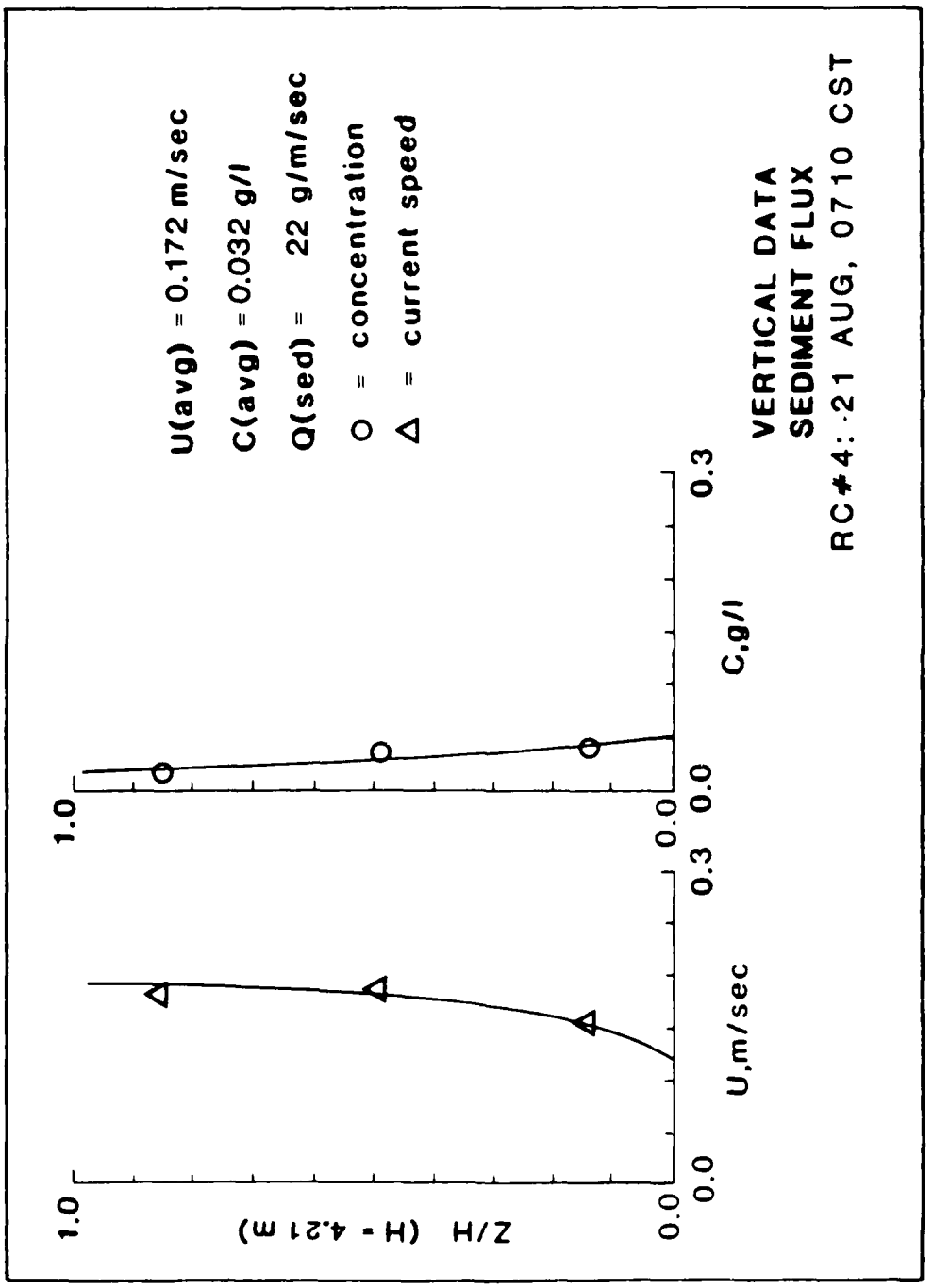
U(avg) = 0.172 m/sec
C(avg) = 0.032 g/l
Q(sed) = 22 g/m/sec
O = concentration
Δ = current speed
VERTICAL DATA
SEDIMENT FLUX
RC#4: 21 AUG, 0710 CST
Z/H (H = 4.21 m)
1.0
0.0
U,m/sec
0.0
0.3
C,g/l
0.0
0.3

PLATE A32

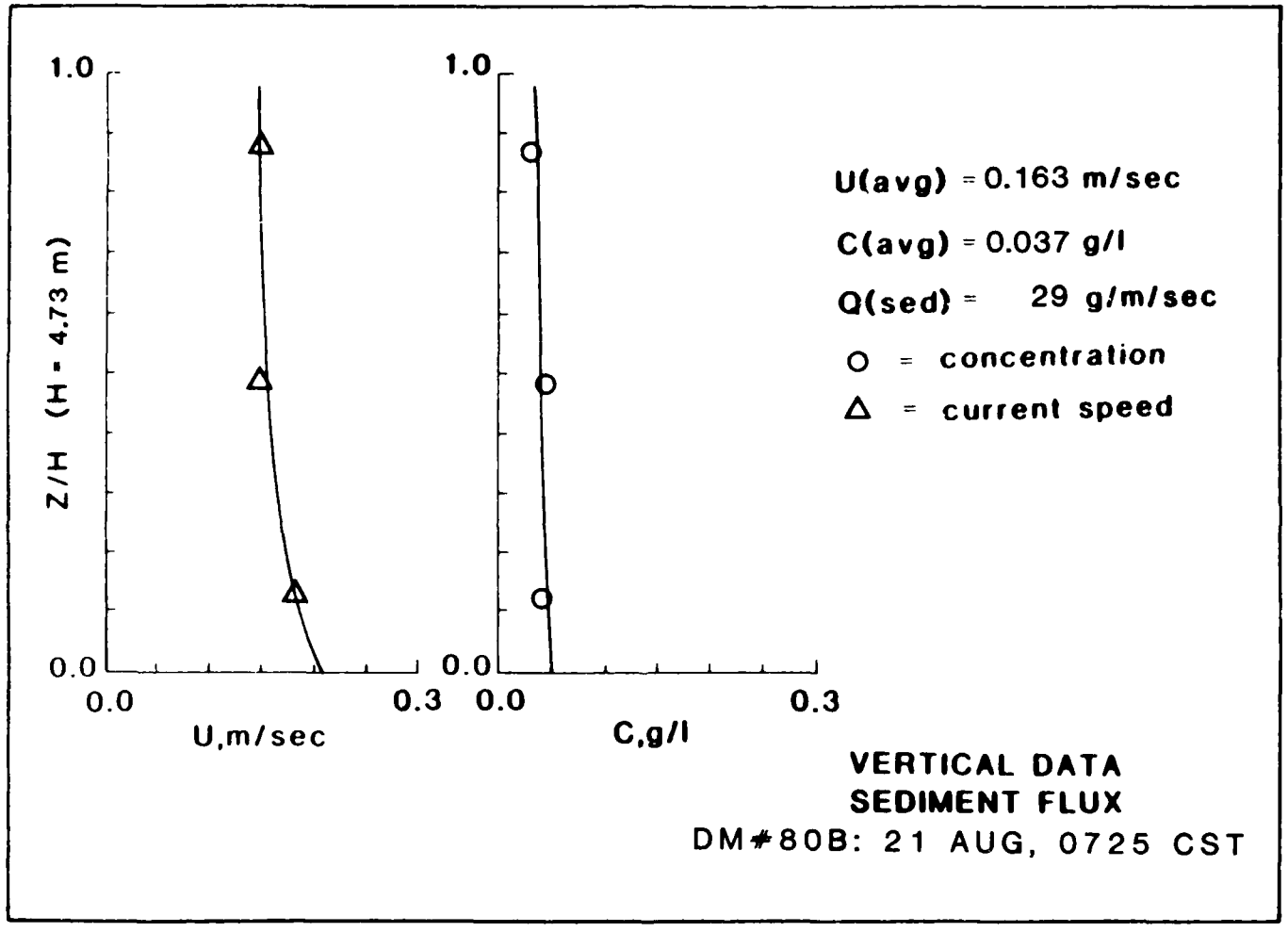
1.0
Z/H (H - 4.73 m)
0.0
0.0
0.3
U,m/sec
1.0
0.0
0.0
0.3
C,g/l
U(avg) = 0.163 m/sec
C(avg) = 0.037 g/l
Q(sed) = 29 g/m/sec
O = concentration
Δ = current speed
VERTICAL DATA
SEDIMENT FLUX
DM#80B: 21 AUG, 0725 CST

PLATE A33

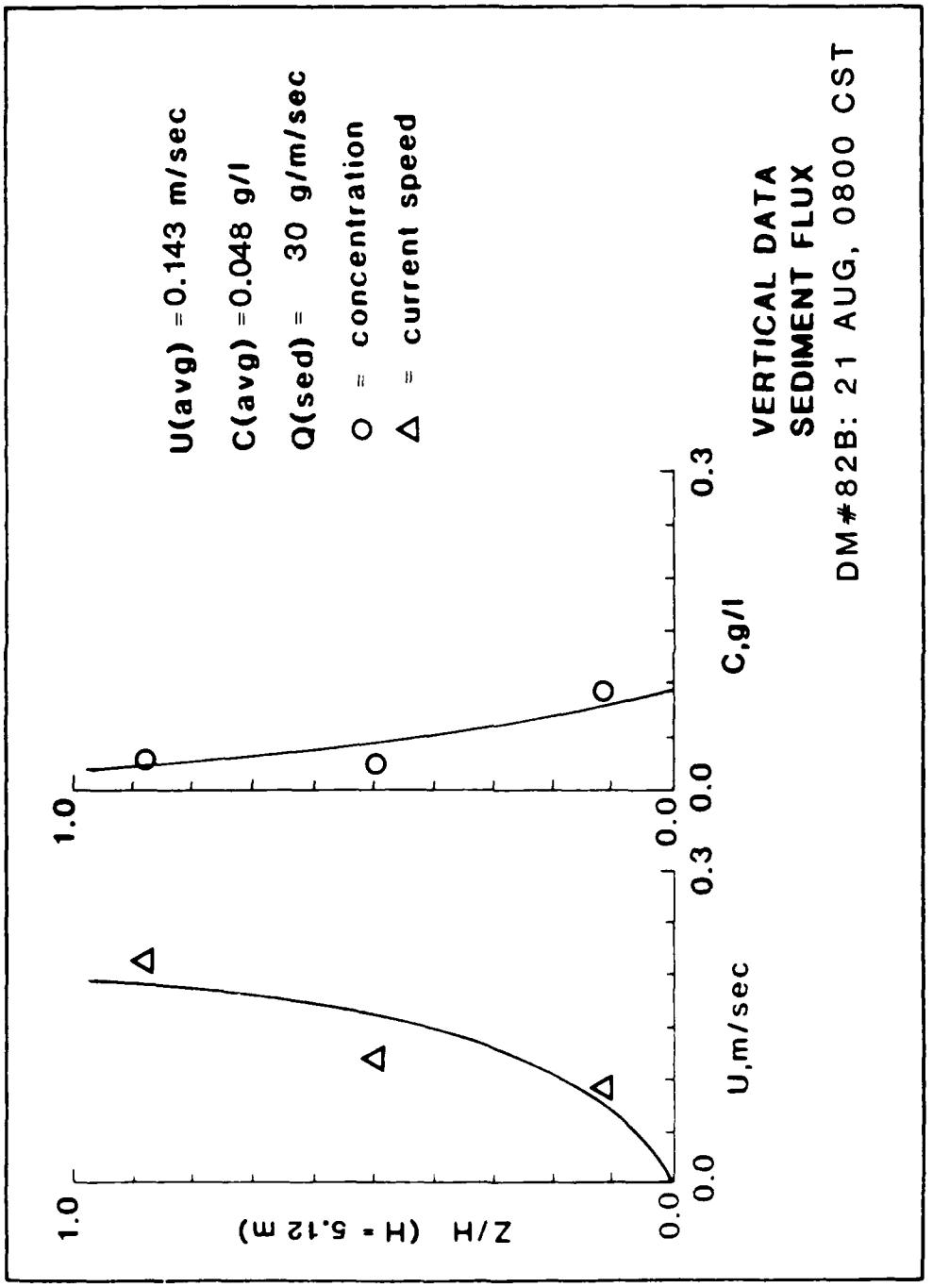
U(avg) =0.143 m/sec
C(avg) =0.048 g/l
Q(sed) = 30 g/m/sec
○ = concentration
Δ = current speed
VERTICAL DATA
SEDIMENT FLUX
DM#82B: 21 AUG, 0800 CST
Z/H (H = 5.12 m)
1.0
0.0
U,m/sec
0.0
0.3
C,g/l
0.0
0.3

PLATE A34

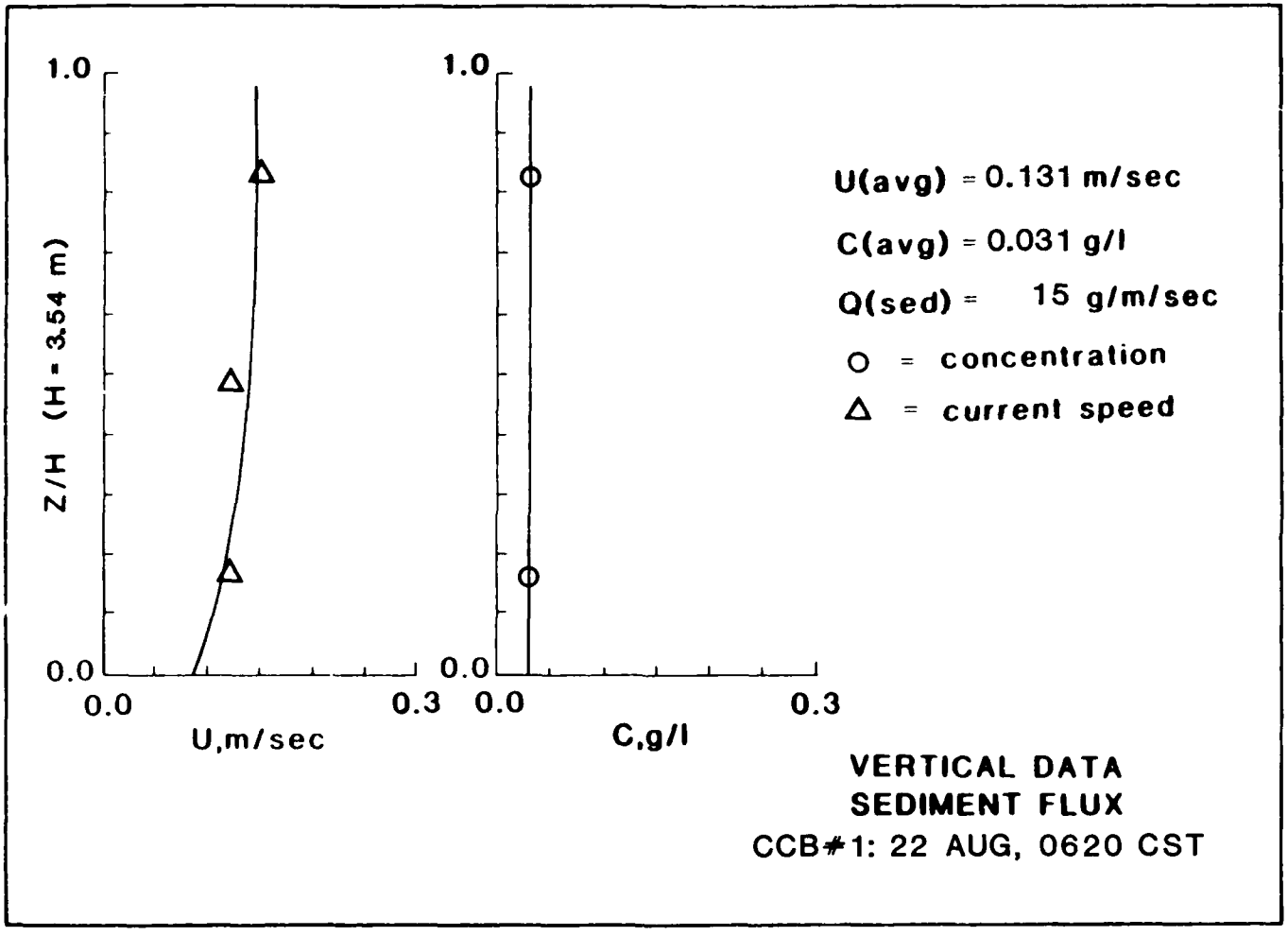
1.0
Z/H (H = 3.54 m)
0.0
0.0
0.3
U,m/sec
1.0
0.0
0.0
0.3
C,g/l
U(avg) = 0.131 m/sec
C(avg) = 0.031 g/l
Q(sed) = 15 g/m/sec
○ = concentration
△ = current speed
VERTICAL DATA
SEDIMENT FLUX
CCB#1: 22 AUG, 0620 CST

PLATE A35

PLATE A36

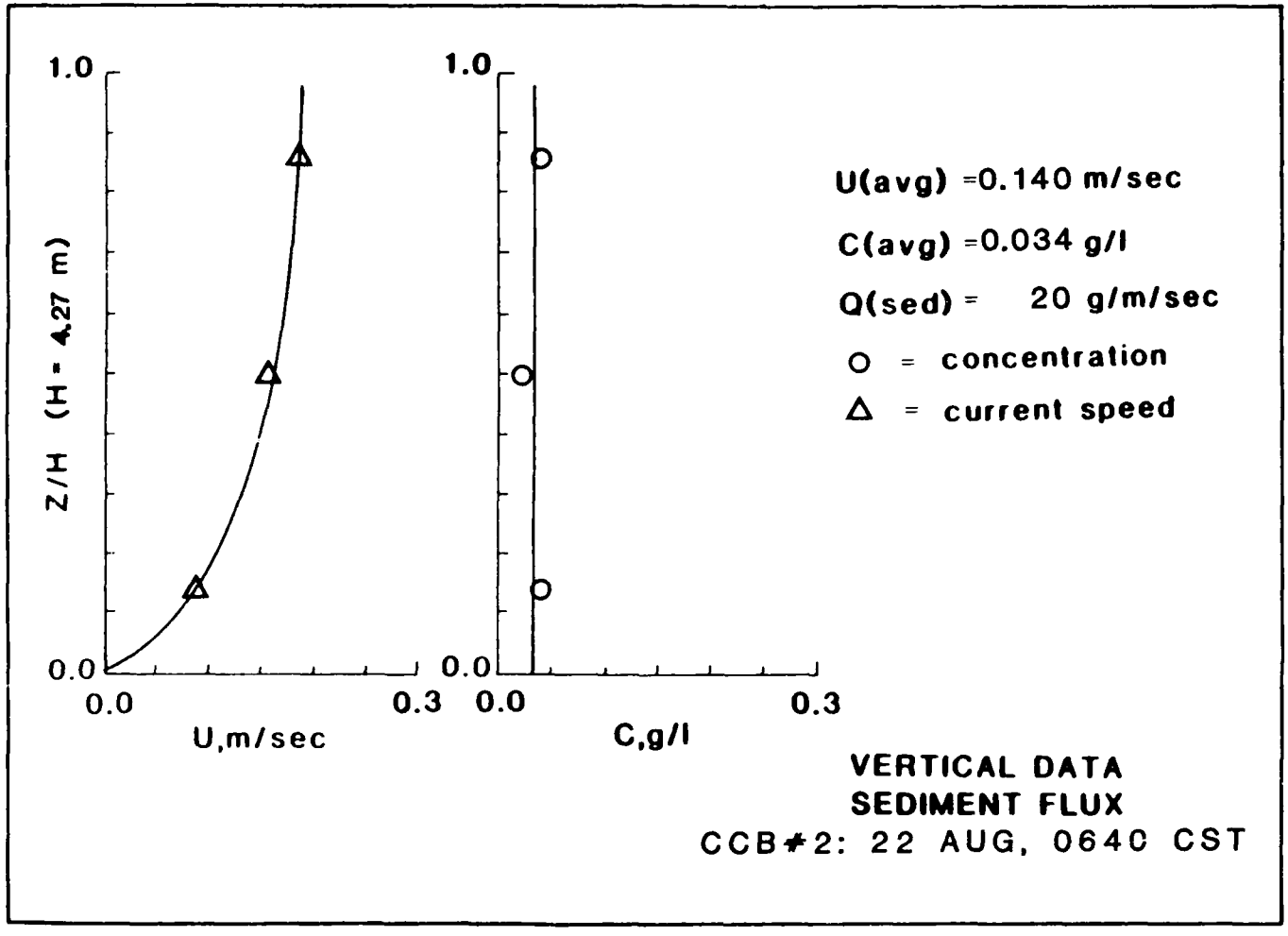
1.0
Z/H (H = 4.27 m)
0.0
0.0
0.3
U,m/sec
1.0
0.0
0.0
0.3
C,g/l
U(avg) =0.140 m/sec
C(avg) =0.034 g/l
Q(sed) = 20 g/m/sec
O = concentration
Δ = current speed
VERTICAL DATA
SEDIMENT FLUX
CCB#2: 22 AUG, 0640 CST

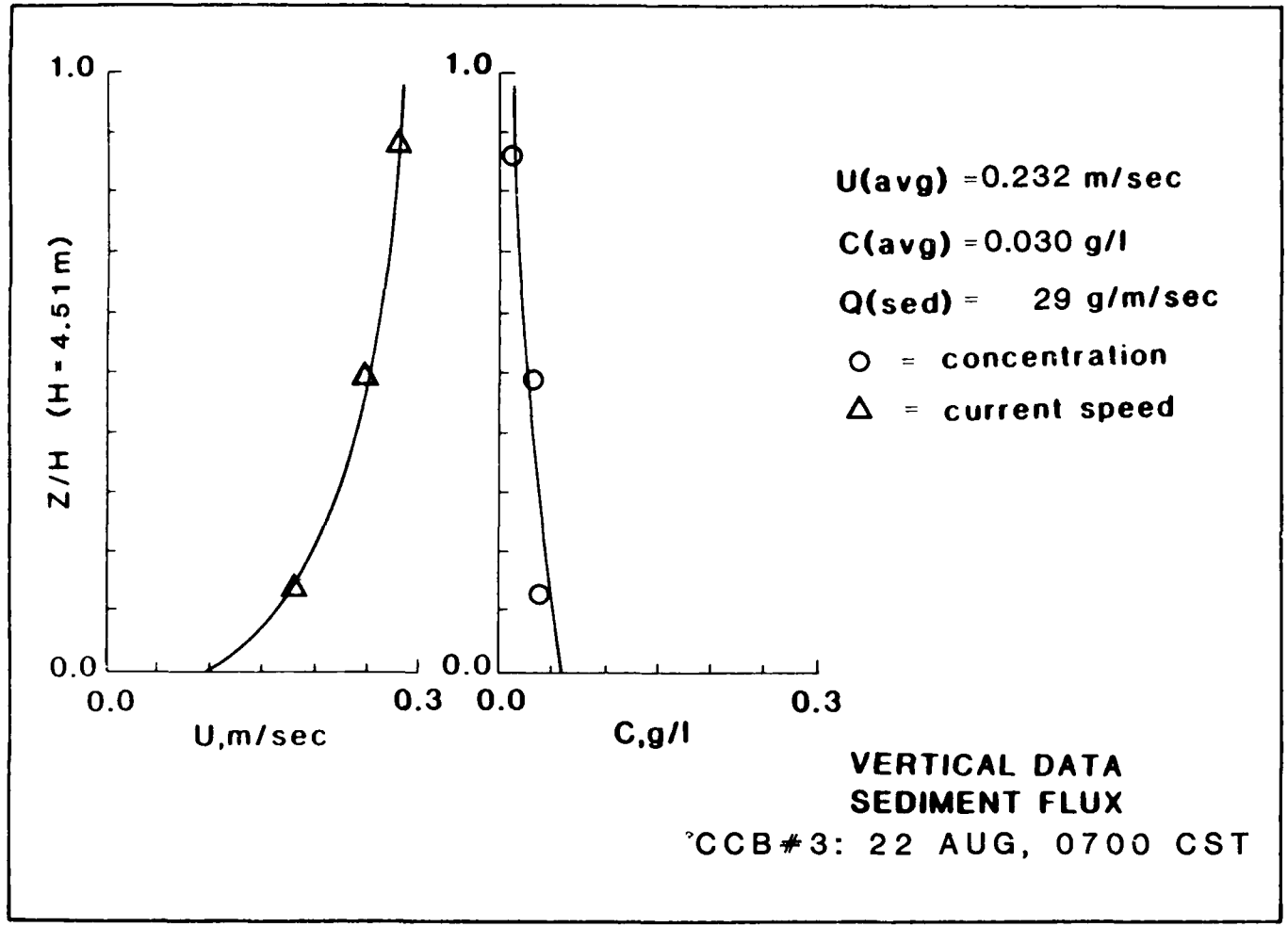
1.0
Z/H (H = 4.51m)
0.0
0.0
0.3
U,m/sec
1.0
0.0
0.0
0.3
C,g/l
U(avg) =0.232 m/sec
C(avg) =0.030 g/l
Q(sed) = 29 g/m/sec
○ = concentration
△ = current speed
VERTICAL DATA
SEDIMENT FLUX
°CCB#3: 22 AUG, 0700 CST

PLATE A37

PLATE A38

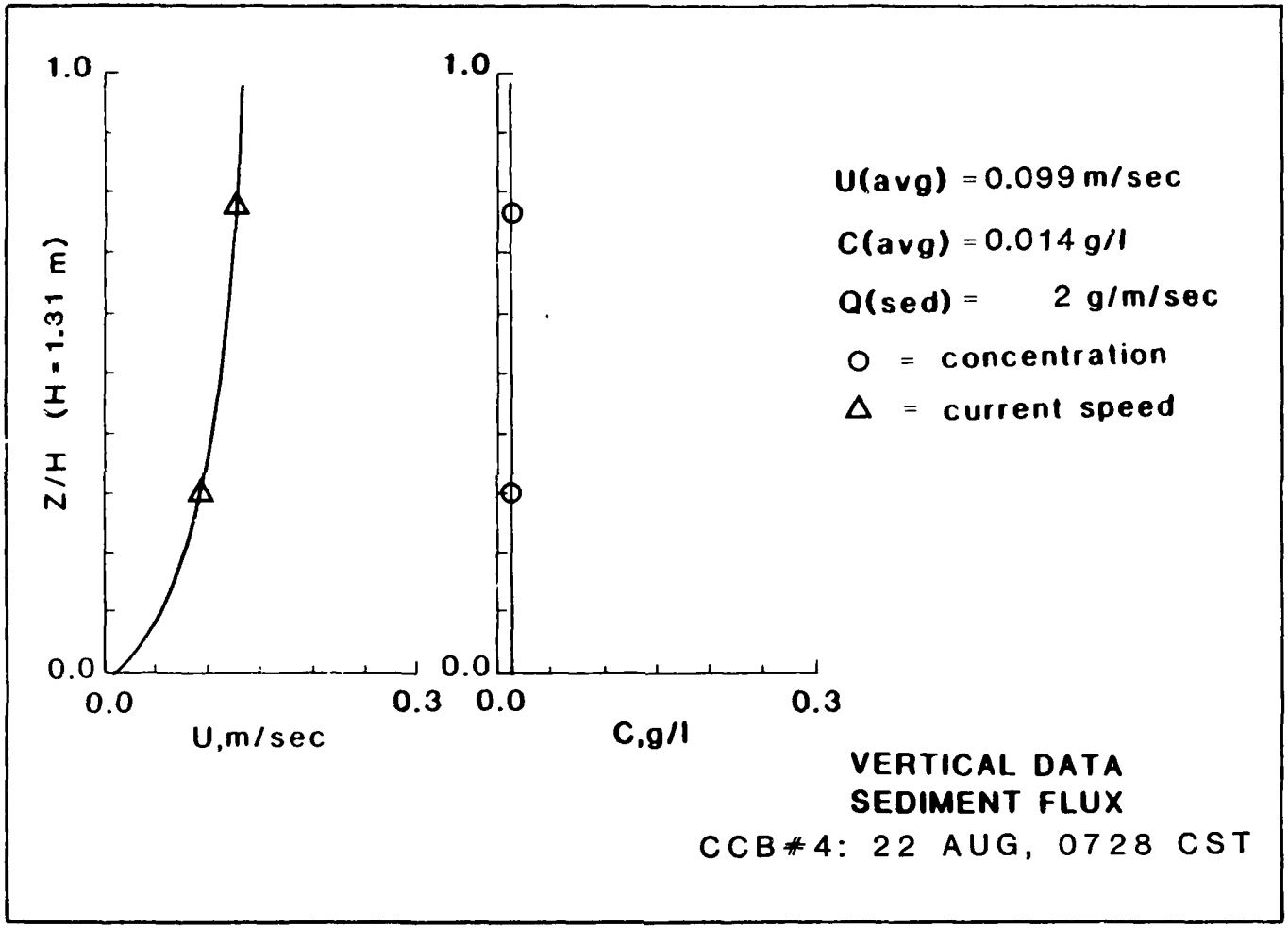
1.0
Z/H (H = 1.31 m)
0.0
0.0
0.3
U,m/sec
1.0
0.0
0.0
0.3
C,g/l
U(avg) = 0.099 m/sec
C(avg) = 0.014 g/l
Q(sed) = 2 g/m/sec
○ = concentration
△ = current speed
VERTICAL DATA
SEDIMENT FLUX
CCB#4: 22 AUG, 0728 CST

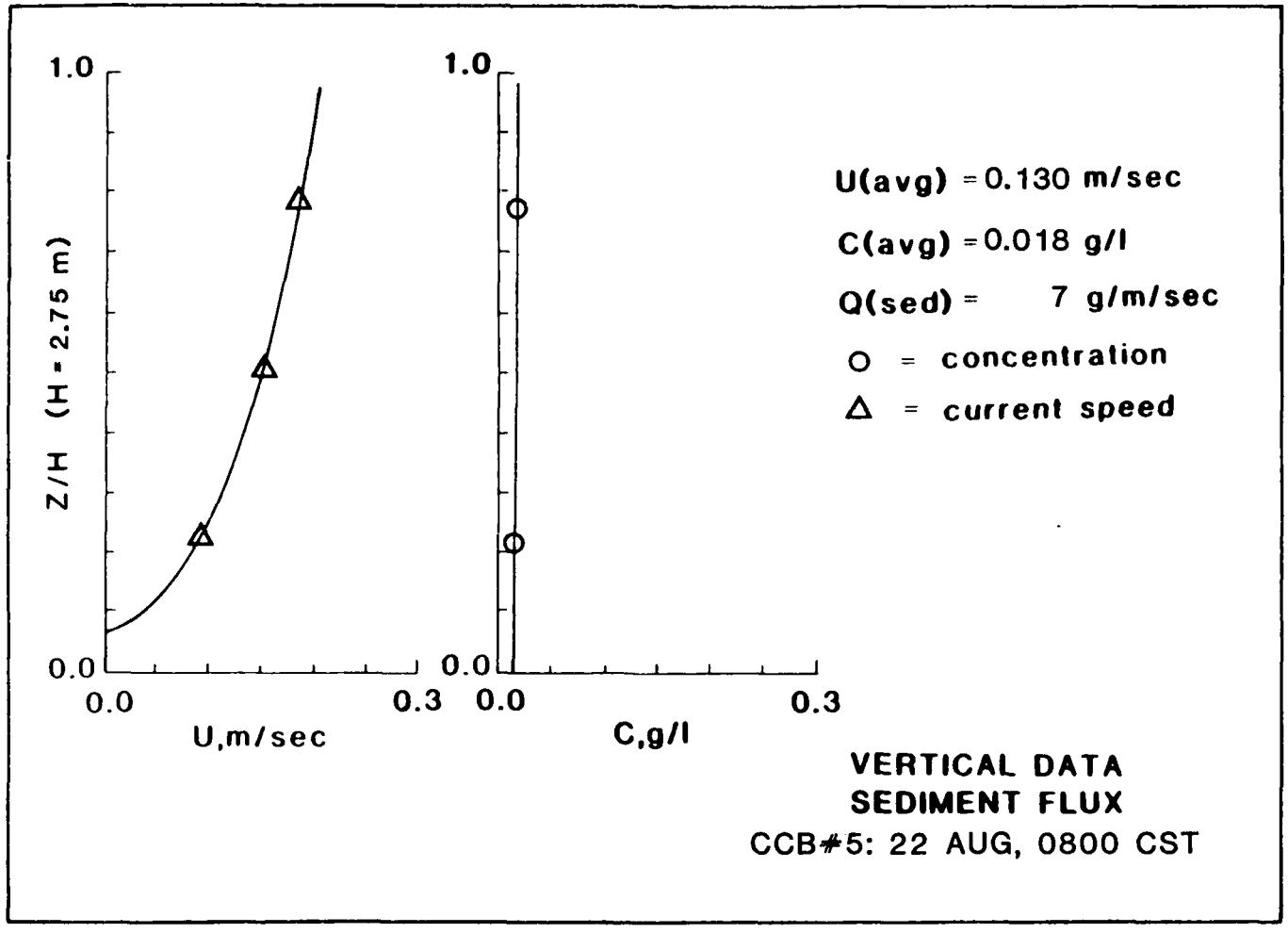
1.0
Z/H (H = 2.75 m)
0.0
0.0
0.3
U,m/sec
1.0
0.0
0.0
0.3
C,g/l
U(avg) = 0.130 m/sec
C(avg) = 0.018 g/l
Q(sed) = 7 g/m/sec
O = concentration
Δ = current speed
VERTICAL DATA
SEDIMENT FLUX
CCB#5: 22 AUG, 0800 CST

PLATE A39

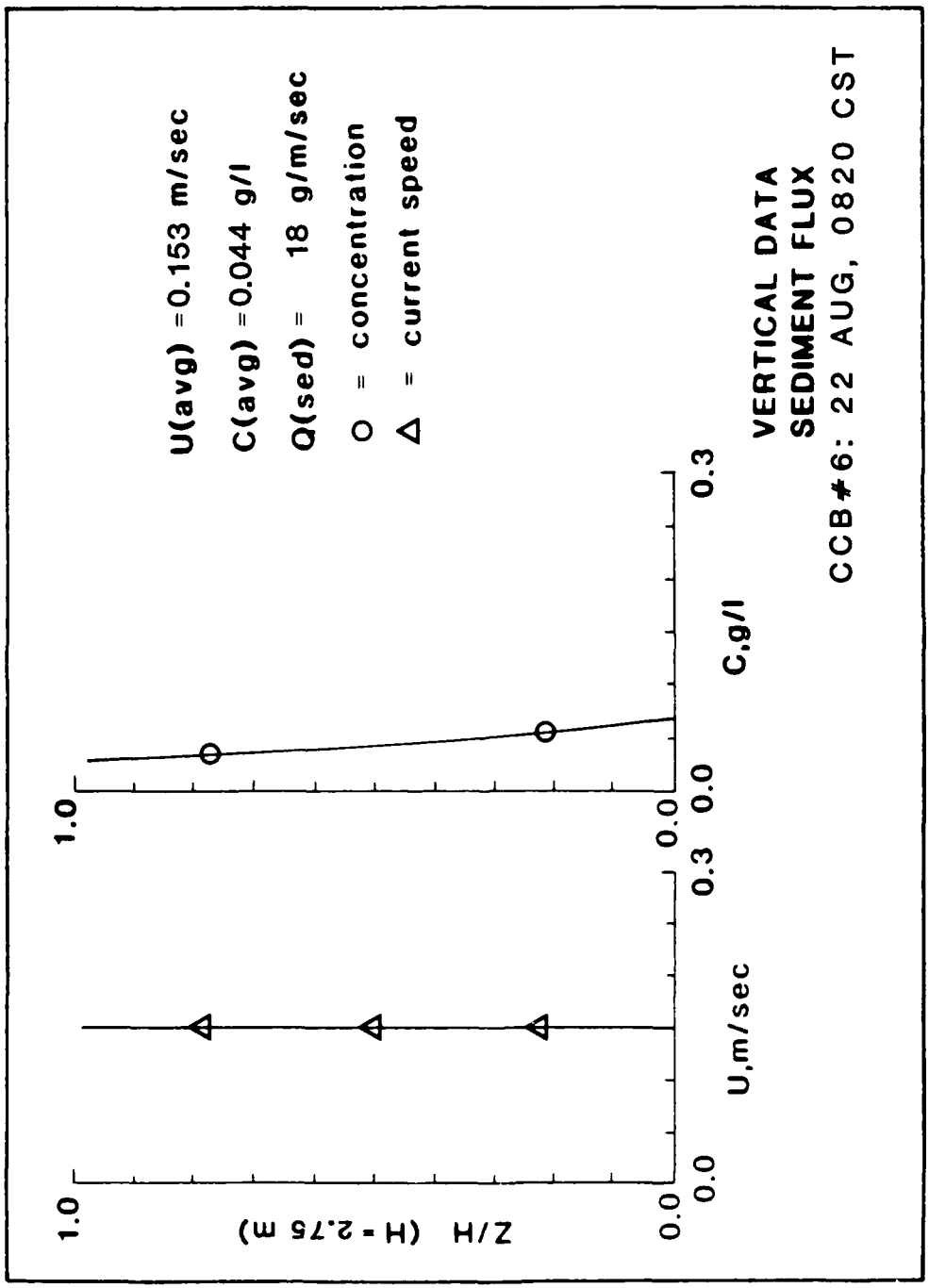
VERTICAL DATA
SEDIMENT FLUX
CCB#6: 22 AUG, 0820 CST
U(avg) =0.153 m/sec
C(avg) =0.044 g/l
Q(sed) = 18 g/m/sec
O = concentration
Δ = current speed
Z/H (H = 2.75 m)
1.0
0.0
U,m/sec
0.0
0.3
C,g/l
0.0
0.3

PLATE A40

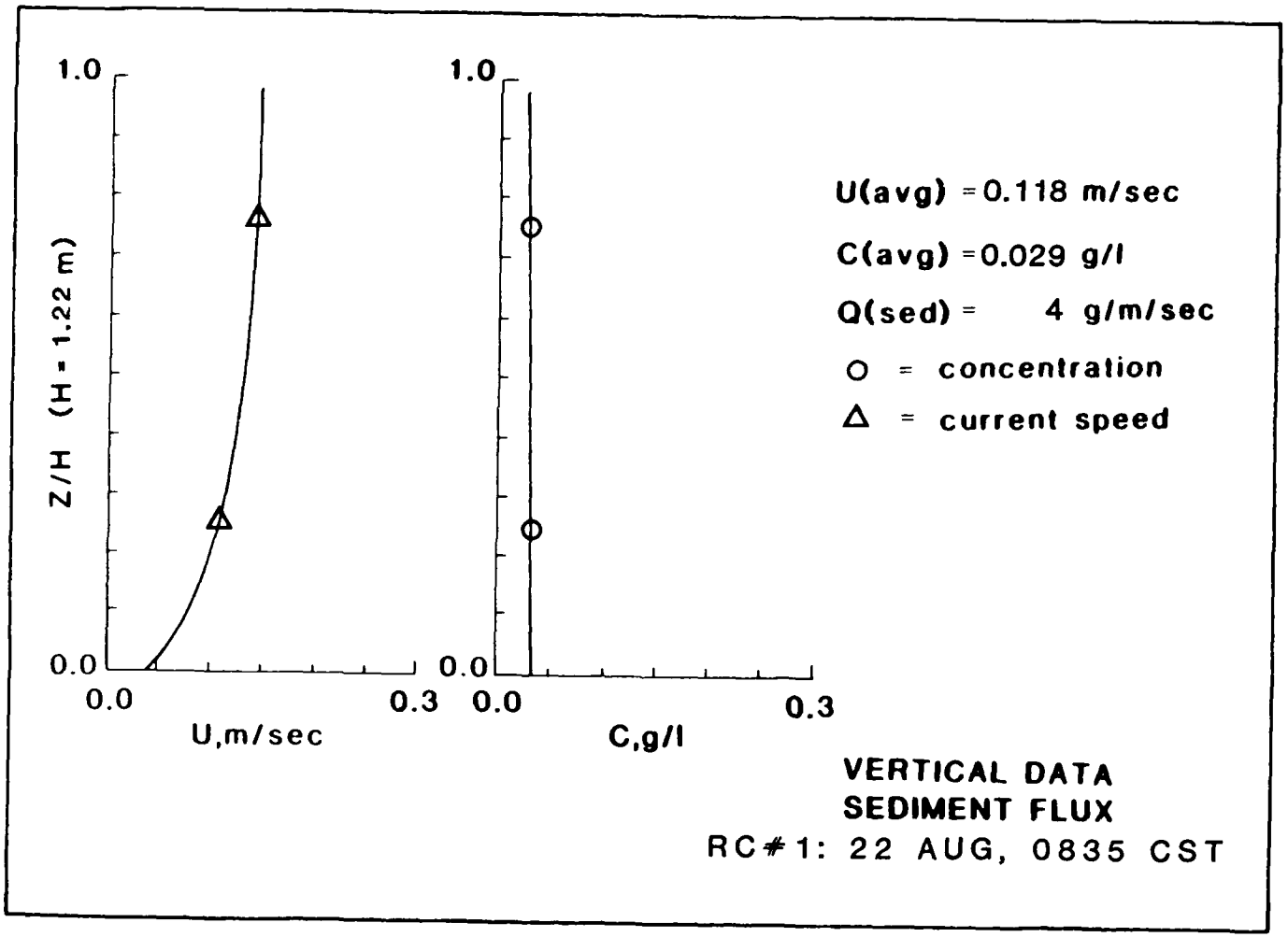
1.0
Z/H (H = 1.22 m)
0.0
0.0
0.3
U,m/sec
1.0
0.0
0.0
0.3
C,g/l
U(avg) = 0.118 m/sec
C(avg) = 0.029 g/l
Q(sed) = 4 g/m/sec
O = concentration
Δ = current speed
VERTICAL DATA
SEDIMENT FLUX
RC#1: 22 AUG, 0835 CST

PLATE A41

PLATE A42

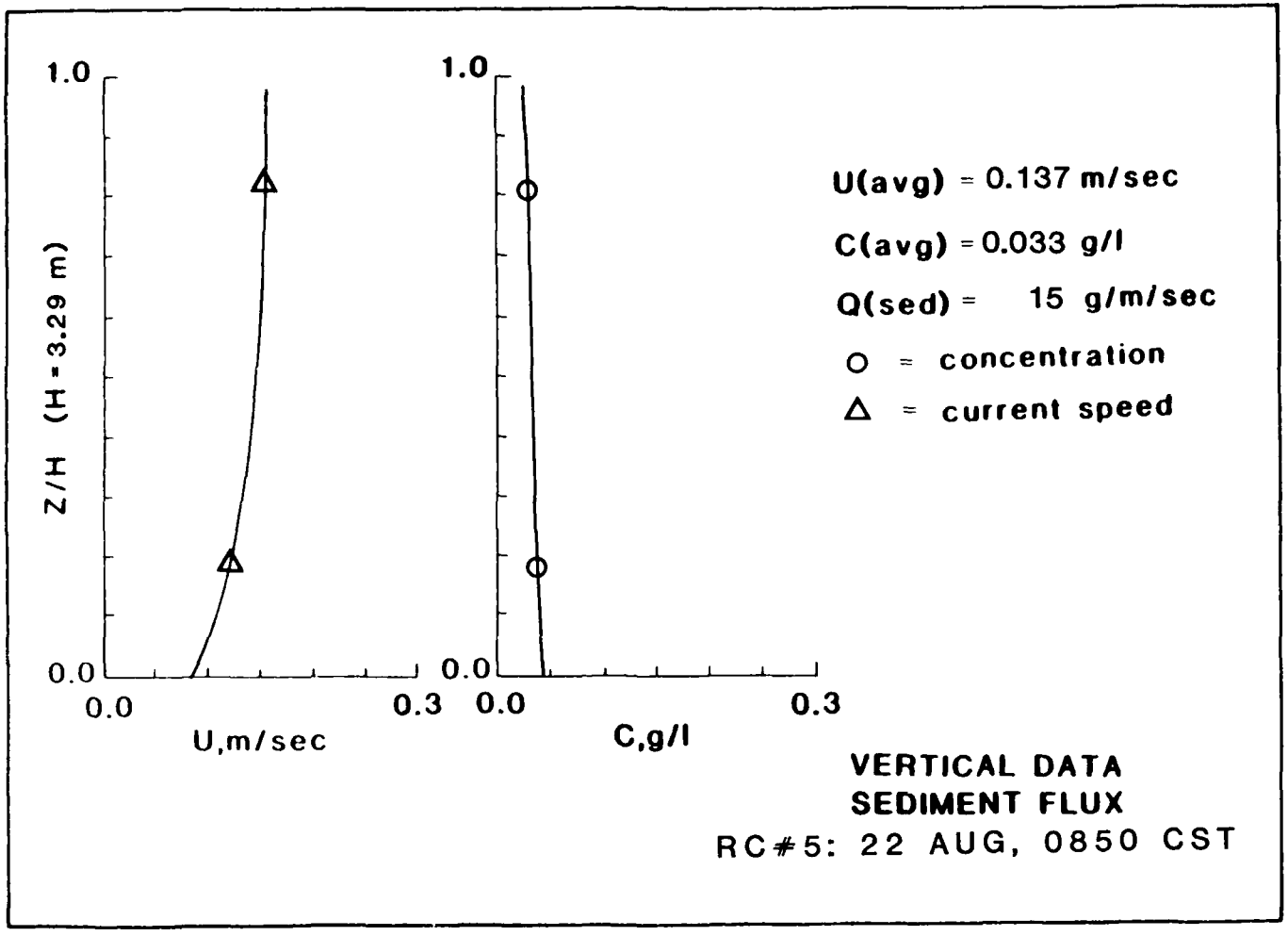
1.0
Z/H (H = 3.29 m)
0.0
0.0
0.3
U,m/sec
1.0
0.0
0.0
0.3
C,g/l
U(avg) = 0.137 m/sec
C(avg) = 0.033 g/l
Q(sed) = 15 g/m/sec
○ = concentration
△ = current speed
VERTICAL DATA
SEDIMENT FLUX
RC#5: 22 AUG, 0850 CST

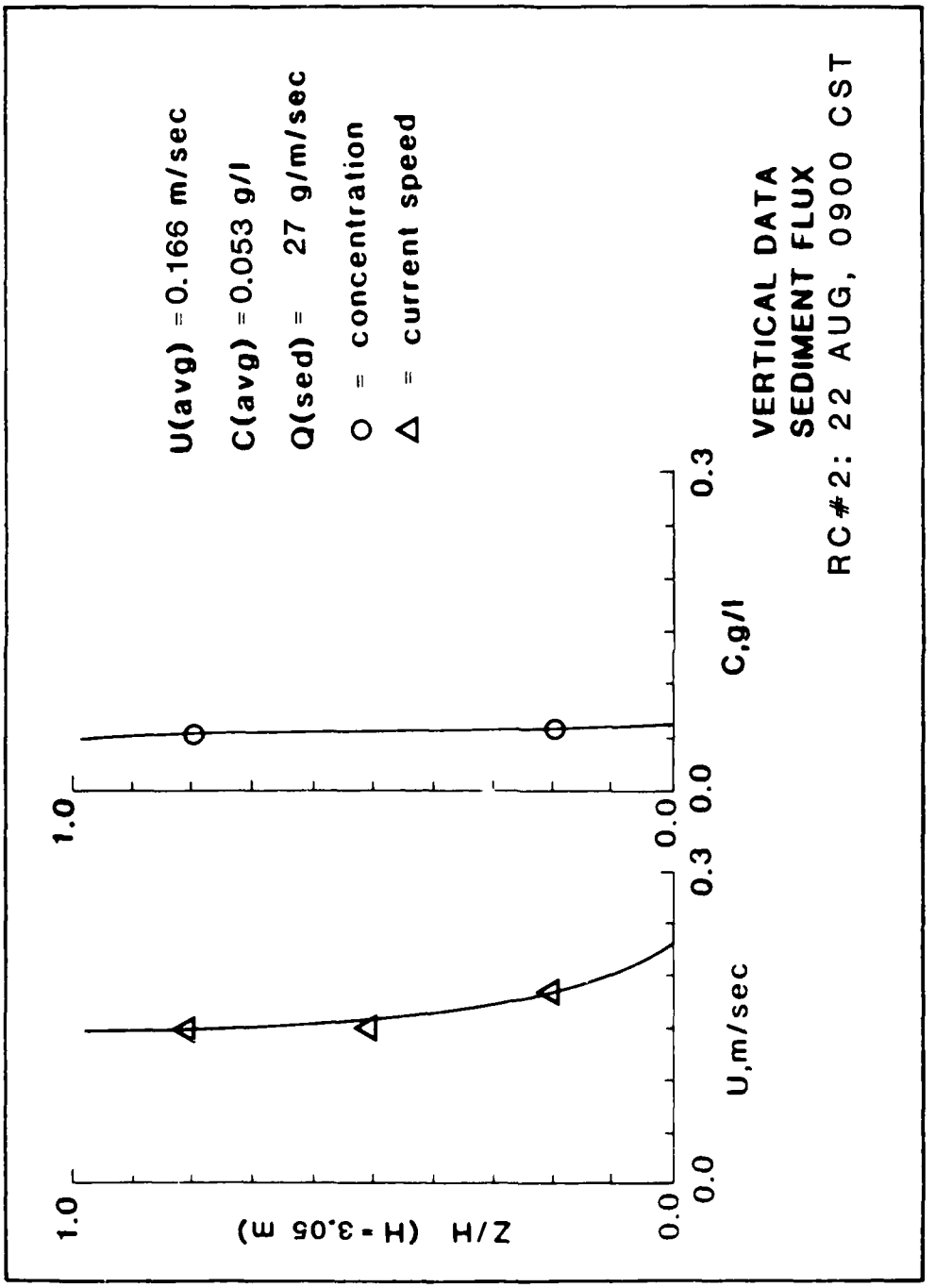
U(avg) = 0.166 m/sec
C(avg) = 0.053 g/l
Q(sed) = 27 g/m/sec
○ = concentration
△ = current speed
VERTICAL DATA
SEDIMENT FLUX
RC#2: 22 AUG, 0900 CST
Z/H (H = 3.05 m)
1.0
0.0
U,m/sec
0.0
0.3
C,g/l
0.0
0.3

PLATE A43

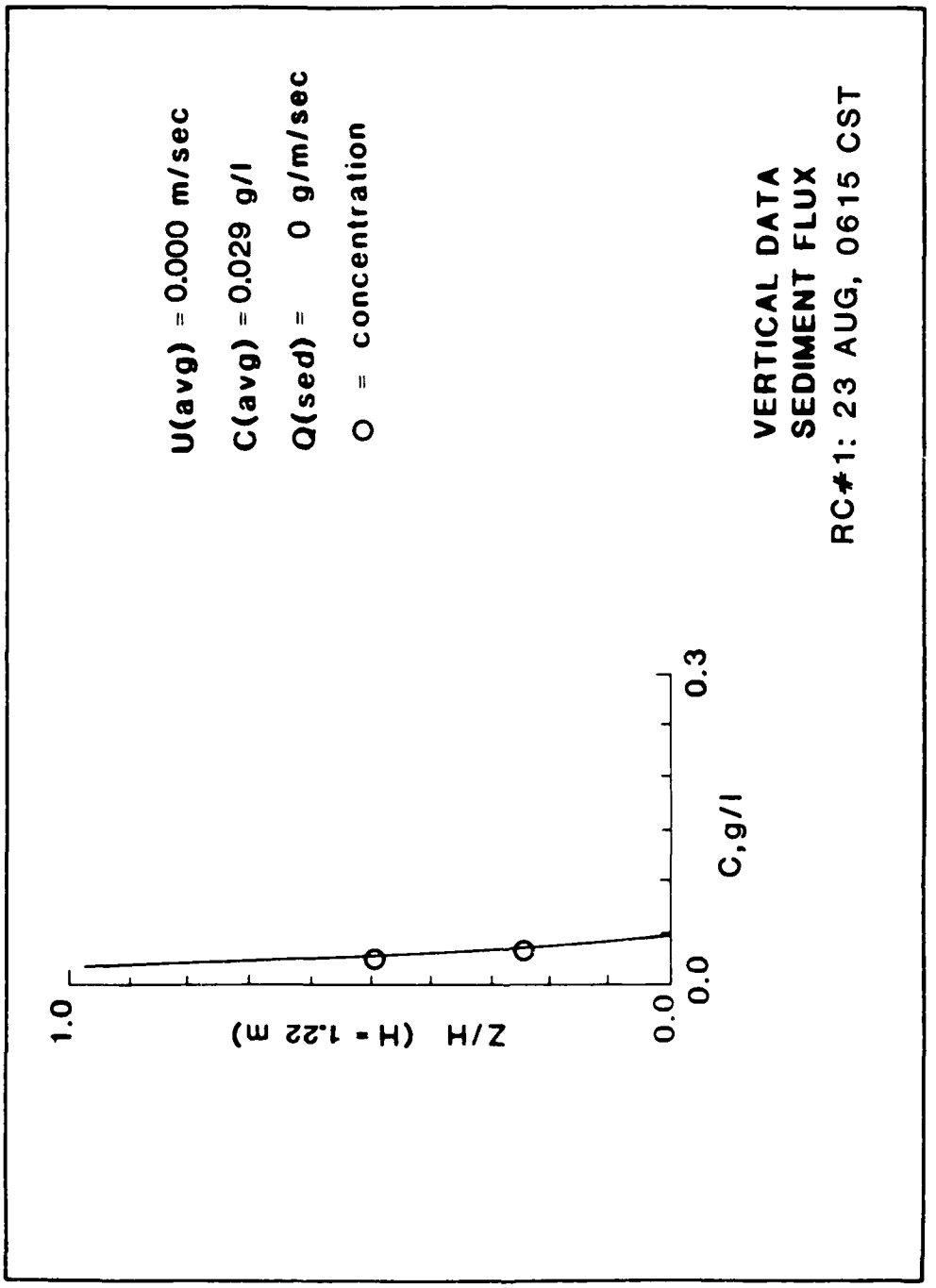
U(avg) = 0.000 m/sec
C(avg) = 0.029 g/l
Q(sed) = 0 g/m/sec
O = concentration
VERTICAL DATA
SEDIMENT FLUX
RC#1: 23 AUG, 0615 CST
1.0
0.0
Z/H (H = 1.22 m)
0.0
0.3
C,g/l

PLATE A44

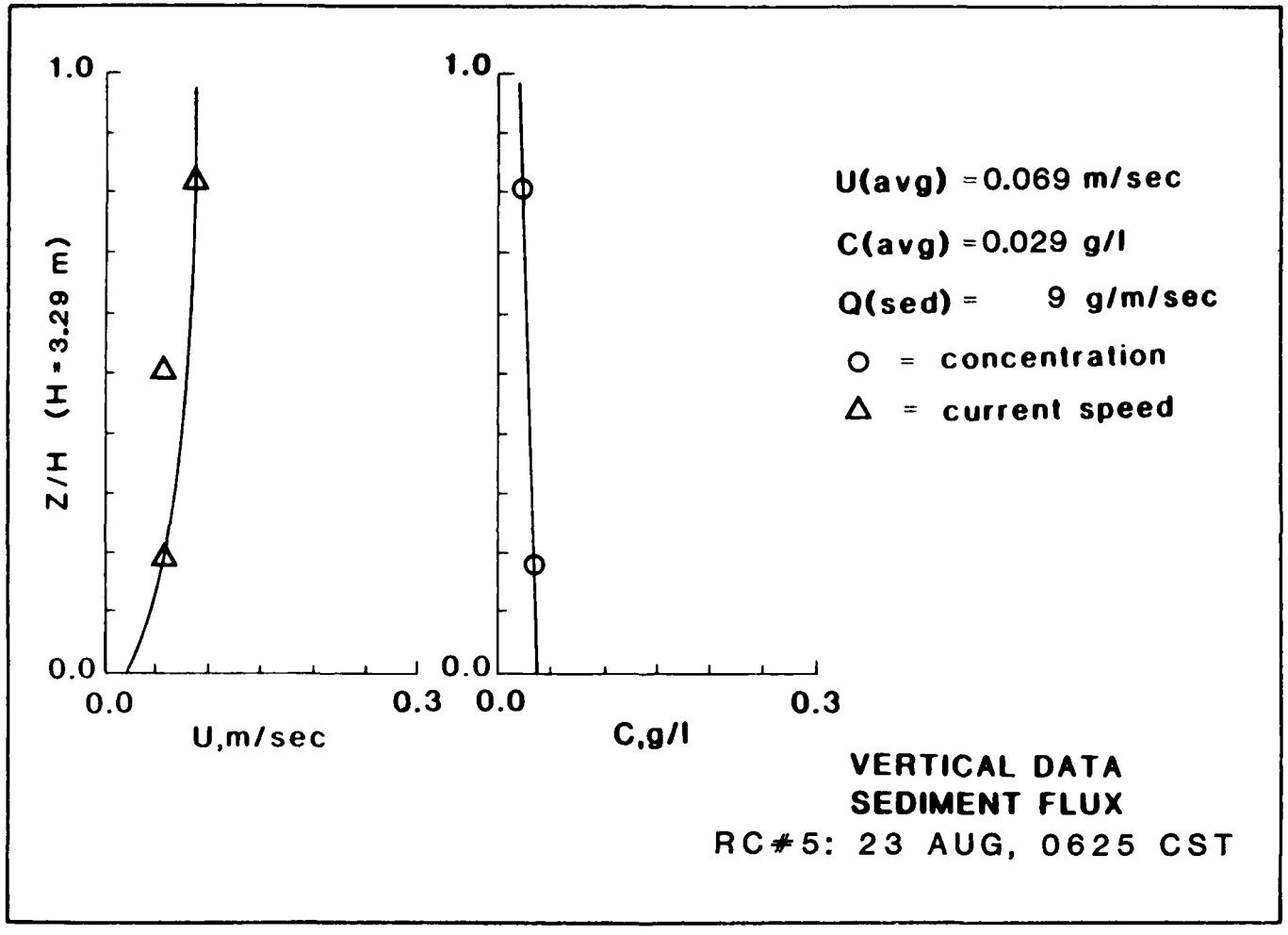
1.0
Z/H (H = 3.29 m)
0.0
0.0
0.3
U,m/sec
1.0
0.0
0.0
0.3
C,g/l
U(avg) = 0.069 m/sec
C(avg) = 0.029 g/l
Q(sed) = 9 g/m/sec
○ = concentration
△ = current speed
VERTICAL DATA
SEDIMENT FLUX
RC#5: 23 AUG, 0625 CST

PLATE A45

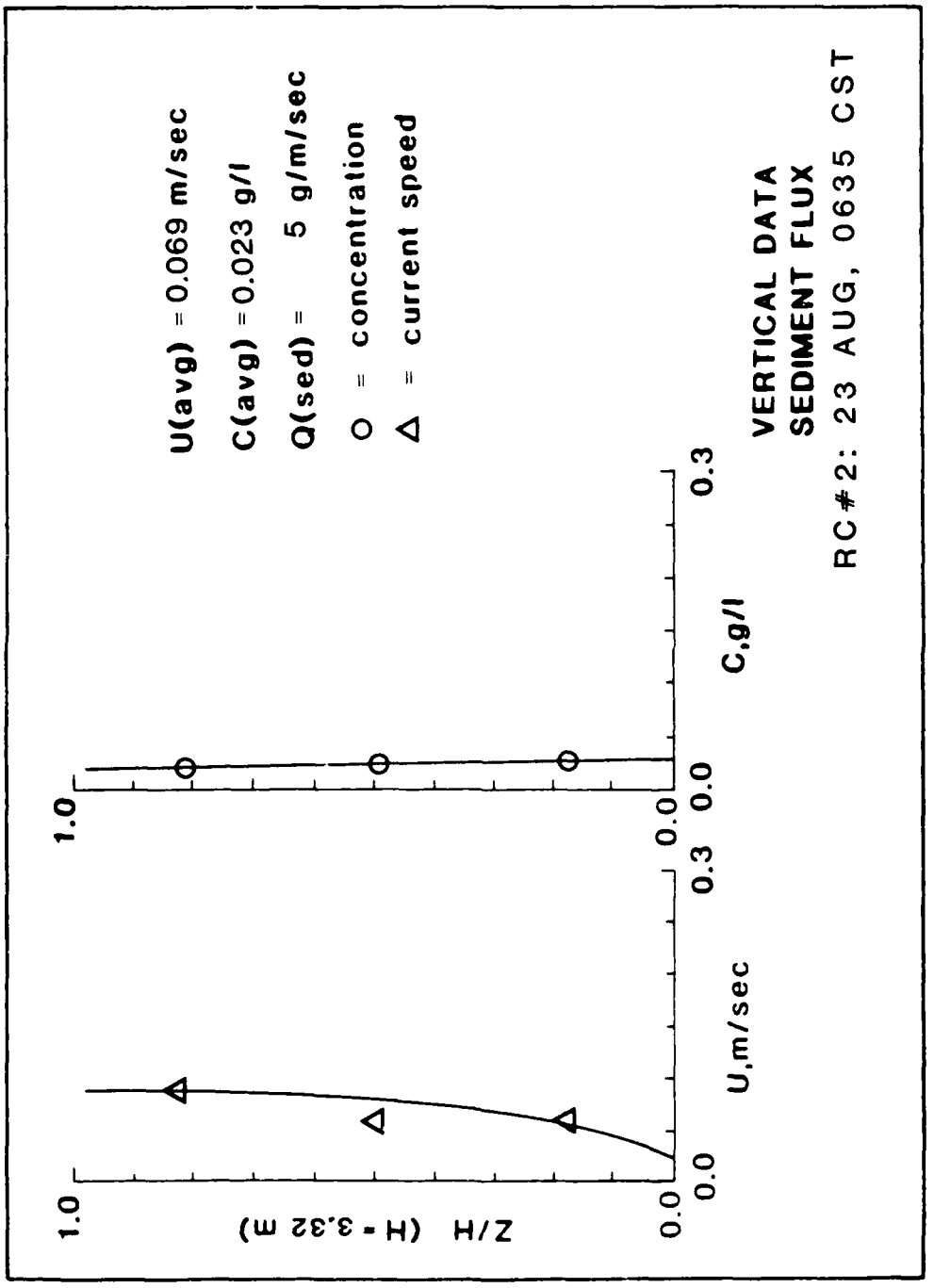
U(avg) = 0.069 m/sec
C(avg) = 0.023 g/l
Q(sed) = 5 g/m/sec
O = concentration
Δ = current speed
VERTICAL DATA
SEDIMENT FLUX
RC#2: 23 AUG, 0635 CST
Z/H (H = 3.32 m)
1.0
0.0
U,m/sec
0.0
0.3
C,g/l
0.0
0.3

PLATE A46

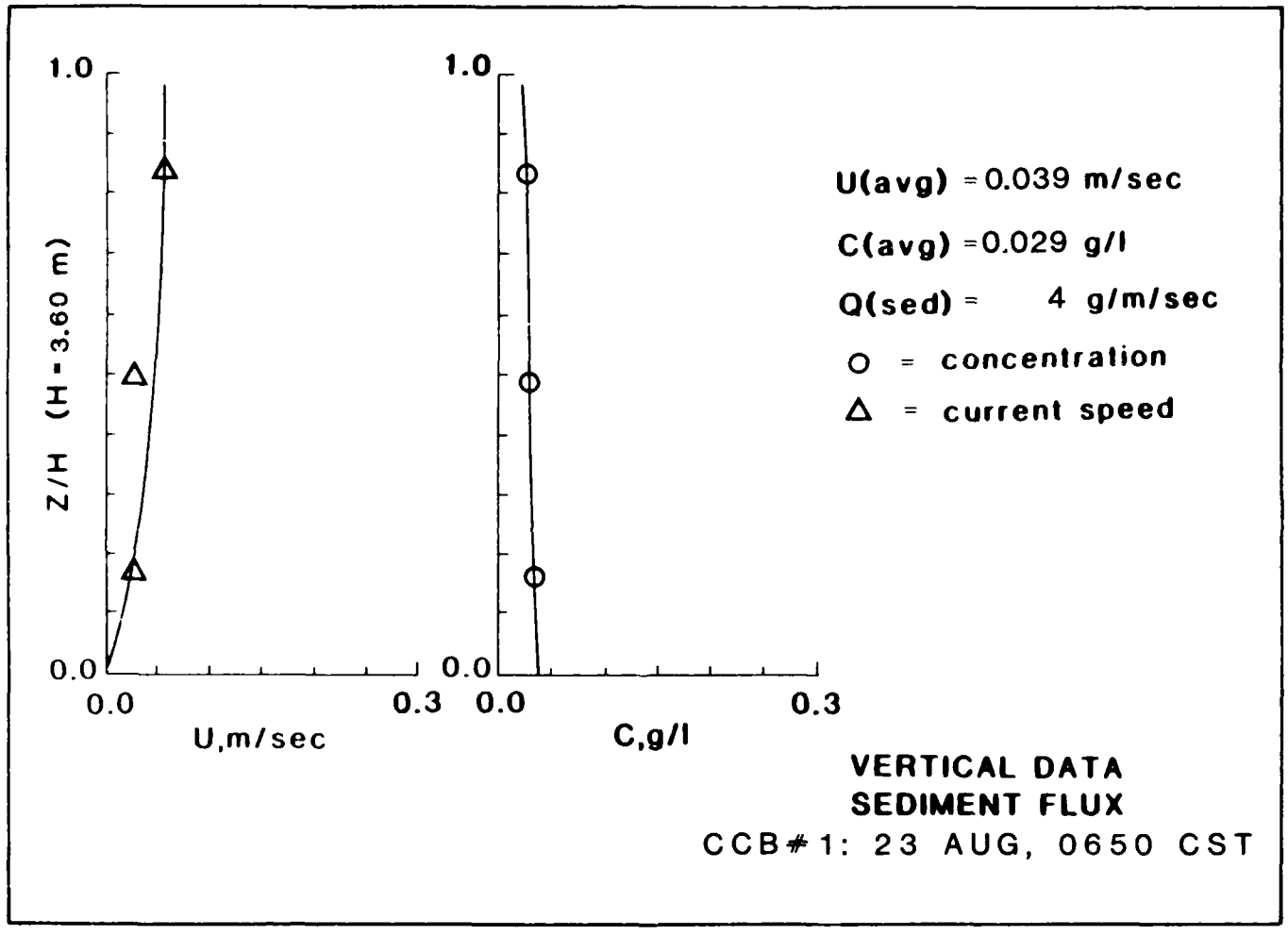
1.0
Z/H (H = 3.60 m)
0.0
0.0
0.3
U,m/sec
1.0
0.0
0.0
0.3
C,g/l
U(avg) = 0.039 m/sec
C(avg) = 0.029 g/l
Q(sed) = 4 g/m/sec
○ = concentration
△ = current speed
VERTICAL DATA
SEDIMENT FLUX
CCB#1: 23 AUG, 0650 CST

PLATE A4/

PLATE A48

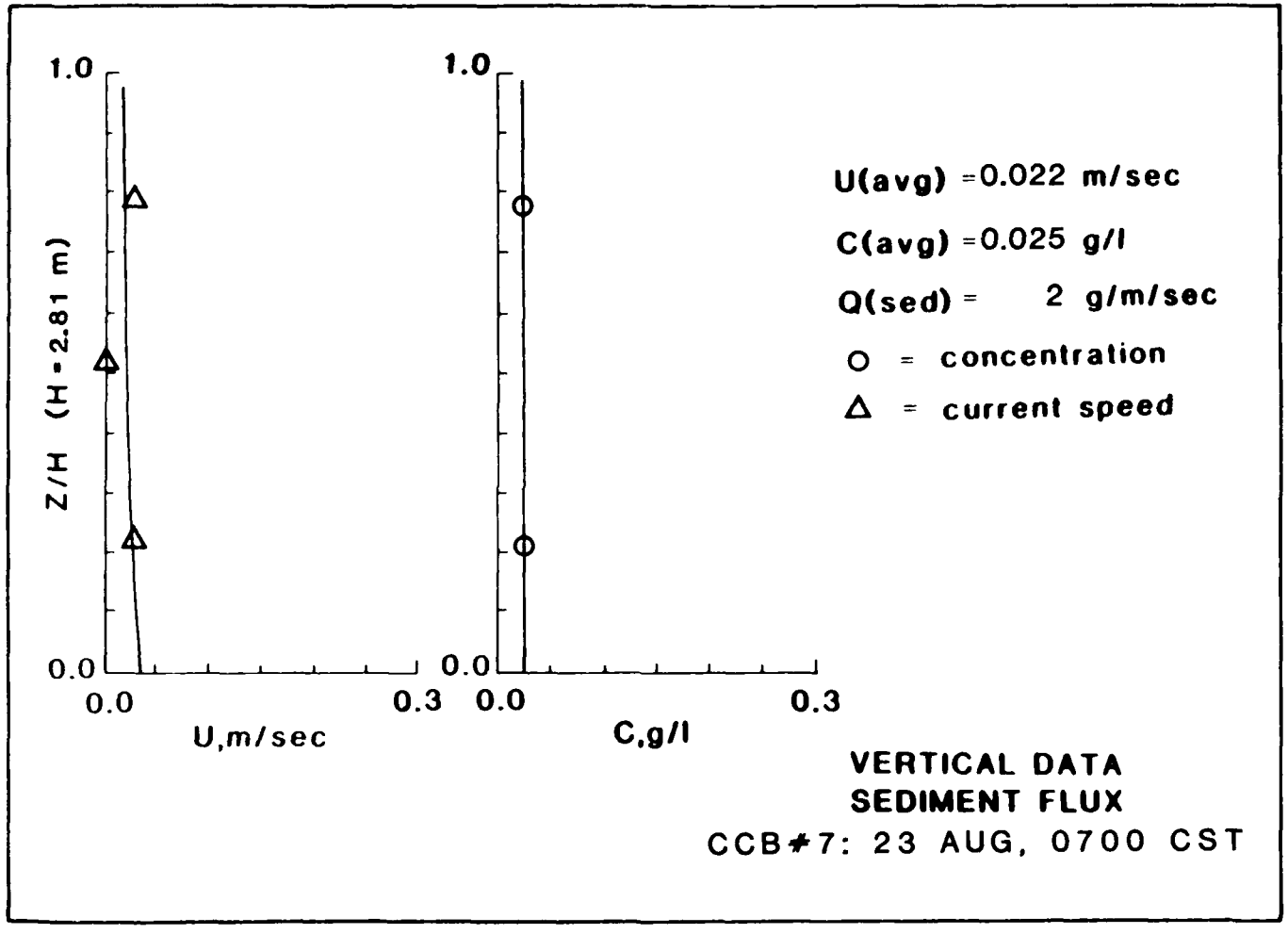
1.0
Z/H (H = 2.81 m)
0.0
0.0
0.3
U,m/sec
1.0
0.0
0.0
0.3
C,g/l
U(avg) =0.022 m/sec
C(avg) =0.025 g/l
Q(sed) = 2 g/m/sec
O = concentration
Δ = current speed
VERTICAL DATA
SEDIMENT FLUX
CCB#7: 23 AUG, 0700 CST

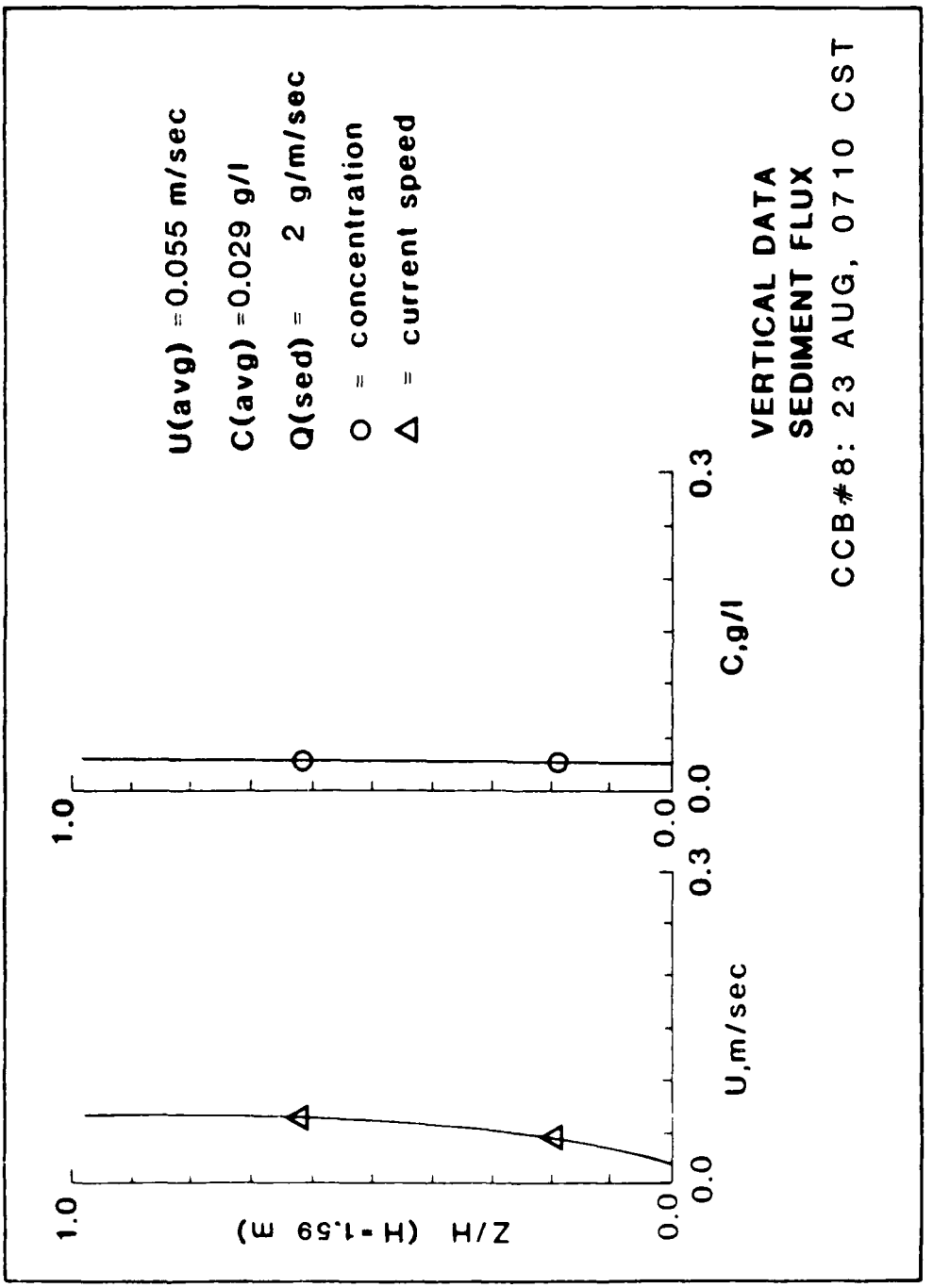
U(avg) =0.055 m/sec
C(avg) =0.029 g/l
Q(sed) = 2 g/m/sec
O = concentration
Δ = current speed
VERTICAL DATA
SEDIMENT FLUX
CCB#8: 23 AUG, 0710 CST
Z/H (H=1.59 m)
U,m/sec
C,g/l
1.0
0.0
0.3

PLATE A49

PLATE A50

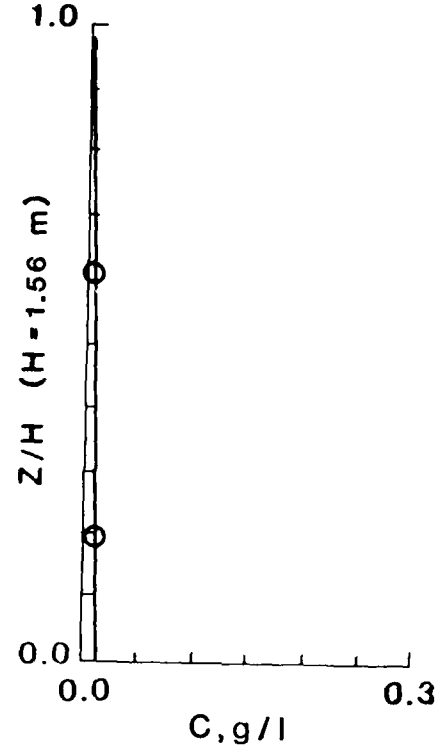

U(avg) =0.055 m/sec

C(avg) =0.010 g/l

Q(sed) = 1 g/m/sec

O = concentration

VERTICAL DATA
SEDIMENT FLUX
DM#82B: 23 AUG, 0720 CST

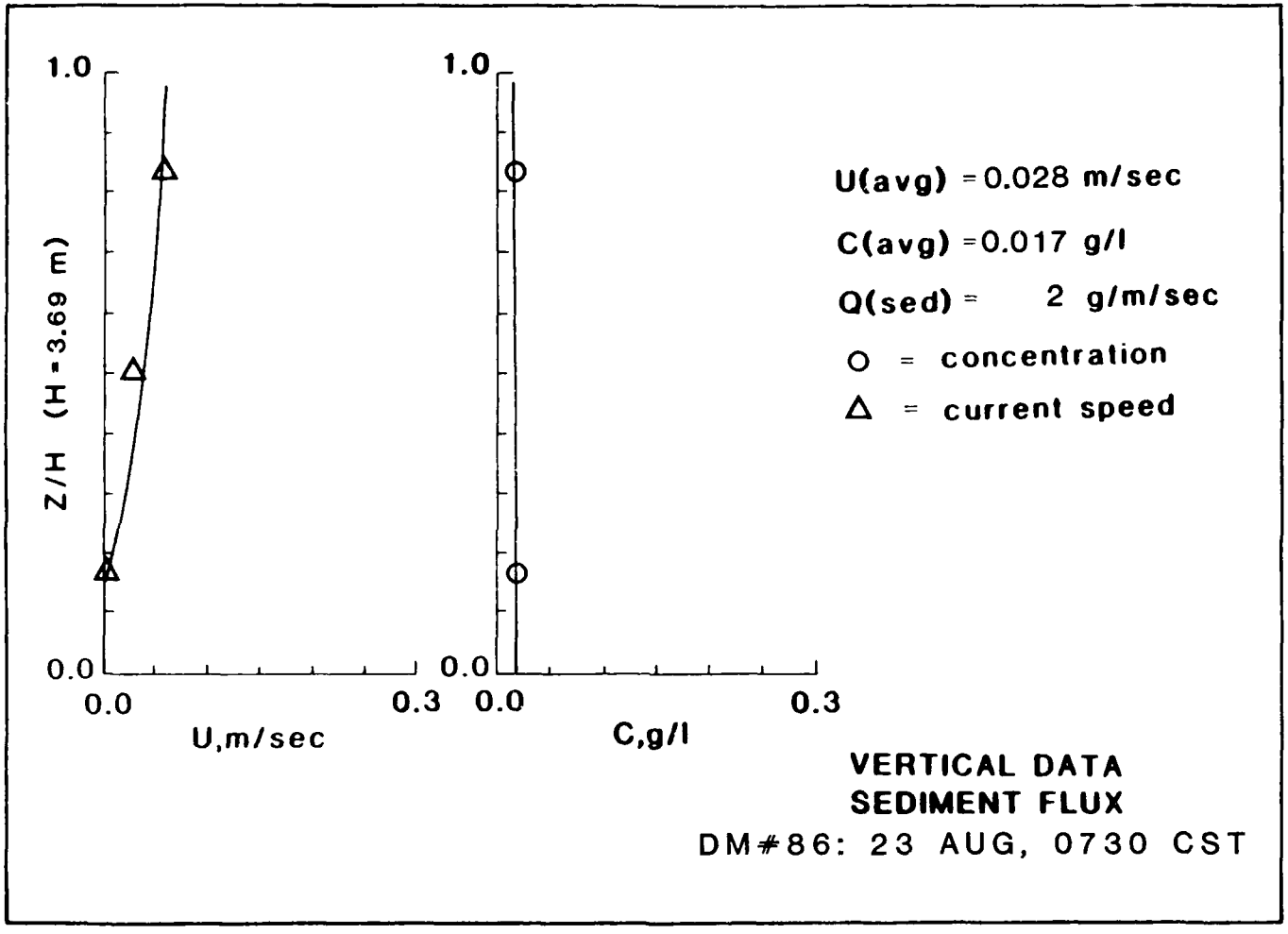
1.0
0.0
Z/H (H-3.69 m)
0.0
0.3
U,m/sec
1.0
0.0
0.0
0.3
C,g/l
U(avg) = 0.028 m/sec
C(avg) = 0.017 g/l
Q(sed) = 2 g/m/sec
○ = concentration
△ = current speed
VERTICAL DATA
SEDIMENT FLUX
DM#86: 23 AUG, 0730 CST

PLATE A51

PLATE A52

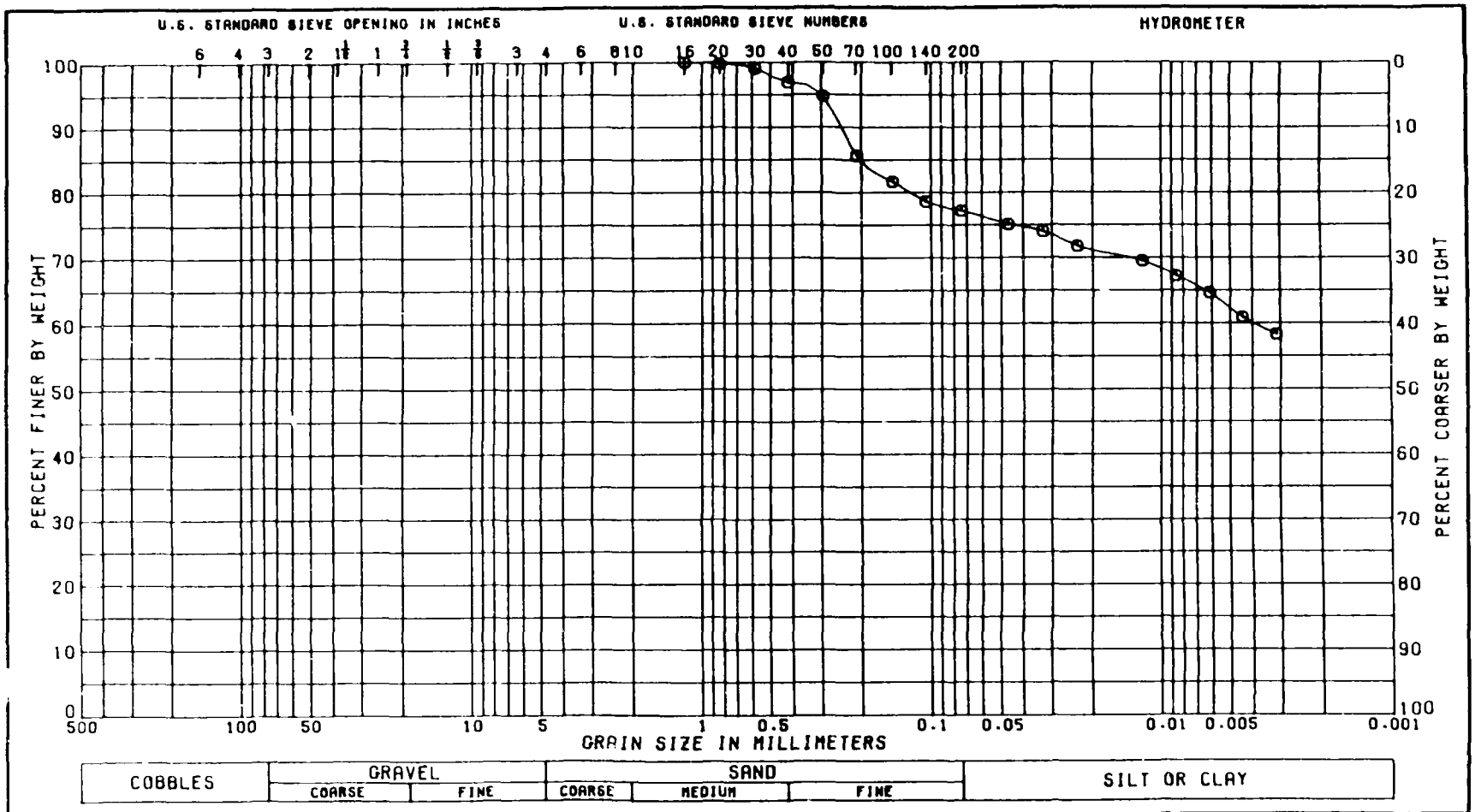

LL	PL	PI	GS 2.70 EST	NAT W.%	

CLASSIFICATION

GRADATION CURVE

PARTICLE SIZE DISTRIBUTION

BORING NO. 0 SAMPLE NO. 1

DEPTH/ELEV 0 DATE 29 OCT 84

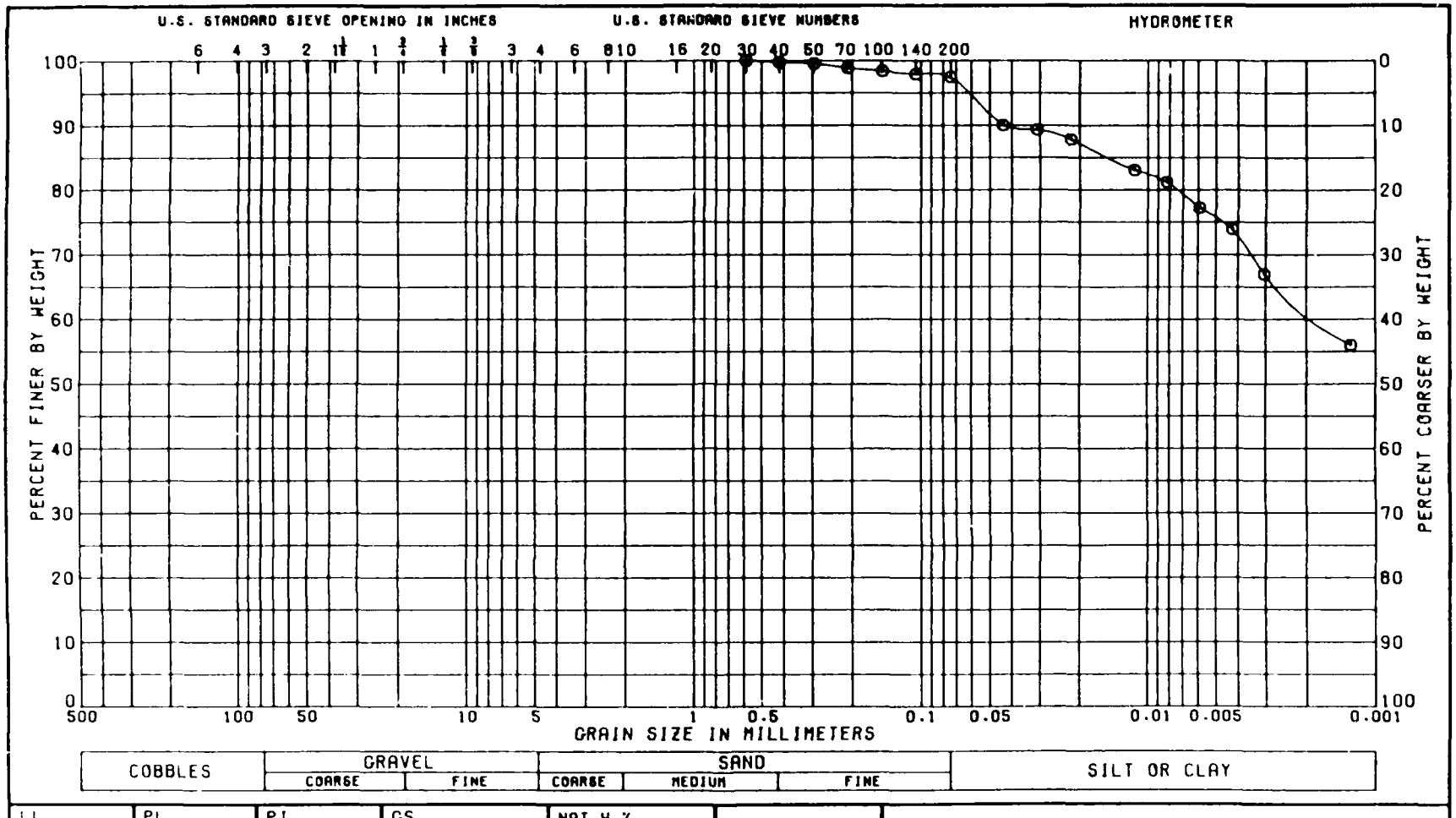

LL	PL	PI	GS 2.70 est	NAT W.%	
CLASSIFICATION					

GRADATION CURVE

PARTICLE SIZE DISTRIBUTION

BORING NO. 0 SAMPLE NO. 2

DEPTH/ELEV 0 DATE 29 OCT 84

PLATE A53

PLATE A54

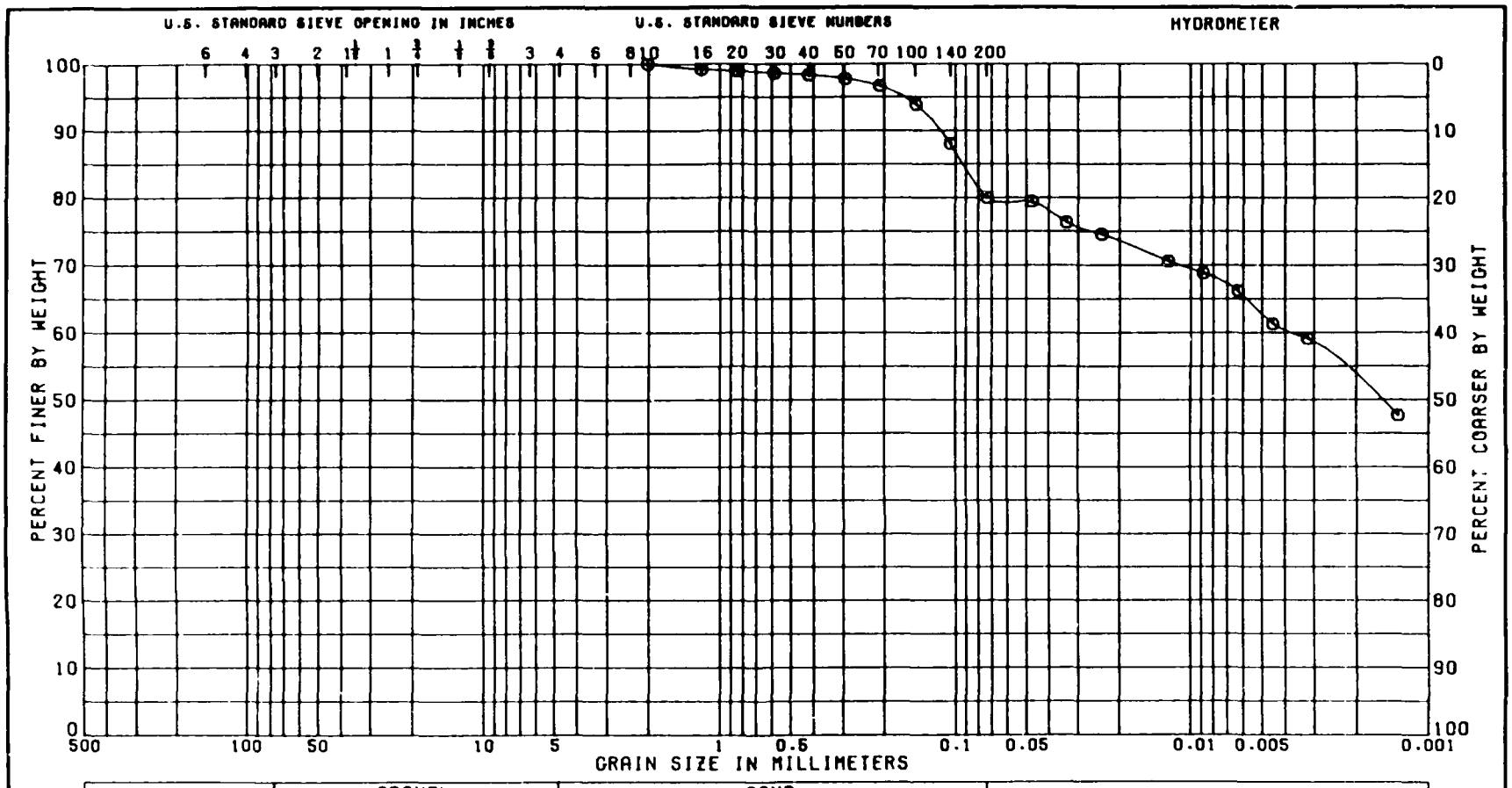

LL	PL	PI	GS 2.70 EST	NAT W.%	
CLASSIFICATION					

GRADATION CURVE

PARTICLE SIZE DISTRIBUTION

BORING NO. 0 SAMPLE NO. 3

DEPTH/ELEV 0 DATE 29 OCT 84

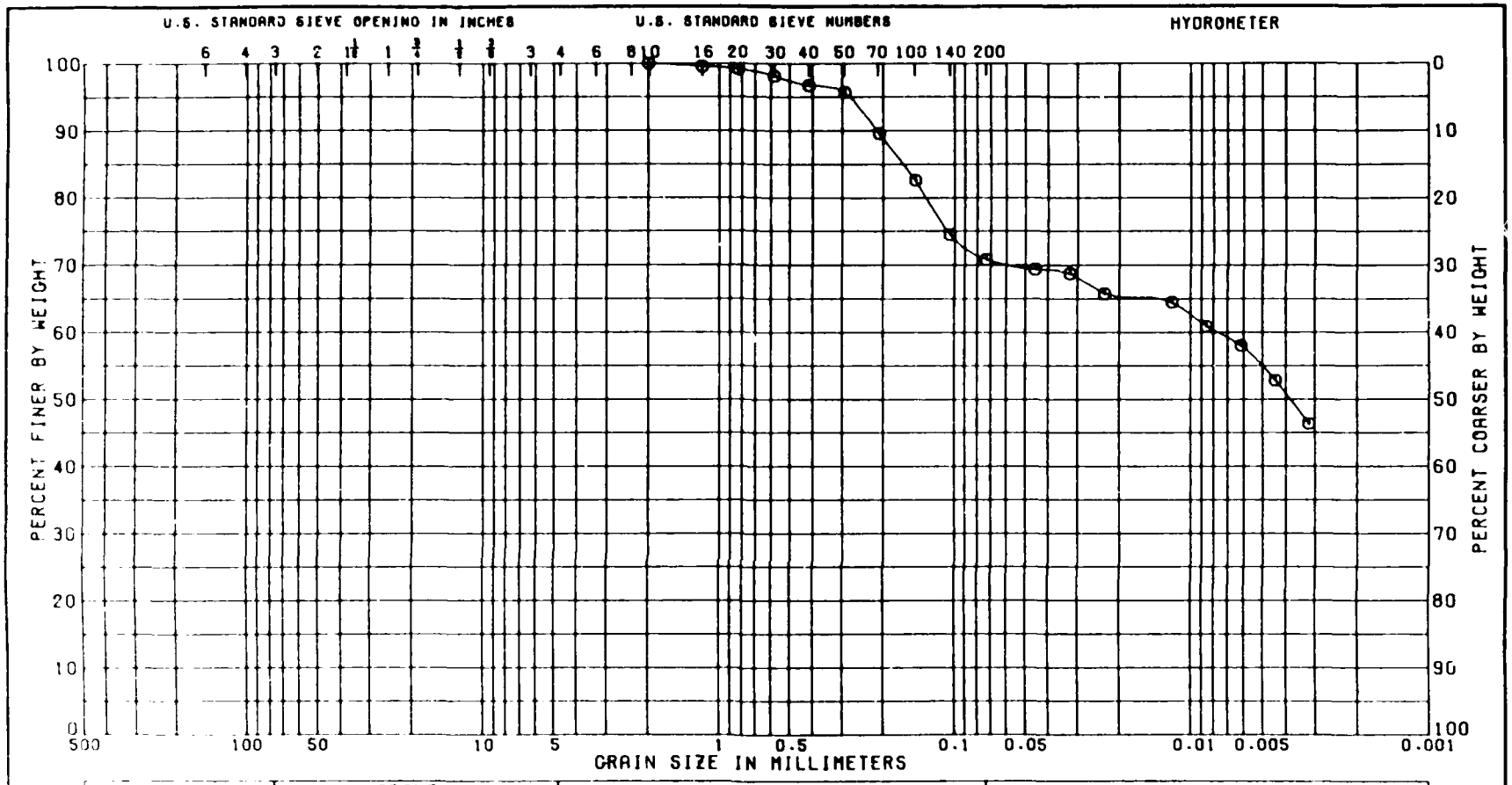

LL	PL	PI	GS 2.70 EST	NAT W.%	

CLASSIFICATION

GRADATION CURVE

PARTICLE SIZE DISTRIBUTION

BORING NO. 0 SAMPLE NO. 4

DEPTH/ELEV 0 DATE 29 OCT 84

PLATE A56

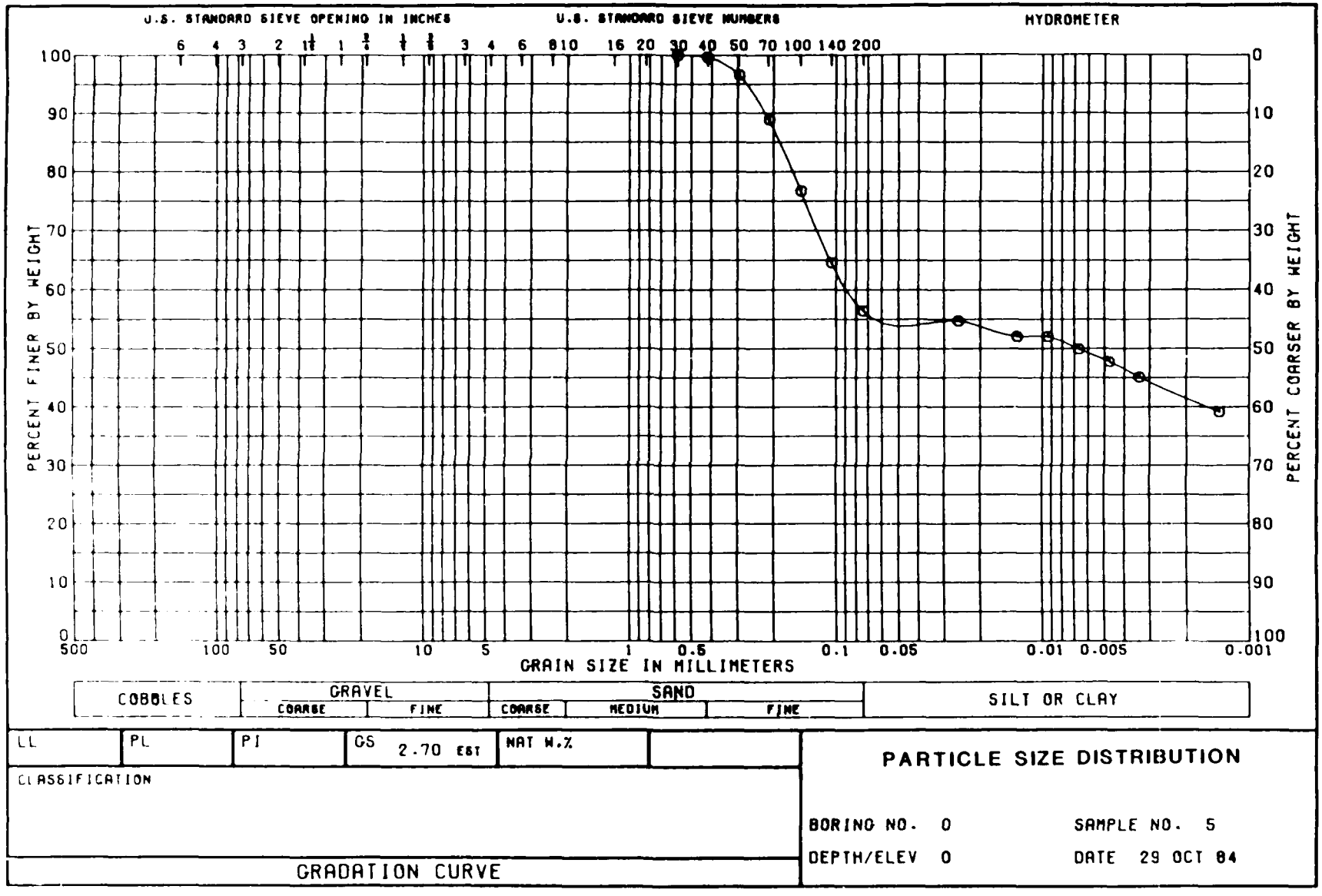

LL	PL	PI	GS 2.70 EST	NAT W.%	

CLASSIFICATION

GRADATION CURVE

PARTICLE SIZE DISTRIBUTION

BORING NO. 0 SAMPLE NO. 5

DEPTH/ELEV 0 DATE 29 OCT 84

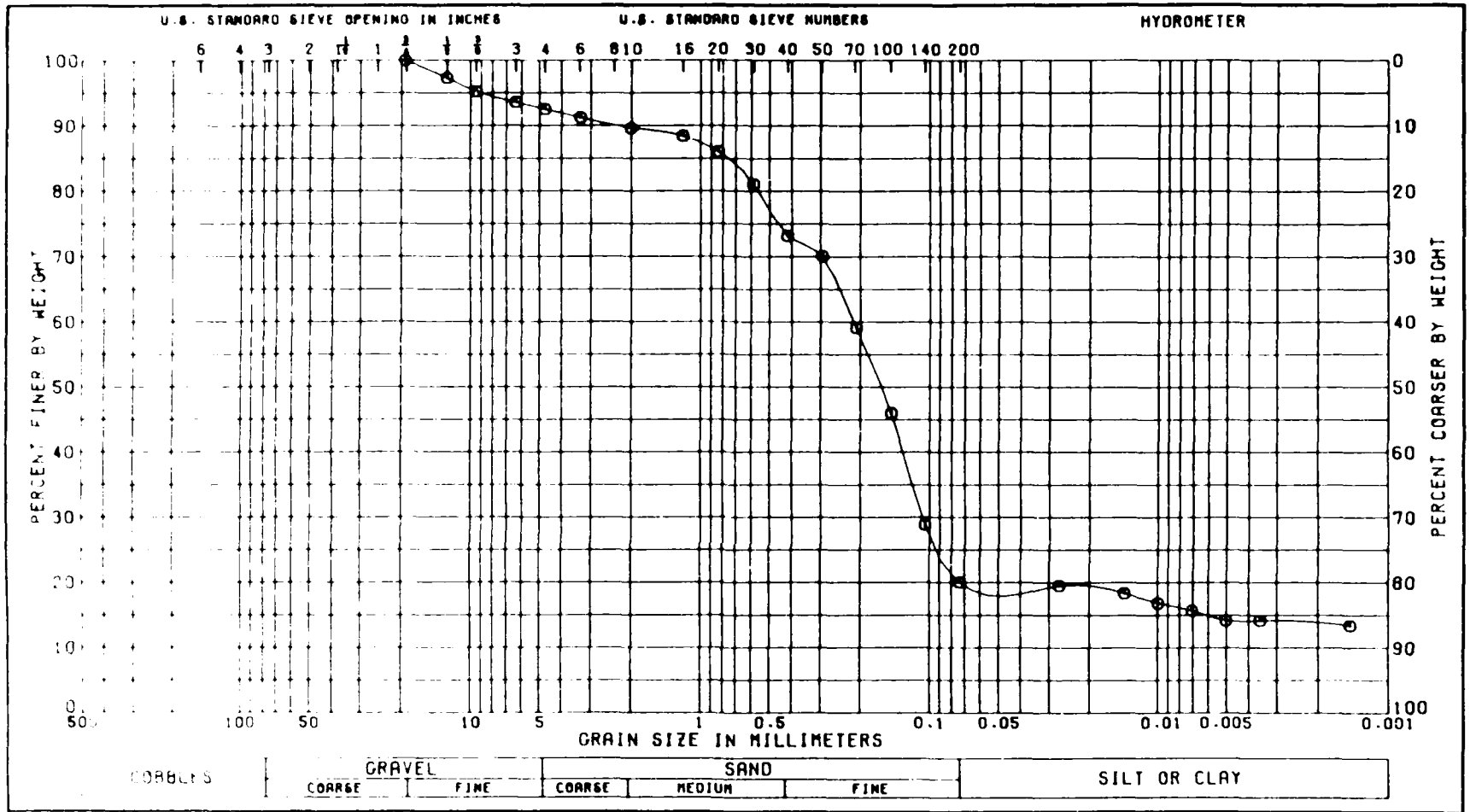

LL	PL	PI	GS 2.65 EST	NAT W.%	
CLASSIFICATION					

GRADATION CURVE

PARTICLE SIZE DISTRIBUTION

BORING NO. 0 SAMPLE NO. 6

DEPTH/ELEV 0 DATE 29 OCT 84

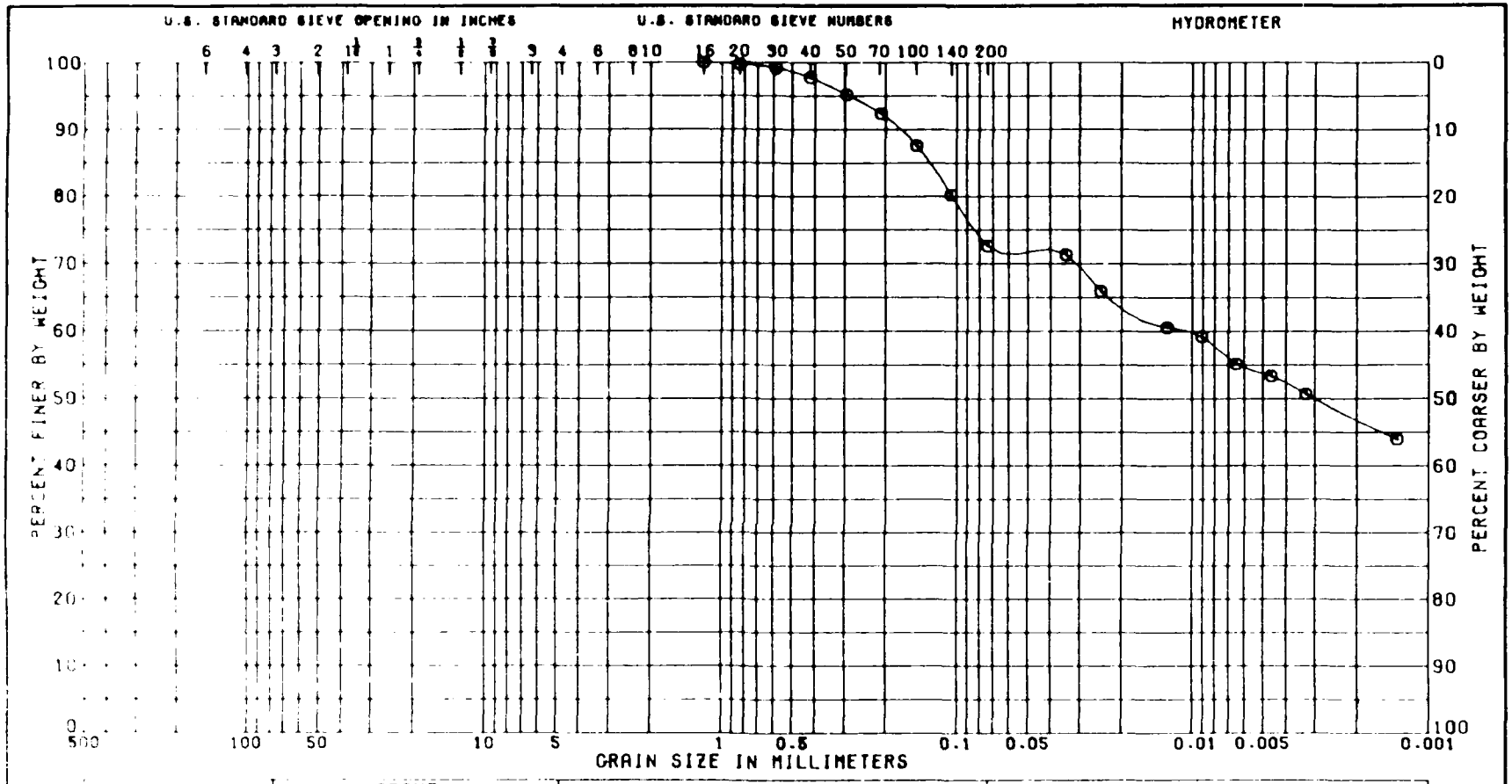

LL	PL	PI	GS 2.70 EST	NAT W.%	
CLASSIFICATION					

GRADATION CURVE

PARTICLE SIZE DISTRIBUTION

BORING NO. 0 SAMPLE NO. 7

DEPTH/ELEV 0 DATE 29 OCT 84

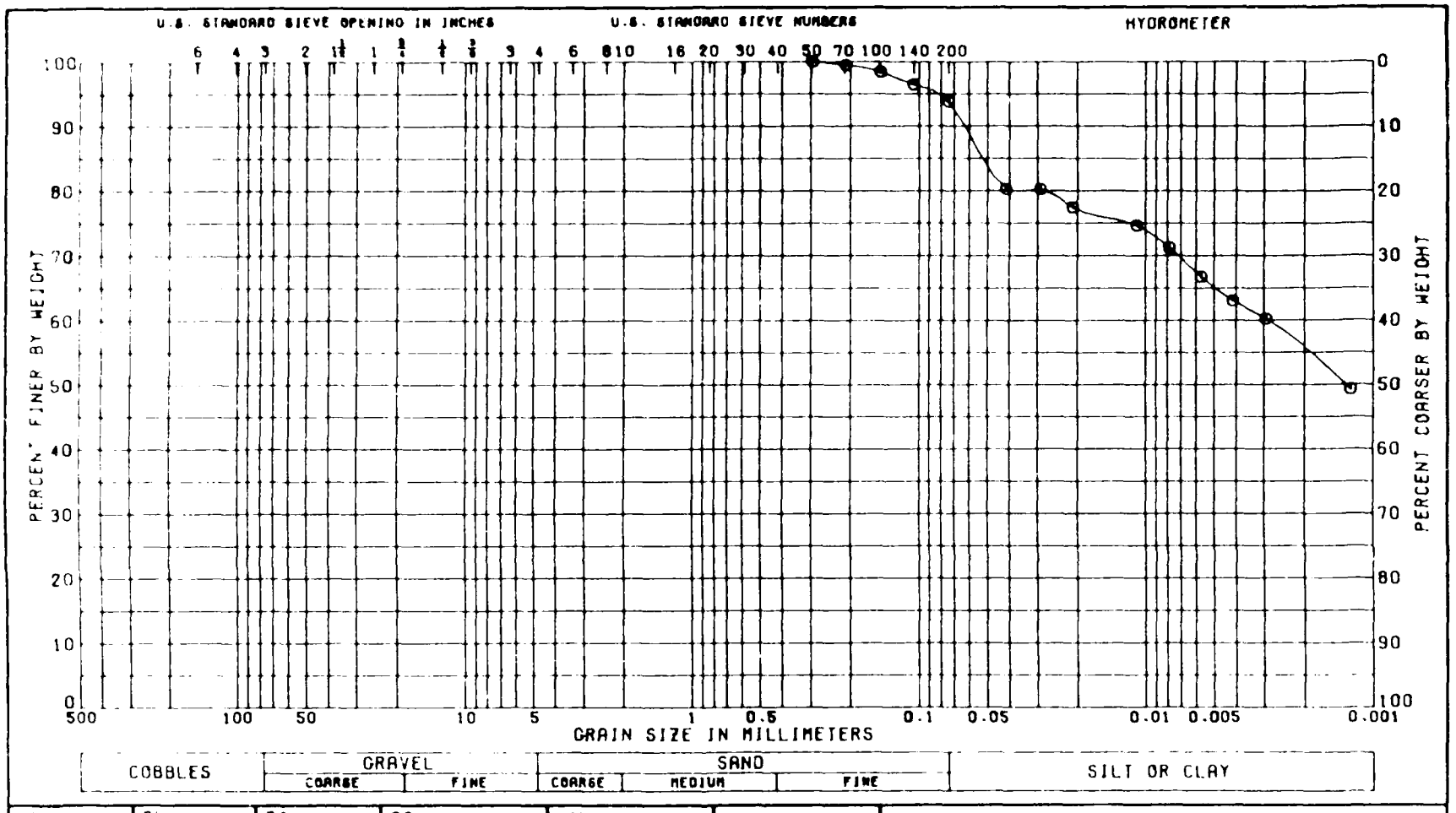

LL	PL	PI	GS 2.70 EST	NAT W.%	

CLASSIFICATION

GRADATION CURVE

PARTICLE SIZE DISTRIBUTION

BORING NO. 0 SAMPLE NO. 8

DEPTH/ELEV 0 DATE 29 OCT 84

PLATE A60

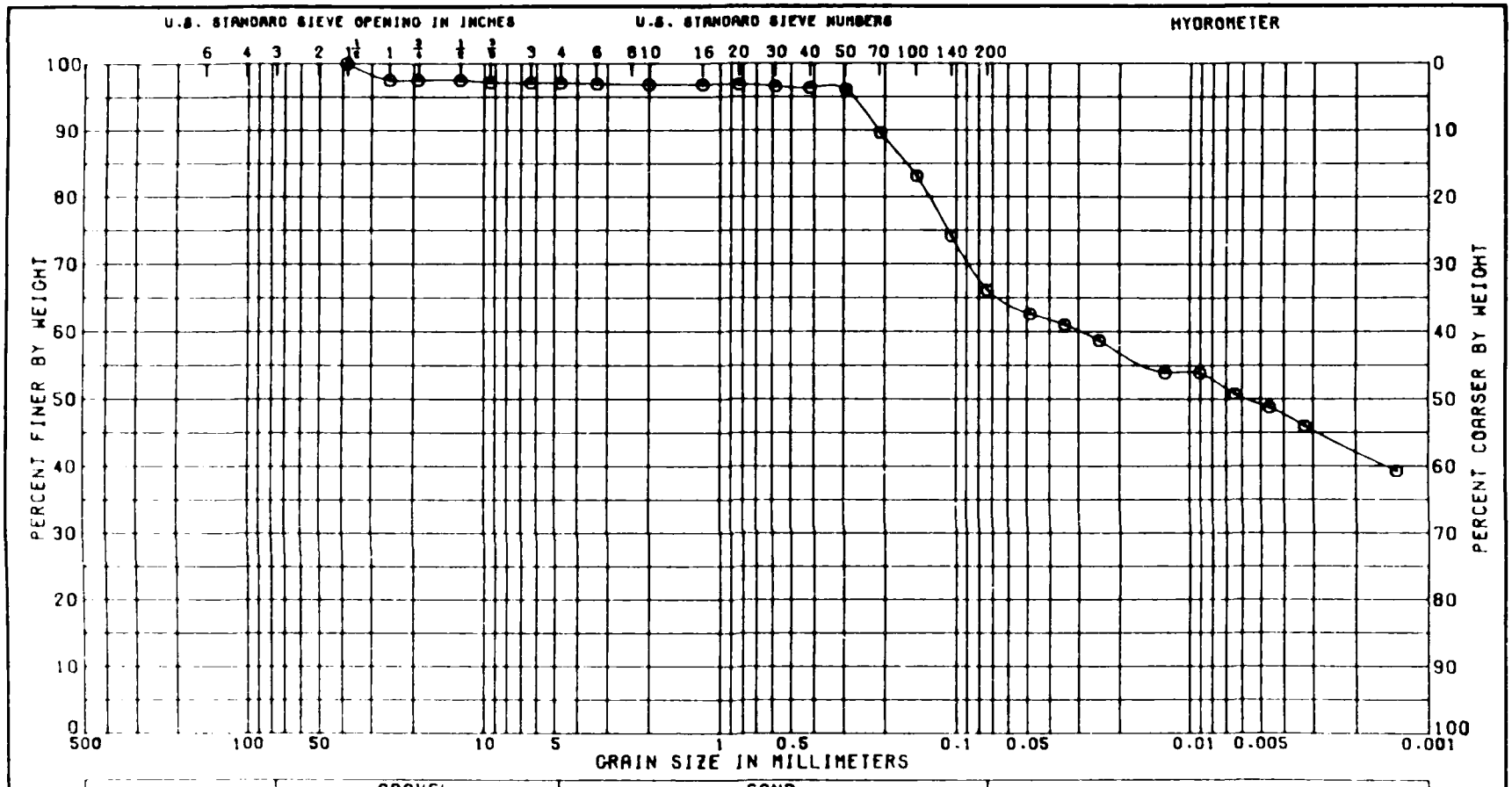

LL	PL	PI	GS 2.70 EST	NAT W.%	
CLASSIFICATION					

GRADATION CURVE

PARTICLE SIZE DISTRIBUTION

BORING NO. 0 SAMPLE NO. 9

DEPTH/ELEV 0 DATE 29 OCT 84

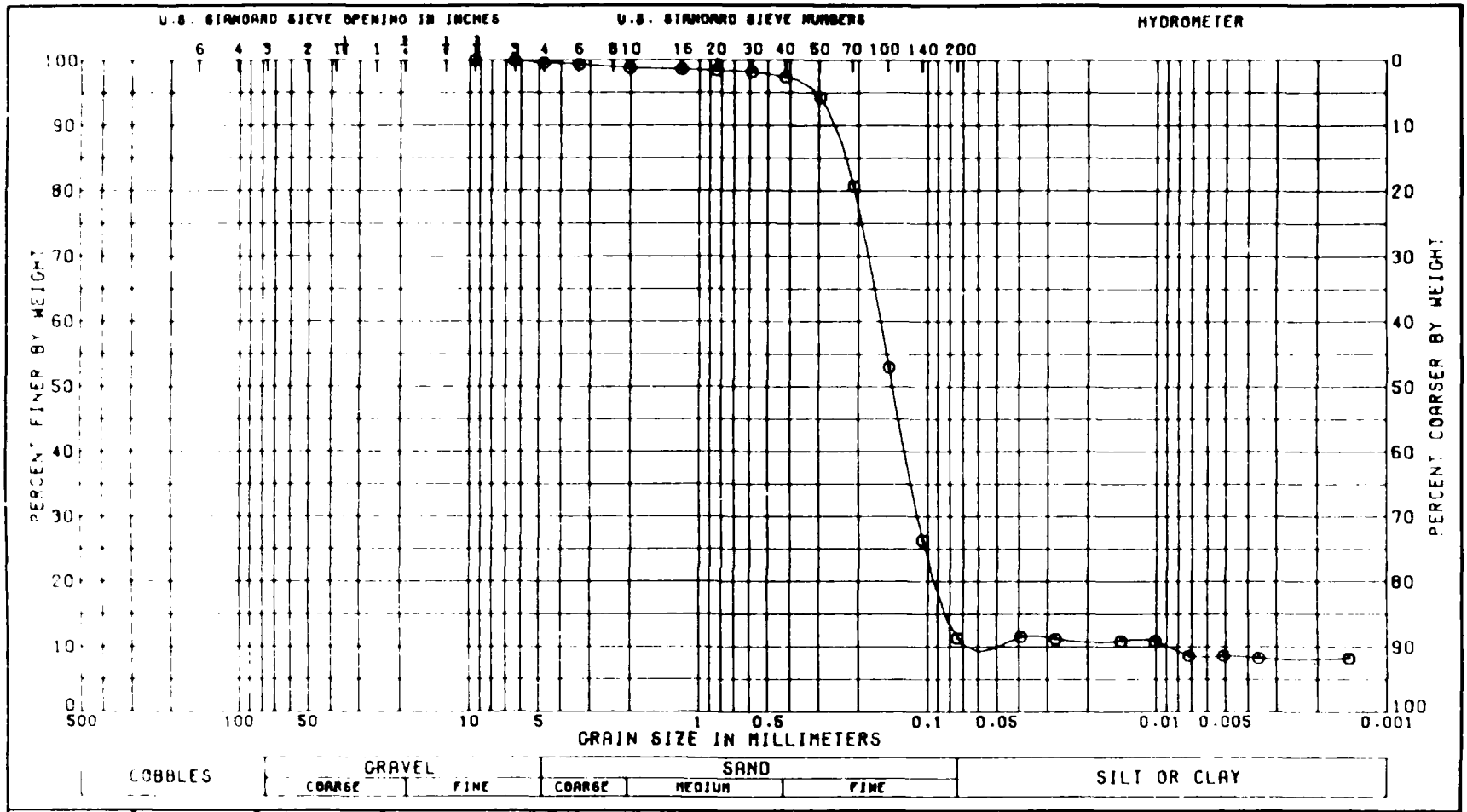

LL	PL	PI	GS 2.65 EST	NAT W.%	
CLASSIFICATION					

GRADATION CURVE

PARTICLE SIZE DISTRIBUTION

BORING NO. 0 SAMPLE NO. 10

DEPTH/ELEV 0 DATE 29 OCT 84

PLATE A62

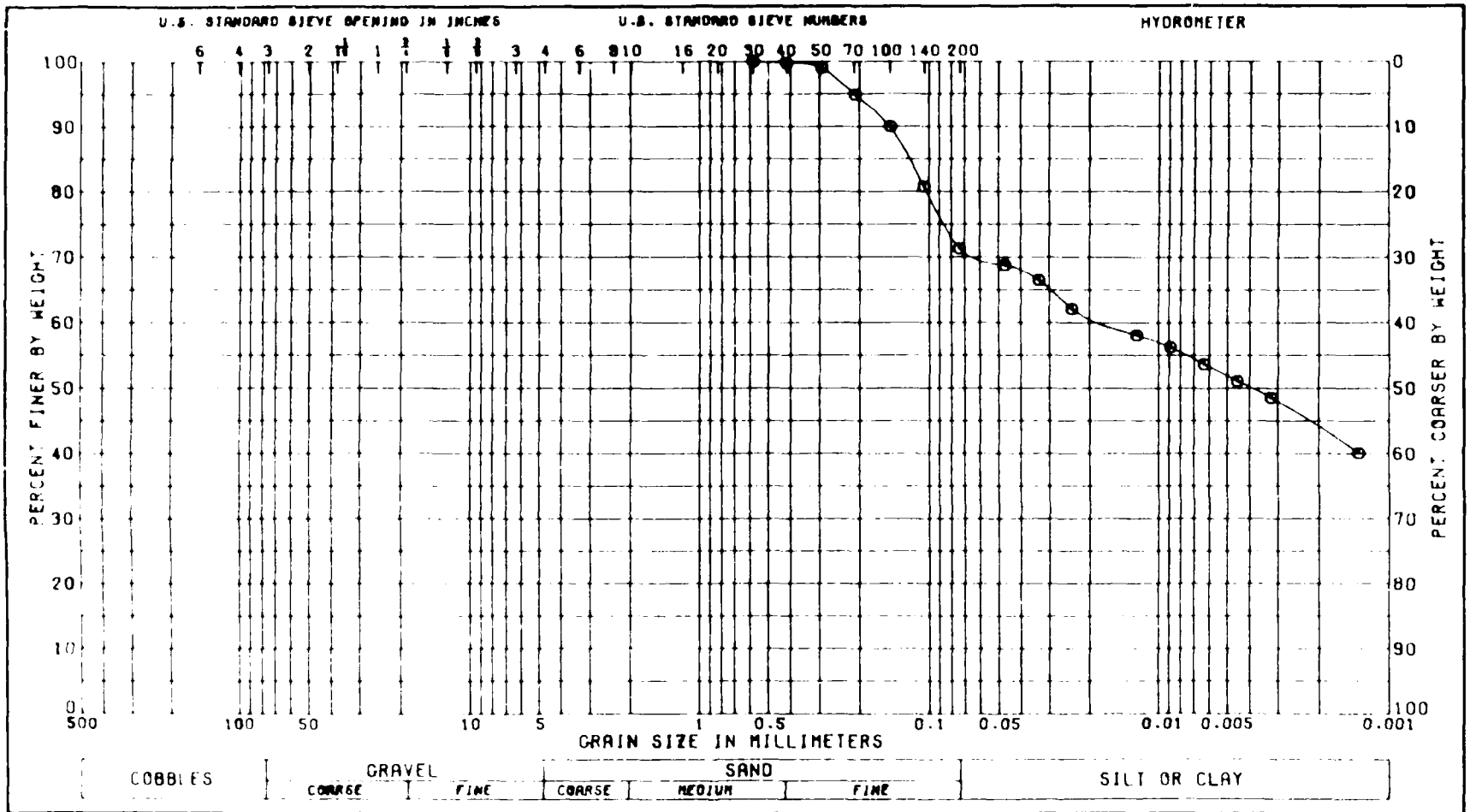

LL	PL	PI	GS 2.70 Est	NAT W.%	

CLASSIFICATION

GRADATION CURVE

PARTICLE SIZE DISTRIBUTION

BORING NO. 0 SAMPLE NO. 11

DEPTH/ELEV 0 DATE 29 OCT 84

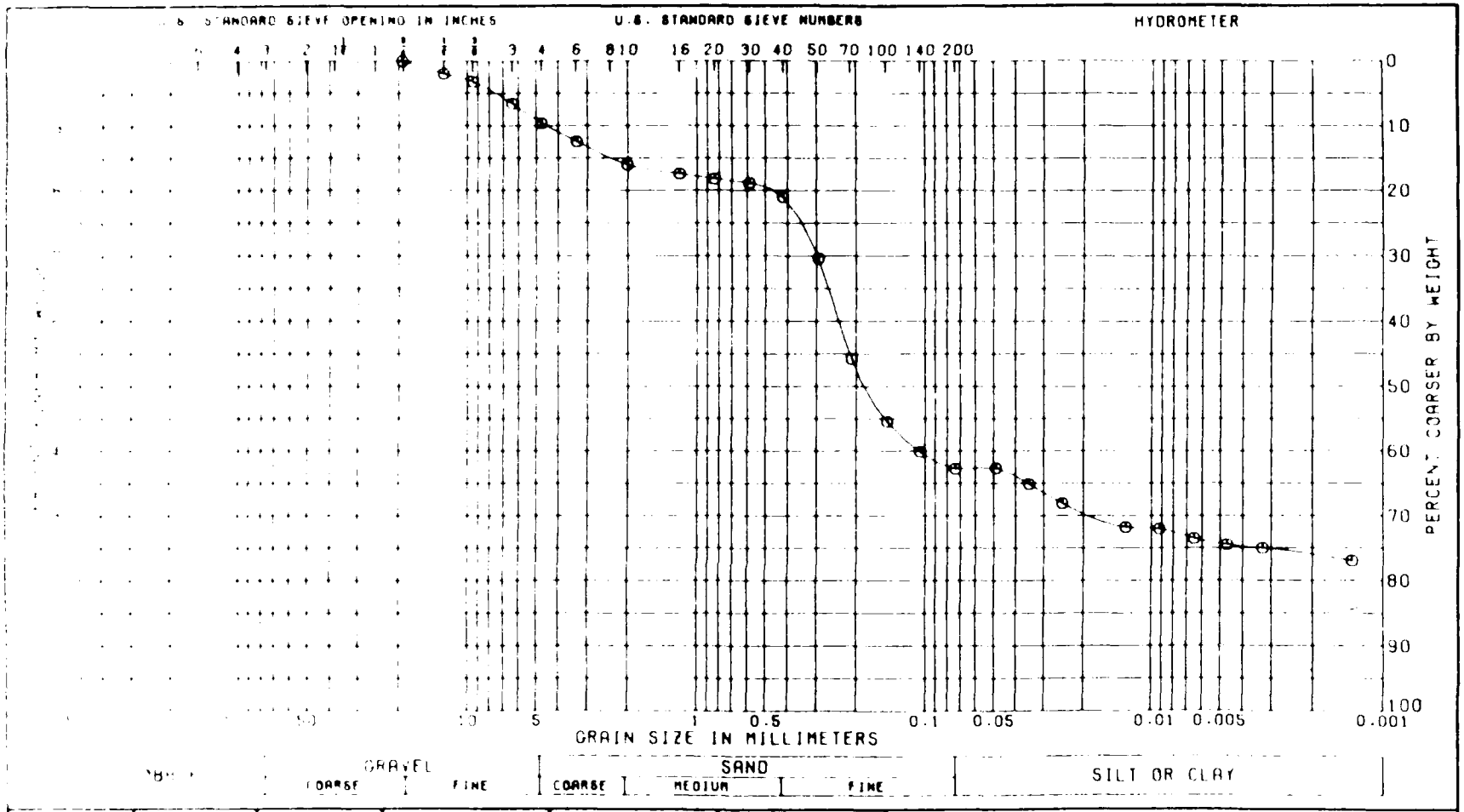

			GS 2.70 EST	NAT W.%	

GRADATION CURVE

PARTICLE SIZE DISTRIBUTION

BORING NO. 0 SAMPLE NO. 12

DEPTH/ELEV 0 DATE 29 OCT 64

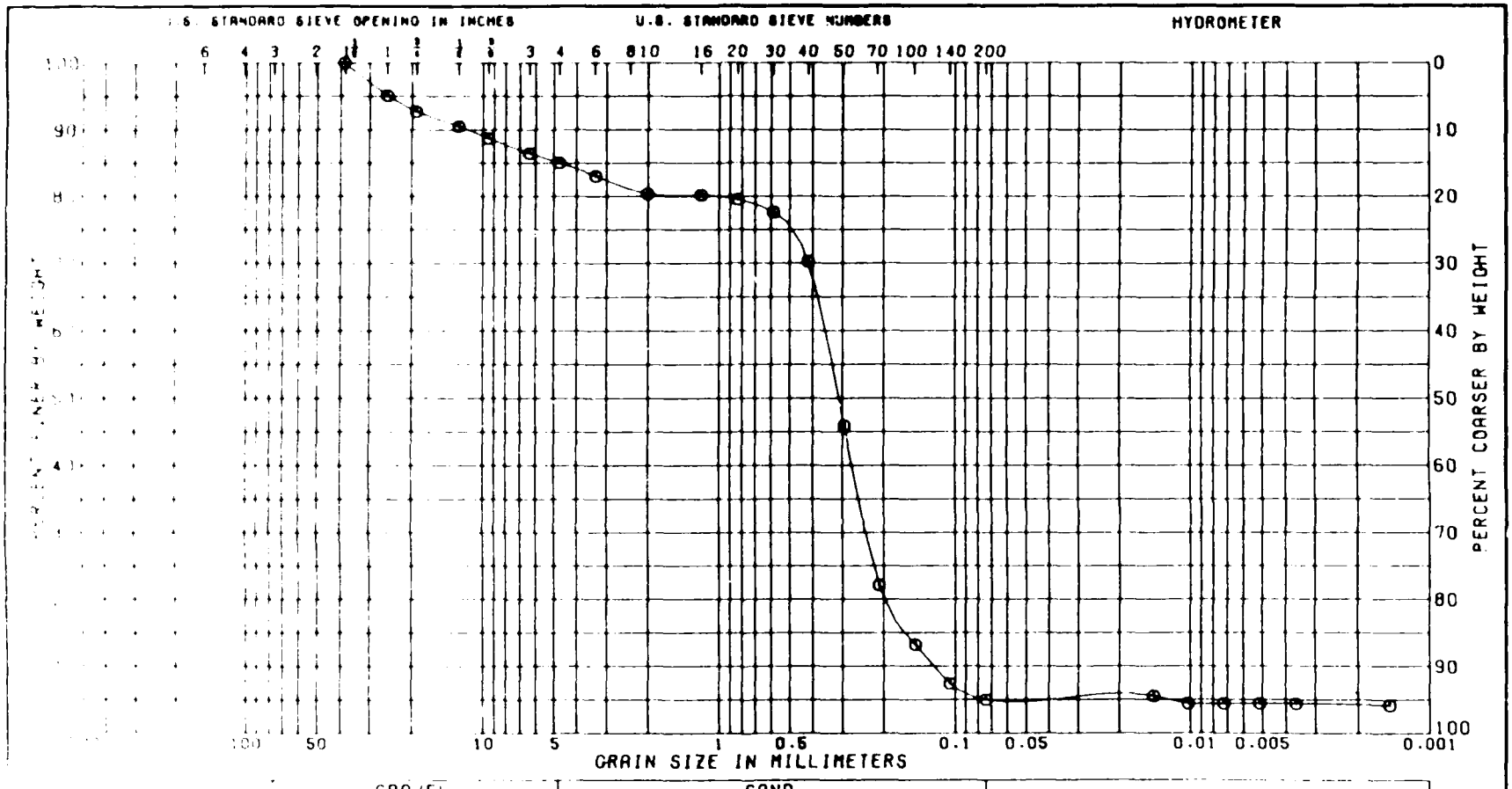

	P	PI	GS 2.65 EST	NAT W.%	

GRADATION CURVE

PARTICLE SIZE DISTRIBUTION

BORING NO. 0 SAMPLE NO. 13

DEPTH/ELEV 0 DATE 29 OCT 84

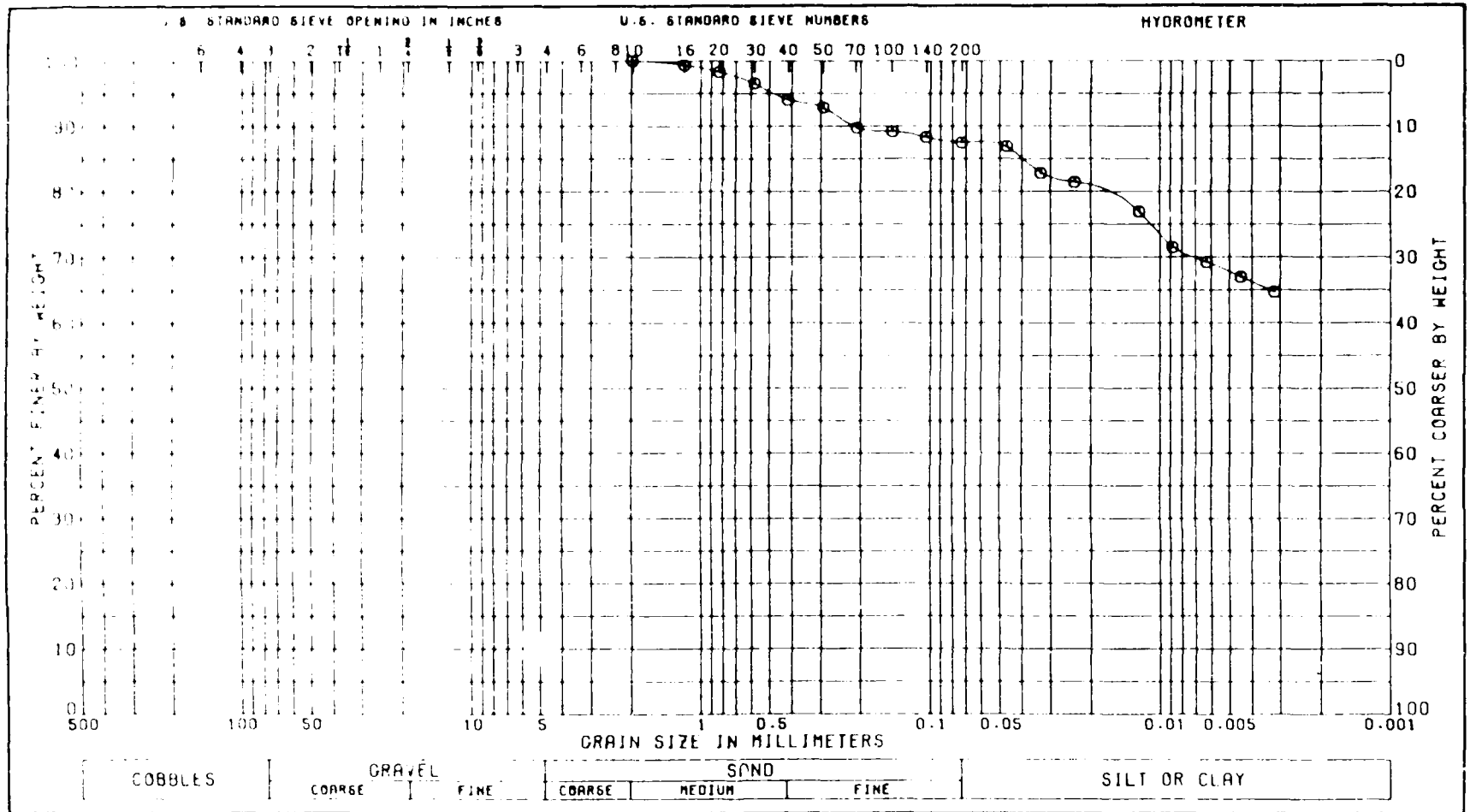

LL	PL	PI	GS 2.70 EST	NAT W.%	

CLASSIFICATION

GRADATION CURVE

PARTICLE SIZE DISTRIBUTION

BORING NO. 0 SAMPLE NO. 14

DEPTH/ELEV 0 DATE 29 OCT 84

PLATE A65

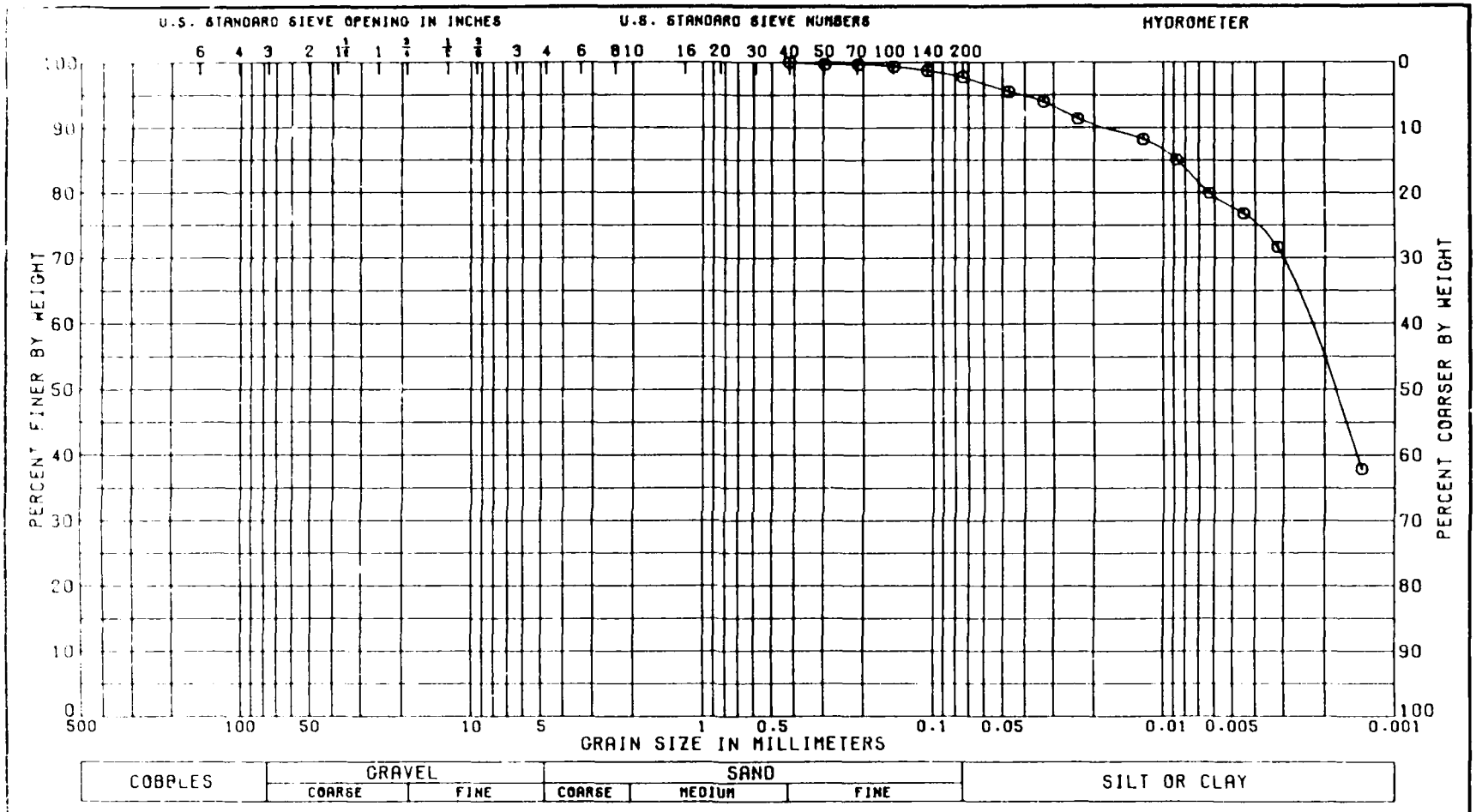

LL	PL	PI	GS 2.70 EST	NAT W.%	

CLASSIFICATION

GRADATION CURVE

PARTICLE SIZE DISTRIBUTION

BORING NO. 0 SAMPLE NO. 15

DEPTH/ELEV 0 DATE 29 OCT 84

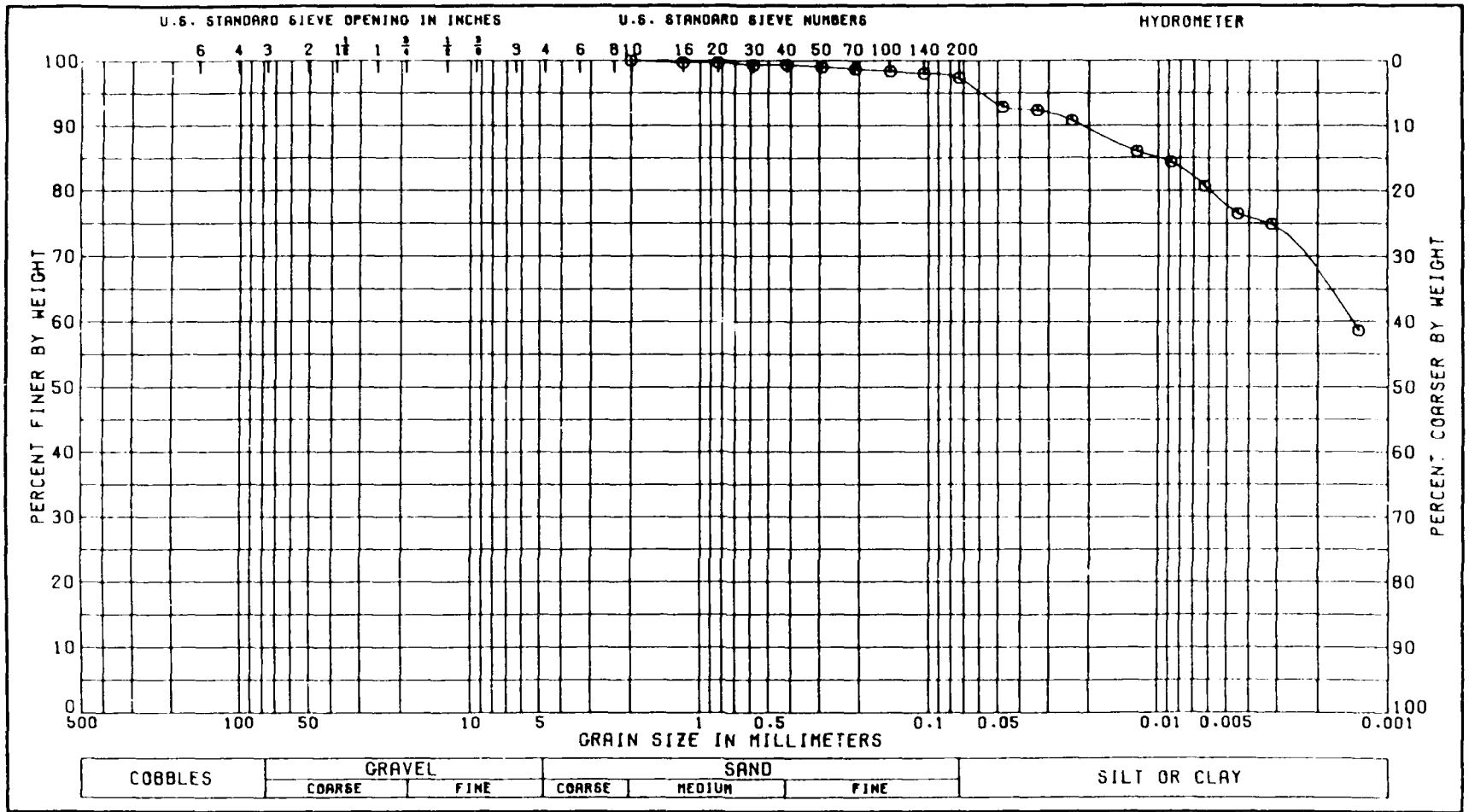

LL	PL	PI	GS 2.70 EST	NAT W.%	
CLASSIFICATION					
GRADATION CURVE					

PARTICLE SIZE DISTRIBUTION

BORING NO. 0 SAMPLE NO. 16

DEPTH/ELEV 0 DATE 29 OCT 84

PLATE A67

PLATE A68

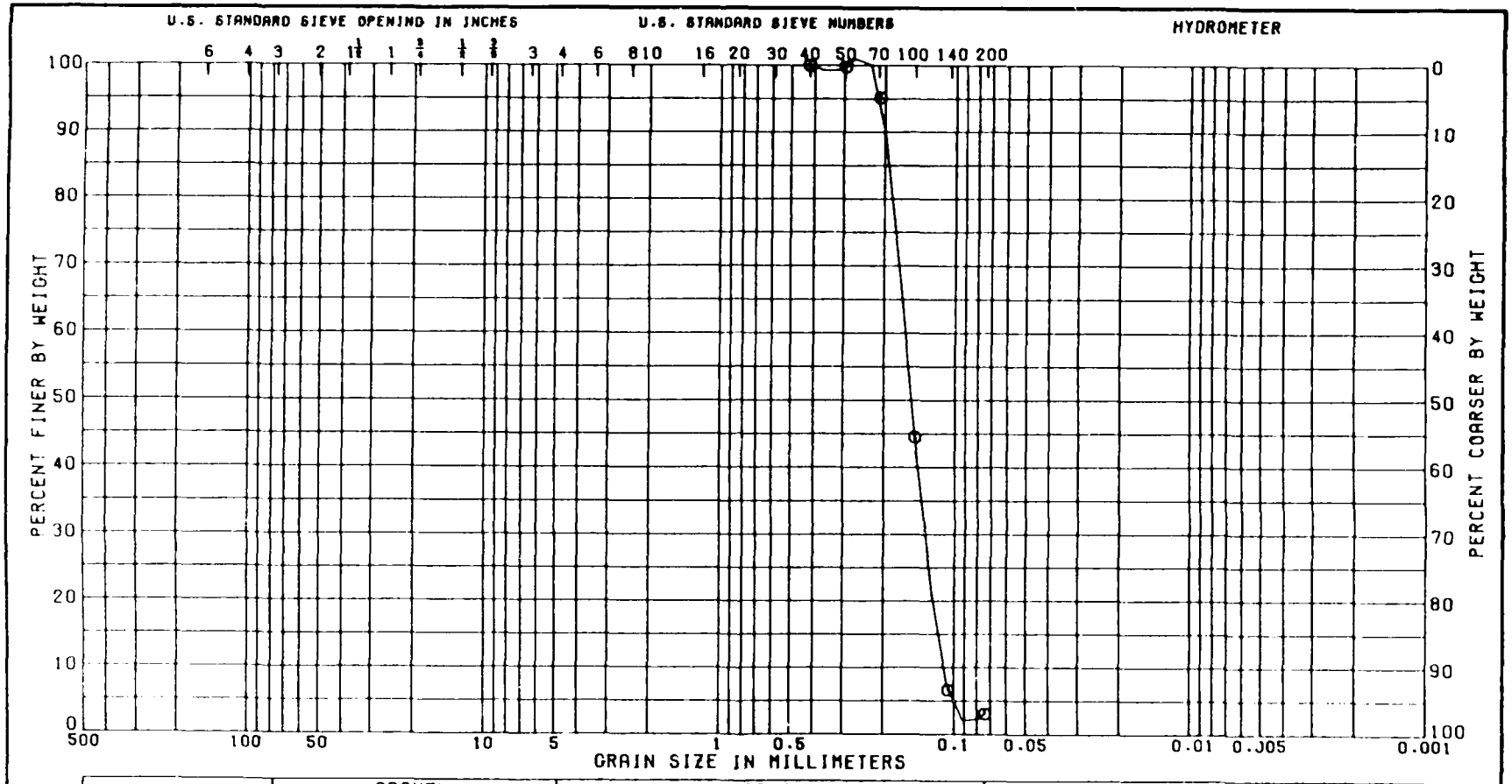

LL	PL	PI	GS 2.65 EST	NAT W.%	

CLASSIFICATION

GRADATION CURVE

PARTICLE SIZE DISTRIBUTION

BORING NO. 0 SAMPLE NO. 17

DEPTH/ELEV 0 DATE 29 OCT 84

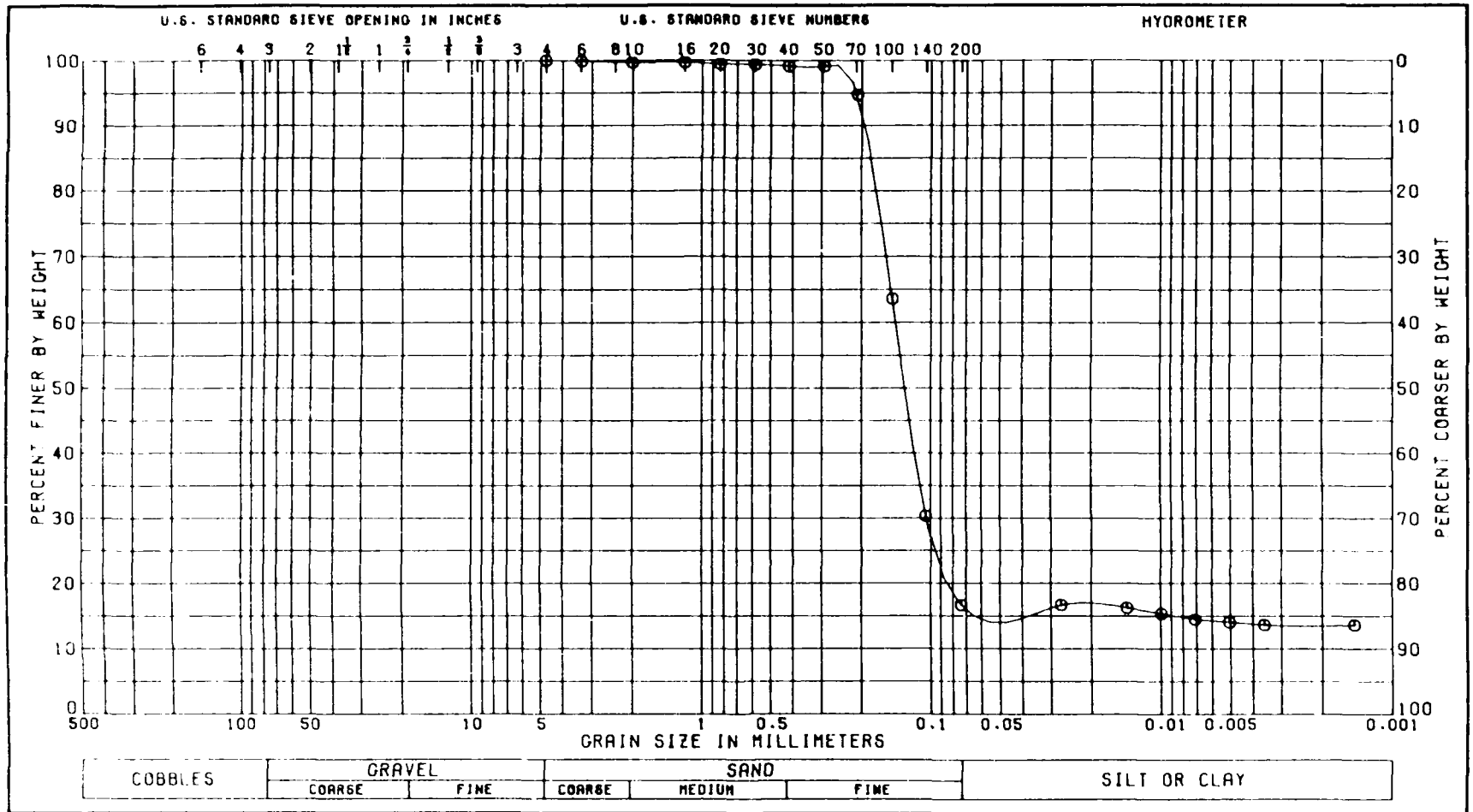

LL	PL	PI	GS 2.65 EST	NAT W.%	
CLASSIFICATION					
GRADATION CURVE					

PARTICLE SIZE DISTRIBUTION

BORING NO. 0 SAMPLE NO. 18

DEPTH/ELEV 0 DATE 29 OCT 84

Figure 11-7d

PLATE A70

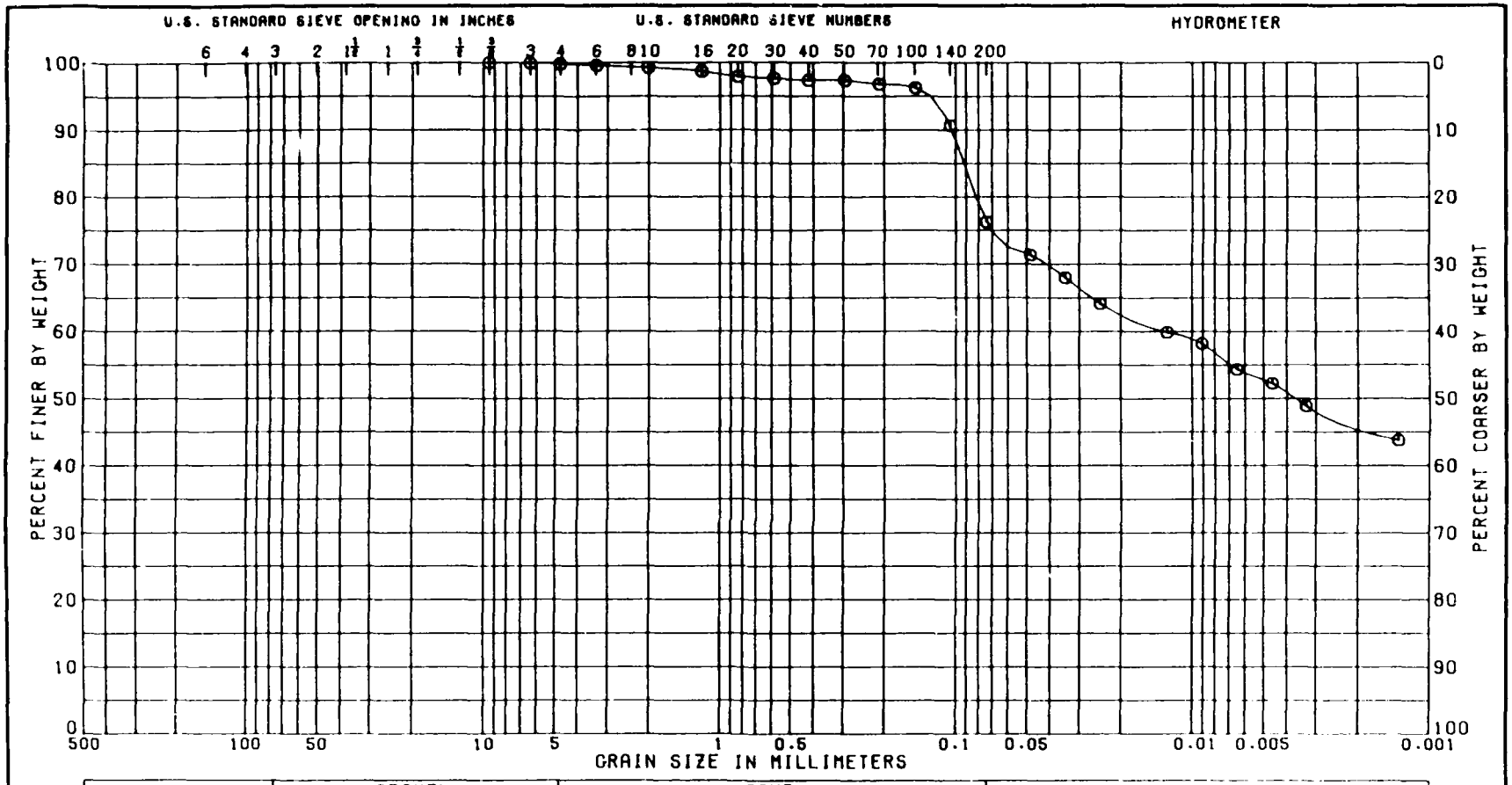

LL	PL	PI	GS 2.70 EST	NAT W.%	

CLASSIFICATION

GRADATION CURVE

PARTICLE SIZE DISTRIBUTION

BORING NO. 0 SAMPLE NO. 19

DEPTH/ELEV 0 DATE 29 OCT 84

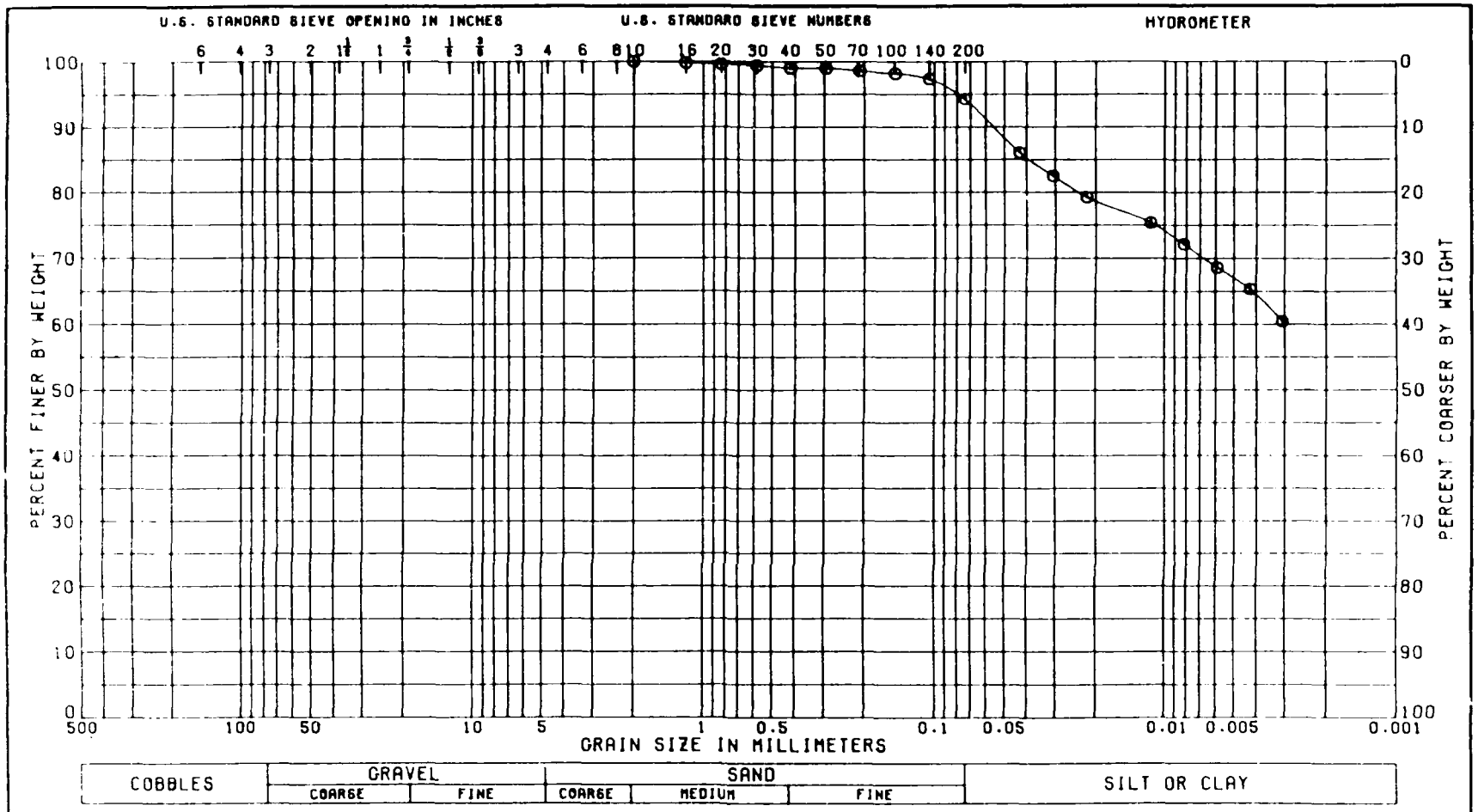

LL	PL	PI	GS 2.70 EST	NAT W.%	

CLASSIFICATION

GRADATION CURVE

PARTICLE SIZE DISTRIBUTION

BORING NO. 0 SAMPLE NO. 20

DEPTH/ELEV 0 DATE 29 OCT 84

PLATE A72

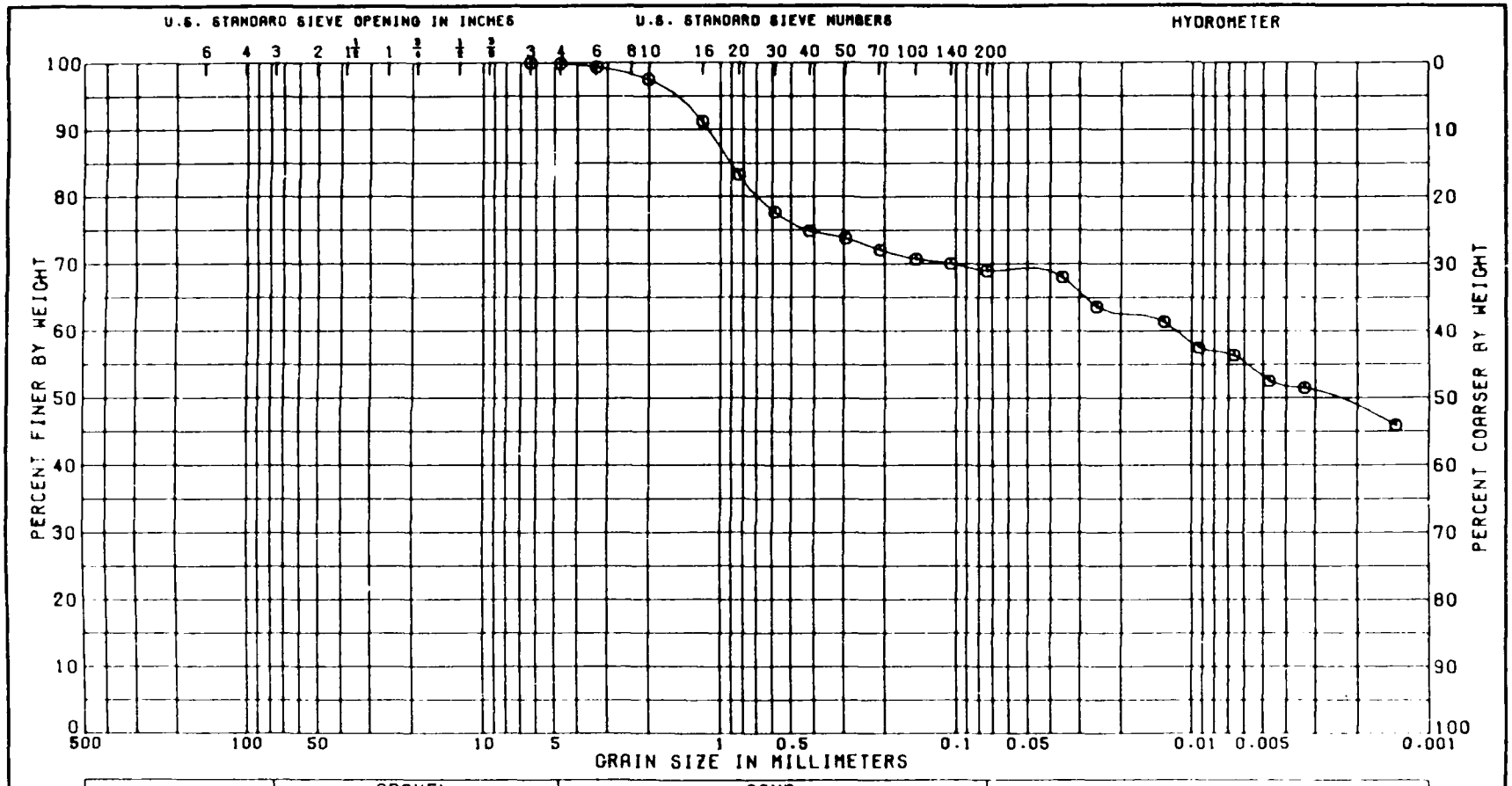

LL	PL	PI	GS 2.70 EST	NAT W.%	

CLASSIFICATION

GRADATION CURVE

PARTICLE SIZE DISTRIBUTION

BORING NO. 0 SAMPLE NO. 21

DEPTH/ELEV 0 DATE 29 OCT 84

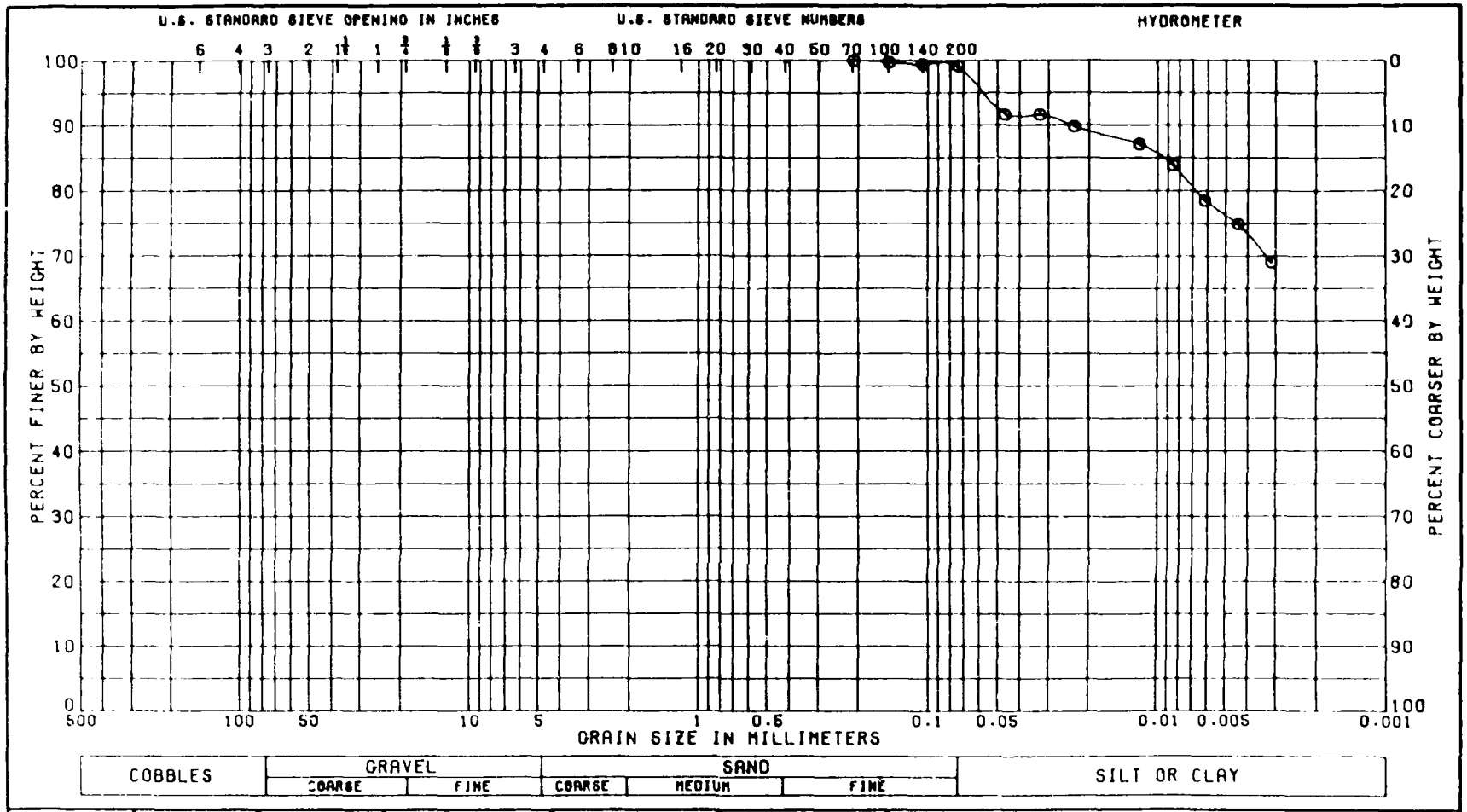

LL	PL	PI	GS 2.70 EST	NAT W.%	

CLASSIFICATION

GRADATION CURVE

PARTICLE SIZE DISTRIBUTION

BORING NO. 0 SAMPLE NO. 22

DEPTH/ELEV 0 DATE 29 OCT 84

PLATE A/3

PLATE A74

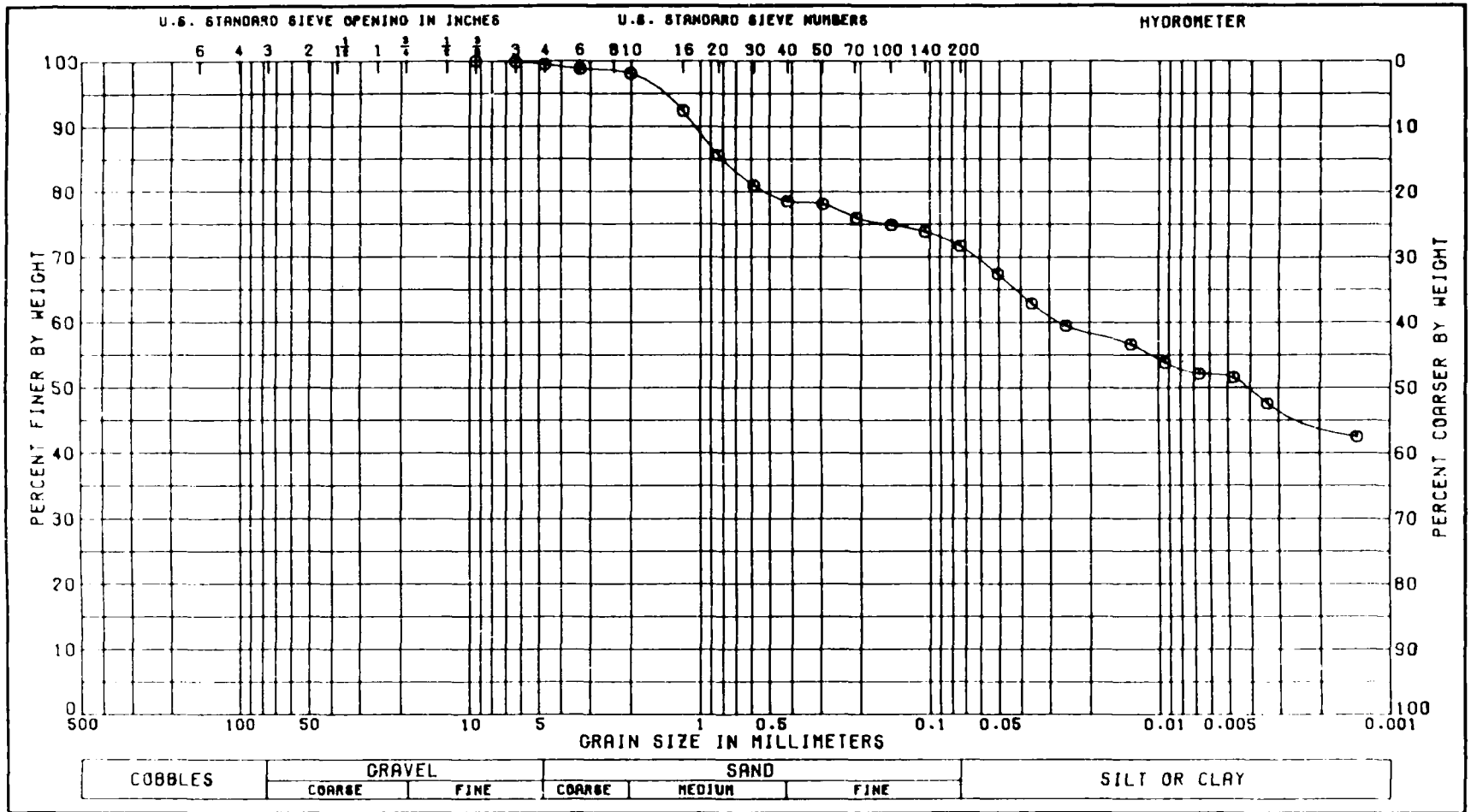

LL	PL	PI	GS 2.70 EST	NAT W.%	

CLASSIFICATION

GRADATION CURVE

PARTICLE SIZE DISTRIBUTION

BORING NO. 0 SAMPLE NO. 23

DEPTH/ELEV 0 DATE 29 OCT 84

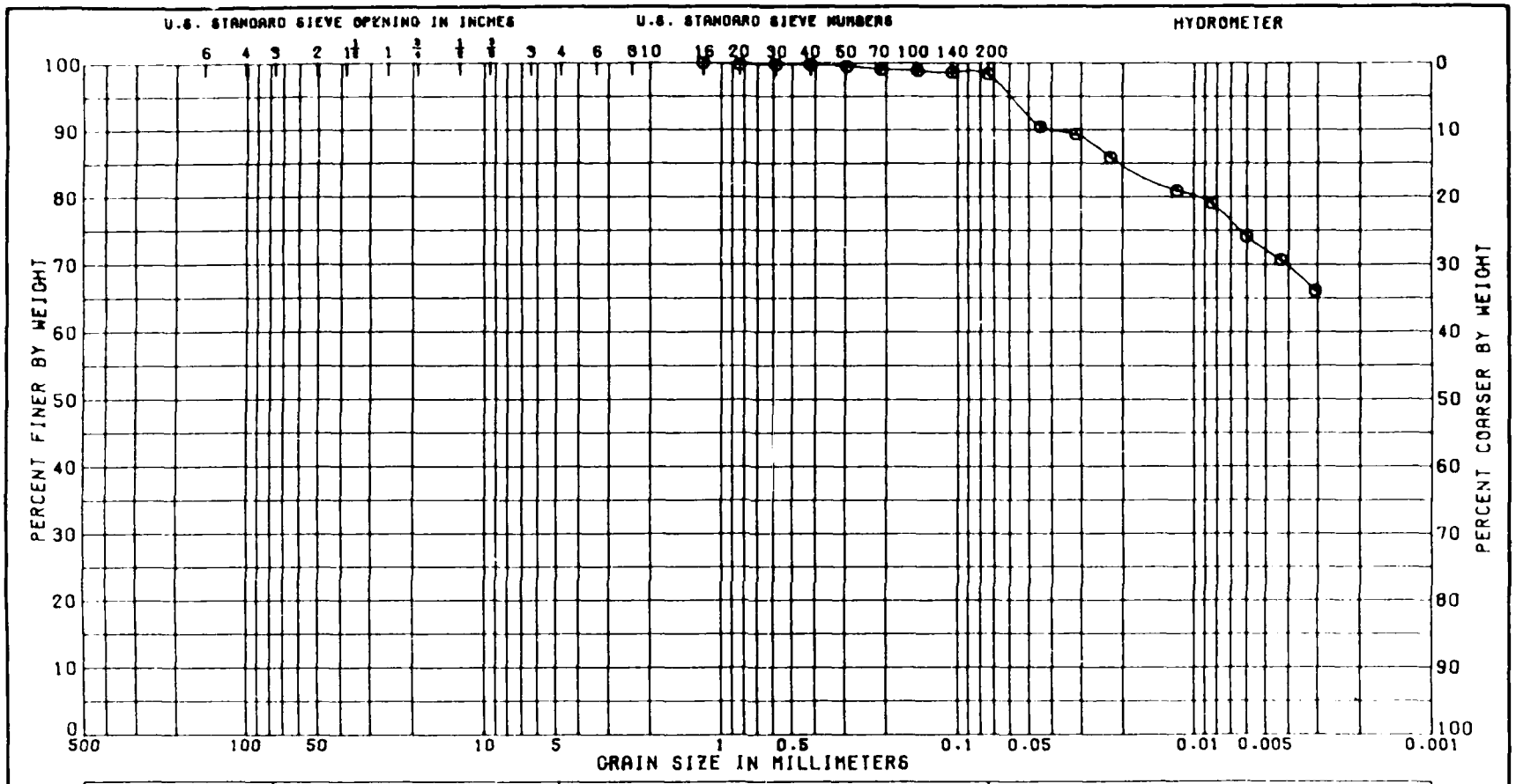

LL	PL	PI	GS 2.70 est	NAT W.%	

CLASSIFICATION

GRADATION CURVE

PARTICLE SIZE DISTRIBUTION

BORING NO. 0 SAMPLE NO. 24

DEPTH/ELEV 0 DATE 29 OCT 84

PLATE A75

PLATE A76

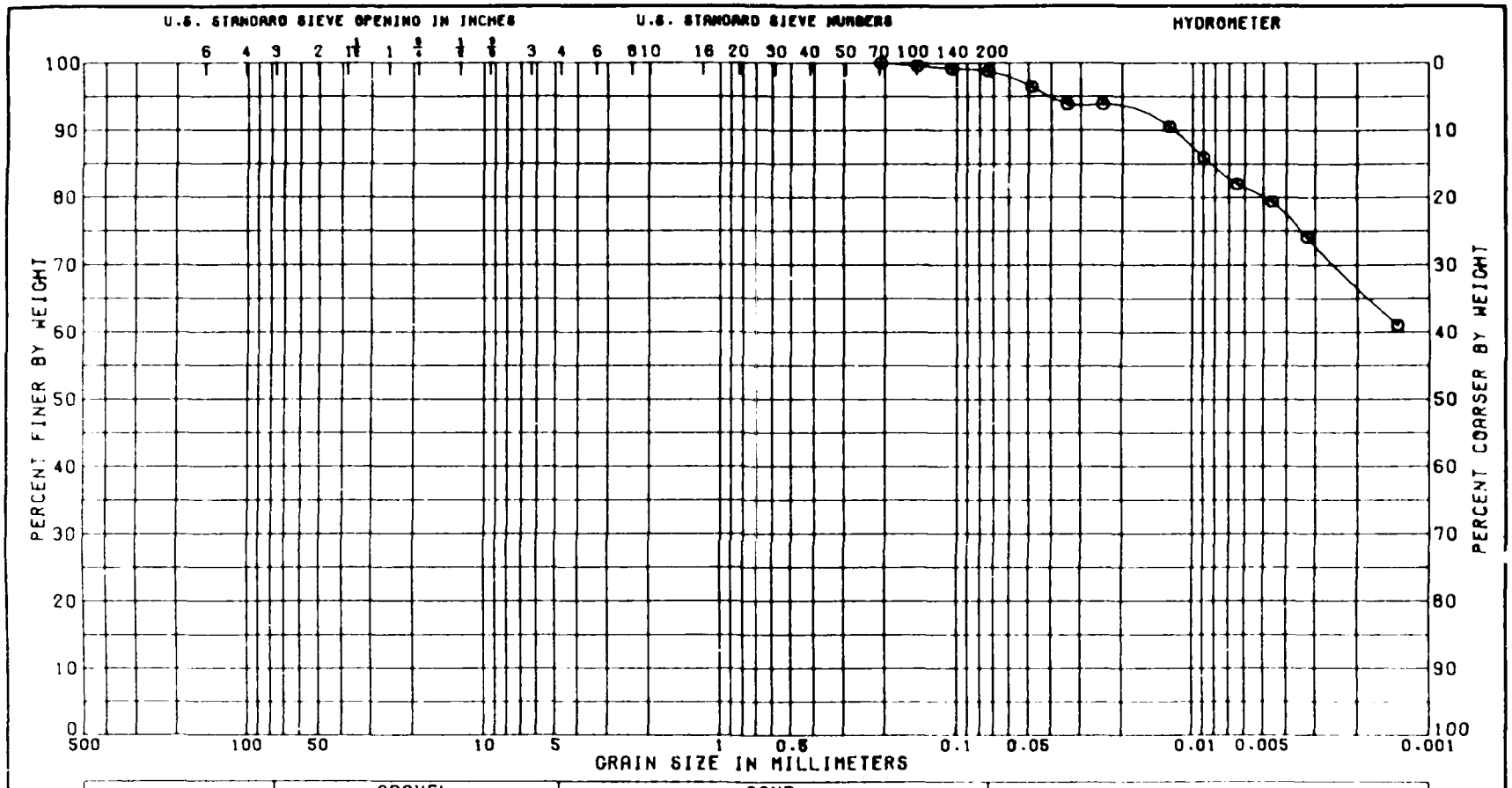

LL	PL	PI	GS 2.70 EST	NAT W.%	

CLASSIFICATION

GRADATION CURVE

PARTICLE SIZE DISTRIBUTION

BORING NO. 0 SAMPLE NO. 25

DEPTH/ELEV 0 DATE 29 OCT 84

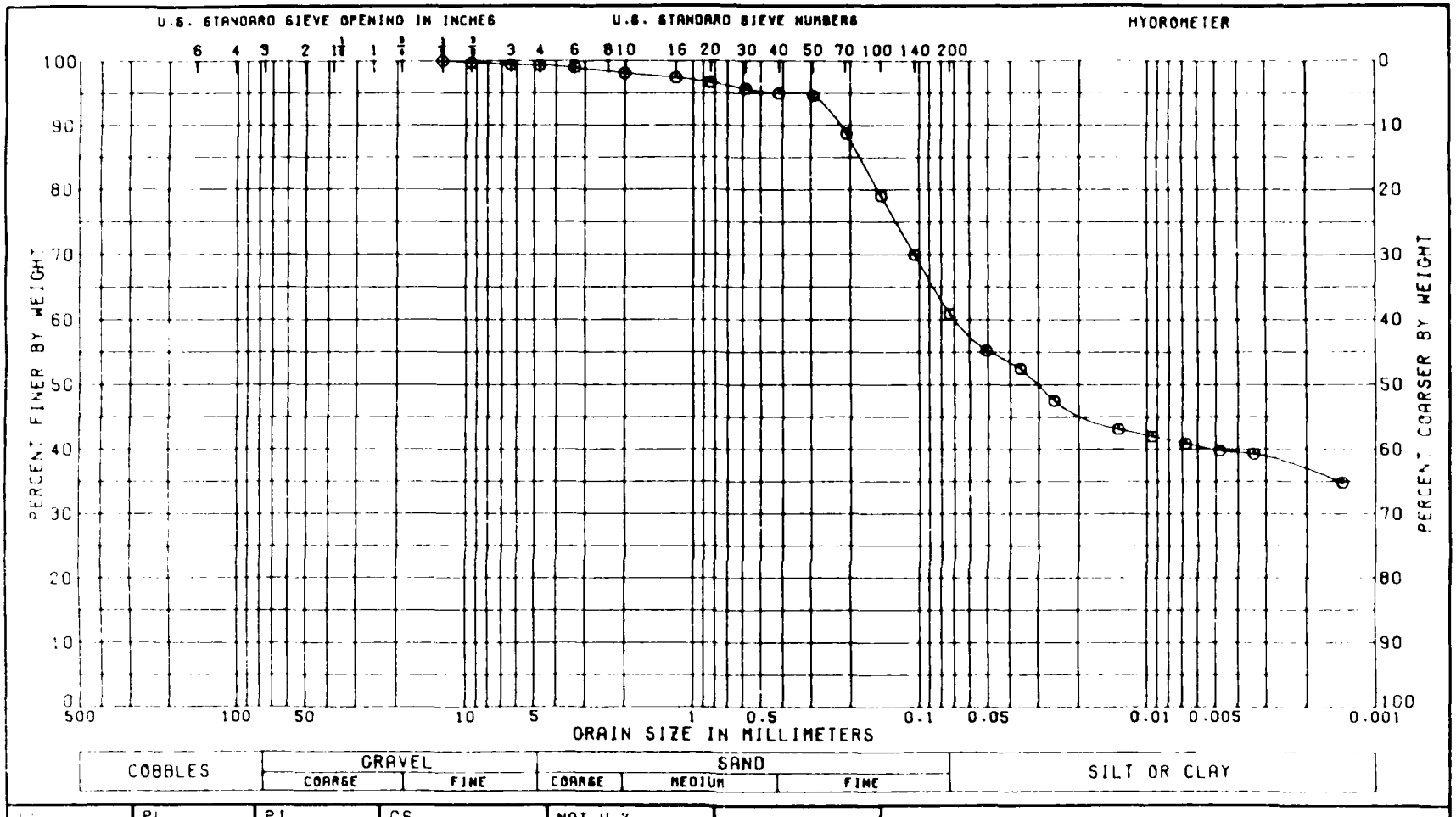

LL	PL	PI	GS 2.70 EST	NAT W.%	
CLASSIFICATION					

GRADATION CURVE

PARTICLE SIZE DISTRIBUTION

BORING NO. 0 SAMPLE NO. 26

DEPTH/ELEV 0 DATE 29 OCT 84

APPENDIX B: THE TABS-2 SYSTEM

1. TABS-2 is a collection of generalized computer programs and utility codes integrated into a numerical modeling system for studying two-dimensional hydrodynamics, sedimentation, and transport problems in rivers, reservoirs, bays, and estuaries. A schematic representation of the system is shown in Figure B1. It can be used either as a stand-alone solution technique or as a step in the hybrid modeling approach. The basic concept is to calculate water-surface elevations, current patterns, sediment erosion, transport and deposition, the resulting bed surface elevations, and the feedback to hydraulics. Existing and proposed geometry can be analyzed to determine the impact on sedimentation of project designs and to determine the impact of project designs on salinity and on the stream system. The system is described in detail by Thomas and McAnally (1985a).*

2. The three basic components of the system are as follows:

   a. "A Two-Dimensional Model for Free Surface Flows," RMA-2V.

   b. "Sediment Transport in Unsteady 2-Dimensional Flows, Horizontal Plane," STUDH.

   c. "Two-Dimensional Finite Element Program for Water Quality," RMA-4.

3. RMA-2V is a finite element solution of the Reynolds form of the Navier-Stokes equations for turbulent flows. Friction is calculated with Manning's equation and eddy viscosity coefficients are used to define the turbulent losses. A velocity form of the basic equation is used with side boundaries treated as either slip or static. The model automatically recognizes dry elements and corrects the mesh accordingly. Boundary conditions may

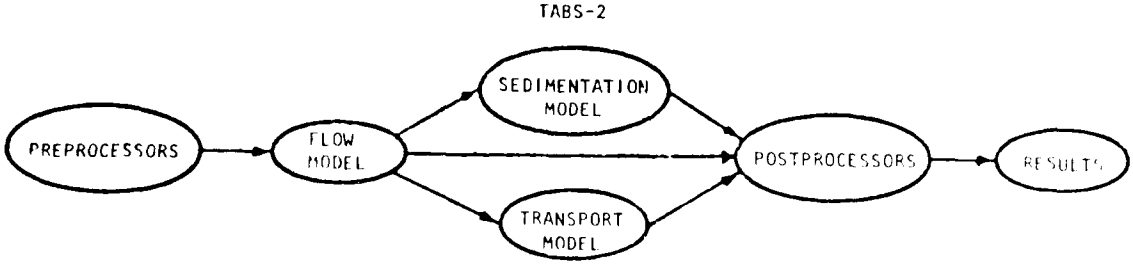

Figure B1. TABS-2 schematic

* References in this Appendix are located in the References section of the main text.

be water-surface elevations, velocities, or discharges and may occur inside the mesh as well as along the edges.

4. The sedimentation model, STUDH, solves the convection-diffusion equation with bed source terms. These terms are structured for either sand or cohesive sediments. The Ackers-White (1973) procedure is used to calculate a sediment transport potential for the sands from which the actual transport is calculated based on availability. Clay erosion is based on work by Ariathurai and Partheniades and the deposition of clay utilizes Krone's equations (Ariathurai, MacArthur, and Krone 1977). Deposited material forms layers, as shown in Figure B2, and bookkeeping allows up to 10 layers at each node for maintaining separate material types, deposit thickness, and age. The code uses the same mesh as RMA-2V.

5. Salinity calculations, RMA-4, are made with a form of the convective-diffusion equation which has general source-sink terms. Up to seven conservative substances or substances requiring a decay term can be routed. The code uses the same mesh as RMA-2V.

6. Each of these generalized computer codes can be used as a stand-alone program, but to facilitate the preparation of input data and to aid in analyzing results, a family of utility programs was developed for the following purposes:

a. Digitizing
b. Mesh generation
c. Spatial data management
d. Graphical output
e. Output analysis
f. File management
g. Interfaces
h. Job control language

Finite Element [illegible]

7. The TABS-2 numerical [illegible] element method to solve the [illegible] familiar with the meth[illegible] of the method is [illegible]

a. [illegible]

AD-A189 323 CORPUS CHRISTI INNER HARBOR SHOALING INVESTIGATION(U) 3/3
CAVER (TROY V) DOVER NJ T M SMITH ET AL. SEP 87
WES/TR/HL-87-13

UNCLASSIFIED F/G 13/2 NL

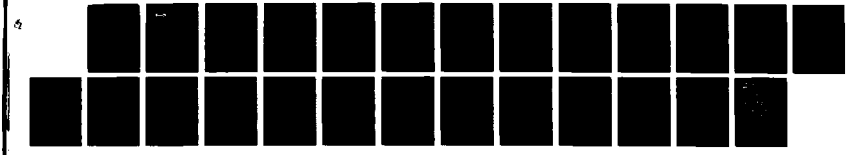

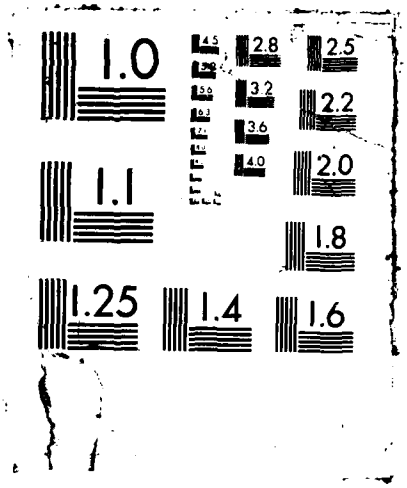
1.0
1.1
1.25
1.4
1.6
1.8
2.0
2.2
2.5
2.8
3.2
3.6
4.0
4.5

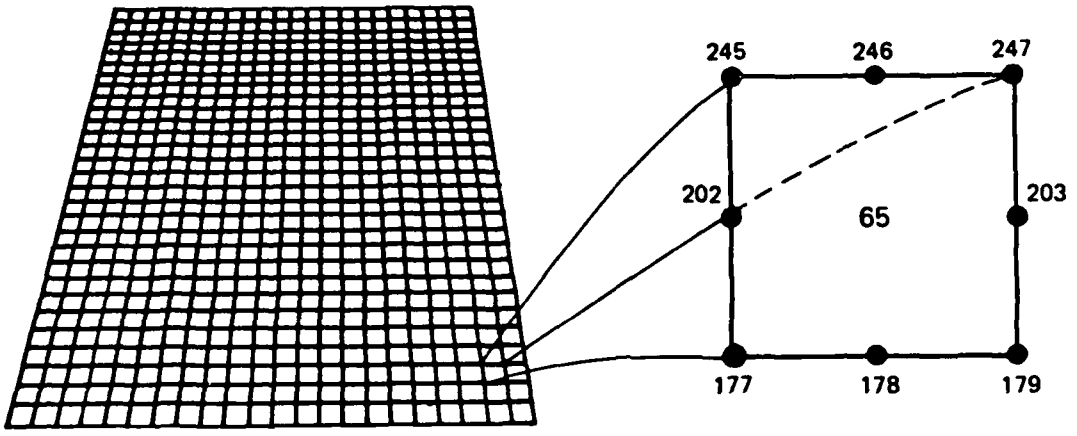

a. Eight nodes define each element

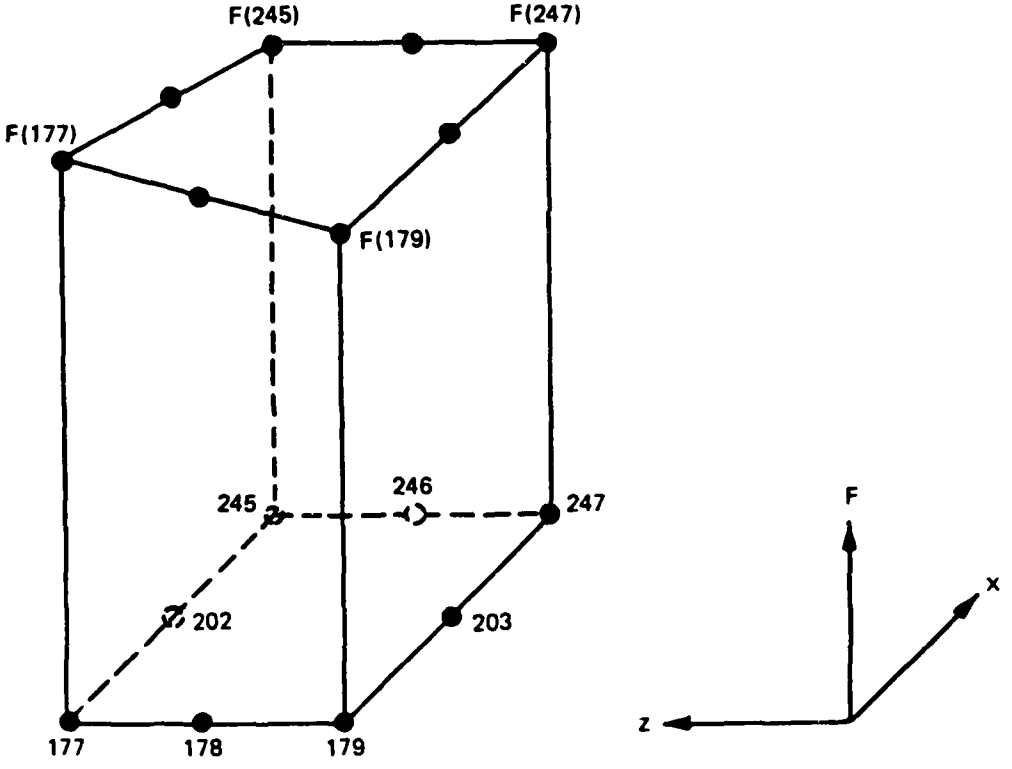

b. Linear interpolation function

Figure B2. Two-dimensional finite element mesh

dividing the area of interest into smaller subareas, which are called elements. The dependent variables (e.g., water-surface elevations and sediment concentrations) are approximated over each element by continuous functions which interpolate in terms of unknown point (node) values of the variables. An error, defined as the deviation of the approximation solution from the correct solution, is minimized. Then, when boundary conditions are imposed, a set of solvable simultaneous equations is created. The solution is continuous over the area of interest.

9. In one-dimensional problems, elements are line segments. In two-dimensional problems, the elements are polygons, usually either triangles or quadrilaterals. Nodes are located on the edges of elements and occasionally inside the elements. The interpolating functions may be linear or higher order polynomials. Figure B2 illustrates a quadrilateral element with eight nodes and a linear solution surface.

10. Most water resource applications of the finite element method use the Galerkin method of weighted residuals to minimize error. In this method the residual, the total error between the approximate and correct solutions, is weighted by a function that is identical with the interpolating function and then minimized. Minimization results in a set of simultaneous equations in terms of nodal values of the dependent variable (e.g. water-surface elevations or sediment concentration). The time portion of time-dependent problems can be solved by the finite element method, but it is generally more efficient to express derivatives with respect to time in finite difference form.

The Hydrodynamic Model, RMA-2V

11. The generalized computer program RMA-2V solves the depth-integrated equations of fluid mass and momentum conservation in two horizontal directions. The form of the solved equations is

$$h\frac{\partial u}{\partial t} + hu\frac{\partial u}{\partial x} + hu\frac{\partial u}{\partial y} - \frac{h}{\rho}\left(\epsilon_{xx}\frac{\partial^2 u}{\partial x^2} + \epsilon_{xy}\frac{\partial^2 u}{\partial y^2}\right) + gh\left(\frac{\partial a}{\partial x}\frac{\partial h}{\partial x}\right)$$

$$+ \frac{gun}{\left(1.486h^{1/6}\right)^2}\left(u^2 + v^2\right)^{1/2} - \zeta V_a^2 \cos\psi - 2h\omega v \sin\phi = 0 \qquad \text{(B1)}$$

$$h\frac{\partial v}{\partial t} + hv\frac{\partial v}{\partial x} + hv\frac{\partial v}{\partial y} - \frac{h}{\rho}\left(\epsilon_{yx}\frac{\partial^2 v}{\partial x^2} + \epsilon_{yy}\frac{\partial^2 v}{\partial y^2}\right) + gh\left(\frac{\partial a}{\partial y} + \frac{\partial h}{\partial y}\right)$$

$$+ \frac{gun}{\left(1.486h^{1/6}\right)^2}\left(u^2 + v^2\right)^{1/2} - \zeta V_a^2 \sin\psi + 2\omega hu \sin\phi = 0 \qquad \text{(B2)}$$

$$\frac{\partial h}{\partial t} + h\left(\frac{\partial u}{\partial x} + \frac{\partial v}{\partial y}\right) + u\frac{\partial h}{\partial x} + v\frac{\partial h}{\partial y} = 0 \qquad \text{(B3)}$$

where

h = depth

u,v = velocities in the Cartesian directions

x,t,y = Cartesian coordinates and time

ρ = density

ϵ = eddy viscosity coefficient, for xx = normal direction on x-axis surface; yy = normal direction on y-axis surface; xy and yx = shear direction on each surface

g = acceleration due to gravity

a = elevation of bottom

n = Manning's n value

1.486 = conversion from SI (metric) to non-SI units

ζ = empirical wind shear coefficient

V_a = wind speed

ψ = wind direction

ω = rate of earth's angular rotation

ϕ = local latitude

12. Equations B1, B2, and B3 are solved by the finite element method using Galerkin weighted residuals. The elements may be either quadrilaterals or triangles and may have curved (parabolic) sides. The shape functions are quadratic for flow and linear for depth. Integration in space is performed by Gaussian integration. Derivatives in time are replaced by a nonlinear finite difference approximation. Variables are assumed to vary over each time interval in the form

$$f(t) = f(0) + at + bt^c \qquad t_0 \leq t < t \qquad \text{(B4)}$$

which is differentiated with respect to time, and cast in finite difference form. Letters a , b , and c are constants. It has been found by experiment that the best value for c is 1.5 (Norton and King 1977).

13. The solution is fully implicit and the set of simultaneous equations is solved by Newton-Raphson iteration. The computer code executes the solution by means of a front-type solver that assembles a portion of the matrix and solves it before assembling the next portion of the matrix. The front solver's efficiency is largely independent of bandwidth and thus does not require as much care in formation of the computational mesh as do traditional solvers.

14. The code RMA-2V is based on the earlier version RMA-2 (Norton and King 1977) but differs from it in several ways. It is formulated in terms of velocity (v) instead of unit discharge (vh), which improves some aspects of the code's behavior; it permits drying and wetting of areas within the grid; and it permits specification of turbulent exchange coefficients in directions other than along the x- and z-axes. For a more complete description, see Thomas and McAnally (1985b).

The Sediment Transport Model, STUDH

15. The generalized computer program STUDH solves the depth-integrated convection-dispersion equation in two horizontal dimensions for a single sediment constituent. A detailed description can be found in Thomas and McAnally (1985c). The form of the solved equation is

$$\frac{\partial C}{\partial t} + u \frac{\partial C}{\partial x} + v \frac{\partial C}{\partial y} = \frac{\partial}{\partial x}\left(D_x \frac{\partial C}{\partial x}\right) + \frac{\partial}{\partial y}\left(D_y \frac{\partial C}{\partial y}\right) + \alpha_1 C + \alpha_2 = 0 \qquad \text{(B5)}$$

where

C = concentration of sediment

u = depth-integrated velocity in x-direction

v = depth-integrated velocity in y-direction

D_x = dispersion coefficient in x-direction

D_y = dispersion coefficient in y-direction

α_1 = coefficient of concentration-dependent source/sink term

α_2 = coefficient of source/sink term

16. The source/sink terms in Equation B5 are computed in routines that treat the interaction of the flow and the bed. Separate sections of the code handle computations for clay bed and sand bed problems.

Sand transport

17. The source/sink terms are evaluated by first computing a potential sand transport capacity for the specified flow conditions, comparing that capacity with the amount of sand actually being transported, and then eroding from or depositing to the bed at a rate that would approach the equilibrium value after sufficient elapsed time.

18. The potential sand transport capacity in the model is computed by the method of Ackers and White (1973), which uses a transport power (work rate) approach. It has been shown to provide superior results for transport under steady-flow conditions (White, Milli, and Crabbe 1975) and for combined waves and currents (Swart 1976). Flume tests at the US Army Engineer Waterways Experiment Station have shown that the concept is valid for transport by estuarine currents.

19. The total load transport function of Ackers and White is based upon a dimensionless grain size

$$D_{gr} = D\left[\frac{g(s-1)}{\nu^2}\right]^{1/3} \tag{B6}$$

where

D = sediment particle diameter

s = specific gravity of the sediment

ν = kinematic viscosity of the fluid

and a sediment mobility parameter

$$F_{gr} = \left[\frac{\tau^{n'}\tau'^{(1-n')}}{\rho g D(s-1)}\right]^{1/2} \tag{B7}$$

where

τ = total boundary shear stress

n' = a coefficient expressing the relative importance of bed-load and suspended-load transport, given in Equation B9

τ' = boundary surface shear stress

The surface shear stress is that part of the total shear stress which is due to the rough surface of the bed only, i.e., not including that part due to bed forms and geometry. It therefore corresponds to that shear stress that the flow would exert on a plane bed.

20. The total sediment transport is expressed as an effective concentration

$$G_p = C\left(\frac{F_{gr}}{A} - 1\right)^m \frac{sD}{h} \left(\frac{\rho}{\tau} U\right)^{n'} \tag{B8}$$

where U is the average flow speed, and for $1 < D_{gr} \leq 60$

$$n' = 1.00 - 0.56 \log D_{gr} \tag{B9}$$

$$A = \frac{0.23}{\sqrt{D_{gr}}} + 0.14 \tag{B10}$$

$$\log C = 2.86 \log D_{gr} - (\log D_{gr})^2 - 3.53 \tag{B11}$$

$$m = \frac{9.66}{D_{gr}} + 1.34 \tag{B12}$$

For $D_{gr} < 60$

$$n' = 0.00 \tag{B13}$$

$$A = 0.17 \tag{B14}$$

$$C = 0.025 \tag{B15}$$

$$m = 1.5 \tag{B16}$$

21. Equations B6-B16 result in a potential sediment concentration G_p. This value is the depth-averaged concentration of sediment that will occur if an equilibrium transport rate is reached with a nonlimited supply of sediment.

The rate of sediment deposition (or erosion) is then computed as

$$R = \frac{G_p - C}{t_c} \tag{B17}$$

where

C = present sediment concentration

t_c = time constant

For deposition, the time constant is

$$t_c = \text{larger of} \begin{cases} \Delta t \\ \text{or} \\ \dfrac{C_d h}{V_s} \end{cases} \tag{B18}$$

and for erosion it is

$$t_c = \text{larger of} \begin{cases} \Delta t \\ \text{or} \\ \dfrac{C_e h}{U} \end{cases} \tag{B19}$$

where

Δt = computational time-step

C_d = response time coefficient for deposition

V_s = sediment settling velocity

C_e = response time coefficient for erosion

The sand bed has a specified initial thickness which limits the amount of erosion to that thickness.

Cohesive sediments transport

22. Cohesive sediments (usually clays and some silts) are considered to be depositional if the bed shear stress exerted by the flow is less than a critical value τ_d. When that value occurs, the deposition rate is given by Krone's (1962) equation

$$S = \begin{cases} -\frac{2V_s}{h} C \left(1 - \frac{\tau}{\tau_d}\right) & \text{for } C < C_c \quad \text{(B20)} \\ -\frac{2V_s}{hC_c^{4/3}} C^{5/3} \left(1 - \frac{\tau}{\tau_d}\right) & \text{for } C > C_c \quad \text{(B21)} \end{cases}$$

where

τ = bed shear stress

C_c = critical concentration = 300 mg/ℓ

If the bed shear stress is greater than the critical value for erosion τ_e, material is removed from the bed. The source term is then computed by Ariathurai's (Ariathurai, MacArthur, and Krone 1977) adaptation of Partheniades' (1962) findings:

$$S = \frac{P}{h} \left(\frac{\tau}{\tau_e} - 1\right) \quad \text{(B22)}$$

where P is the erosion rate constant, unless the shear stress is also greater than the critical value for mass erosion τ_s. When τ_s is exceeded, mass failure of a sediment layer occurs and

$$S = \frac{T_L P_L}{h\Delta t} \quad \text{(B23)}$$

where

T_L = thickness of the failed layer

P_L = density of the failed layer

23. The cohesive sediment bed consists of 1 to 10 layers, each with a distinct density and erosion resistance. The layers consolidate with overburden and time.

Bed shear stress

24. Bed shear stresses are calculated from the flow speed according to one of four optional equations: the smooth-wall log velocity profile or Manning equation for flows alone; and a smooth bed or rippled bed equation for

combined currents and wind waves. Shear stresses are calculated using the shear velocity concept where

$$\tau_b = \rho u_*^2 \tag{B24}$$

where

τ_b = bed shear stress

u_* = shear velocity

and the shear velocity is calculated by one of four methods:

a. Smooth-wall log velocity profiles

$$\frac{\bar{u}}{u_*} = 5.75 \log \left(3.32 \frac{u_* h}{\nu}\right) \tag{B25}$$

which is applicable to the lower 15 percent of the boundary layer when

$$\frac{u_* h}{\nu} > 30$$

where u is the mean flow velocity.

b. The Manning shear stress equation

$$u_* = \frac{\sqrt{g\bar{u}n}}{CME\ h^{1/6}} \tag{B26}$$

where CME is a coefficient of 1 for SI (metric) units and 1.486 for non-SI units of measurement.

c. A Jonsson-type equation for surface shear stress (plane beds) caused by waves and currents

$$u_* = \frac{1}{2}\left(\frac{f_w u_{om} + f_c \bar{u}}{u_{om} + \bar{u}}\right)\left(\bar{u} + \frac{u_{om}}{2}\right) \tag{B27}$$

where

f_w = shear stress coefficient for waves

u_{om} = maximum orbital velocity of waves

f_c = shear stress coefficient for currents

d. A Bijker-type equation for total shear stress caused by waves and current

$$u_* = \sqrt{\frac{1}{2} f_c \bar{u}^2 + \frac{1}{4} f_w u_{om}^2} \tag{B28}$$

For further information on the shear stress computation equations, see McAnally and Thomas.*

Solution method

25. Equation B5 is solved by the finite element method using Galerkin weighted residuals. Like RMA-2V, which uses the same general solution technique, elements are quadrilateral and may have parabolic sides. Shape functions are quadratic. Integration in space is Gaussian. Time-stepping is performed by a Crank-Nicholson approach with a weighting factor (θ) of 0.66. A front-type solver similar to that in RMA-2V is used.

* W. H. McAnally, Jr., and W. A. Thomas. 1980. "Shear Stress Computations in Numerical Model for Estuarine Sediment Transport," Memorandum for Record, US Army Engineer Waterways Experiment Station, Vicksburg, Miss.

APPENDIX C: THEORETICAL ASPECTS OF LAEMSED

1. Under the Environmental and Water Quality Operational Studies (EWQOS) program of the US Army Corps of Engineers, developmental work was conducted on a two-dimensional (2-D) laterally averaged, free-surface, variable-density, and heat-conducting model for use in simulating flows in thermally stratified reservoirs. This effort, which extended the earlier work funded by the US Army Engineer Division, Ohio River (Edinger and Buchak 1979),* resulted in a numerically efficient model that is known as LARM (Laterally Averaged Reservoir Model). Under a contract with the US Army Engineer District, Savannah, LARM was modified for use in computing stratified flows in estuaries as a result of both salinity and thermal effects. This model is known as LAEM (Laterally Averaged Estuarine Model) (Edinger and Buchak 1981). An application of LAEM to a channel deepening study by Johnson, Boyd, and Keulegan (1987) on the Lower Mississippi River demonstrated the general applicability of LAEM to such problems. A version of LAEM which allows the modeling of interconnecting channels has been modified by Johnson (Johnson, Trawle, and Kee, in preparation). This model, which computes suspended sediment transport and simulates the erosion/deposition process at the bed, is called LAEMSED (Laterally Averaged Estuarine Model with Sediment).

Governing Flow-Transport Equations

2. The basic set of flow and transport equations that are solved in LAEMSED are statements of the conservation of mass and momentum of the flow field plus the conservation of the heat, salt, and suspended sediment in the water body. The governing equations are developed by first performing a temporal averaging of the three-dimensional equations for laminar flow. Boussinesq's eddy coefficient concept is then employed to account for the effect of turbulence in the flow field. Next, the time-averaged equations are averaged over the estuary width and finally over an individual vertical layer with boundaries at $z = k + 1/2$ and $z = k - 1/2$ where z is the positive downward Cartesian coordinate and k is the integer layer number, to yield

---

* References in this Appendix are located in the References section of the main text.

the following equations that are solved in the water column in LAEMSED (symbols used in these equations are defined following Equation C9):

Longitudinal (x-direction) momentum

$$\frac{\partial}{\partial t}(UBh) + \frac{\partial}{\partial x}(U^2Bh) + \left(u_b w_b b\right)_{k+1/2} - \left(u_b w_b b\right)_{k-1/2}$$

$$+ \frac{1}{\rho}\frac{\partial}{\partial x}(PBh) - A_x \frac{\partial^2}{\partial x^2}(UBh) + \left(\tau_z b\right)_{k+1/2} - \left(\tau_z b\right)_{k-1/2} = 0 \qquad (C1)$$

with

$$\tau_z = C^* \rho_a \Big/ \left(\rho W_a^2 \cos\phi\right) \quad \text{(surface)}$$

$$= A_z \, \partial U/\partial z \quad \text{(interlayer)}$$

$$= gU|U|/c^2 \quad \text{(bottom)}$$

Internal continuity

$$\left(w_b b\right)_{k-1/2} = \left(w_b b\right)_{k+1/2} + \frac{\partial}{\partial x}(UBh) - q_1 \frac{Bh}{V} \qquad (C2)$$

Total depth continuity

$$\frac{\partial(\xi b)}{\partial t} - \sum_k \frac{\partial}{\partial x}(UBh) = \frac{q_2 Bh}{V} + \sum_k \frac{q_1 Bh}{V} \qquad (C3)$$

where q_2 is computed from

$$q_2 = \frac{A_f \Delta\xi}{\Delta t} \qquad (C4)$$

Vertical (z-directional) momentum

$$\frac{\partial P}{\partial z} = \rho g \qquad (C5)$$

Heat balance

$$\frac{\partial}{\partial t}(BhT) + \frac{\partial}{\partial x}(UBhT) + \left(w_b bT\right)_{k+1/2} - \left(w_b bT\right)_{k-1/2}$$

$$- \frac{\partial}{\partial x}\left(D_x \frac{\partial BhT}{\partial x}\right) - \left(D_x \frac{\partial BT}{\partial z}\right)_{k+1/2} + \left(D_z \frac{\partial BT}{\partial z}\right)_{k-1/2} = \frac{H_n Bh}{V} \qquad (C6)$$

Salinity balance

$$\frac{\partial}{\partial t}(BhS) + \frac{\partial}{\partial x}(UBhS) + \left(w_b bS\right)_{k+1/2} - \left(w_b bS\right)_{k-1/2} - \frac{\partial}{\partial x}\left(D_x \frac{\partial BhS}{\partial x}\right)$$

$$- \left(D_z \frac{\partial BS}{\partial z}\right)_{k+1/2} + \left(D_z \frac{\partial BS}{\partial z}\right)_{k-1/2} = \frac{\left(Sq_1 + S_{kT}q_2\right) Bh}{V} \qquad (C7)$$

Suspended sediment balance

$$\frac{\partial}{\partial t}\left(BhC_s\right) + \frac{\partial}{\partial x}\left(UBhC_s\right) + \left(w_b bC_s\right)_{k+1/2} - \left(w_b bC_s\right)_{k-1/2} - \frac{\partial}{\partial x}\left(D_x \frac{\partial BhC_s}{\partial x}\right)$$

$$- \left(D_z \frac{\partial BC_s}{\partial z}\right)_{k+1/2} + \left(D_z \frac{\partial BC_s}{\partial z}\right)_{k-1/2} = H_s Bh + \frac{C_s q_2 Bh}{V} \qquad (C8)$$

Equation of state

$$\rho = \frac{1{,}000\ P_o}{LA + 0.698P_o} + \frac{\left(\gamma_s - 1\right)}{\gamma_s} C_s \qquad (C9)$$

where

$$P_o = 5890 + 38T - 0.375T^2 + 3S$$
$$LA = 1779.5 + 11.25T - 0.0745T^2 - (3.8 + 0.01T)S$$

Variables in Equations C1-C9 are defined as follows:

A_f = plan area of overbank storage, m^2

A_x = x-direction momentum dispersion coefficient, m^2/sec

A_z = z-direction momentum dispersion coefficient, m^2/sec

b = estuary or river width, m

B = laterally averaged width integrated over h , m

c = Chezy resistance coefficient, $m^{1/2}/sec$

C* = resistance coefficient associated with wind

C_s = suspended sediment concentration, kg/m^3

D_x = x-direction temperature and salinity dispersion coefficient, m^2/sec

D_z = z-direction temperature and salinity dispersion coefficient, m^2/sec

g = acceleration due to gravity, m/sec^2

h = horizontal layer thickness, m

H_n = source strength for heat balance, °C m^3/sec

H_s = sediment source, $kg/m^3/sec$

k = integer layer number, positive downward

P = pressure, N/m^2

q_1 = tributary inflow or withdrawal, m^3/sec

q_2 = exchange of flow between channel and overbank, m^3/sec

S = laterally averaged salinity integrated over h , ppt

S_{kT} = laterally averaged salinity in top layer, ppt

t = time, sec

T = laterally averaged temperature integrated over h , °C

u_b = x-direction laterally averaged velocity, m/sec

U = x-direction laterally averaged velocity integrated over h , m/sec

V = cell volume ($B \cdot h \cdot \Delta x$), m^3

W_a = wind speed, m/sec

w_b = z-direction laterally averaged velocity, m/sec

x and z = Cartesian coordinates: x is along the estuary center line at the water surface, positive to the right, and z is positive downward from the x-axis, m

Δx = longitudinal spatial step, m

Δt = time-step, sec

$\Delta \xi$ = change in surface elevation, m

γ_s = specific gravity of sediment

ξ = surface elevation, m

ρ = density, kg/m^3

ρ_a = air density, kg/m^3

τ_z = water density times tangential stress in positive x-direction, m^2/sec^2

ϕ = wind direction, rad

3. Basic assumptions in addition to the reduced dimensionality are that the Boussinesq approximation (ρ is constant except where multiplied by the acceleration of gravity) is applicable and that vertical accelerations are negligible so that the pressure can be considered hydrostatic. In addition, the concept of eddy coefficients is used to represent the effect of both time averaging, as previously noted, and spatial averaging of the equations. The horizontal dispersion coefficients, A_x and D_x, are assumed to be constant, whereas the vertical dispersion coefficients, A_z and D_z, are dependent upon the stratification as reflected by the local Richardson number R_i, i.e.,

$$A_z = A_{z_o}\left(1 + 3.33R_i\right)^{-3/2}$$
$$D_z = D_{z_o}\left(1 + 10R_i\right)^{-1/2} \qquad \text{(C10)}$$

where

$$R_i = \frac{\frac{g}{\rho}\frac{\partial \rho}{\partial z}}{\left(\frac{\partial U}{\partial z}\right)^2} \qquad \text{(C11)}$$

and A_{z_o} and D_{z_o} are the vertical coefficients for no stratification. Due to the hydrostatic pressure assumption, unstable stratification cannot be modeled in a convective fashion and thus is handled in a diffusive manner by increasing D_z to its stability limit of $h^2/2\Delta t$, where Δt is the computation time-step.

4. The laterally averaged horizontal pressure gradient in the longitudinal momentum equation contains the density driving force. Using the expression for the hydrostatic pressure, the horizontal pressure gradient can be divided into its two components of the barotropic (surface slope) gradient and the baroclinic (density) gradient to yield:

$$\frac{\partial P}{\partial x} = -g\rho\frac{\partial \xi}{\partial x} + g\int_{\xi}^{z}\frac{\partial P}{\partial x}\,dz \qquad (C12)$$

Numerical Solution Scheme

5. Finite difference techniques are employed to solve the governing equations. The particular scheme employed is structured such that the water-surface elevations are computed implicitly. Using the new water-surface elevations, the x-component of the flow velocity is then explicitly computed from the longitudinal momentum equation. As in other hydrostatic models, the vertical component of the velocity is computed from the continuity equation which is reduced to the incompressibility condition as a result of the Boussinesq approximation. The solution begins at the bottom and progresses up the column of layers. With the flow field computed, the water temperature and salt and suspended sediment concentrations are then computed from their respective transport equations in a semi-implicit fashion. Details can be found in Edinger and Buchak (1979).

6. A note concerning the treatment of the vertical advection term $\left(w_b bC_s\right)_{k+1/2} - \left(w_b bC_s\right)_{k-1/2}$ in the transport equation for the suspended sediment concentration is required. In the equations for temperature and salinity, the vertical advection term is handled explicitly. However, if the settling velocity is relatively large and/or the vertical layer spacing is small, an explicit representation in the sediment transport equation will result in a severe restriction on the computational time-step. Therefore, an approximate factorization scheme has been used to implicitly handle the vertical advection term in Equation C8. This is accomplished in the following manner. Before averaging, Equation C8 had the form

$$\frac{\partial C_s}{\partial t} + \frac{\partial UC_s}{\partial x} + \frac{\partial w_b C_s}{\partial z} = \text{R.H.S.} \qquad (C13)$$

where R.H.S. contains all other terms in Equation C8.

Using

$$\frac{\partial C_s}{\partial t} = \frac{C_s^{n+1} - C_s^n}{\Delta t} + O(\Delta t) \qquad (C14)$$

where n represents the time level and $O(\Delta t)$ refers to additional terms multiplied by Δt and higher powers of Δt and substituting into Equation C13 yields

$$C_s^{n+1} + \Delta t \frac{\partial UC_s}{\partial x} + \frac{\partial w_b C_s}{\partial z} = C_s^n + \Delta t \text{ (R.H.S.)} + O(\Delta t^2) \qquad (C15)$$

However, the left-hand side, written in operator form, can be factored as

$$\left(1 + \Delta t\ D_x'\right)\left(1 + \Delta t\ D_z'\right) C_s^{n+1} = C_s^{n+1} + \Delta t\ D_x' C_s^{n+1} + \Delta t\ D_z' C_s^{n+1} + O(\Delta t^2) \qquad (C16)$$

where D_x' and D_z' are differential operators defined such that

$$D_x'\ C_s^{n+1} = \left(\frac{\partial UC_s}{\partial x}\right)^{n+1} \quad ; \quad D_z'\ C_s^{n+1} = \left(\frac{\partial w_b C_s}{\partial z}\right)^{n+1}$$

The following sequence of equations can then be written for Equation C16.

$$\left(1 + \Delta t\ D_x'\right) \bar{C}_s = C_s^n + \Delta t \text{ (R.H.S.)} \qquad (C17a)$$

$$\left(1 + \Delta t\ D_z'\right) C_s^{n+1} = \bar{C}_s + O(\Delta t^2) \qquad (C17b)$$

Thus, with Equation C17a, computations are first made along the channel without considering the vertical advection term. This solution is then used in a vertical sweep with Equation C17b to yield the final suspended sediment concentration field at the new time level. Unlike standard alternating-direction-implicit (ADI) schemes, to an accuracy of $O(\Delta t^2)$ no iteration is required. With this solution procedure, the settling velocity of the suspended sediment does not influence the allowable computational time-step.

7. The major advantage of the basic solution scheme employed in LAEMSED

is that the extremely restrictive stability criterion based upon the speed of the free-surface gravity wave, i.e., $\Delta t < (\Delta x/\sqrt{gH_{max}})$, where H_{max} is the maximum water depth, is removed. However, since the convective terms and baroclinic term in the longitudinal momentum equation, as well as the vertical diffusion and advection terms in the temperature and salt transport equations, are lagged in an explicit fashion, the following stability criteria still remain:

$$\Delta t < \frac{\Delta x}{U}$$

$$\Delta t < \frac{\Delta x}{\frac{\Delta \rho}{\rho} g h_w}$$

$$\Delta t < \frac{h^2}{2D_z} \tag{C18}$$

$$\Delta t < \frac{h}{w_b}$$

where $\Delta \rho$ is the density difference of the fresh and saline water, and h_w is the height of the density flow.

Governing Bed Equations

8. The routines in LAEMSED that compute the exchange of sediment between the sediment bed and the water column are modifications of those found in a vertically averaged sediment transport model called STUDH (Thomas and McAnally 1985c). The sediment may be treated as either cohesive (clay) or noncohesive (sand). A single, effective grain size is considered for each.

Conceptual basis

9. The following are basic assumptions:

   a. Basic processes in sedimentation can be grouped into erosion, entrainment, transportation, and deposition.

   b. Flowing water has the potential to erode, entrain, and transport sediment whether or not sediment particles are present.

c. Sediment on the streambed will remain immobile only as long as the energy forces in the flow field remain less than the critical shear stress threshold for erosion.

d. Even when sand particles become mobile, there may be no net change in the surface elevation of the bed. A net change in the surface would result only if the rate of erosion was different from the rate of deposition--two processes which go on continually and independently.

e. Cohesive sediments in transport will remain in suspension as long as the bed shear stress exceeds the critical value for deposition. In general, simultaneous deposition and erosion of cohesive sediments do not occur.

f. The structure of cohesive sediment beds changes with time, overburden, and ambient water conditions.

g. The major portion of sediment in transport can be characterized as being transported in suspension, even that part of the total load that is transported close to the bed.

Bed shear stress

10. Several options are available for computing the shear velocity used in the bed shear stress equation

$$\tau_b = \rho u_*^2 \tag{C19}$$

where

ρ = water density

u_* = shear velocity

a. Smooth-wall log velocity profile,

$$\frac{\bar{u}}{u_*} = 5.75 \log \left(3.32 \frac{u_* h}{\nu}\right) \tag{C20}$$

where

$\bar{u}$ = flow velocity in bottom computational cell

h = bottom layer thickness

ν = kinematic viscosity of water

b. The Manning shear stress equation,

$$u_* = \frac{\sqrt{g\bar{u}n}}{\text{CME } h^{1/6}} \tag{C21}$$

where

n = Manning's roughness value

CME = coefficients of 1 for SI (metric) units and 1.486 for non-SI units

c. A Jonsson-type equation for surface shear stress (plane beds) caused by waves and currents,

$$u_* = \sqrt{\frac{1}{2}\left(\frac{f_w u_{om} + f_c \bar{u}}{u_{om} + \bar{u}}\right)\left(\bar{u} + \frac{u_{om}}{2}\right)} \tag{C22}$$

where

f_w = shear stress coefficient for waves

u_{om} = maximum orbital velocity of waves

f_c = shear stress coefficient for currents

Bed source term

11. The transport equation for suspended sediment, Equation C8, contains a bed source term, H_s. The form of this term is

$$H_s = \alpha_1 C_{s_b} + \alpha_2 \tag{C23}$$

where C_{s_b} is the sediment concentration near the bottom and α_1 and α_2 are computed as discussed below. Equation C23 is the same for deposition and erosion of both sands and clays. Naturally, if deposition is occurring, H_s will be negative, whereas a positive value will result if erosion is taking place. In Equation C23, α_1 is in units of 1 per second while α_2 is the equilibrium concentration portion of the source term and is in units of kilograms per cubic metre per second. Methods of computing α_1 and α_2 depend on the sediment type and whether erosion or deposition is occurring.

12. Sand transport. The supply of sediment from the bed (i.e., the sediment reservoir) is controlled by the transport potential of the flow and availability of material in the bed. The bed source term is

$$H_s = \frac{C_{eq} - C_{s_b}}{t_c} \tag{C24}$$

where

C_{eq} = equilibrium concentration

t_c = characteristic time for effecting the transition

There are many transport relationships for calculating C_{eq} for sand. The Ackers-White (1973) formula was adopted for STUDH and thus is also used in LAEMSED.

13. The characteristic time t_c is somewhat subjective. It should be the amount of time required for the concentration in the bottom layer to change from C_{s_b} to C_{eq}. In the case of deposition, t_c is related to fall velocity. The following expression is employed:

$$t_c = \text{larger of } C_d \frac{h}{W_s} \text{ or } \Delta t \tag{C25}$$

where

C_d = coefficient for deposition

W_s = fall velocity of sediment particle

Δt = computation time interval

In the case of erosion, there are no simple parameters to employ. The following expression is used:

$$t_c = \text{larger of } C_e \frac{h}{u} \text{ or } \Delta t \tag{C26}$$

where

C_e = coefficient for entrainment

u = flow velocity

14. Clay transport. Deposition rates of clay beds are calculated with the equations of Krone (1962):

$$H_s = -\frac{2W_s}{h} C_{s_b} \left(1 - \frac{\tau}{\tau_d}\right) \quad \text{for} \quad C_{s_b} < C_c \tag{C27}$$

$$H_s = -\frac{2W_s}{C_c^{4/3} h} C_{s_b}^{5/3} \left(1 - \frac{\tau}{\tau_d}\right) \quad \text{for} \quad C_{s_b} > C_c \tag{C28}$$

where

τ = bed shear stress

τ_d = critical shear stress for deposition

C_c = critical concentration = 300 mg/ℓ

Erosion rates are computed by Ariathurai's simplification (Ariathurai, MacArthur, and Krone 1977) of Parthenaides' (1962) results for particle by particle erosion. The source term is computed by

$$H_s = \frac{P}{h}\left(\frac{\tau}{\tau_e} - 1\right) \tag{C29}$$

where

P = erosion rate constant

τ_e = critical shear stress for particle erosion

15. When bed shear stress is high enough to cause mass failure of a bed layer, the erosion source term is

$$H_s = \frac{T_L P_L}{h \Delta t_f} \quad \text{for} \quad \tau > \tau_s \tag{C30}$$

where

T_L = thickness of the failed layer

P_L = density of the failed layer

Δt_f = time interval over which failure occurs

τ_s = bulk shear strength of the layer

Bed model

16. The sink/source term H_s in Equation C8 becomes a source/sink term for the bed model, which keeps track of the elevation, composition, and character of the bed. A basic assumption is that the width over which deposition or erosion occurs is the input width of the bottom computational cell.

17. Sand beds. Sand beds are considered to consist of a sediment reservoir of finite thickness, below which is a nonerodible surface. Sediment is added to or removed from the bed at a rate determined by a weighted value of the sink/source term at the previous and present time-steps. The mass rate of exchange with the bed is converted to a volumetric rate of change by the bed porosity parameter.

18. Clay beds. Clay beds are treated as a succession of layers. Each layer has its own characteristics as follows:

a. Thickness

b. Density

c. Age

d. Bulk shear strength

e. Type

In addition, the layer type specifies a second list of characteristics:

a. Critical shear stress for erosion

b. Erosion rate constant

c. Initial and 1-year densities

d. Initial and 1-year bulk shear strengths

e. Consolidation coefficient

New clay deposits form layers up to a specified initial thickness and then increase in density and strength with increasing overburden pressure and age. Variation with overburden occurs by increasing the layer type value by one for each additional layer deposited above it. Change with time is governed by the equations

$$f(t) = \begin{cases} f(t_0) + [f(t_1) - f(t_0)] \log (9t + 1) & 0 \leq t \leq 1 \text{ year} \\ f(t_1) + M \log t & 1 \text{ year} \leq t \end{cases} \tag{C31}$$

where

f = time-varying characteristics of density or bulk strength

t_0 = time = zero

t_1 = time = 1 year

M = consolidation coefficient

Mass deposition rates are converted to volumetric deposits by the specified density for the type 1 layer, and erosion rates are converted to a corresponding volume by the actual density of the eroding layer.

Data Requirements

19. The major data input required by LAEMSED is the geometry data describing the system. At the center of each computational cell, the width of the estuary or river must be prescribed. In addition, overbank areas that contribute to the storage of water during flood tide must be included in the model geometry. Other data required are the boundary conditions that drive the internal flow field. At a river (upstream) boundary, a discharge hydrograph must be prescribed along with the temperature, salinity, and concentration of suspended sediment associated with the inflow. At the ocean boundary, the tide must be prescribed. At tidal boundaries, vertical distributions of temperature, salinity, and suspended sediment concentrations must also be prescribed. Water temperature is often assumed constant and surface heat exchange is usually set to zero. However, for problems in which thermal effects are considered, shortwave solar radiation, air temperature, dew-point temperature, and wind speed must be known in order to compute the coefficients required in the computation of the rate of surface heat exchange.

20. In addition to these water column data described, information about the sediment and the initial bed structure must be input. A constant settling velocity is currently assumed. Default values for the characteristic parameters of the different type layers that can make up a sediment bed are provided in LAEMSED, e.g., the density of a freshly deposited type 1 layer is defaulted to 90 kg/m^3. However, any of these values can be changed through input data, if desired.

END

DATE

FILMED

MARCH

1988

DTIC